Bedside Measurements of Oxygen Consumption and End-expiratory Lung Volume in Mechanically Ventilated Patients

A Thesis Submitted for the Degree of Doctor of Philosophy

University of Oxford

Jessica Luiz Segel

Green Templeton College

Michaelmas Term 2025

To Kayhan

We shall not cease from exploration,
And the end of all our exploring
Will be to arrive where we started
And know the place for the first time.

Four Quartets, T. S. Eliot, 1943

ABSTRACT: BEDSIDE MEASUREMENTS OF OXYGEN CONSUMPTION AND END-EXPIRATORY LUNG VOLUME IN MECHANICALLY VENTILATED PATIENTS

Jessica Luiz Segel, Green Templeton College *DPhil Thesis, Michaelmas Term 2025*

Critical care medicine relies heavily on physiological monitoring, however, several fundamental variables remain difficult to measure at the bedside. This thesis focuses on two of these variables: oxygen consumption ($\dot{V}_{O2}$) and end-expiratory lung volume (EELV). Both are central to understanding metabolic and respiratory function, but their reliable quantification in mechanically ventilated patients has historically been challenging. The overarching aim of this work was to determine whether $\dot{V}_{O2}$ and EELV can be measured with sufficient accuracy to provide clinically meaningful information in the intensive care setting.

Chapters 1 and 2 provide the physiological background to $\dot{V}_{O2}$ and EELV, outlining their importance and the challenges associated with their measurement in critical care.

Chapter 3 introduces Computed Cardiopulmonography (CCP), a technique composed of in-airway highly-precise and time-resolved measurements of respired gas composition and flow (Molecular Flow Sensor; MFS) along with robust cardiopulmonary modelling.

The first experimental strand (*Chapters 4 and 5*) investigated $\dot{V}_{O2}$ measurement using the MFS. In healthy volunteers, the MFS showed strong agreement with the Douglas bag method, and in mechanically ventilated patients it provided precise $\dot{V}_{O2}$ assessments over a prolonged measurement window. A novel quality control approach based on nitrogen balance was developed to construct confidence intervals around each individual $\dot{V}_{O2}$ measurement. $\dot{V}_{O2}$ trends were captured in tandem with fluctuations in body temperature, muscle activity, and haemodynamic status, supporting the feasibility of its real-time monitoring in critical care.

The second experimental strand (*Chapters 6 and 7*) examined the estimation of EELV using CCP. In healthy volunteers, CCP-derived volumes agreed with body plethysmography. EELV values obtained by CCP under partial and full multi-breath nitrogen washout stimulus were compared and proven to provide equivalent results. In mechanically ventilated patients, CCP delivered reproducible EELV estimates. An application of such estimates was conducted to assess the changes in absolute volume induced by lung recruitment manoeuvres: the total lung volume change was highly variable and did not correlate with existing predictors of lung recruitability.

Chapter 8 summarises the main conclusions of the thesis. Together, these studies demonstrate that $\dot{V}_{O2}$ and EELV can be made measurable at the bedside with sufficient accuracy to inform clinical care and potentially aid in decision-making.

Acknowledgements

It has been a privilege and an honour to be supervised by Professor Peter A Robbins and Professor Matthew C Frise. Peter, thank you for your patience and support, even when my questions were met with the gentle reminder that I "should know this from school"; for the after-hours meetings; and for lightening our long conversations with photos and stories of your dog. Matthew, ever the optimist, always found the brightest side of every challenge I faced – and provided the best coffee from his hidden stashes. His depth of medical knowledge was both inspiring and, at times, almost intimidating, but it continually pushed me to deepen my own understanding of physiology.

Working alongside other members of the Robbins' and Ritchie's group has been a pleasure. A special thank you to Asma Alamoudi, Haopeng Xu, and Tishan Wellalagodage for your day-to-day assistance, thoughtful sharing, and the enjoyable nights out. To Graham Richmond, Nicholas Smith, Dominic Sandhu, John Couper, and Grant Ritchie, I could not have completed this work without your continuous backing and brilliance in physics, chemistry, coding, and engineering. To Nayia Petousi and Nick Talbot, your clinical and managerial efforts have enabled me to conduct several studies across multiple sites as smoothly as possible.

The bulk of my recruitment took place at the Royal Berkshire Hospital, and I am deeply grateful to all the research nurses who facilitated recruitment on site. To the families of participants who were unable to provide consent for themselves, my genuine gratitude. Even in the face of life-threatening illness, you demonstrated a remarkable selfless commitment to advancing knowledge that may help improve the lives of others in the future. Professor Liza Keating deserves a special mention: she has been a role model to me and a source of endless encouragement and advice – whether clinical, research-related, or personal.

For my husband, Kayhan – my greatest cheerleader – my heartfelt thanks. You believed in me and encouraged me to pursue this degree even when I struggled to believe in myself. Thank you for your love, your unwavering support, and the countless cups of coffee and tea that kept me going. Most of all, thank you for the many nights and weekends you sacrificed to stay by my side so that I could make this possible.

Finally, I would like to thank my family. Mom and Dad, your unconditional love and dedication have enabled me to achieve things I once only dreamed of. Your thoughts and prayers from across the ocean, together with the many video calls, have been invaluable in keeping me going and easing the immense *saudade* I feel every single day. To Xuru, thank you for all the calls just to chat about nothing – they kept me grounded and sane. To Ezi and Kerry, your encouragement has truly been essential. And to my uncle, Huederfidel Viana (in memoriam), my greatest professional inspiration – this achievement is dedicated to you.

I am profoundly grateful to all who have walked alongside me on this journey; this thesis is as much yours as it is mine.

Contents

Abbreviations

2,3-DPG	2,3-diphosphoglycerate
ANOVA	Analysis of variance
ARDS	Acute respiratory distress syndrome
ATP	Adenosine triphosphate
ATPS	Ambient temperature and pressure, saturated
ATS	American Thoracic Society
BPleth	Body plethysmography
CABGS	Circulation and body gas stores
CaO_2	Arterial oxygen content
C_{ARM}	Dynamic compliance after recruitment manoeuvre
C_{BRM}	Dynamic compliance before recruitment manoeuvre
CC	Closing capacity
C_{CO2}	Molar concentration of carbon dioxide
CCP	Computed cardiopulmonography
C_{dyn}	Dynamic compliance of the respiratory system
CEAS	Cavity enhanced absorption spectroscopy
C_{error}	Oxygen consumption error associated with gas concentration inaccuracies
C_{H2O}	Molar concentration of water
C_{linear}	Linear compliance of the quasistatic pressure-volume curve
C_{N2}	Molar concentration of nitrogen
C_{O2}	Molar concentration of oxygen
CO_2	Carbon dioxide
COPD	Chronic obstructive pulmonary disease
CPET	Cardiopulmonary exercise testing
CRF	Case report form
CT	Computerised tomography
CV	Coefficient of variation from the mean
CVC	Central venous catheter
C_{VD}	Anatomical dead space compliance
$C_{VOL}(CO_2)$	Cumulative uptake of carbon dioxide over time
$C_{VOL}(H_2O)$	Cumulative uptake of water vapour over time
$C_{VOL}(N_2)$	Cumulative uptake of nitrogen over time
$C_{VOL}(O_2)$	Cumulative uptake of oxygen over time

$C\bar{v}O_2$	Mixed venous oxygen content
DB	Douglas bag
D_{max}	Maximal distance between the limbs of a quasistatic pressure-volume curve
D_{O2}	Oxygen delivery
ECR	Electronic clinical record
EELV	End-expiratory lung volume
$EELV_{BRM}$	End-expiratory lung volume before recruitment manoeuvre
$EELV_{ARM}$	End-expiratory lung volume after recruitment manoeuvre
$EELV_{ZEEP}$	End-expiratory lung volume change at zero positive end-expiratory pressure
EIT	Electric impedance tomography
$err\dot{V}_{O2}$	$\dot{V}_{O2}$ error
ERV	Expiratory reserve volume
FeN_2	Dry fraction of expired nitrogen
FeO_2	Dry fraction of expired oxygen
FEV1	Forced expired volume in one second
FHS	Final Honours School
$FiCO_2$	Dry fraction of inspired carbon dioxide
FiN_2	Dry fraction of inspired nitrogen
FiO_2	Dry fraction of inspired oxygen
$FmeCO_2$	Dry fraction of mixed expired carbon dioxide
$FmeO_2$	Dry fraction of mixed expired oxygen
FRC	Functional residual capacity
FVC	Forced vital capacity
GCP	Good Clinical Practice
GDPR	General Data Protection Regulation
GLI	Global Lung Function Initiative
Hb	Haemoglobin concentration
H_2O	Water
HME	Heat and moisture exchanger
IC	Inspiratory capacity
ICC	Intraclass correlation coefficient
ICU	Intensive Care Unit
ID / PID	Patient identity number
IPPV	Invasive positive-pressure ventilation
IRV	Inspiratory reserve volume

LB	Lower bound
LNL	Lognormal lung
LoA	Limits of agreement
MBNW	Multi-breath nitrogen washout
MFS	Molecular flow sensor
N_2	Nitrogen
NIPPV	Non-invasive positive pressure ventilation
NLLSOR	Nonlinear least squares optimisation routine
NMD%	Normalised maximum distance percentage
O_2	Oxygen
P	Airway pressure
$PaCO_2$	Arterial partial pressure of carbon dioxide
P_{alv}	Alveolar pressure
PaO_2	Arterial oxygen tension
PAO_2	Alveolar partial pressure of oxygen
P_B	Barometric pressure
PBW	Predicted body weight
PEEP	Positive end-expiratory pressure
PEF	Peak expiratory flow
P_{el}	Elastic pressure
pFRC	Predicted functional residual capacity (Global Lung Function Initiative)
P_{H2O}	Partial pressure of water vapour
$PiCO_2$	Modelled ideal partial pressure of carbon dioxide
PIF	Peak inspiratory flow
PIP	Peak inspiratory pressure
P_{pl}	Pleural pressure
P_{plat}	Plateau pressure
P_{res}	Airway resistance pressure
P_{start}	Airway pressure at the beginning of a recruitment manoeuvre
P_{top}	Maximal airway pressure held during a recruitment manoeuvre
P_{tp}	Transpulmonary pressure
PV	Pressure-volume
Q	Cardiac output
R/I	Recruitment-to-inflation ratio
REE	Resting Energy Expenditure

RM	Recruitment manoeuvre
RQ	Respiratory Quotient
RQ^{mod}	Modelled respiratory quotient
RR	Respiratory rate
RSS	Root sum of squares
RV	Residual volume
SaO_2	Arterial oxygen saturation
$ScvO_2$	Central venous oxygen saturation
SD	Standard deviation
STPD	Standard temperature and pressure, dry conditions
T	Ambient temperature
TLC	Total lung capacity
T_{pause}	Time period of sustained inflation recruitment manoeuvre
UB	Upper bound
V/Q	Ventilation/perfusion
V_A	Alveolar volume
VC	Vital capacity
V_D	Anatomical dead space at the end of expiration
V_D^{APP}	Apparatus dead space
V_D^{INS}	Anatomical dead space at the end of inspiration
V_D^{TOT}	Total dead space
V^{insp}	Inspired gas volume
V^{mexp}	Mixed expired gas volume
V_{PEEP}	End-expiratory lung volume added by positive end-expiratory pressure
V_{rec}	Volume change during the sustained inflation of a recruitment
V_T	Tidal volume
$\dot{V}$	Flow
$\dot{V}_{CO2}$	Carbon dioxide production
$\dot{V}_{error}$	Oxygen consumption error associated with flow inaccuracies
$\dot{V}_{H2O}$	Water vapour production
$\dot{V}_{N2}$	Nitrogen balance
$\dot{V}_{O2}$	Oxygen consumption
$V_{\Delta PEEP}$	Volume change caused by a change in positive end-expiratory pressure
$Z\sigma C_L$	Z-score for ventilation inhomogeneity
ΔEELV	End-expiratory lung volume change following recruitment manoeuvre

ΔP	Driving pressure
ΔRM	End-expiratory lung volume change after RM; discounted from $V_{\Delta PEEP}$
ΔV_A	Total change in alveolar volume following recruitment manoeuvre
σC_d	Alveolar vascular conductance (perfusion) distribution
σC_L	Alveolar compliance (ventilation) distribution
σV_D	Expiratory anatomical dead space distribution

Chapter 1. Introduction to oxygen consumption in critical illness

Oxygen is fundamental for cellular respiration and metabolism – processes essential for sustaining life. In small organisms, oxygen diffuses directly from the environment into cells; however, in larger organisms, diffusion alone is insufficient due to the greater distances between cells and the external environment. To overcome this limitation, a specialised cardiopulmonary system evolved to ensure efficient oxygen delivery (D_{O2}) throughout the body. This process, known as the oxygen cascade, involves the sequential transfer of oxygen from the atmosphere to the alveoli, through the circulation, and finally to the mitochondria, the ultimate site of oxygen consumption ($\dot{V}_{O2}$).

In critically ill patients, disruption at any stage of this cascade can lead to inadequate oxygenation, resulting in hypoxia, shock, organ dysfunction, and eventually death if not rapidly corrected. Maintaining sufficient oxygenation is, therefore, a paramount concern in the management of this group. Historically, various strategies have been developed to monitor and manipulate D_{O2} and $\dot{V}_{O2}$. Early approaches focused on achieving supranormal

delivery targets in an attempt to improve outcomes. Subsequently, more conservative strategies were introduced, utilising surrogates such as central venous oxygen saturation ($ScvO_2$) to assess the adequacy of D_{O2} in response to therapeutic interventions. However, despite its physiological significance, a convenient and reliable method for the direct measurement of $\dot{V}_{O2}$ has remained elusive, even though it might provide crucial insights into metabolic demand and oxygenation status.

This section introduces the fundamental principles of oxygen metabolism, defines and classifies hypoxia, and reviews historical and contemporary approaches to monitoring and managing shock, with a focus on how D_{O2}, $ScvO_2$, blood lactate, and $\dot{V}_{O2}$ relate to patient outcomes in the critical care setting.

1.1. The oxygen cascade

The oxygen cascade begins when dry atmospheric air is inspired and is subsequently warmed and humidified in the upper airways. This process reduces the inspired oxygen partial pressure at sea level from about 21.2 kPa to roughly 19.9 kPa, in accordance with Dalton's law of partial pressures. As the convective airflow reaches the alveoli, it mixes with carbon dioxide produced by ongoing gas exchange, further diluting the alveolar oxygen pressure to approximately 13.3 kPa. This alveolar oxygen tension reflects the balance between ventilation, $\dot{V}_{O2}$, and pulmonary blood flow; any disruption in these factors can compromise gas exchange.

At the alveolar level, oxygen diffuses passively across the alveolar-capillary membrane into the pulmonary capillaries, driven by the partial pressure gradient between the alveolar gas and the blood. Although complete equilibrium would halt diffusion, physiological

right-to-left shunts – such as those in the bronchial circulation and via Thebesian veins – as well as regional ventilation-perfusion mismatches, prevent perfect equilibrium, resulting in a residual gradient of about 2 kPa between alveolar and arterial oxygen pressures[1]. Variations in ventilation-perfusion matching, whether due to changes in shunt fraction or increases in alveolar dead space, can significantly alter this gradient and thereby affect overall gas exchange efficiency[2].

Once in the circulation, only approximately 1% of oxygen is physically dissolved in plasma, while the remaining 99% is transported bound to haemoglobin. Haemoglobin's capacity to carry oxygen, its binding affinity, and its ability to release oxygen to tissues are influenced by factors such as the arterial partial pressure of carbon dioxide ($PaCO_2$), pH, and levels of 2,3-diphosphoglycerate (2,3-DPG). In metabolically active tissues, elevated $PaCO_2$ and reduced pH trigger the Bohr effect, shifting the oxygen-haemoglobin dissociation curve to the right and promoting oxygen unloading. Oxygen then diffuses from the capillaries into tissues and is ultimately utilised in the mitochondria for adenosine triphosphate (ATP) production through the citric acid cycle and oxidative phosphorylation. Within the mitochondria, where oxygen partial pressures range from 0.5 to 3 kPa, the oxygen cascade culminates. Should oxygen levels fall below a critical threshold – known as the Pasteur Point (approximately 0.15 to 0.3 kPa) – cells switch to anaerobic metabolism, leading to a substantially lower energy yield and lactate accumulation.

The efficient flow of oxygen down the cascade is vital to meet metabolic demands (Figure 1). In critically ill patients, simultaneous impairments at multiple stages of the cascade may occur, potentially leading to organ dysfunction and, if uncorrected, death[3].

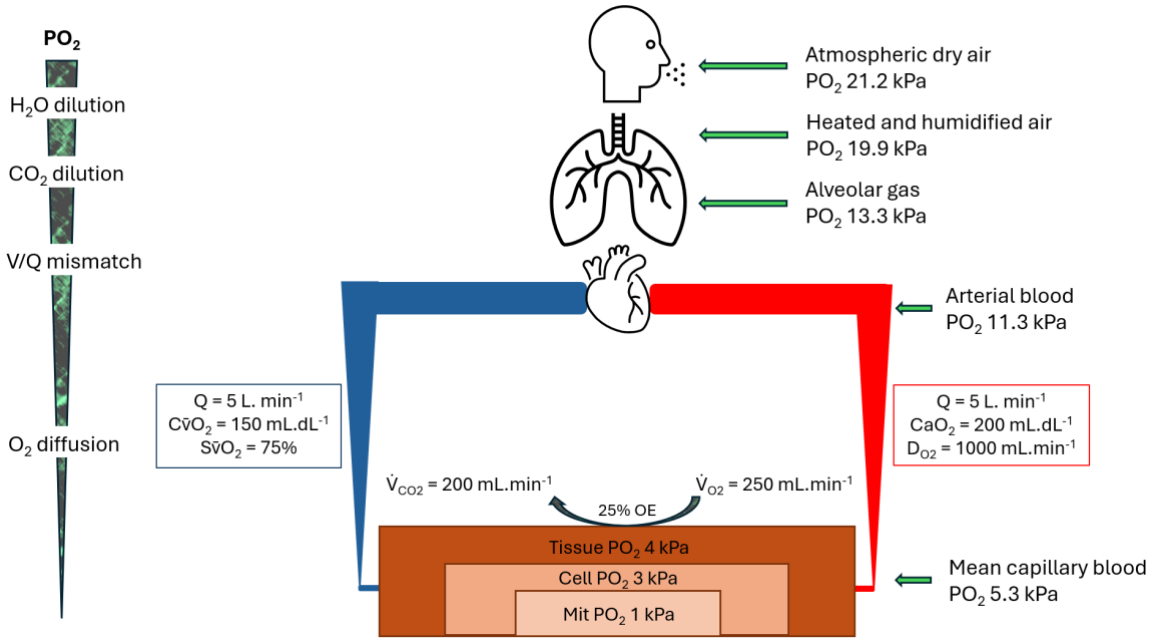

Figure 1. The oxygen cascade.

Transport of O_2 is demonstrated from inspired atmospheric air to the mitochondria, where it is consumed. The values are considered for a standard healthy individual, weighing 75 kg, breathing air at 0.21 FiO_2 and sea level atmospheric pressure (P_B 101 kPa). Q = cardiac output; CaO_2 = oxygen arterial content; D_{O2} = oxygen delivery; Mit = mitochondria; $C\bar{v}O_2$ = oxygen mixed venous content; $S\bar{v}O_2$ = mixed venous oxygen saturation; $\dot{V}_{O2}$ = oxygen consumption; $\dot{V}_{CO2}$ = carbon dioxide production; V/Q = ventilation/perfusion; OE = oxygen extraction.

1.2. Hypoxia

Hypoxia occurs when tissue oxygen levels fall below normal[4]. It can be classified into two main categories: impaired D_{O2}, which includes hypoxaemic, stagnant, and anaemic hypoxia, and impaired $\dot{V}_{O2}$, as seen in histotoxic hypoxia[4, 5].

1.2.1. Impaired D_{O2}

D_{O2} is the total amount of oxygen supplied to the body per minute, calculated as the product of cardiac output (Q; in $L.min^{-1}$) and arterial oxygen content (CaO_2; in mL of O_2 per dL of blood):

$$D_{O2} = Q \times CaO_2 \rightarrow D_{O2} = Q \times [(1.34 \times Hb \times SaO_2) + (0.003 \times PaO_2)]$$

where Hb is haemoglobin concentration ($g.dL^{-1}$), SaO_2 arterial oxygen saturation, and PaO_2 arterial oxygen tension (mmHg).

When oxygen demand increases, physiological compensations enhance cardiac output to maintain adequate tissue oxygenation. However, any impairment in cardiac function (e.g., myocardial infarction, heart failure, arrhythmia) or systemic circulation (e.g., hypovolaemia, cardiac outflow obstruction) reduces D_{O2}, leading to stagnant hypoxia.

The oxygen content of arterial blood is primarily determined by haemoglobin-bound oxygen, as only a small fraction of oxygen is dissolved in plasma. The amount of oxygen carried depends on haemoglobin concentration and arterial oxygen saturation – the proportion of haemoglobin binding sites occupied by oxygen. For a given cardiac output, a reduction in haemoglobin levels significantly decreases D_{O2}, leading to anaemic hypoxia[2].

The dissolved oxygen fraction, though small, is crucial in determining arterial oxygen tension. PaO_2 is influenced by multiple steps of the oxygen cascade, including: (i) fraction of inspired oxygen (FiO_2) and barometric pressure (P_B), which together determine alveolar partial pressure of oxygen (PAO_2); (ii) oxygen diffusion efficiency across the alveolar-capillary membrane, dependent on surface area and thickness; (iii) ventilation-perfusion matching, which promotes optimal gas exchange between alveoli and blood. A failure in

any of these processes impairs arterial oxygenation, lowering PaO_2 and SaO_2, with progression to hypoxaemic hypoxia[6].

1.2.2. Impaired $\dot{V}_{O2}$

$\dot{V}_{O2}$ refers to the amount of oxygen utilised by the body per minute, reflecting metabolic demand. Even if oxygen is adequately delivered, cellular dysfunction can impair oxygen use. This occurs when mitochondrial activity is disrupted, often due to toxins or inflammatory mediators that inhibit the electron transport chain. Conditions such as cyanide poisoning, hydrogen sulphide poisoning, and septic shock interfere with oxygen-dependent ATP production, rendering cells incapable of utilising the available oxygen[4]. This state is known as histotoxic hypoxia.

1.3. Shock

1.3.1. Definition

Shock is a state of acute circulatory failure in which tissue perfusion and oxygenation are compromised, leading to impaired cellular oxygen utilisation[7, 8]. This definition makes clear that the ultimate indicator of adequate tissue oxygenation is the cell's ability to utilise oxygen efficiently. Cellular oxygen utilisation can be impaired through two primary mechanisms. The first involves a direct insult to the mitochondria, often triggered by toxins and inflammatory mediators, which disrupts the electron transport chain and reduces oxidative phosphorylation. The second mechanism results from an inadequate oxygen supply, leading to decreased ATP production. As ATP levels fall, ATP-dependent ion pumps such as the sodium-potassium ATPase and calcium ATPase become dysfunctional, causing ionic imbalances that result in cellular oedema, structural damage, and further

mitochondrial impairment. This vicious cycle of energy depletion and ionic dysregulation culminates in cellular injury and death. For this reason, patients with shock are continuously monitored within dedicated intensive care units (ICUs).

1.3.2. D_{O2}-$\dot{V}_{O2}$ relationship

In a healthy, resting individual, only approximately 25% of the oxygen available in systemic arterial blood is extracted and consumed (i.e., normal global oxygen extraction ratio ranging between 20% and 30% at rest), with the remainder returning to the lungs as mixed venous blood[2]. Under normal conditions, when D_{O2} decreases, the body compensates by increasing the oxygen extraction ratio, maintaining $\dot{V}_{O2}$ in a supply-independent manner. However, once D_{O2} falls below a critical threshold, the compensatory mechanisms fail, and $\dot{V}_{O2}$ begins to decline proportionally with D_{O2} (Figure 2)[9-11]. The critical D_{O2} point marks the tipping point at which shock ensues[12]. This transition signals the onset of supply-dependent oxygenation, where D_{O2} fails to meet metabolic demands. Consequently, there is a forced cellular shift to anaerobic metabolism with significantly reduced energy yield and lactate accumulation, further exacerbating the metabolic crisis in critically ill patients, and precipitating dysoxia[7] – a state in which cellular oxygen utilisation is impaired despite the presence of oxygen.

1.3.3. Types of shock

Shock can be classified into four types according to the main circulation component affected[13]. Hypovolaemic shock results from significant fluid or blood loss leading to reduced circulatory volume. Cardiogenic shock is caused by cardiac dysfunction resulting in inadequate cardiac output. Obstructive shock occurs due to obstruction of blood flow from conditions such as pulmonary embolism or cardiac tamponade, directly affecting afterload. Finally, distributive shock, a disturbance of vascular tone, is characterised by

inappropriate vasodilation leading to altered blood flow distribution and impaired perfusion – e.g. septic, anaphylactic, and neurogenic shock. In reality, several components of the circulation may be simultaneously affected in a given critically ill patient, with overlapping features across different shock types and commonly shared treatments.

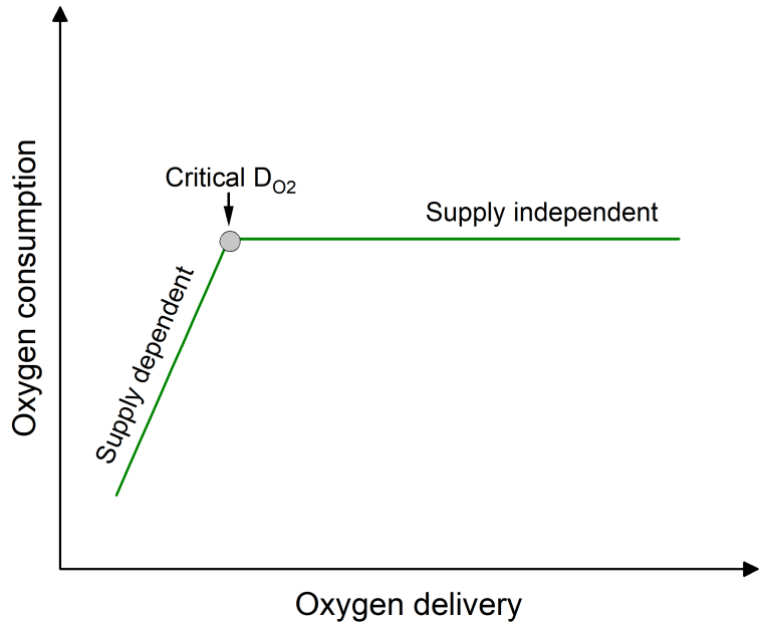

Figure 2. The D_{O2}-$\dot{V}_{O2}$ relationship*.

In a physiologic compensation to decreased D_{O2}, oxygen extraction increases, maintaining consumption at constant level – supply independent portion of the curve. Below a critical delivery point, further reduction in supply cannot be fully compensated, resulting in proportional decline in consumption – supply dependent portion of the curve. *Except for the kidneys.

1.3.4. Monitoring strategies in shock

The specific treatment of shock depends upon its underlying cause. For instance, septic shock requires treatment of the underlying infection, whereas obstructive shock necessitates relief of the obstruction. Broadly speaking, common treatment principles for all shock types include restoring cardiac output – either by fluid resuscitation, enhancing

cardiac contractility, or both – and optimising vascular tone. Although specific recommendations regarding the type and amount of fluids and drugs have evolved over time, the fundamental goal remains consistent: to reverse acute circulatory failure and restore tissue perfusion by balancing D_{O2} with $\dot{V}_{O2}$[7, 8, 13]. Effective monitoring strategies are essential for clinicians to evaluate treatment effectiveness. The most valuable monitoring methods are those capable of reflecting the adequacy of cellular $\dot{V}_{O2}$. Recently, clinical practice has trended away from highly invasive monitoring strategies and strict physiological targets. Historical and contemporary examples of such monitoring approaches are described in the following sections.

1.3.4.1. Oxygen delivery

Historically, D_{O2} was monitored invasively via pulmonary artery catheters in patients with shock. Efforts to enhance D_{O2} were, in reality, attempts to improve tissue $\dot{V}_{O2}$. Early studies employed fluid resuscitation, blood transfusions, and vasoactive drugs to boost D_{O2}, and initial observations suggested that only patients with high lactate – presumed to be in the supply-dependent range of the D_{O2}-$\dot{V}_{O2}$ relationship – experienced significant increases in $\dot{V}_{O2}$[14-16].

Shoemaker et al. reported improved outcomes in high-risk surgical patients when supranormal D_{O2} targets were achieved, sparking interest in maximising D_{O2} though the adoption of such targets[17-19]. However, subsequent trials in heterogeneous critical care populations failed to demonstrate a survival benefit to support this practice[20, 21]. Indeed, *Hayes et al.* showed that, provided that patients were adequately fluid-resuscitated and maintained good perfusion pressure, attaining supranormal D_{O2} targets did not alter $\dot{V}_{O2}$ and was, in fact, associated with increased in-hospital mortality[21].

These findings demonstrate that the assumption that D_{O2} is a reasonable surrogate for $\dot{V}_{O2}$ is flawed. In patients with already adequate D_{O2}, further increases do not enhance $\dot{V}_{O2}$, as the tissues are already extracting the maximum oxygen possible. In cases of histotoxic hypoxia, where cellular oxygen utilisation is impaired due to mitochondrial dysfunction, boosting D_{O2} fails to completely rectify the underlying metabolic deficits[22]. Additionally, the invasive nature of D_{O2} measurements, relying on pulmonary artery catheters, is associated with increased morbidity with no demonstrable survival benefit[23-25]. As a result, D_{O2} measurements have largely given way to the surrogate markers of D_{O2}-$\dot{V}_{O2}$ relationship adequacy, such as $ScvO_2$ and blood lactate concentration.

1.3.4.2. Central venous oxygen saturation

$ScvO_2$ represents the percentage oxygenation of haemoglobin in central venous blood – sampled from the superior vena cava or right atrium – that remains saturated with oxygen after tissue oxygen extraction, serving as an index of the balance between D_{O2} and $\dot{V}_{O2}$.

Early studies in septic shock, notably the Early Goal Directed Therapy trial by *Rivers et al.* – which enrolled patients with very low $ScvO_2$ – suggested that raising $ScvO_2$ above 70% could substantially reduce mortality[26]. The therapeutic bundle employed to achieve this target involved optimising preload (fluid resuscitation), afterload (maintaining mean arterial pressure with vasopressors), and cardiac contractility (using inotropes) to ensure adequate end-organ perfusion[26]. However, subsequent multicentre trials, such as ProCESS, ProMISe, and ARISE[27-29]– which enrolled patients with higher baseline $ScvO_2$ values – failed to demonstrate the same benefits. These trials used more flexible treatment protocols that avoided unnecessary fluid or drug administration and yet achieved similar outcomes to those adopting a strict $ScvO_2$ target[30].

The use of $ScvO_2$ as a therapeutic target has important limitations. As a central venous measure, it does not account for myocardial oxygen extraction and may overestimate systemic oxygenation[31]. It also fails to detect regional hypoperfusion, such as that which occurs from microvascular shunting[7] or impaired cellular oxygen utilisation due to mitochondrial dysfunction. A patient with normal or high $ScvO_2$ may still have impaired D_{O2} or $\dot{V}_{O2}$ at tissue level – a situation where solely relying on $ScvO_2$ to assess oxygenation adequacy could be misleading. Consequently, routine insertion of a central venous catheter (CVC) solely for $ScvO_2$ monitoring is no longer recommended[7]. In patients who already have a CVC, $ScvO_2$ monitoring is primarily useful when low values occur alongside hyperlactatemia, indicating compromised D_{O2}[7].

1.3.4.3. Lactate

Lactate is primarily produced by cells during anaerobic respiration in response to inadequate D_{O2}. In shock, reduced tissue perfusion and oxygen supply stimulate increased lactate production, resulting in hyperlactataemia. Even mild elevations (above 1.5 $mmol.L^{-1}$) are associated with increased mortality, especially in septic shock[32], highlighting the importance of lactate as an early marker of impaired oxygen utilisation.

In clinical practice, lactate is valuable both for monitoring shock progression and guiding resuscitation strategies. Its predictive value for patient outcomes often surpasses that of traditional parameters, such as blood pressure[33]. A rapid decrease in lactate following initial resuscitation efforts signals improved tissue oxygenation and correlates with reduced mortality[34].

However, lactate levels must be interpreted cautiously, as they can rise due to mechanisms other than tissue hypoxia – such as impaired clearance in liver dysfunction or increased

aerobic glycolysis during stress responses – limiting lactate's specificity as an isolated tool. Therefore, lactate measurements are most informative when integrated into a comprehensive clinical assessment, alongside other physiological markers of oxygen delivery and utilisation[7].

1.3.4.4. Oxygen consumption

$\dot{V}O_2$ serves as an index of metabolic rate and is influenced by the oxygen demands of individual tissues and organs[2]. Early research has demonstrated that reduced $\dot{V}O_2$ correlates with increased mortality among critically ill patients[35]. In septic shock specifically, $\dot{V}O_2$ has an inverse relationship with arterial blood lactate levels[36].

Impaired cellular $\dot{V}O_2$ is recognised as the fundamental pathophysiological consequence of shock[7, 8, 13]. The primary factor limiting $\dot{V}O_2$ may differ according to the type of shock, whether due to inadequate DO_2, cellular dysfunction, or a combination of both. Regardless of the underlying cause, the ultimate result is invariably inadequate cellular oxygen utilisation.

Therefore, an ability accurately to measure $\dot{V}O_2$ in critically ill patients in a straightforward way would be highly desirable. Theoretically, once maximum $\dot{V}O_2$ is achieved through resuscitation, additional interventions aimed at further increasing DO_2 would not confer further benefit. However, reliably measuring $\dot{V}O_2$ in this patient population remains extremely challenging.

1.4. Clinical value of $\dot{V}O_2$ measurements

Measurement of $\dot{V}O_2$ in critical care provides valuable insights into a patient's metabolic state, potentially informing clinical decision-making and therapeutic interventions.

The assessment of $\dot{V}_{O2}$ and $\dot{V}_{CO2}$ enables clinicians to determine Resting Energy Expenditure (REE), reflecting a patient's basal metabolic rate. Accurate REE estimation supports personalised nutritional support, which may help optimising recovery and clinical outcomes in the critically ill[37]. Additionally, measuring these respiratory gases enables calculation of the Respiratory Quotient (RQ) – the ratio of $\dot{V}_{CO2}$ to $\dot{V}_{O2}$ – offering insight into predominant metabolic substrates: carbohydrates (RQ $\sim$ 1.0), proteins ($\sim$ 0.8), or lipids ($\sim$ 0.7).

In critically ill patients, $\dot{V}_{O2}$ can vary significantly, reflecting changes in metabolic demand driven by clinical conditions (e.g., sepsis, trauma, surgery), physiological stress responses (e.g., fever, shivering), or medical interventions (e.g., sedation, analgesia). Such variations carry important prognostic and therapeutic implications. Monitoring $\dot{V}_{O2}$ might help clinicians detect inadequate tissue perfusion before conventional clinical signs become apparent, assess the effectiveness of treatments aimed at enhancing D_{O2} (e.g., fluid therapy, inotropes, blood transfusion), and evaluate interventions intended to reduce metabolic demands.

Moreover, direct measurement of $\dot{V}_{O2}$ may offer greater specificity when compared with surrogate markers such as blood lactate or $ScvO_2$. It might allow clinicians to tailor therapies to individual metabolic profiles, enhancing personalised care and potentially improving outcomes.

The following sections review both historical and current techniques for measuring $\dot{V}_{O2}$ in mechanically ventilated patients in addition to discussing the technical and practical limitations associated with these methods. Direct respiratory gas-exchange methods as well as indirect approaches based on the reverse Fick principle are examined.

1.5. Measurements of $\dot{V}_{O2}$ in mechanically ventilated patients

1.5.1. Brief historical timeline of $\dot{V}_{O2}$ measurements

The earliest documented measurement of $\dot{V}_{O2}$ in humans dates back to 1790 and is credited to Antoine Lavoisier[38]. His recognition of respiration as a slow combustion – where oxygen facilitates the production of carbon dioxide, heat, and water – established foundational concepts for contemporary gas exchange understanding and indirect calorimetry, a technique that estimates energy expenditure from $\dot{V}_{O2}$ and $\dot{V}_{CO2}$ measurements rather than direct heat quantification[38, 39].

Early measurements of human $\dot{V}_{O2}$ relied primarily on closed-circuit respirometry, a method in which individuals rebreathed air from a sealed container, resulting in gradual oxygen depletion and limited experiment duration. Opening the circuit would lead to variable inspired volumes and complicate the calculation of $\dot{V}_{O2}$[39]. A critical breakthrough occurred in 1912 with Haldane's introduction of a mathematical approach – the Haldane transformation – which permitted accurate estimation of inspired gas volumes from measured expired volumes, assuming nitrogen remained inert during respiration[40]. This innovation allowed closed respirometers to evolve into open-circuit systems, greatly enhancing practicality and the length of measurement acquisition.

Simultaneously, Oxford physiologist Claude Douglas developed the Douglas bag (DB) technique, a pioneering open-circuit method that involved collecting mixed expired gases in a bag for subsequent chemical analysis[41]. By employing the Haldane transformation, researchers could estimate inspired volumes and thus determine $\dot{V}_{O2}$. This approach became

the gold standard in respiratory physiology, enabling validation of subsequent technological developments – including more recent indirect calorimeters, which quantify metabolism through indirect heat estimation based on $\dot{V}_{O2}$ and $\dot{V}_{CO2}$[42-44].

During the twentieth century, measurement methods advanced significantly: pulmonary artery catheters allowed $\dot{V}_{O2}$ estimation using Fick's principle and modern indirect calorimeters[45, 46], equipped with rapid gas analysers and pneumotachographs, enabled faster and clinically applicable $\dot{V}_{O2}$ measurements. Despite these advancements, accurately quantifying $\dot{V}_{O2}$ in critically ill, mechanically ventilated patients remains methodologically challenging.

1.5.2. Direct measurement of $\dot{V}_{O2}$

$\dot{V}_{O2}$ can be directly measured from respiratory gas exchange by subtracting expired from inspired oxygen volumes:

$$\dot{V}_{O2} = \left(FiO_2 \times MV^{insp}\right) - \left(FeO_2 \times MV^{exp}\right)$$

where FiO_2 and FeO_2 are inspired and expired fractions of oxygen; and MV^{insp} and MV^{exp} are the inspired and expired minute-volumes, respectively, in $mL.min^{-1}$.

Accurate measurement of $\dot{V}_{O2}$ depends on dynamic assessment of respiratory gas composition and flow rates. Direct respiratory $\dot{V}_{O2}$ measurement methods include the DB, mixing chamber, and breath-by-breath analysis (Figure 3). As these techniques measure both $\dot{V}_{O2}$ and $\dot{V}_{CO2}$, they will collectively be referred to as indirect calorimeters.

1.5.2.1. Gas composition assessment

Respired gases (oxygen, O_2; and carbon dioxide, CO_2) are typically analysed using rapid-response analysers as their response time – the time required for changes in gas composition to be accounted for – is shorter. Commonly employed technologies for O_2 measurement include paramagnetic analysers (detecting O_2 concentration via changes in a magnetic field), fuel cell analysers (generating current proportional to O_2 concentration via chemical reactions), and mass spectrometry (ionising gases and distinguishing them by mass-to-charge ratio). CO_2 is usually measured via broadband infrared spectroscopy, detecting infrared absorption proportional to gas concentration.

In mechanically ventilated patients, a small gas sample can be withdrawn from the ventilator circuit for sidestream gas analysis. The sampling location depends on the measurement method used (DB, mixing chamber, or breath-by-breath).

1.5.2.2. Flow assessment

Respiratory flow measurements can be obtained using flow meters (usually pneumotachographs), volume meters, or calculated indirectly via the Haldane transformation. Pneumotachographs measure flow by detecting pressure differences across a fixed resistance and can be unidirectional (expiratory flow only) or bidirectional (both inspiratory and expiratory flows).

When inspiratory flow is not directly measured, the Haldane transformation is employed. This method relies on the assumption that nitrogen (N_2) remains inert during respiration, such that the amount of N_2 entering the lungs equals the amount leaving them. Based on this equivalence, inspired flow can be estimated from measured expired flow:

$$FiN_2 \times MV^{insp} = FeN_2 \times MV^{exp} \quad \rightarrow \quad MV^{insp} = \frac{FeN_2}{FiN_2} \times MV^{exp}$$

where FiN_2 and FeN_2 are the inspired and expired fractions of nitrogen. Nitrogen fractions are obtained indirectly by subtracting measured O_2 and CO_2 fractions from the total gas mixture (disregarding other inert gases, such as argon). The Haldane transformation helps minimise discrepancies and integration errors between inspired and expired flows, since the former is estimated from the latter.

1.5.2.3. Douglas bag

The Douglas bag technique consists of collecting mixed expired gases over a defined period into a flexible rubbery bag connected to the mechanical ventilator's exhaust port[43]. Gas composition is determined by running a sample of gas syringed out of the bag into a gas analyser. Gas volume is subsequently analysed using a volume meter. Inspired flow is determined via the Haldane transformation, as inspired gas fractions are known.

1.5.2.4. Mixing chamber

The mixing chamber method involves expired gas flowing through a chamber for homogenisation prior to undertaking gas composition assessment and flow measurements. Mixed expired samples are drawn from the chamber's outlet for gas analysis. Expired flow is also measured at the chamber's outlet by an interposed flow sensor, with inspired flow estimated via using the Haldane transformation. Here, inspired gas is sampled from the inspiratory limb of the ventilator circuit to determine FiO_2. Some mixing chamber devices (e.g., Deltatrac II) employed an additional air dilution step at a known constant flow, allowing $\dot{V}_{O2}$ determination without explicitly measuring minute-volumes[37].

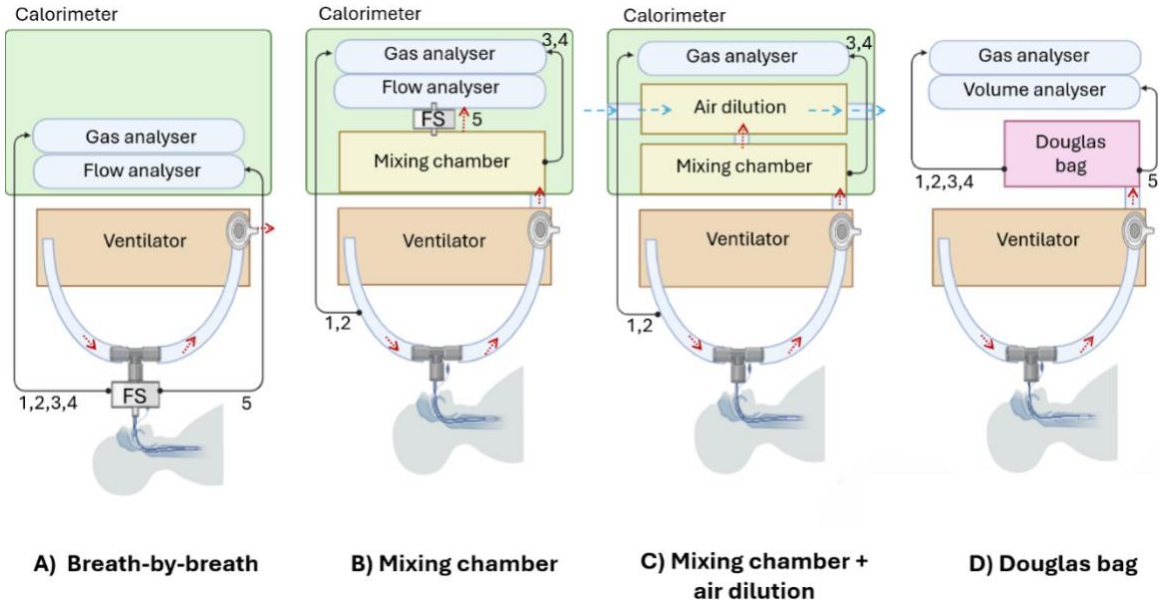

Figure 3. Schematic representation of direct oxygen consumption measurements in critically ill mechanically ventilated patients.

(A) The breath-by-breath technique continuously measures inspired and expired gas composition and flow, using a flow sensor placed at the airway and a gas analyser that samples gases from the ventilator circuit. (B) The mixing chamber method collects expired gas into a chamber where it is homogenised before analysis. Inspired gas composition is sampled separately from the inspiratory limb of the ventilator, and expired flow is measured at the chamber outlet. The Haldane transformation is applied to estimate inspired volume. (C) A variation of this method, known as mixing chamber with air dilution, eliminates the need for direct flow measurement by further diluting the homogenised expired gas with a known airflow before analysis. (D) The Douglas bag technique involves collecting expired gas into a sealed bag over a fixed time period, after which the volume and composition of the collected gas are analysed. Inspiratory volume is estimated using the Haldane transformation, while inspired gas composition is typically known from the administered gas mixture. Red dotted line and arrows point towards flow direction. Black continuous line and arrows show gas sampling direction. Blue dashed lines and arrows reveal the direction of airflow in dilutional methods. FS = flow sensor. 1, 2, 3, 4, 5 represent, respectively, fraction of inspired O_2, fraction of inspired CO_2, fraction of expired O_2, fraction of expired CO_2, and respired flow. Created with BioRender.com.

1.5.2.5. Breath-by-breath

The breath-by-breath method continuously samples inspired and expired gas from the ventilator circuit for concentration analyses and simultaneously measures expired flow, typically through a pneumotachograph positioned at the airway opening. Inspired flow is either directly measured (bidirectional flow sensors, e.g., Medgraphics Ultima[43]) or indirectly estimated by applying the Haldane transformation[47]. These data are synchronised by computational software to calculate $\dot{V}_{O2}$ and $\dot{V}_{CO2}$ breath-by-breath.

1.5.3. Indirect measurement of $\dot{V}_{O2}$

$\dot{V}_{O2}$ can be indirectly calculated as the product of cardiac output by the arteriovenous difference in O_2 content, a rearrangement of the Fick equation, which considers only systemic consumption:

$$Q = \dot{V}_{O2}/\left(C_{aO_2} - C_{\bar{v}O_2}\right) \quad \rightarrow \quad \dot{V}_{O2} = Q \times \left(C_{aO_2} - C_{\bar{v}O_2}\right)$$

where, Q is cardiac output, in $L.min^{-1}$; $\dot{V}_{O2}$ is oxygen consumption in $mL.min^{-1}$; CaO_2 is the arterial oxygen content in mL of O_2 per dL of blood; $C\bar{v}O_2$ is the mixed venous oxygen content in mL of O_2 per dL of blood.

1.5.3.1. Reverse Fick

The Fick principle, established in the 1870s and later refined by Stuart and Hamilton, laid the foundation for measuring cardiac output and indirectly assessing oxygen metabolism. This understanding advanced with the mid-20th-century development of pulmonary artery catheters, a Nobel-Prize worthy innovation which revolutionised hemodynamic monitoring[45, 46]. Inserted via a central vein into the pulmonary artery, these catheters allow direct sampling of mixed venous blood for $C\bar{v}O_2$ calculation. CaO_2 is obtained from

systemic arterial blood, while cardiac output is typically measured via thermodilution. Using these variables, $\dot{V}_{O2}$ is indirectly estimated through the reverse Fick method.

1.5.4. Direct measurement challenges and limitations

Direct measurement methods for $\dot{V}_{O2}$ rely on calculating the relatively small difference between two large numerical values: the inspired and expired oxygen volumes. Consequently, even minor inaccuracies in measuring these large volumes can result in significant magnification of errors in the final $\dot{V}_{O2}$ value, limiting the precision and reliability of the method.

1.5.4.1. Gas composition and flow measurements

Respiratory gases are typically analysed using sidestream rather than mainstream measurements, requiring gas samples to be withdrawn remotely from the ventilator circuit. Sampling lines and flow sensors are susceptible to condensation, which impairs accurate gas composition and flow assessments. Additionally, because gas composition and flow are measured by separate devices at different locations, significant time-alignment errors can occur. Although software corrections attempt to reduce such mismatches, residual inaccuracies remain. Furthermore, several gas analysers – despite advances – have relatively long response times (over a hundred milliseconds), limiting the accurate representation of dynamic changes in gas exchange [48].

1.5.4.2. Haldane transformation

The Haldane transformation relies on the assumption of zero nitrogen exchange to estimate inspired flow. At higher FiO_2 values (particularly above 0.6), the reduced inspired nitrogen fraction can substantially amplify measurement errors, as even small inaccuracies in gas composition analyses significantly impact $\dot{V}_{O2}$ calculations[43]. Leaks anywhere in the

mechanical ventilator circuit will result in unreliable $\dot{V}_{O2}$ measurements. Moreover, critically ill patients often undergo dynamic changes in inspired oxygen concentration; this violates the steady-state nitrogen assumption required by Haldane's method, necessitating prolonged equilibration periods (approximately 30 minutes) before reliable measurements can resume, restricting clinical utility.

1.5.4.3. Accuracy and inter-device variability

Overall, reported accuracy of indirect calorimetry devices is limited (± 20% or greater)[43]. Even short-term consecutive measurements often exhibit low precision; for instance, a coefficient of variation up to 14% over five consecutive single-minute $\dot{V}_{O2}$ measurements[43]. Furthermore, the lack of standardised validation methods in mechanically ventilated patients complicates reliability assessments. Historically, DBs were the validation standard, though contemporary studies have relied heavily on the discontinued Deltatrac II device, an outdated mixing chamber calorimeter[42, 47, 49, 50]. Comparisons between devices frequently reveal systematic and random errors, characterised by wide limits of agreement, emphasising the unresolved issue of inter-device consistency[43].

1.5.4.4. Douglas-bag-specific drawbacks

The DB technique introduces additional practical limitations: gas diffusion through the bag's membrane alters gas composition over time, incomplete emptying into gas meters compromises volume accuracy, and insufficient gas mixing within the bag affects composition analyses[51]. Perhaps most importantly, DBs do not support continuous monitoring. These drawbacks, combined with a cumbersome design, relegate DB use primarily to research contexts rather than routine critical care practice.

1.5.5. Indirect measurement challenges and limitations

The reverse Fick method requires invasive placement of a pulmonary artery catheter, with the risk of significant complications that limit its routine clinical use[23-25]. Being an indirect measurement, the method introduces additional sources of random error due to reliance on multiple derived physiological variables. Furthermore, this method quantifies only systemic $\dot{V}O_2$, omitting pulmonary oxygen utilisation, thereby systematically underestimating total $\dot{V}O_2$ by as much as 16% when compared with direct respiratory measurement techniques[52]. Lastly, when examining the relationship between DO_2 and $\dot{V}O_2$, the use of the same cardiac output measurement for calculating both variables may lead to mathematical coupling errors, artificially strengthening their correlation[53].

1.6. Motivation & Objectives

$\dot{V}O_2$ measurement in critically ill, mechanically ventilated patients provides a crucial insight into metabolism. It serves both as a marker of basal nutritional requirements and as an index of oxygen utilisation at the cellular level, helping clinicians assess metabolic stress, recovery, and response to interventions.

Despite its clinical relevance, accurately measuring $\dot{V}O_2$ in this cohort remains challenging. Current techniques require complex assumptions and synchronisations that introduce errors. As a result, clinicians often rely on surrogate markers such as lactate or $ScvO_2$ which may not fully capture real-time metabolic changes. A direct, continuous, and precise method of measuring $\dot{V}O_2$ could provide valuable insight into the adequacy of DO_2 and cellular respiration.

One potential approach uses the Molecular Flow Sensor (MFS), a gas analyser that integrates laser gas spectroscopy with a bespoke bidirectional flow sensor to measure respired gas concentrations and flows directly within the mainstream airway [54]. As it will be discussed in Chapter 3, its features address several of the limitations of conventional indirect calorimeters. While this approach has been successfully deployed in an operating theatre environment, where $\dot{V}_{O2}$ was tracked in a single mechanically ventilated patient undergoing abdominal aortic aneurysm repair[54], its application to a critically ill mechanically ventilated patient cohort has not yet been systematically examined.

This thesis aims to explore the measurement of $\dot{V}_{O2}$, using the MFS, in a cohort of critically ill mechanically ventilated patients. It seeks to: (i) examine the reproducibility of serial $\dot{V}_{O2}$ measurements; (ii) compare $\dot{V}_{O2}$ values obtained by the MFS against a reference method (the DB); and (iii) determine whether $\dot{V}_{O2}$ measurements obtained with the MFS are sufficiently accurate to support this as an approach for continuous metabolic monitoring in intensive care settings.

Chapter 2. Introduction to lung volumes in critical care

2.1. Normal lung physiology

The respiratory system is the site of gas exchange between the body and environment. To support this function, inspired air moves through the upper airways into a branching network that progressively narrows and thins from the trachea to the alveoli, maximising the surface area available for exchange at the alveolar-capillary interface.

The upper airways – comprising the nasal and oral cavities, pharynx, and larynx – warm, humidify, and filter the incoming air. The air then passes into the conductive airways, a non-gas-exchanging zone extending from the trachea to the terminal bronchioles. The trachea divides into lobar and segmental bronchi and finally into multiple smaller bronchioles. Structural support in these airways, which become progressively thinner distally, is provided by cartilage and smooth muscle.

The respiratory zone, where gas exchange occurs, begins with the respiratory bronchioles, which derive from terminal bronchioles and lead into alveolar ducts and sacs. Each alveolus is lined by a single layer of epithelial cells, including type II pneumocytes that secrete surfactant to reduce surface tension and help keep the alveoli open. Surrounding the alveoli is a dense network of pulmonary capillaries. The thin barrier between the alveolar epithelium and the capillary endothelium forms the site of gas exchange.

The lungs are housed within the thoracic cage and rest on the diaphragm. They are enclosed by pleural membranes, which line the inner surface of the chest wall and diaphragm, and the outer surface of the lungs.

There is a natural tendency of the lungs to recoil inward due to their elastic properties, which are primarily attributable to alveolar surface tension and the abundant presence of elastic fibres in the lung parenchyma. Despite this inward recoil, the lungs do not collapse at rest because they are held open by an opposing outward force – the transpulmonary pressure, defined as the difference between alveolar pressure and pleural pressure. At FRC – the volume of the lungs at the end of a normal passive expiration – alveolar pressure is equal to atmospheric pressure, and pleural pressure is slightly sub-atmospheric, typically around - 5 cmH_2O at mid-lung level in upright individuals, becoming more negative toward the apices. This results in a positive transpulmonary pressure that balances lung recoil and keeps the alveoli open (Figure 4).

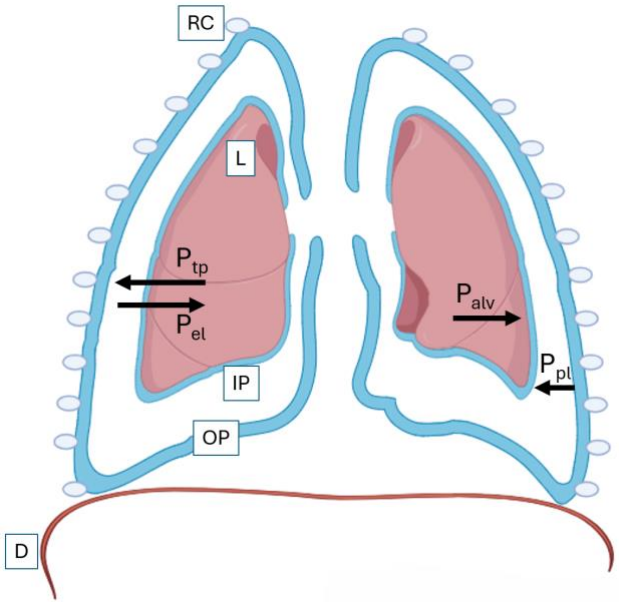

Figure 4. Factors driving lung expansion and recoil.

At FRC, alveolar pressure equals atmospheric pressure and the inward recoil of the lungs is balanced by the outward recoil of the chest wall. This balance is reflected in the transpulmonary pressure (P_{tp}), which is the difference between alveolar pressure (P_{alv}) and pleural pressure (P_{pl}). At FRC, P_{tp} is of equal magnitude and opposite direction to the elastic pressure (P_{el}), such that the lungs are held open against their tendency to collapse. D = diaphragm; OP = parietal pleural; IP = visceral pleura; L = lung; RC = ribcage. Created with BioRender.com.

Lung volume changes are entirely driven by forces external to the lungs. During spontaneous inspiration, an active process, the increase in lung volume is initiated by contraction of the inspiratory muscles. The diaphragm moves downward, and the external intercostal muscles lift the ribcage upward and outward. This increases intrathoracic volume and further lowers pleural pressure, thereby increasing transpulmonary pressure. The rise in transpulmonary pressure causes alveolar expansion, which lowers alveolar pressure below atmospheric, creating a pressure gradient that drives airflow into the lungs. Air continues to flow until alveolar and atmospheric pressures reach equilibrium.

Expiration, by contrast, is passive under resting conditions. As the inspiratory muscles relax, the thoracic cavity returns to its original dimensions. Pleural pressure becomes less negative, transpulmonary pressure decreases, and the elastic recoil of the lungs reduces alveolar volume. As alveolar volume falls, alveolar pressure rises above atmospheric pressure, creating a gradient that facilitates airflow out of the lungs. Expiration is completed once alveolar and atmospheric pressures equalise once again at FRC.

To some extent, FRC represents a point of mechanical equilibrium in the respiratory system. Lung volumes are conventionally described in relation to this baseline. Tidal breathing produces small fluctuations around FRC, while the full range of possible lung volumes extends from residual volume (RV) at the end of maximal expiration to total lung capacity (TLC) at the end of maximal inspiration. These variations in lung volume relative to FRC during the respiratory cycle are illustrated in Figure 5.

FRC can be broadly divided into two functional compartments: alveolar volume, which consists of alveoli that receive both fresh gas and pulmonary blood flow and thus participate in gas exchange, and dead space volume, which includes the conducting airways (anatomical dead space) and any alveoli that are ventilated but not perfused (alveolar dead space). In healthy individuals at rest, approximately 30% of each tidal breath is directed to dead space while the remaining 70% contributes to effective alveolar ventilation[2].

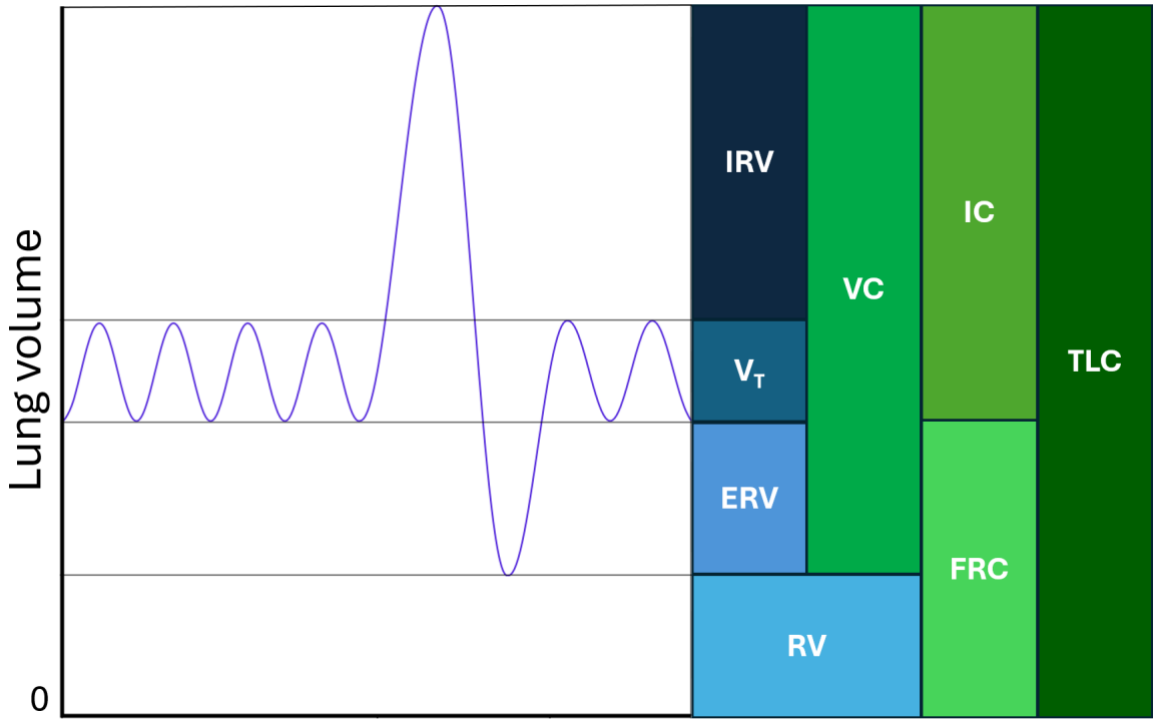

Figure 5. Schematic representation of lung volume and capacities.

The diagram illustrates individual lung volumes and their combinations (capacities). Tidal volume (V_T) represents the volume of air inspired and expired during normal breathing. Inspiratory reserve volume (IRV) is the additional volume that can be breathed in upon a maximal inspiration, while expiratory reserve volume (ERV) is the extra volume that can be breathed out after a maximal expiration. Residual volume (RV) is the amount of air remaining in the lungs after maximal expiration and it cannot be voluntarily expelled. At the end of a tidal expiration, the volume remaining in the lungs is named functional residual capacity (FRC), composed by the sum of RV and ERV. When combined, lung volumes form larger capacities: inspiratory capacity (IC), the sum of IRV and VT; vital capacity (VC), the sum of IRV, VT, and ERV; total lung capacity (TLC), the sum of IRV, VT, ERV, and RV.

As discussed in more detail in Chapter 1, the primary function of the cardiopulmonary system is to enable efficient gas exchange and delivery – supplying oxygen to the tissues and removing carbon dioxide. Effective gas exchange depends on the appropriate matching of ventilation and perfusion within the lungs. Although straightforward in principle, this

matching is influenced by complex anatomical and physiological factors. In the upright lung, both ventilation and perfusion are greater at the bases and decrease toward the apices, largely due to the effects of gravity. In dependent regions, alveoli are smaller and more compliant, allowing greater expansion and therefore increased ventilation. Perfusion also displays a gravity-dependent component, but decreases more steeply than ventilation as it moves from base to apex. As a result, the apex displays higher ventilation-to-perfusion (V/Q) ratios, while the bases have lower V/Q ratios. At the extremes of mismatch – alveolar dead space (ventilated but unperfused regions) and physiological shunt (perfused but unventilated regions) – gas exchange does not occur. However, in healthy individuals, these mismatched regions typically account for a very small proportion of the lungs and do not significantly impair overall gas exchange.

In order to accommodate ventilation and promote gas exchange, the lung needs to be able to expand. This expansion is determined by three key mechanical properties of the respiratory system: compliance, elastance, and resistance. Compliance reflects how easily the lungs and chest wall can stretch and is defined as the change in volume per unit change in distending pressure (i.e., the pressure gradient). When evaluating lung compliance in isolation, the relevant pressure gradient is the transpulmonary pressure. When assessing the compliance of the entire respiratory system, including the chest wall, the gradient used is that between alveolar and airway opening pressure (or simply airway pressure, when flow is zero). Elastance is the inverse of compliance, reflecting the tendency of the lungs and chest wall to recoil after being stretched. The higher the elastance, the stiffer the system is, requiring more elevated pressures to achieve the same change in volume. Resistance, on the other hand, refers to the opposition to airflow through the airways. It depends on factors such as airway diameter, gas density, and the speed and pattern of flow. Resistance influences the total pressure required to expand the lungs during dynamic breathing.

Dynamic compliance is calculated on a breath-by-breath basis, using the change in volume and the pressure measured during airflow – from the beginning of inspiration to the point of peak inspiratory pressure – reflecting both elastic and resistive components of the respiratory system. Static compliance, on the other hand, requires an inspiratory hold manoeuvre to pause airflow and allow pressure equilibration and volume redistribution across alveoli, which is impractical in healthy spontaneously breathing individuals. This enables the isolation of elastic recoil properties from the influence of resistance components and time-dependent effects. In healthy lungs, static and dynamic compliance are similar, but as airway resistance increases in disease states, dynamic compliance tends to fall below its static counterpart.

From observing the relationship between pressure and volume during tidal breathing it is evident that inflation and deflation follow different paths. The asymmetry in the pressure-volume curve is known as hysteresis, and it reflects the time-dependent mechanical behaviour of the lungs. During inflation, a higher pressure is required to reach a given volume when compared with deflation. This asymmetry arises from several interacting mechanisms. First, as alveoli expand, surfactant becomes more thinly distributed within the alveoli, transiently increasing surface tension and requiring greater pressure for inflation. During deflation, surfactant concentrates, lowering surface tension and helping maintain alveolar stability and, thus, volume. Second, alveolar recruitment is gradual and individual units have specific time constants. While some alveoli open early, others require more time or even higher pressures to open during inflation depending on the product of their own compliance and resistance. However, once open, they remain open throughout deflation at lower pressures, supported by greater alveolar stability generated both by surfactant concentration and by mechanical tethering from adjacent alveoli. This contributes to the higher volume observed during deflation at equivalent pressures. Third, the viscoelastic

properties of the lung mean that tissue deformation depends on time. Volume changes lag behind pressure changes during both inflation and deflation periods.

There is, however, a component of airflow resistance during tidal breathing that contributes to the separation between inflation and deflation limbs. This effect can be minimised by generating pressure-volumes curves at low-flow, quasi-static conditions. While this smooths the curve by reducing resistive influences, a difference between inflation and deflation still remains, reflecting not only the time-dependent elastic properties of the lung but also small changes in alveolar gas volume due to ongoing $\dot{V}_{O2}$ and $\dot{V}_{CO2}$.

2.2. An overview of mechanical ventilation

Invasive positive-pressure mechanical ventilation (IPPV) constitutes an essential therapy to support the patient with respiratory failure and provide airway protection in neurologically compromised patients. The need for mechanical ventilation is more often driven by respiratory failure than a need for neuroprotection. In excess of 85,000 adult patients are mechanically ventilated in UK ICUs annually[55].

The term "invasive" in IPPV refers to the insertion of a tube that bypasses the upper airways and terminates with its tip in the trachea. The external end of the tube emerges through the mouth (orotracheal), nose (nasotracheal), or neck (tracheostomy), depending on the route of insertion. During the acute phase of mechanical ventilation, patients are typically sedated and given analgesia for comfort, particularly when the tube passes through the upper airway. The tube connects to a Y-piece, which joins a corrugated ventilator circuit with separate inspiratory and expiratory limbs, forming a closed-loop system with the ventilator.

In adult patients, the tube usually contains an inflatable cuff to minimise air leakage and ensure effective ventilation.

The term “positive pressure” in IPPV refers to the fact that ventilation is delivered at pressures above atmospheric. Airway pressure within the closed circuit is measured proximally to the endotracheal tube, at the interface between the patient and the ventilator. The sequence of events during inspiration differs from that of a healthy, spontaneously breathing individual, mostly because there is no reliance on respiratory muscle activity to generate the pressure gradient needed to drive airflow. During inspiration, the ventilator responds to a trigger – which can be time, a change in airway pressure or flow, or diaphragmatic activity – by actively increasing proximal airway pressure, creating a gradient which drives airflow into the lungs. As air enters, alveolar pressure rises, increasing transpulmonary pressure and thereby expanding lung volume. The extent of lung volume gain depends not only on the compliance and resistance of the respiratory system, but also on how the breath is delivered by the ventilator (i.e., at which pressure and flow). Expiration remains a passive process, as in normal physiology, and begins when the ventilator cycles off, allowing airway pressure to drop and the lung’s elastic recoil to drive air out.

During invasive mechanical ventilation, diaphragmatic tone and chest wall activity are often reduced or absent. Without muscle activity, the pleural pressure becomes less negative, leading to a reduction in transpulmonary pressure and an increased tendency for alveoli and small airways to collapse at the end of expiration. To counteract this, most mechanically ventilated patients receive positive end-expiratory pressure (PEEP), which maintains airway pressure above atmospheric levels at the end of expiration, helping to keep alveoli open and prevent atelectasis (i.e., lung collapse).

As a result, in patients ventilated with PEEP, lung inflation does not begin from FRC, but from a baseline end-expiratory lung volume (EELV) which includes the additional volume contributed by the applied positive pressure. In normal spontaneously breathing individuals, EELV and FRC are equivalent, as no external pressure is present at the end of expiration. In contrast, during mechanical ventilation with PEEP, EELV differs from FRC due to the inflation of the lung above its natural resting volume. For a given respiratory system compliance, the increase in volume above FRC can be can be approximated as the product of compliance and the applied PEEP. In this context, EELV is the preferred term to describe the total lung volume at the end of expiration.

Understanding the concept of PEEP sets the stage for interpreting pressure delivery throughout the respiratory cycle. This is best visualised by examining the pressure waveform, which captures the pattern of airway pressure changes during inspiration and expiration (Figure 6). Peak inspiratory pressure (PIP) is the maximum proximal airway pressure measured during the respiratory cycle, and reflects both resistive and elastic forces. The resistive pressure arises from airflow through the airways and is proportional to airway resistance and flow. If an inspiratory pause is applied – momentarily halting flow – this resistive pressure drops to zero, allowing isolation of the elastic pressure. The pressure measured at the beginning of this pause is known as the plateau pressure (P_{plat}) and reflects the pressure required to maintain lung inflation at a given point in the absence of flow. The difference between PIP and P_{plat} corresponds to the pressure lost to airway resistance (P_{res}). The difference between P_{plat} and PEEP represents the elastic pressure driving tidal ventilation, commonly referred to as the driving pressure, which is directly related to static compliance.

The relationships between these components is described by the equation of motion of the respiratory system. In a passively ventilated patient, airway pressure (P_{aw}) at any moment can be viewed as the sum of three terms: PEEP, an elastic pressure proportional to the volume above end-expiration (V), and a resistive pressure proportional to flow ($\dot{V}$). In essence, the equation states that for gas to enter the lungs, the pressure applied to the respiratory system must be sufficient to overcome both resistive and elastic loads. In shorthand:

$$P_{aw} \approx PEEP + P_{el} + P_{res}$$

with

$$P_{el} = E_{rs} \times V, \qquad P_{res} = R_{rs} \times \dot{V}$$

where E_{rs} represents elastance and R_{rs} represents resistance of the respiratory system.

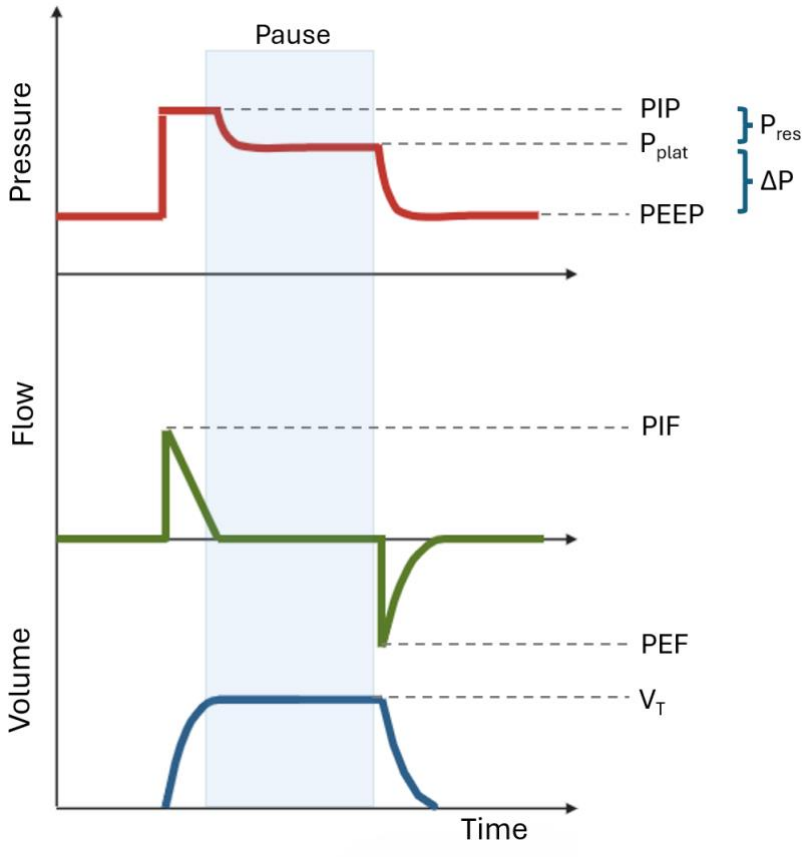

Figure 6. Typical ventilator waveforms during pressure-controlled ventilation with an end-inspiratory pause.

The figure displays airway pressure (top), flow (middle), and volume (bottom) waveforms over time for a single breath. During inspiration, airway pressure rises from baseline (PEEP) to a peak value (PIP). When an inspiratory pause is applied, flow ceases, and pressure plateaus (P_{plat}) following a resistive drop in pressure (P_{res}). The difference between P_{plat} and PEEP defines the driving pressure (ΔP). Aligned with changes in flow and pressure, lung volume increases during inspiration, remaining constant during the inspiratory pause, before decreasing during passive expiration. PIP = peak inspiratory pressure; PEEP = positive end-expiratory pressure; P_{plat} = plateau pressure; P_{res} = resistive pressure; ΔP = driving pressure; PIF = peak inspiratory pressure; PEF = peak expiratory pressure; V_T = tidal volume.

Invasive mechanical ventilation affects several physiological functions of the respiratory system, including the natural warming and humidification of inspired air provided by the

upper airways. When an endotracheal tube or tracheostomy bypasses these structures, inspired gas no longer receives adequate heat and moisture. This results in increased respiratory heat and water loss, and more importantly, leads to impaired humidification of the airways. Inadequate humidification compromises the function of the airway epithelium, particularly ciliated cells responsible for mucus clearance. This impairment reduces the ability to clear secretions and defend against pathogens, increasing the risk of airway plugging and respiratory infections. To prevent these complications, artificial humidification is always provided – either passively, using heat and moisture exchangers (HMEs), or actively, through heated humidifiers integrated to the ventilator circuit[13].

Mechanical ventilation also alters the relationship between dead space and total ventilation. While bypassing the upper airways with a tracheal tube can reduce anatomical dead space by up to 50%, this benefit may be offset by the addition of external monitoring and sampling devices (e.g., filters, capnography sensors), which contribute to apparatus dead space. As a result, a larger proportion of each tidal breath may fail to reach the alveoli and participate in gas exchange. To maintain adequate alveolar ventilation and prevent CO_2 retention, higher tidal volumes or respiratory pressures may be required. This, in turn, increases the risk of ventilator-induced lung injury (VILI; Figure 7), particularly barotrauma (i.e., pressure-related injury) and volutrauma (i.e., volume-related injury). Although traditionally described separately, barotrauma and volutrauma are mechanically inseparable. The pressure applied to the lung (stress) is proportional to the delivered tidal volume relative to FRC (strain), scaled by the specific elastance of the lung. In other words, barotrauma and volutrauma represent the same underlying process of excessive lung stress.

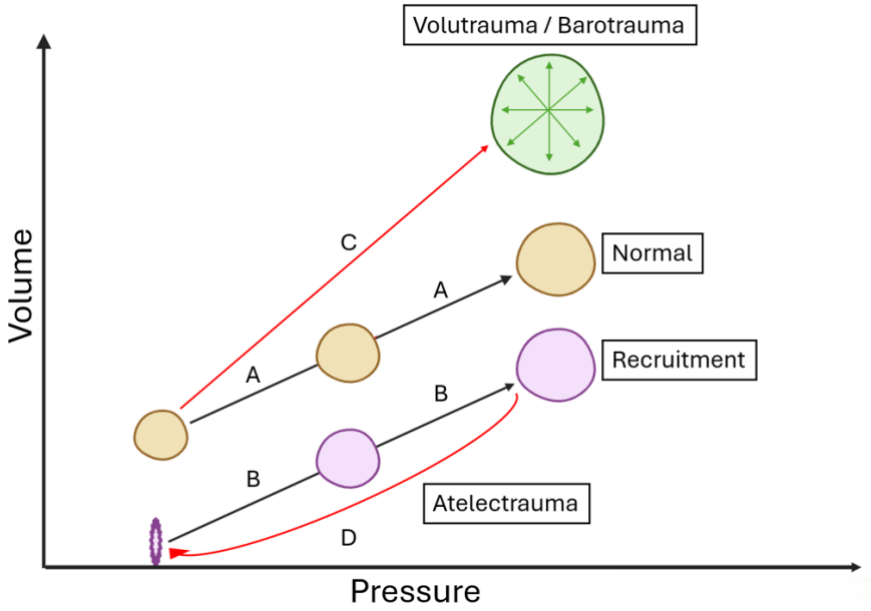

Figure 7. Schematic representation of ventilator-induced lung injury.

The pressure-volume relationship illustrates how different mechanisms contribute to lung injury during mechanical ventilation. Path A represents healthy alveolar inflation under optimal ventilation. Path B depicts recruitment of an alveolus from collapsed to aerated. Path C shows alveolar overstretching due to excessive volume and pressure (volutrauma / barotrauma). Path D demonstrates atelectrauma, caused by the repetitive collapse and reopening of alveoli leading to shear stress and injury. Additionally, mechanical ventilation can trigger biotrauma, an inflammatory response characterised by the systemic release of inflammatory mediators that may contribute to multiorgan dysfunction. Created with BioRender.com.

Another major alteration introduced by mechanical ventilation is the redistribution of ventilation and perfusion. In spontaneously breathing individuals, both ventilation and perfusion favour dependent lung regions (posterior and basal when supine). During positive pressure ventilation, however, ventilation is preferentially directed toward non-dependent regions. Perfusion, by contrast, retains its gravity-dependent characteristics and favours dorsal regions at supine position, which results in increased V/Q mismatch. This mismatch, along with reduced diaphragm activity, contributes to an impaired gas exchange in the

dependent lung. Adequate application of PEEP can help reopen collapsed alveoli and restore ventilation to these regions, improving oxygenation. A central determinant of these effects is the EELV, which reflects the functional size of the ventilated lung. Maintaining sufficient EELV is essential to prevent atelectasis, minimise shunt and alveolar dead space, and support more physiological V/Q relationships during MV.

2.3. FRC and EELV in health and disease

An understanding of FRC and EELV is relevant in critical care, where both insufficient and excessive lung volumes can impair gas exchange, influence mechanical ventilation settings, and increase the risk of VILI. As discussed, FRC is the volume of gas remaining in the lungs at the end of a passive expiration. Both the magnitude and the partitioning of FRC (i.e., between alveolar and dead space volumes) vary widely depending on individual physiology and clinical condition.

FRC reflects a balance between the inward recoil of the lungs and the outward recoil of the chest wall[56]. In healthy individuals, this balance is shaped by factors such as age, body size, and posture. For instance, FRC increases by approximately 16 mL per year of age due to reduced elastic recoil, increased chest wall stiffness, and air trapping in enlarged alveoli[57]. It decreases by 10% to 33% in obesity owing to an upward displacement of the diaphragm and reduced chest wall compliance[58]; and falls by around 25% when moving from an upright to a supine position[59, 60].

Pathological changes further affect this balance. Restrictive diseases (e.g., pulmonary fibrosis) reduce FRC via increased lung stiffness, while obstructive diseases (e.g., COPD) increase FRC through gas trapping and dynamic hyperinflation[61]. An important related

concept is closing capacity (CC), the volume at which small airways begin to close during expiration – normally sitting between residual volume and FRC. When CC exceeds FRC, airway closure occurs during tidal breathing, worsening gas exchange. This mismatch is especially relevant in individuals with higher residual volume (e.g., the elderly) or reduced FRC (e.g., mechanically ventilated patients).

Under mechanical ventilation, additional factors reduce FRC, including sedation, muscle paralysis, and loss of diaphragmatic tone. These changes lead to lower pleural and transpulmonary pressures, predisposing to alveolar collapse[62]. *Bikker et al.* reported that, in supine mechanically ventilated patients without primary lung disease, EELV was 34% lower than predicted values, and this reduction exceeded 60% in patients with acute respiratory distress syndrome (ARDS)[63]. The application of PEEP proportionally elevates EELV above passive FRC, potentially restoring lung volume and improving gas exchange[63].

2.4. Measurement of EELV in mechanically ventilated patients

Accurately measuring EELV in mechanically ventilated patients remains a major clinical challenge. Conventional pulmonary function tests are not feasible in this setting, and available bedside methods are limited in accuracy and accessibility. The following sections explore the main existing measurement techniques for the assessment of EELV in mechanically ventilated patients and their limitations.

2.4.1.1. Helium dilution method

The helium dilution technique for measuring lung volume was first introduced by Meneely and Kaltreider in 1941[64]. It is based on the principle of mass conservation in a closed circuit using helium as an inert tracer gas. Helium is an ideal choice because it is non-toxic and has low blood solubility, limiting its diffusion across the alveolar-capillary membrane and ensuring it remains largely confined to the gas phase within the lungs and circuit.

In mechanically ventilated patients, the method typically involves disconnecting the patient from the ventilator and connecting their endotracheal tube to a closed rebreathing system filled with a helium-oxygen gas mixture of known concentration (C_i) and volume (V_i)[65]. Manual ventilation is then performed for a set number of breaths, allowing the helium to mix with the gas within the lungs[66]. Once equilibrium is reached, the final helium concentration (C_e) is measured. Since helium does not leave the system, EELV can be calculated by:

$$EELV = (\frac{C_i - C_e}{C_e}) \times V_i$$

As V_i is known, the main measurement instrument required is a helium analyser. However, even the most modern analysers are sensitive to pressure and temperature changes, as well as to CO_2, H_2O and O_2 fluctuations, which may be problematic if the final equilibrium gas is a product of rebreathing from a bag[67]. Conversion to body temperature, ambient pressure, and saturated water conditions (BTPS) is required, and, as measurements are made independently by different instruments and at different sites, errors may be introduced to the retrieved lung volume.

There are several physiological limitations associated with this technique, particularly when adapting it to mechanically ventilated patients. First, in diseased or heterogenous lungs, helium may not mix uniformly. Dead space ventilation or regions of poor ventilation can lead to underestimation of true EELV or prolong the time to equilibrium. Second, manual ventilation may alter the usual tidal volume and pattern, affecting EELV. Finally, disconnecting the patient from the ventilator can cause rapid lung derecruitment and lead to atelectrauma – a type of VILI associated with cyclic opening and closing of alveolar units – compromising both patient safety and measurement validity[68].

Though some systems have been developed to allow helium rebreathing without disconnection, these setups are often complex and not suited for routine clinical use[69-71]. As a result, helium dilution is now largely restricted to research settings in critical care.

2.4.1.2. Electric impedance tomography

Electrical impedance tomography (EIT) is a non-invasive imaging technique first introduced by Barber and Brown in 1984[72]. It estimates the regional distribution of lung ventilation by measuring changes in thoracic electrical impedance during breathing. As the lungs fill with air during inspiration, impedance increases – air is a poor electrical conductor – and decreases during expiration as air is replaced by more conductive tissue and blood. These changes are detected using 16 to 32 surface electrodes placed circumferentially around the thorax. A small alternating current is applied through one electrode pair, while voltages are measured from the others. By cycling through multiple pairs, a real-time, cross-sectional image of thoracic impedance distribution is reconstructed.

Unlike the other methods described in this section, EIT captures only relative changes in lung volume over time. The point of lowest impedance is assumed to correspond to end-

expiration and thus represents EELV. When interventions such as increased PEEP elevate lung volume, a rise in end-expiratory impedance is observed. Comparing impedance before and after such changes allows estimation of regional changes in EELV, reflecting local recruitment or derecruitment. Studies such as that by *Hinz et al.* have demonstrated that these relative changes correlate well with EELV variations measured by nitrogen washout techniques[73].

However, commercially available EIT does not measure absolute lung volumes[74]. Additionally, technical limitations such as motion artifact, anatomical variability (e.g., obesity or oedema), and electrode misplacement can compromise accuracy[74]. Although limited in its ability to quantify lung volumes, EIT is valuable for monitoring regional ventilation inhomogeneity and is increasingly used to guide ventilator management[75]. Its application in lung volume assessment, though, should be interpreted with caution, for the reasons stated above.

2.4.1.3. Computerised tomography

Computerised tomography (CT) generates cross-sectional images based on the differences in attenuation of ionising radiation upon crossing tissues of varying density[76]. In the lungs, this differential attenuation reflects the relative proportions of gas and soft tissue, allowing for the classification of lung regions into compartments: non-aerated (gasless), poorly aerated, normally aerated, and hyperinflated. By quantifying these compartments, CT can characterise the extent and distribution of aeration in both healthy and diseased lungs.

EELV is assessed by performing an expiratory hold to eliminate airflow, acquiring the CT scan at this static point. Regions of interest are then segmented, and gas volume is summed across all lung slices[66]. Compared with other techniques described in this section, CT is the

only one capable of identifying gas trapped behind closed small airways – an important distinction – by comparing inspiratory and expiratory scans and identifying areas that fail to deflate on expiration[61].

Some regard CT as the reference standard for EELV measurement in mechanically ventilated patients, given its anatomical resolution and ability to distinguish aeration compartments[65]. However, the requirement to transfer critically ill patients to the radiology suite, combined with the exposure to ionising radiation, time constraints, cost, and the need for specialised software and expertise, limit its feasibility for routine use[77]. Furthermore, inconsistency in definitions and methodologies across studies – even despite efforts to standardise terminology (e.g., the glossary proposed by *Austin et al.*[78]) and technique[79] – adds to the challenge. As Desai and Hansell suggest, CT should be reserved for resolving specific clinical questions rather than routine bedside monitoring[80].

2.4.1.4. Multi-breath nitrogen washout

The use of open-circuit inert gas washout during tidal breathing to estimate EELV was first described by *Darling et al.* in 1940[81]. Nitrogen is the most widely used tracer, given it is already naturally present in atmospheric air and conventional inspired gas mixtures. The technique exploits the changes in alveolar nitrogen concentration – a washin, washout, or both – following a step change in FiO_2 (Figure 8). Assuming that nitrogen behaves as an inert gas and that both lung volume and gas exchange remain stable over the measurement period, the cumulative difference in nitrogen content before and after the FiO_2 change can be used to estimate the absolute gas volume in the lungs at end-expiration.

This volume is calculated under the assumption that the changes in nitrogen fraction are equal in magnitude but opposite in sign to the change in oxygen fraction (ΔFiO_2), based on

the fact that nitrogen, oxygen and carbon dioxide together account for nearly all of the inspired and expired gases[65]. Therefore, EELV can be estimated from:

$$EELV = \Delta N_2 / \Delta FiO_2$$

Where ΔN_2 corresponds to the cumulative volume of nitrogen exchanged over the course of the test until a new alveolar gas steady state is reached.

To compute this, simultaneous measurement of inspiratory and expiratory flows and gas concentration is necessary. Given that direct measurement of nitrogen is technically challenging and costly, most commercial systems calculate nitrogen concentration indirectly by subtracting measured O_2 and CO_2 fractions from 1.0 (i.e., $FiN_2 = 1 - FiO_2 - FiCO_2$), assuming that no other gases are present and that both $\dot{V}_{O2}$ and $\dot{V}_{CO2}$ remain constant throughout the reading[82].

In mechanically ventilated patients, applying this technique introduces several physiological and technical challenges. First, the ventilator circuit acts as a closed system, which affects the dynamics of gas delivery and mixing. Second, changes in gas composition due to a step change in FiO_2 affect gas viscosity, which can alter accurate flow sensor readings. Larger FiO_2 alterations lead to larger changes in viscosity and hence greater measurement error, which are difficult to fully correct for[83-85].

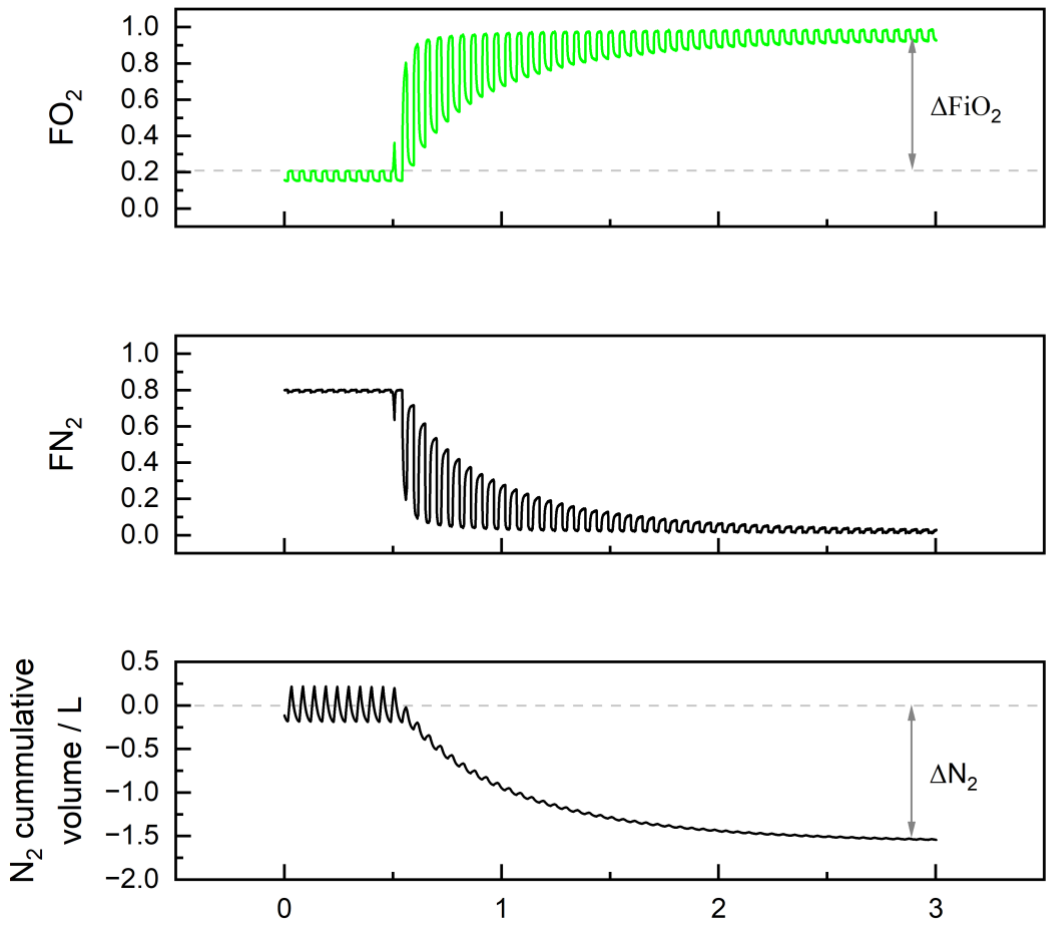

Figure 8. Conventional (full) multi-breath nitrogen washout.

A step increase in the FiO_2 from baseline (0.21 to 1.0) initiates the washout (top panel), displacing nitrogen from the lungs. This results in a corresponding decline in nitrogen fraction (middle panel). The last breath before the FiO_2 change is used as a reference. The cumulative volume of nitrogen eliminated from the lungs (bottom panel) is integrated over time. EELV is estimated as the total nitrogen volume washed out (ΔN_2) divided by the change in oxygen fraction (ΔFiO_2), assuming complete gas mixing and stable ventilation during the procedure. FO_2 = fraction of oxygen; FN_2 = fraction of nitrogen.

A further challenge in this context is that many patients are already ventilated with significantly higher baseline FiO_2 concentrations than found in ambient air. This limits the magnitude of any additional FiO_2 step that can be safely applied for washout or washin

manoeuvres, traditionally conducted under a 0.79 ΔFiO_2. Additionally, the clinical use of large FiO_2 steps has been associated with absorption atelectasis, which reduces EELV and alters gas distribution[86]. This not only complicates interpretation of nitrogen washout data but also may compromise adequate gas exchange in critically ill patients.

Another critical assumption of the technique that is violated in mechanical ventilation is that FiO_2 remains constant throughout each inhalation. After a step change in FiO_2, the newly composed gas may not reach the airway opening immediately due to the circuit length, humidification devices, and turbulent flow[84]. This creates a "gas front" that may not be fully mixed by the time it reaches the lungs, violating the assumption of homogeneous FiO_2 and introducing error into the nitrogen balance calculation[87].

Additionally, delays in the measurement of gas concentrations – especially in systems that use sidestream gas analysers – result in misalignment between intra-breath gas flow and composition. These delays are nontrivial in mechanically ventilated patients, where precise timing is needed to ensure volume and composition measurements correspond to the same breath phase[83]. Robust synchronisation software is required to align flow and gas concentration data, but this approach is still not perfect. For example, *Fretschner et al.* found that with a 0.3 step change in FiO_2, the method could not reliably detect EELV changes smaller than 20%, which limits clinical sensitivity[84].

Subsequent efforts to improve synchronisation included the development of faster gas sensors and improved correction algorithms. *Weismann et al.* designed a system (LUFU) incorporating high-fidelity synchronisation for the measurement of oxygen concentration changes throughout washin and washout manoeuvres, while correcting for volume change[83]. However, this system exhibited measurement errors nearing 10% under

conditions of low compliance, low tidal volume, and high pressures[83, 88] – common in critically ill patients.

In contrast, *Olegard et al.* proposed a simplified method using only end-tidal gas concentrations rather than continuous intra-breath analysis[85]. By focusing only on end-expiratory and end-inspiratory plateaus, the method avoids some synchronisation problems, assuming these plateaus represent alveolar gas[85]. However, this simplification risks under- or over-estimating EELV by ignoring intra-breath volume changes, particularly in patients with uneven ventilation or significant dead space. Comparisons with CT scan and He dilution resulted in an EELV bias ± SD of 15% ± 18% and 40% ± 26%, respectively[65].

Lastly, conventional nitrogen washout methods estimate EELV based on the end-expiratory volume of the last stable breath before the inspired oxygen concentration is increased. This breath serves as the baseline from which nitrogen washout is calculated[89]. The method assumes a consistent tidal volume and breathing pattern throughout the measurement. If baseline breathing is unstable or if variability occurs during the washout, the accuracy of the EELV estimate may be compromised.

2.5. Clinical value of EELV measurements

In 1993, Goran Hedenstierna highlighted the clinical value of measuring EELV in mechanically ventilated patients[90]. His concise statement captures the principle behind this section:

> *"...Any manoeuvre that recruits lung tissue and increases the amount of aerated lung up to a normal value can be expected to improve gas exchange."*[90]

EELV measurement provides a practical estimate of the volume of lung available for gas exchange. In critical care, this information is valuable not only for optimising ventilator settings, but also for understanding the impact of common interventions and potentially minimising VILI.

Studies have demonstrated the clinical utility of EELV in various contexts. During elective surgery, *Pelosi et al.* found that repositioning patients from supine to prone increased EELV and PaO_2, with obese patients also showing improved respiratory system compliance[91]. In patients with ARDS, *Maggiori et al.* demonstrated that endotracheal suctioning – particularly with ventilator disconnection – led to significant reductions in EELV, oxygenation, and compliance, suggesting alveolar derecruitment[92]. These effects were less pronounced with closed suctioning[92]. *Heinze et al.* showed that switching to a lower level of ventilatory support – from dual to single level pressure support – during weaning, despite maintaining equivalent PEEP, led to reductions in both EELV and oxygenation – again indicating some level of derecruitment[93].

Beyond procedural applications, EELV also plays a critical role in estimating lung stress and strain – central determinants of VILI[94]. Stress refers to the internal force exerted by transpulmonary pressure, while strain describes the deformation of lung tissue, calculated as the ratio of tidal volume to EELV. Assuming a linear relationship between these variables, stress can be estimated by multiplying strain by the lung's specific elastance, which *Chiumello et al.* proposed to be approximately 13 cmH_2O[56]. In patients with ARDS, where aerated lung volume is significantly reduced, even low tidal volumes can result in disproportionately high stress and strain, increasing the risk of overdistension and lung injury[94].

As Heinze and Eichler stated:

> *"FRC could be the basis for setting lung-protective ventilation."* [95]

Lung-protective strategies aim to limit end-inspiratory strain and avoid end-expiratory collapse by controlling tidal volume, plateau and driving pressures, and applying appropriate PEEP. While low tidal volume ventilation has improved ARDS outcomes[96, 97], it may also induce atelectasis or hypoventilation when used without individualisation[94]. EELV offers a means to personalise ventilator settings based on the size of the aerated lung compartment, enabling more precise control over both stress and strain, and, therefore, reduce the risk of VILI[65].

EELV monitoring can support PEEP titration by identifying patients who respond with meaningful volume gains. In a study by *Bikker et al.*, ICU patients with healthy lungs or ARDS showed proportional increases in EELV when PEEP was raised from 5 to 15 cmH_2O, though those with ARDS had lower baseline volumes and greater potential for recruitment[63]. Similarly, *Maisch et al.* demonstrated EELV increases during incremental and decreases during decremental PEEP trials, with higher volumes observed during the decremental procedure following a recruitment manoeuvre[98]. While EELV cannot by itself distinguish between alveolar recruitment and inflation[98], combining it with complementary parameters – such as compliance, PaO_2/FiO_2 ratio, dead space fraction, and inhomogeneity indexes – could guide clinicians toward a more balanced and personalised approach to setting PEEP[98, 99].

Finally, serial EELV measurements may provide useful information about the trajectory of lung injury and recovery[90]. Increases in EELV could reflect successful alveolar recruitment, whereas declining values may signal ongoing derecruitment or lung deterioration. While

this potential application warrants further investigation, it may provide additional value in managing patients undergoing prolonged mechanical ventilation.

2.5.1. Recruitment manoeuvres

2.5.1.1. Physiological basis and definition

In patients with respiratory failure requiring mechanical ventilation, the lung is characterised by an enhanced tendency to collapse. This collapse not only worsens hypoxaemia but also amplifies stress and strain on the remaining aerated regions, leading to VILI[56]. Alveolar recruitment – the re-aeration of previously collapsed alveoli – can potentially mitigate these effects, improving oxygenation and preventing lung injury[100, 101].

Recruitment manoeuvres (RMs) are sometimes applied after intubation or during the course of critical illness to counteract alveolar collapse. *Hodgson et al.* defined a RM as:

> *"…any technique that transiently increased alveolar pressure above normal tidal ventilation (which may have included an increase in any pressure, such as plateau, peak or end-expiratory pressure) and sustained that pressure beyond the normal time."*[102]

The most common form, sustained inflation, involves increasing airway pressure from baseline PEEP to a peak (often exceeding 40 cmH_2O) and holding it for several seconds before returning to baseline or, more typically, to a higher PEEP (Figure 9). This approach aims to overcome the opening pressures of collapsed units by a transient increase in transpulmonary pressure. Owing to lung hysteresis, lower pressures may suffice to keep them open thereafter. Since most alveolar units reopen within the first few seconds of inflation, pressure – rather than inflation duration – appears to be the key determinant of effective lung recruitment[103, 104].

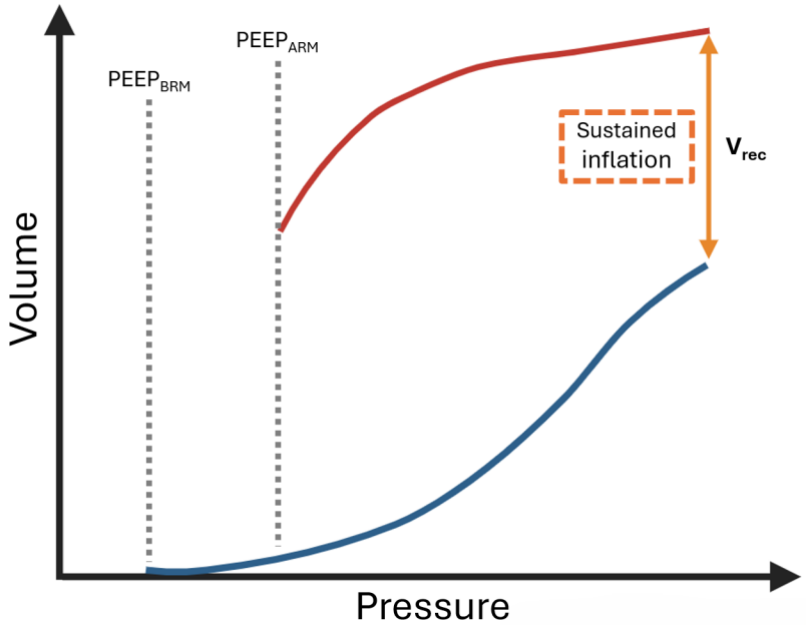

Figure 9. Illustration of a sustained inflation recruitment manoeuvre.

The blue curve represents the inspiratory phase, with airway pressure increased from a baseline PEEP (PEEP$_{BRM}$) to a high inflation pressure. This pressure is then statically sustained for a set duration (orange line) to allow time for alveolar recruitment. The difference between inspiratory and expiratory volumes at sustained inflation (V_{rec}) gives an estimate of the recruited lung volume achieved during the manoeuvre. Following this, the expiratory phase takes place (red curve), returning to a PEEP that may be equal to or higher than the initial setting (PEEP$_{ARM}$), to help maintain the recruited volume. Created with BioRender.com.

2.5.1.2. Clinical context

The main and most studied clinical application for RMs is in patients with ARDS. A recent definition by *Matthay et al.* describes ARDS as:

> *"…an acute, diffuse, inflammatory lung injury precipitated by a predisposing risk factor, such as pneumonia, nonpulmonary infection, trauma, transfusion, burn, aspiration, or shock. The resulting injury leads to increased pulmonary vascular and epithelial permeability, lung edema, and gravity-dependent atelectasis, all of which contribute to loss of aerated lung tissue. The clinical hallmarks are arterial hypoxemia and diffuse radiographic opacities associated with increased shunting, increased alveolar dead space, and decreased lung compliance."*[105]

CT imaging has shown that much of the lung in ARDS is collapsed or fluid-filled, with only a small functional fraction – the "baby lung" – remaining aerated[106]. This limited volume, though compliant, is vulnerable to overdistension, cyclical tidal collapse and reopening, and overall VILI, prompting the need for lung-protective strategies[106]. The ARDSNet trial demonstrated that low tidal volume ventilation with limited plateau pressures reduces mortality and increases ventilator-free days in this cohort of patients[96].

RMs in the context of moderate-to-severe ARDS aim to reopen collapsed alveoli, improve gas exchange and ventilation-perfusion matching. *Amato et al*. reported a significant mortality reduction using a strategy that included low tidal volumes, higher PEEP, and frequent RMs[97]. However, their findings have been questioned due to the small sample size, unblinded design, and an unusually high mortality in the control group, who received lower PEEP and much higher tidal volumes – practice now considered harmful. Later large trials were less positive. The LOVS trial found improved oxygenation and fewer rescue interventions in the high PEEP/RM group but no mortality benefit[107]. The ART trial, which applied staircase RMs with decremental PEEP titration to best compliance, was terminated early due to increased mortality and cardiovascular events[108]. Similarly, the PHARLAP trial found no difference in ventilator-free days and reported more cardiovascular complications[109]. A Cochrane review by *Hodgson et al.* and a meta-analysis by *Pensier et*

al. concluded that while RMs may transiently improve oxygenation, evidence for survival benefit is lacking and potential harms remain[102, 110]. These findings support a more cautious, individualised use of RMs, especially targeting those with higher recruitability. The difficulty, of course, is in determining who is likely to benefit before doing a RM.

Beyond ARDS, RMs have also been explored perioperatively, particularly in obese patients, who experience larger reductions in lung volume and more atelectasis under general anaesthesia. In a randomised trial, *Futier et al.* showed that morbidly obese patients receiving both non-invasive positive pressure ventilation (NIPPV) before intubation and an immediate RM afterward had greater improvements in PaO_2, EELV, and compliance, and required lower driving pressures than those with NIPPV alone[111]. *Reinius et al.* further demonstrated that while PEEP alone increases lung volume, a RM plus PEEP was more effective in reducing atelectasis and improving compliance[112]. A large trial by the PROVEnet group found that, although intraoperative oxygenation improved with RMs and high PEEP in obese patients without pre-existing lung disease, this approach was associated with increased intraoperative haemodynamic instability and only a small, non-significant reduction in postoperative pulmonary complications compared with a low PEEP strategy[113].

RMs are also used as a rescue strategy following alveolar derecruitment, such as after ventilator disconnection for endotracheal suctioning. *Dyhr et al.* observed that post-suction RMs in ARDS patients restored EELV and oxygenation more effectively than simply resuming prior ventilator settings[114]. *Heinze et al.*, in a larger cohort of post-cardiac surgery patients, found that those with a drop in EELV greater than 6% after suctioning experienced the greatest improvement in lung volume and oxygenation following RMs[93].

These examples illustrate that the effects of RMs are highly context-dependent. While RMs can be beneficial in settings of high lung recruitability, their success is not universal[115]. This raises the importance of individualised assessment of lung recruitability, which will be the focus of the following section.

2.5.1.3. Lung recruitability assessment

The volume of lung that can be reopened during mechanical ventilation – known as lung recruitability – varies widely between patients[115-117]. It depends on factors such as the underlying disease precipitating respiratory failure (pulmonary vs. extrapulmonary), the distribution of lung injury (focal vs. diffuse), and the time elapsed since injury onset[118-121]. Given the potential risks of RMs, including barotrauma and hemodynamic instability, assessing recruitability is essential to guide their safe and effective use.

The gold standard for quantifying recruitability is a CT scan performed at two different airway pressures[117] (Figure 10). *Gattinoni et al.* defines recruitment as the mass of lung tissue that transitions from a non-aerated state to an aerated state between scans[79] – though other definitions exist[122]. As previously discussed, this approach is impractical in the ICU due to radiation exposure, cost, and the need to transport critically ill patients.

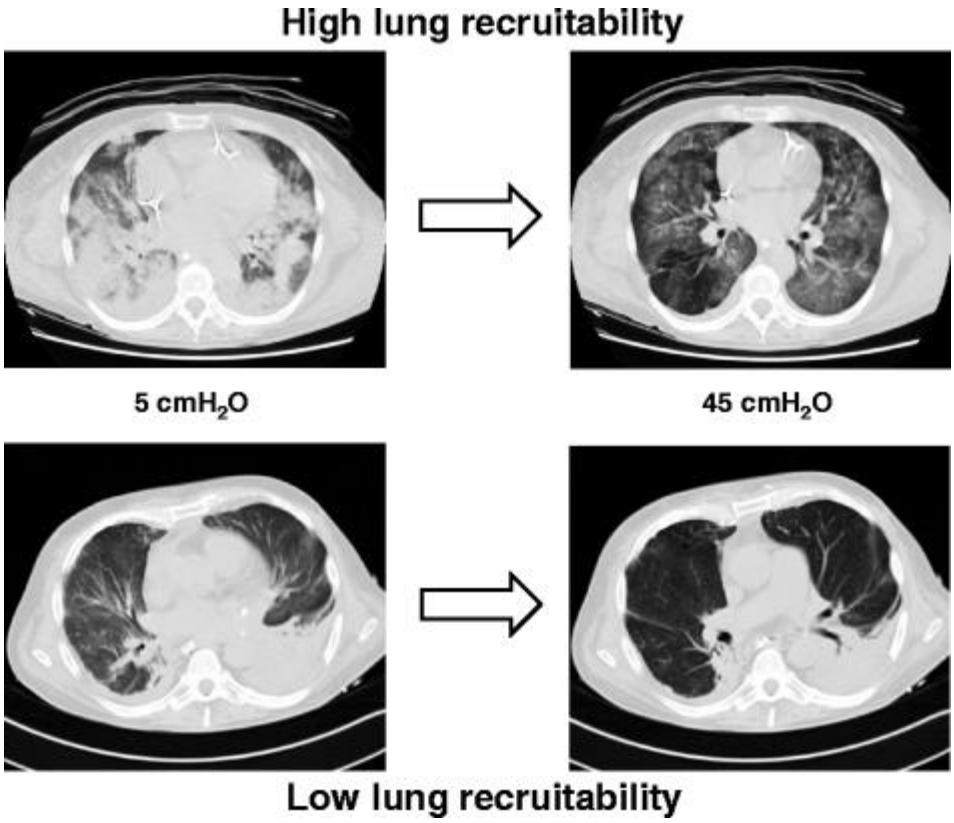

Figure 10. Lung recruitability assessment by CT scan.

CT scans obtained in two mechanically ventilated patients at airway pressures of 5 cmH_2O (left) and 45 cmH_2O (right). The upper row shows a patient with high lung recruitability, where substantial re-aeration is visible at higher pressure, particularly in dependent regions. The bottom row shows a low recruitability patient, with less pronounced radiological change following pressure increase, indicating that this individual is less likely to benefit from a RM. Figure reproduced from *Chiumello et al.*[123], licensed under CC BY 4.0.

At the bedside, recruitability is often assessed through respiratory mechanics[124]. A common approach involves comparing quasi-static PV curves obtained at different PEEP levels[125, 126]. An increase in lung volume at a given airway pressure suggests recruitment and reflects changes in respiratory system compliance[125]. With the integration of automated PV loop tools into modern ventilators, this technique has become more accessible in routine clinical practice[127]. However, it cannot reliably differentiate true re-aeration of collapsed

alveoli from greater inflation of already open units. Consequently, it is relatively insensitive to hyperinflation, and the volume changes inferred from PV curve analysis do not correlate consistently with CT-derived measurements of lung recruitment[124].

Several hysteresis-based PV curve metrics have been proposed to predict recruitability, including: (i) the area between the inspiratory and expiratory limbs (hysteresis); (ii) the linear compliance between lower and upper inflection points; and (iii) the normalised maximal distance between the limbs – a simpler proxy of lung hysteresis[127-130] (Figure 11). These provide qualitative assessments and are limited by their inability to differentiate recruitment from overdistension[131].

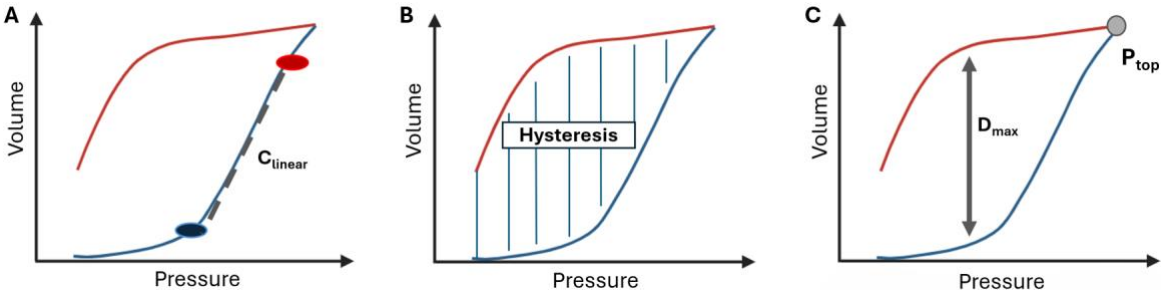

Figure 11. Lung recruitability assessment using parameters derived from a quasi-static pressure-volume curve.

(A) Linear compliance (C_{linear}) is the slope of the mid-inspiratory limb, between lower and upper inspiratory points, where alveolar recruitment is ideal. A high compliance in a pressure-volume curve derived from zero PEEP indicates good potential for alveolar recruitment. (B) Hysteresis, the area enclosed between the inspiratory and expiratory limbs, reflects recruitment and retention of alveolar volume during the breathing cycle. A larger area suggests higher recruitability. (C) The normalised maximum distance percentage represents the percentage ratio of the largest vertical separation between inspiratory and expiratory curves (D_{max}) and the volume at maximal pressure (P_{top}). High ratios indicate high recruitability. Created with BioRender.com.

The recruitment-to-inflation (R/I) ratio offers a simplified, single-breath estimate of recruitability. It compares the compliance of the volume recruited between two PEEP levels with baseline compliance at low PEEP. A higher ratio suggests a greater proportion of recruitable lung[132]. However, like other mechanical measures, it lacks specificity for true alveolar recruitment[131].

Electrical Impedance Tomography, as previously discussed, has been explored as a tool for visualizing regional volume changes and guiding PEEP titration[133]. While promising for tailoring mechanical ventilation settings, its use for pre-RM assessment of recruitability remains limited.

Across recruitability assessment methods, definitions of "high" versus "low" recruitability rely on arbitrary thresholds (e.g. the median values of a small cohort study) and lack standardization. Even CT-based approaches vary in technique – such as voxel-by-voxel analysis versus anatomical region-based methods – leading to inconsistent analyses[122, 124, 131, 134].

Assessing the immediate and, especially, the long term effectiveness of RMs is even more challenging. Volume gains during a sustained inflation RM may reflect recruitment[127], but also include overdistension, which cannot be differentiated without further analysis. Similarly, improvements in oxygenation (PaO_2) are unreliable markers, as they may result from haemodynamic or perfusion changes rather than true alveolar recruitment[117, 130, 135].

In summary, to date, most bedside tools for the assessment of lung recruitability and the effectiveness of RM provide only qualitative or semi-quantitative assessments, and cannot reliably distinguish beneficial recruitment from harmful overinflation.

2.6. Motivation & Objectives

The accurate measurement of EELV has the potential to guide ventilatory strategies, assess the impact of common interventions, and support more physiologically grounded decisions. However, as discussed earlier, bedside tools currently available are either impractical, or lack the accuracy, resolution, or interpretability required for meaningful clinical application.

A pertinent example is the use of RMs, which are commonly applied based on individual clinician judgement rather than a precise understanding of lung recruitability or the physiological effects of the manoeuvre. The same increase in EELV following a RM may reflect either a beneficial recruitment of collapsed alveoli, an increase in lung inhomogeneity, or both. Without knowing the nature of the volume gained, clinicians remain uncertain about whether the intervention was effective, necessary, or even potentially harmful.

Despite the long-standing interest in lung recruitment, there is no international consensus on how or when RMs should be applied. UK joint guidance has concluded that "the evidence supporting the role of RMs was so poor and the concept so ill-defined that we were unable to make a recommendation"[136]. Thoracic Society, European Society of Intensive Care Medicine, and Society of Critical Care Medicine have issued only a conditional recommendation, highlighting ongoing uncertainty[137].

Computed cardiopulmonography (CCP), which combines a laser-based gas analyser with a detailed computational cardiopulmonary model, offers a non-invasive means to obtain precise measurements of lung volumes, gas exchange, and ventilation heterogeneity at the bedside[54, 138]. This allows the estimation of EELV in addition to tracking how uniformly

the lung inflates during a breathing cycle. These capabilities present a unique opportunity to revisit fundamental questions around lung physiology during mechanical ventilation.

This research does not aim to validate CCP as a clinical device. Instead, its focus is exploratory and physiological. Through a series of observational studies, we aim to: (i) investigate how lung volume changes can be measured and interpreted using CCP; (ii) assess the repeatability (precision) of these measurements across time; (iii) assess how lung volumes measured with CCP compare with a physiological standard; and (iv) explore the lung volume changes measured via CCP before and after a lung RM and how they correlate with established lung recruitability techniques.

In doing so, this work seeks to better understand whether CCP might provide new physiological insights to support future research and more individualised approaches to ventilatory management.

Chapter 3. Computed Cardiopulmonography

Computed Cardiopulmonography is a technique developed to measure and model gas exchange. The complex interplay between airways, lung, heart, circulation, metabolism, and body gas stores is carefully considered by this technique in a closed-loop physiological assessment of the cardiopulmonary system. The output of this assessment sheds light on gas exchange behaviour in health and disease.

The technique can be broken down into two steps. First, gas exchange is measured within the mainstream airway by the Molecular Flow Sensor. Here, the composition and flow of respired gases is assessed, along with extrinsic gas properties that may affect their behaviour (e.g., density, viscosity). The data acquired in this stage are then fed into an integrated cardiopulmonary model. Based on patient characteristics, a series of modelled physiological inferences are made pertaining to absolute lung volumes, distribution of ventilation and perfusion, and overall metabolic exchange.

In this chapter, both the measurement and the modelling components of CCP are detailed. All studies designed and described in this thesis involve the application of either one or both of such components, whereby the main intent is to explore $\dot{V}_{O2}$ and EELV measurements, enabled by CCP, in critically ill mechanically ventilated patients.

3.1. The Molecular Flow Sensor

The Molecular Flow Sensor combines laser gas spectroscopy and a precision flow sensor to measure the molar concentrations and flows of respired gases within the mainstream airway every 10 milliseconds[54].

The instrument comprises three main sections: the measurement head, the electronics module, and a laptop controller (Figure 12). Subjects inhale from and exhale into the measurement cell embedded into the measurement head. Data gathered at the measurement head are transmitted through a pair of cables to the electronics module, and a USB connection then streams the information to a laptop controller. Real time gas exchange information is promptly displayed on the laptop controller screen. This information includes, but is not limited to, respired gas concentrations, flows, temperature, pressure, oxygen consumption, and carbon dioxide production.

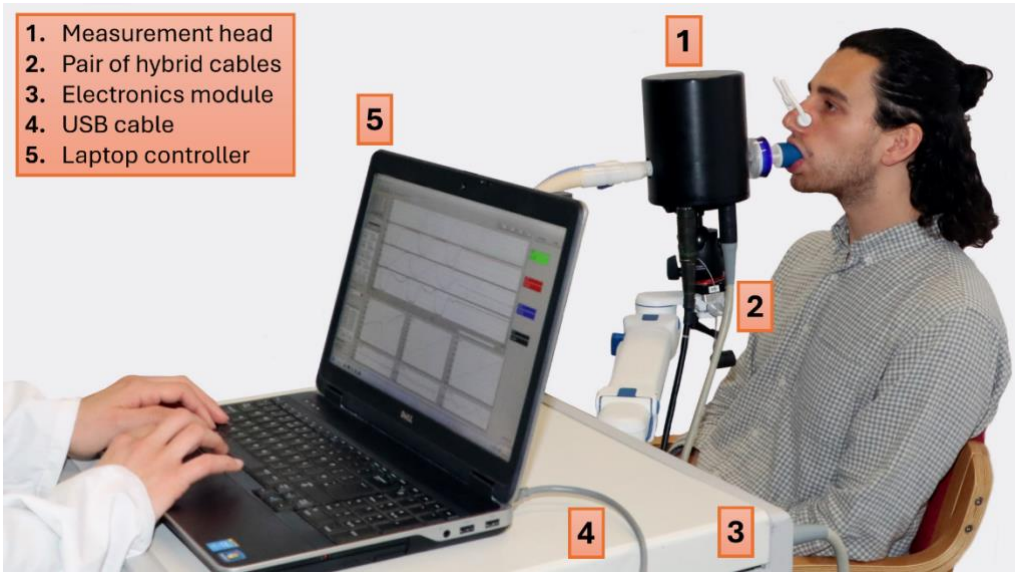

Figure 12. Molecular Flow Sensor.

Subjects breathe in and out through the measurement cell in the measurement head (1). Information is sent via hybrid cables (2) from the head to the electronics module (3) and vice versa, then streamed through USB (4) to the laptop controller (5), where real-time gas exchange information is displayed. Picture taken by Colin Beesley; Robbins' group holds copyright.

The MFS directly measures concentrations and flows of O_2, CO_2, and water (H_2O) vapour. Considering that the sum of fractional contributions of all respired gases equates to 1, the concentration of N_2 can be obtained by subtraction. Other respired gases, such as Argon and Helium, are quantified as N_2 in the balance. Water vapour quantification is invaluable to accurately determine flow, which, in turn, makes it highly relevant to the assessment of O_2 and CO_2 exchanges.

Here, it is established how these measurements are made, compared with other techniques, and the qualities that make them desirable for the study of gas exchange are highlighted.

3.1.1. Gas composition measurement

3.1.1.1. Laser gas spectroscopy

The concentration of respired gases is measured in the MFS by laser absorption spectroscopy. In general terms, absorption spectroscopy is concerned with how matter absorbs electromagnetic radiation. The technique takes advantage of the unique way in which different atoms and molecules interact with radiation. As different gas species absorb radiation at specific wavelength ranges, if radiation source is tuned to a specific species spectrum, its interaction will be directed towards the targeted gas. The nature of such interaction will depend on the frequency, i.e., energy, of the radiation source[139, 140].

Lasers are used in absorption spectroscopy as a source of monochromatic radiation, emitting radiation in a very narrow range of wavelengths, which can be tuned for a specific frequency. When a molecule is hit by incident radiation in the appropriate range and energy, absorption occurs, leading the molecule to transition from ground to excited state. As a consequence, there is a weakening of the radiation as it passes through the molecule. The difference in radiation intensity before and after absorption takes place is referred to as attenuation.

The degree of radiation attenuation (I) from a baseline incident intensity (I_0) is related to the concentration of the absorbing species (c), the absorption cross-section (σ), and the path length (l) through the medium by the Beer-Lambert law[140]:

$$I = I_0 e^{-\sigma c l}$$

If the intrinsic properties of the molecule under investigation, the measured attenuation, and the virtual distance between laser and detector (path length) are known, its concentration can be derived.

Measurements of gas concentrations using laser gas spectroscopy are exceptionally fast, with response times that are nearly instantaneous. The use of tuneable lasers enables very high spectral resolution. Compared with other techniques – such as paramagnetic gas analysers, galvanic fuel cell sensors, and broadband infrared analysers – laser absorption spectroscopy offers far superior precision and accuracy. Moreover, there is less potential for interference from external factors. These characteristics make laser gas spectroscopy an excellent choice for real-time, precise measurements of gas exchange.

3.1.1.2. Carbon dioxide and water measurement

The lasers utilised to measure CO_2 and H_2O are housed within the electronics module of the MFS. Their emitted radiation travels to the measurement head via optic fibre. Both of these gases are relatively easily excited, with good absorbance, thus, the concentration measurements require only a short path length.

As subjects breathe into the MFS head, respired gas flows through the measurement cell with approximately 2.5 cm in length. Laser beams, tuned to the absorption wavelengths of CO_2 and H_2O, traverse the gas and are reflected by a highly reflective mirror arranged in a V-shaped configuration. This arrangement effectively extends the gas path length to 5.4 cm prior to detection (Figure 13).

A single multiplexed optical cable transmits the information obtained from the measurement head to the electronics module, and, subsequently, to the laptop controller.

3.1.1.3. Oxygen measurement

Measuring O_2 concentration using laser absorption spectroscopy is challenging because the symmetric structure of O_2 molecules produces minimal changes in charge distribution during radiation interaction. Since such changes are necessary for effective radiation absorption, O_2 exhibits only weak absorption.

To address this limitation, the MFS incorporates two advanced strategies. First, a vertical-cavity surface-emitting diode laser is employed to generate a focused, intensified radiation beam tuned to oxygen, thereby enhancing the detection of subtle absorption changes[141]. Second, the system increases the effective optical path length through off-axis cavity enhanced absorption spectroscopy (CEAS)[139]. In this technique, the laser radiation is repeatedly reflected between two highly reflective mirrors. Within the MFS measurement head, the O_2 laser and the two highly-reflective mirrors are placed perpendicular to the respired gas flow, with a mirror situated on each side of the optical cavity (Figure 13). Each mirror reflects 99.75% of the radiation and transmits 0.25%, resulting in approximately 400 reflections before a single transmission to the detector occurs. This process extends the effective path length from 2.5 cm to 10 m, significantly amplifying the absorption signal and enabling more sensitive and accurate measurements of O_2 concentration in respiratory gases.

The O_2 laser is housed directly in the MFS head, while its controllers are maintained in the electronics module. Calibration with pure O_2 (N5.0, 99.999% O_2; BOC Limited, UK) allows for accurate path length calculation.

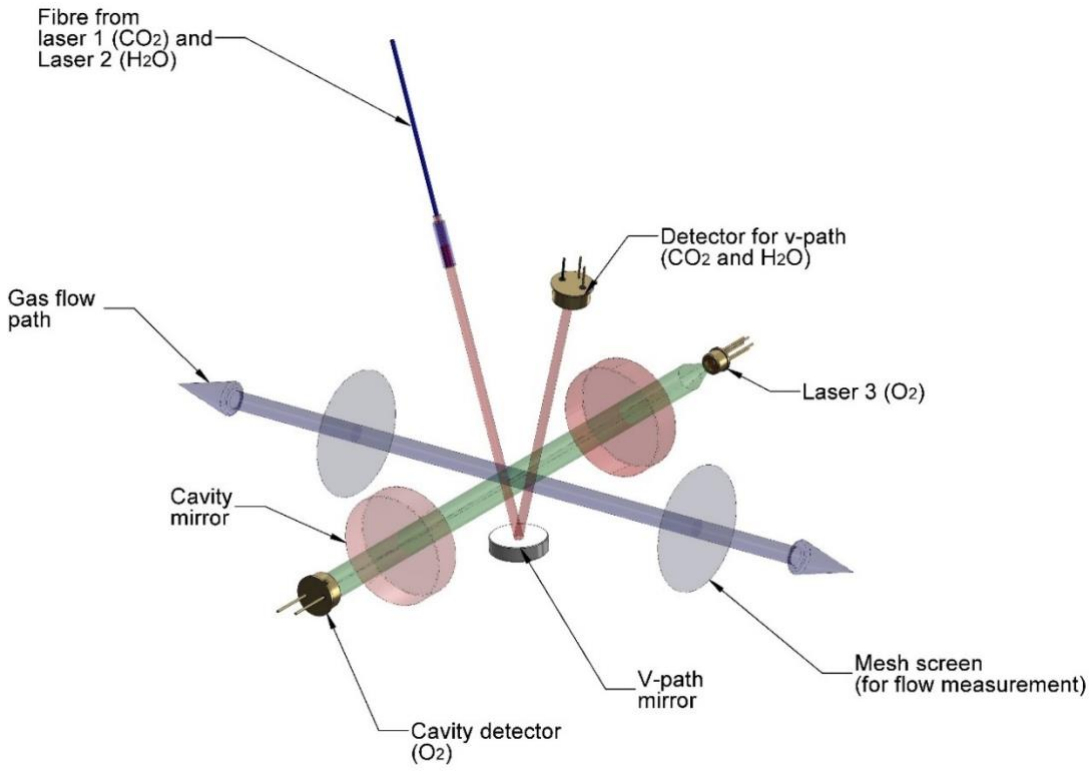

Figure 13. Schematic representation of gas composition and flow measurement pathways in the MFS.

Composition analysis of CO_2 and H_2O follow a v-path, whereby radiation travels vertically through the measurement cell, is reflected, and then detected. To enable O_2 analysis, radiation bounces back and forth between two highly reflective mirrors positioned perpendicular to both gas flow and v-path. A very small portion of this radiation is transmitted and captured by a second detector. Respiratory gas flows inwards and outwards through two mesh screens that record the flow through the pressure drop detected. Authorised reproduction of figure designed by John Couper.

3.1.1.4. Temperature and pressure sensors

According to the ideal gas law, temperature and pressure directly influence gas concentration. Therefore, precise measurement of these parameters is crucial for determining both the total concentration of respired gases and the fractional concentrations of individual components. The MFS measures temperature and pressure within the

measurement cell, ensuring that all relevant variables are spatially and temporally aligned for accurate gas exchange quantification. Initially, these measurements provide the total gas concentration. Subsequently, the fractional concentrations of O_2, CO_2, and H_2O vapour are determined using their respective spectroscopic signals.

A single commercial sensor (HCA0811ARH8, First Sensor AG) is used to measure absolute pressures throughout the breathing cycle, including barometric and peak pressures. When external pressure is applied, the sensor's silicon diaphragm deforms. Piezoresistive elements embedded in the diaphragm detect this deformation through changes in electrical resistance, generating a voltage signal that is proportional to the applied pressure.

Four custom-made thermocouples are used to measure the absolute temperature. Two sensors are positioned at each end of the MFS measurement cell, where the respired gas flows. The readings from all four sensors are averaged to produce the final temperature measurement. The thermocouples are deliberately manufactured with a thin diameter (25 μm) to facilitate rapid response times, which is essential for capturing the dynamic nature of breathing.

The measurement cell is preheated to a minimum of 35 °C prior to initiating MFS measurements. This step prevents condensation on the surface of measurement elements and aligns temperature of the instrument with the typical human body temperature.

Measurements of temperature, pressure, and humidity allow for calculation of density and viscosity of the respired gas, which is crucial for accurate flow measurement.

3.1.2. Respiratory flow measurement

Accurate flow measurement is critical for reliably estimating gas exchange, yet the dynamic nature of respiration presents several challenges. Variations in pressure, temperature, humidity, and gas composition lead to frequent changes in the viscosity and density of respired gas, which in turn affect flow measurements. Therefore, to obtain accurate and precise flow data, a device must: (1) provide rapid measurements, (2) accurately integrate both inspiratory and expiratory flows without depending on the Haldane transformation, (3) ensure temporal and spatial synchronization with gas composition, temperature, and pressure data, and (4) account for changes in density and viscosity. Currently, no commercial device fulfils all these requirements, which contributes to the unreliability of gas exchange measurements, particularly $\dot{V}_{O2}$. The MFS incorporates all these features, rendering it well-suited for precise and accurate flow measurement.

The MFS employs a Lilly-type pneumotachograph, centrally located within the measurement cell. As respired gas crosses two parallel wire-mesh screens with known resistance, the pressure differential is sensed by 8 piezoelectric sensors – 4 symmetrically positioned on each screen. The mechanical deformation induced by the pressure drop in the piezoelectric sensor induces an electrical charge, and the resulting voltage is proportional to the pressure difference. By calibrating this voltage signal, the gas flow rate can be accurately determined.

The calibration takes into consideration the relationship between pressure drop and flow. In a predominantly laminar flow, this would be linear, following Poiseuille's law. Nevertheless, respired flow can also be transitional or turbulent, making the pressure loss, and therefore the flow, less predictable. The model relationship between pressure drop and flow employed by the MFS accounts for laminar, transitional, and turbulent flows by

including major and minor pressure losses. Major pressure losses are proportional to viscosity and flow rate, mostly caused by friction. Minor losses are mainly triggered by geometric changes in the flow path, being proportional to the squared flow rate and to density.

Flow conditioning screens are positioned external to each end of the meshes to help amortize the flow into a less turbulent one. Light traps are interposed between the flow conditioning screens and taper connectors on each end of the measurement cell. These capture and absorb scattered light, preventing optical mismeasurements. Connectors allow for airway integration in-line with mechanical ventilator circuits or with gas supply sources in the spontaneously breathing patient (Figure 14).

The mainstream airway measurement of respired gas compositions and bidirectional flows by the MFS enables highly time-resolved, precise, and accurate measurements of gas exchange. In fact, the precision of the MFS is of an order of magnitude higher than the standardised requirements for commercial gas analysers[54]. Similarly, it offers error margins that are 50% smaller than the standard, indicating excellent accuracy[54].

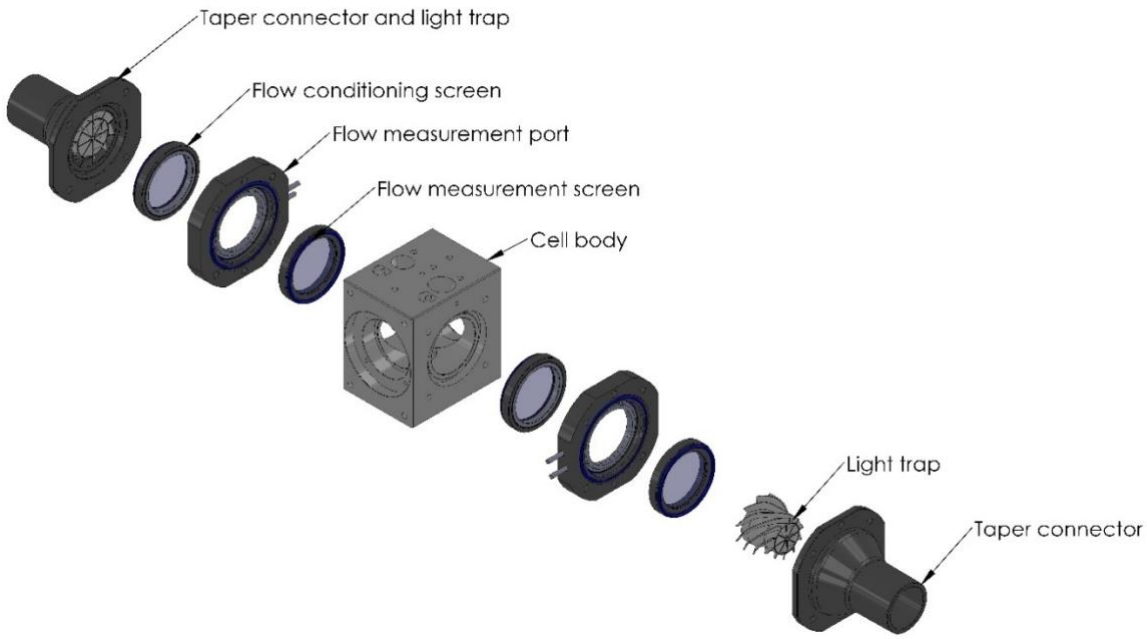

Figure 14. Schematic representation of the flow measurement components within the MFS.

Connectors enable integration with multiple gas supply circuits. Gas flows through the connectors bidirectionally, and are smoothened by flow conditioning screens before crossing the flow measurement meshes. Light traps are positioned between conditioning screens and taper connectors to capture scattered light and prevent measurement errors. Authorised reproduction of figure designed by John Couper.

3.2. The Cardiopulmonary Model

The MFS continuously records the fractional concentrations and flow rates of respired gases during both inspiration and expiration. This enables rapid evaluation of key gas exchange and metabolic parameters, such as oxygen uptake and carbon dioxide elimination. To provide a more comprehensive assessment of an individual's cardiopulmonary function, the data collected by the MFS are further analysed using a computational model that incorporates patient-specific characteristics.

This model functions as a closed-loop system that tracks the entire gas exchange process, from initial inspiration, through alveolar-blood and blood-tissue exchanges, to the return of mixed venous blood to the lungs. It consists of three interconnected sub-models representing the lungs, the blood, and the circulation with body gas stores[142]. The lognormal lung model (LNL) evaluates the unevenness in the distribution of alveolar ventilation, dead space, and pulmonary blood flow across 125 alveolar compartments. The blood sub-model depicts the physicochemical behaviour of gases in the blood, including acid-base buffering, Bohr and Haldane effects, and the dissociation curves of each gas species[143]. The circulation and body gas stores sub-model (CABGS) connects pulmonary venous outflow with pulmonary arterial inflow by simulating the interactions between major blood vessels and organs that influence gas exchange[144].

Simulated data generated by the model are designed to be the best possible match to the MFS measured data whilst accounting for patient-specific characteristics. During inspiration, the model directly incorporates MFS-measured gas fractions and flow rates. For the exhalation phase, while flow rate is taken from measurements, the gas fractions are simulated. A nonlinear least squares optimisation routine (NLLSOR) is employed to minimise the squared differences between the simulated and measured expired gas flux (i.e., the product of flow rate and gas fraction every 10 milliseconds). Progressively to reduce the residual measured-modelled flux difference, the optimisation routine iteratively adjusts physiological parameters initially fed into the model as an experimental file. The final outcome is an optimised parameter set that best characterises the subject's cardiopulmonary physiology[142, 144].

3.2.1. Lognormal lung sub-model

The LNL is the computational framework in the core of CCP: the first point of gas exchange from which the other models stem and to which they reconnect. The end goal of the model is to estimate alveolar and pulmonary end-capillary blood partial pressures for respired gases, initiating the gas exchange process. This goal is achieved by modelling the lung through a series of inhomogeneous gas exchanges.

Lung inhomogeneity refers to the unevenness of ventilation and perfusion across the lung. It occurs physiologically in healthy individuals – where regional distribution is mainly influenced by gravity, posture, and exercise – and is exacerbated in disease. The LNL was originally developed to quantify lung inhomogeneity using non-invasive gas exchange data[138]. The model is predicated on the understanding that effective gas exchange in the lung depends on the adequate matching of ventilation and perfusion. Deviations from this match beyond a certain threshold are indicative of respiratory dysfunction.

In this model, the lung is represented as a series of 125 alveolar compartments that together comprise the total gas-exchanging volume (V_A). Each compartment encompasses 5 key physiological elements (Figure 15): alveolar volume, alveolar compliance (a proxy of ventilation), anatomical dead space, pulmonary vascular conductance (a proxy of perfusion), and dead space compliance. The compartments (each represented as "i") are assumed to have equal alveolar volumes at functional residual capacity ($V_{A,i} = V_A/125$), while fractional shares of alveolar compliance ($F_{CL,i}$), pulmonary perfusion ($F_{Cd,i}$), and anatomical dead space ($F_{VD,i}$) are distributed unevenly across compartments. When an individual inspires, the expansion of an alveolar unit tractions out their adjunct conductive airway, expanding it to some extent: this concept lays the foundation for the model's dead

space compliance (C_{VD}), defined as the fraction of dead space expansion in relation to alveolar compliance.

The anatomical dead space at the end of expiration (V_D) is the sum of each of the 125 $F_{VD,i}$. The apparatus dead space (V_D^{APP}) comprises the non-exchanging volume of all equipment interposed between a measurement plane of the MFS and the mouth when a participant is undertaking a breathing test. This value is calculated and inputted to the model before it runs. The model computes total dead space (V_D^{TOT}) as the sum of V_D and V_D^{APP} – it does not account for true alveolar dead space. Another dead space model variable was developed to describe the inspiratory dead space volume (V_D^{INS}), which is often higher than its expiratory counterpart (V_D) due to the effects of C_{VD}. Once an individual's V_D and V_A are determined, functional residual capacity (FRC) can be calculated as their sum.

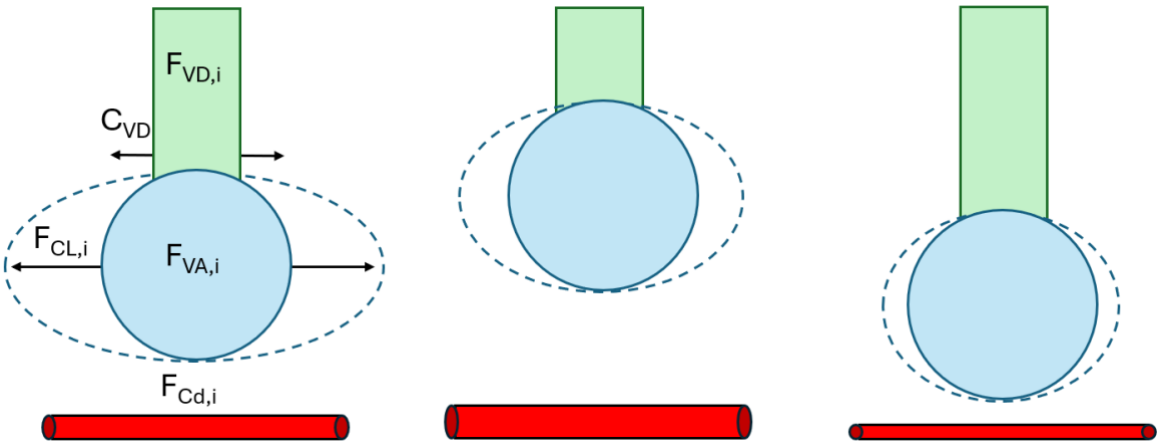

Figure 15. Schematic representation of 3 model compartments.

The LNL encompasses 125 distinct compartments. Each compartment ("i") comprises 5 key elements: alveolar volume (V_A), alveolar compliance (C_L), anatomical dead space (V_D), and vascular conductance (C_d). All compartments receive an equal fraction (F) of alveolar volume ($V_A/125 = F_{VA,i}$) at FRC but variable fractions of anatomical dead space ($F_{VD,i}$), alveolar compliance ($F_{CL,i}$), and vascular conductance ($F_{Cd,i}$). Dead space compliance (C_{VD}) varies as a function of alveolar compliance.

The variations in fractional shares across LNL compartments are characterised using statistical distributions, under the assumptions that: (i) alveolar compliance and pulmonary conductance follow a bivariate lognormal distribution[145, 146] ($F_{CL,i}$:$F_{VA,i}$ and $F_{Cd,i}$:$F_{VA,i}$, respectively) and have a fixed correlation ρ (($F_{CL,i}$:$F_{VA,i}$)/($F_{Cd,i}$:$F_{VA,i}$) = 0.87)[138]; (ii) anatomical dead space follows a normal distribution ($F_{VD,i}$:$F_{VA,i}$). The model variables that represent such distributions are the three key lung inhomogeneity parameters:

i. $\underline{\sigma C_L}$ ($\sigma \ln F_{CL,i}$:$F_{VA,i}$): the standard deviation (SD) of the distribution of the natural logarithm of standardised alveolar compliance; or, simply, the alveolar compliance (or ventilation) distribution.

ii. $\underline{\sigma C_d}$ ($\sigma \ln F_{Cd,i}$:$F_{VA,i}$): the SD of the distribution of the natural logarithm of standardised vascular conductance; or, simply, the vascular conductance (or lung perfusion) distribution.

iii. $\underline{\sigma V_D}$ ($\sigma F_{VD,i}$:$F_{VA,i}$): the SD of the distribution of dead space; or, simply, the anatomical dead space distribution.

Here, inhomogeneity is assessed as a function of the variances of alveolar compliance, vascular conductance, and anatomical dead space. The approach of assessing distributions rather than individual compartment values allows the model to capture the inherent inhomogeneity of the lung using only a few critical parameters.

The variables describing inhomogeneity and absolute lung volumes – outlined above and summarised in Table 1 – are derived from the LNL model and could theoretically be obtained without relying on MFS data, the CABGS, or the blood model. However, this would necessitate alternative measured data sources and considerably more assumptions

about circulation, gas stores, and blood transport to act as inputs to the LNL. Most of the work described in this thesis employs the CCP technique in its entirety: MFS and integrated cardiopulmonary model. Technically, this means that the variables aforementioned are reported as outputs of CCP rather than the LNL alone, being described in the final parameter set file.

Individual compartment values	
$F_{VA,i}$	Fractional share of alveolar volume
$F_{CL,i}$	Fractional share of alveolar compliance (ventilation)
$F_{VD,i}$	Fractional share of expiratory anatomical dead space
$F_{Cd,i}$	Fractional share of vascular conductance (perfusion)
C_{VD}	Anatomical dead space compliance
Lung inhomogeneity parameters	
σC_L	Alveolar compliance distribution across model lung
σV_D	Expiratory anatomical dead space distribution across model lung
σC_d	Perfusion distribution across model lung
ρ	Fixed relationship between σC_L and σC_d
Absolute lung volumes	
V_A	Total alveolar volume
V_D^{TOT}	Total dead space
V_D^{APP}	Apparatus dead space
V_D	Expiratory anatomical dead space
V_D^{INS}	Inspiratory anatomical dead space
FRC	Functional residual capacity

Table 1. LNL individual compartment values and CCP-estimated parameters.

Each of the 125 LNL model compartments are composed of 5 main fractions: alveolar volume, alveolar compliance, anatomic dead space, lung perfusion, and dead space

compliance (in relation to alveolar compliance). MFS and cardiopulmonary modelling by CCP result in a set of physiological parameters which include both lung inhomogeneity and absolute lung volume estimates.

The LNL model operates under the assumption that the gas within each alveolar compartment is perfectly mixed and remains in equilibrium with the blood and lung tissue; diffusive effects are disregarded. Therefore, all governing equations applied to the model can be directed by conservation of masses principles. To maintain equal partial pressures of a gas species in the alveoli, blood, and lung tissue, an iterative time-sensitive process takes place, ensuring that the inward and outward flows and fractions of gases in each of the three areas are adequate.

Given that equilibrium is reached between alveoli and blood, it follows that the total gas exchange at a given time equals the difference between mixed venous and pulmonary end-capillary blood contents. Alveolar and end-capillary partial pressures are given by the LNL model, the conversion from partial pressures to contents in end-capillary blood for each gas species can be estimated utilising the blood model, and the mixed venous blood content can be drawn from the circulation and body gas stores model (Figure 16).

A relevant limitation of the LNL model is that, as it does not incorporate true shunt or alveolar dead space, its ability to accurately assess lung inhomogeneity may be constrained in conditions where these extremes are prevalent, such as in severe lung diseases or in mechanically ventilated patients, who are the main target participants in this work. As a consequence, Chapter 6 and Chapter 7 of this thesis will prioritise the discussion of model parameters related to the characterisation of absolute lung volumes. Modifications to the

model can be implemented to enable the simulation of fractional shunt and alveolar dead space, however, these are not within the scope of this thesis.

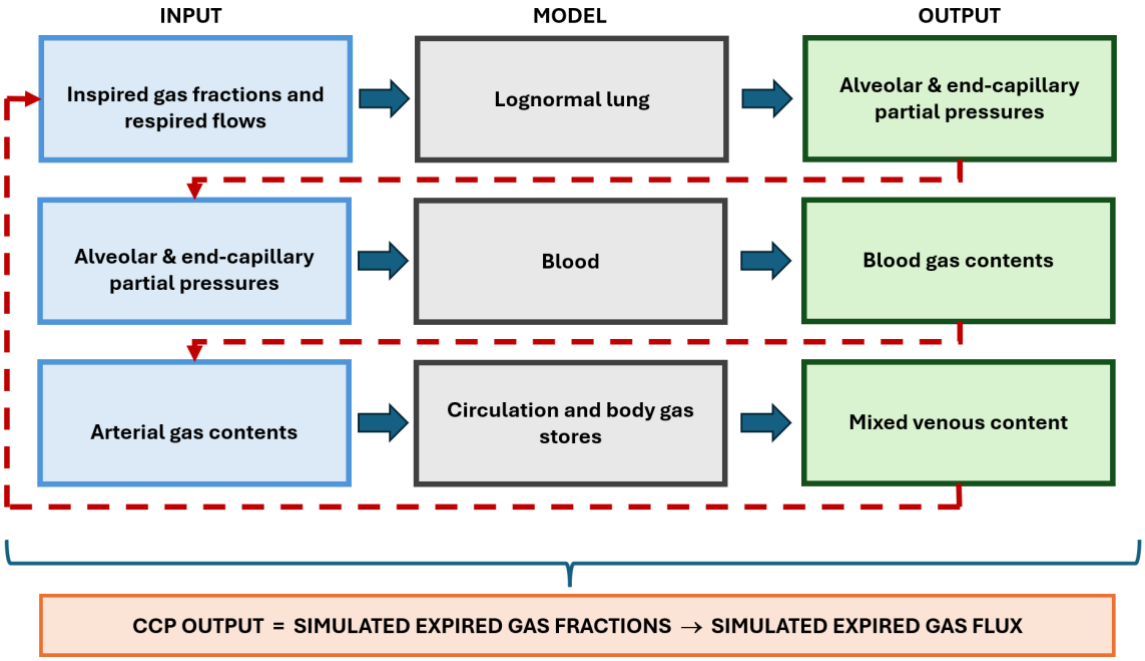

Figure 16. Simulation of flow through the cardiopulmonary model components.

The model takes as inputs MFS-measured inspired gas fractions and respired flows, in addition to patient-specific characteristics and a file containing initial guesses of physiological parameters. Following alveolar-blood exchange, the LNL model provides the relevant partial pressures to the blood model, which will be converted to contents based on the gas behaviour, effects and transport means. The CABGS utilises the arterial contents generated by the blood model to facilitate blood-tissue gas exchange and provides the composition of mixed venous blood returning to the lung. The final outputs of the cardiopulmonary model are the simulated expired gas fractions, allowing for estimation of expired gas flux.

3.2.2. Blood Model

The blood model simulates how respiratory gases behave and are transported within the blood. It is designed to predict the total CO_2 and O_2 content based on the alveolar PCO_2 and PO_2 values provided by the lognormal lung model. For inert gases like N_2, converting

partial pressure to content is straightforward – it only requires multiplication by its solubility coefficient, as described by Henry's law. In contrast, for O_2 and CO_2 the conversion process must account for their dynamic physicochemical properties and interactions, rendering their modelling considerably more complex[143].

CO_2 is transported in blood in three forms: dissolved in plasma, converted to bicarbonate, and bound to proteins as carbamino compounds – with bicarbonate accounting for over half of the circulating CO_2. In both plasma and red blood cells, CO_2 reacts with water to form carbonic acid, which dissociates into bicarbonate and hydrogen ions – a reaction accelerated by carbonic anhydrase within red blood cells. As red cell membranes are relatively impermeable to cations, bicarbonate is exchanged with plasma chloride in a process known as the chloride shift, which continues until Gibbs-Donnan equilibrium is reached. The distribution of CO_2 among these forms is primarily influenced by the conformation of haemoglobin. In tissues, deoxygenated (tense) haemoglobin – being less acidic and a more effective proton acceptor – binds CO_2 to form carbamino compounds while buffering excess hydrogen ions (the Haldane effect). Intracellularly, organic compounds and phosphate also contribute to proton buffering, whereas albumin and bicarbonate perform this role extracellularly. At the alveolar level, as blood becomes oxygenated, haemoglobin transitions to its relaxed form, reducing its affinity for CO_2 and releasing both CO_2 and hydrogen ions. The resulting decrease in free hydrogen ion concentration, facilitated by the conversion of bicarbonate back to CO_2 and water, helps normalise blood pH and promotes efficient CO_2 elimination at the alveolus.

Due to its low solubility, oxygen is primarily transported in blood bound to haemoglobin, with only a small fraction remaining dissolved in plasma. Haemoglobin's affinity for oxygen is dynamic and decreases under conditions of elevated hydrogen ion concentration,

high CO_2 partial pressure, increased temperature, and elevated intracellular levels of 2,3-DPG. In tissues, where CO_2 levels and hydrogen ion concentrations are high, oxygen is released from haemoglobin for tissue uptake – a phenomenon known as the Bohr Effect. Conversely, in the lungs, high inspired oxygen partial pressures facilitate the reloading of haemoglobin, ensuring efficient oxygen transport to the tissues.

All these complexities of oxygen and carbon dioxide transport, including their physicochemical interactions, are mathematically integrated into the model to determine their total contents, as described by *O'Neill and Robbins*[143]. For simplicity, the model assumes that O_2 and CO_2 have equal partial pressures in plasma and within red blood cells. It adheres to the principles of mass conservation, the law of mass action, electroneutrality, and Gibbs-Donnan equilibrium. Key physiological parameters – such as haemoglobin concentration, haematocrit, and the concentrations of major electrolytes, albumin, and 2,3-DPG – are defined using standard literature values. When available, participant laboratory parameters can be inputted to personalise the modelling of gas transport.

For validation, the model has previously been tested against several physiological scenarios, comprising both standard resting conditions and dynamic circumstances – such as hyperoxia, metabolic acidosis, metabolic alkalosis, anaemia, and polycythaemia. Results revealed good agreement with existing literature values[143].

3.2.3. Circulation and Body Gas Stores Model

The circulation and body gas stores model simulate the dynamic storage and exchange of respiratory gases between blood and body tissues, linking pulmonary venous outflow to arterial inflow. This model closes the loop with the LNL framework and delivers mixed venous gas content as an output. This parameter is crucial for determining total gas

exchange, defined as the difference between the mixed venous and pulmonary end-capillary gas contents.

The CABGS model comprises 11 anatomically based major organs and tissue compartments. It includes separate compartments for major organs such as the heart, lungs, liver, kidneys, gastrointestinal tract (stomach, small and large intestine, and, for venous drainage reasons, spleen), and brain, as well as for distributed tissues such as muscle, skin, fat, and bone, and an additional compartment that accounts for the remainder of the body (thyroid, adrenals, pancreas). Each compartment is assigned a tissue volume – calculated from organ mass and density – and corresponding flows, which are further subdivided into arterial, capillary, and venous components. Additionally, each compartment holds a share of the metabolism, represented by oxygen consumption, and its own solubility coefficient for O_2, CO_2, and N_2. The apportionment of volumes, flows, and metabolism across compartments is based on existing literature sources[147-149] and additional model assumptions that are discussed in detail elsewhere by *Magor-Elliott et al*[144].

Circulation of blood takes place between the lungs and all the other compartments via independent circulatory pathways running in parallel (Figure 17). Oxygen-rich blood leaves the pulmonary veins, is delivered, exchanged, and stored by the model compartments, before returning to the lung via the pulmonary artery as mixed venous blood.

The compartmentalised structure of the model enables it to simulate how different regions of the body store and exchange respiratory gases, providing an anatomically informed framework for understanding systemic gas transport.

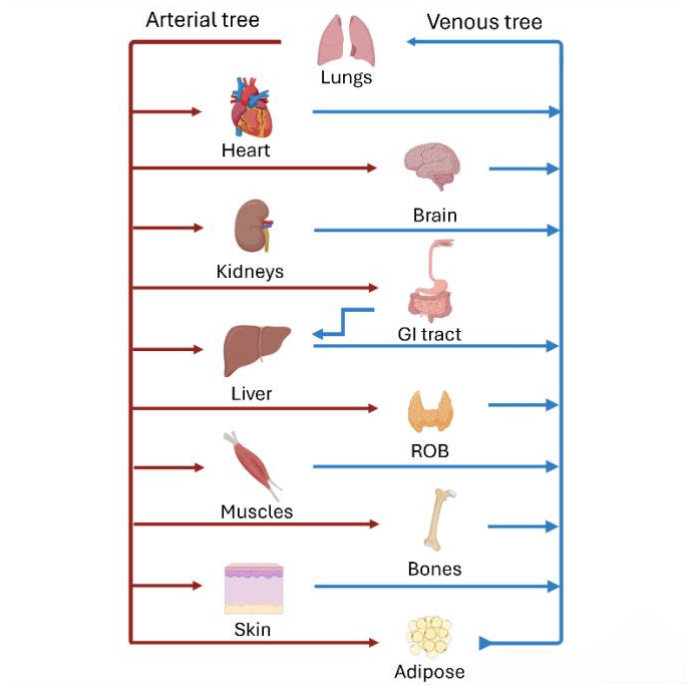

Figure 17. CABGS model cross-compartmental parallel circulation.

The model divides the body into 11 organ and tissue compartments. Blood flows from and drains into the lungs, perfusing target compartments along the circulatory route. The gastrointestinal (GI) tract drains into the liver, as a representation of the portal vein function. Red and blue lines denote arterial and venous trees, respectively, with arrows indicating the direction of circulation. ROB = rest of body (thyroid, adrenal, pancreas). Diagram created with BioRender.com.

To initialise the model, arterial contents of O_2, CO_2, and N_2 are required. Blood from the pulmonary outflow fills the arterial tree and is directed towards organs and tissues under the influence of their apportioned metabolic rates and flows. The extent of gas exchange between blood and tissues depends on the compartment-specific solubility coefficient of the gas being exchanged, the differential partial pressure between blood and compartment, and the potential chemical reactions of the gas species within the blood or tissues.

For inert gases, such as N_2, movement is determined simply by the partial pressure differential: from areas of higher pressure to areas of lower pressure. For O_2 and CO_2, the exchange is more complicated as these gases interact with blood in specific ways. O_2 binds to haemoglobin and is influenced by factors that affect its release to tissues, while CO_2 not only dissolves in blood but also reacts with water to form bicarbonate and protons. These interactions, Bohr and Haldane effects included, couple the behaviour of O_2 and CO_2 during exchange. The CCP blood model carefully accounts for such interactions when modelling exchange between blood and tissues. Ultimately, this means that the gas concentrations in the blood and tissues are continuously changing based on both the physical movement of gases and these chemical reactions. Following exchange, blood returns to the lung through the venous tree at a set flow and a known composition. Once more, the entire model process is predicated on conservation of mass principles.

The model can be tailored to represent the gas exchange properties of different subjects by proportionally scaling the anatomical and physiological parameters to match their specific body composition and size. This is achieved by inputting sex, age, height, and weight to estimate an individual's proportion between adipose tissue mass and lean body mass:

$$F_{fat} = \frac{1.2(BMI) + 0.23(age) - 10.8(sex) - 5.4}{100}$$

$$F_{lean} = 1 - F_{fat}$$

where F_{fat} is the fraction of adipose tissue and F_{lean} the faction of lean body mass; BMI is the body mass index, calculated diving weight by the squared height, in $kg.m^{-2}$; age is measured in years; and sex is inputted as male (1) or female (0). With these numbers, values

can be adjusted from the "standard man" utilised for model development (male, age 25 years, 180 cm height, and 70 kg weight).

3.2.4. MFS and multi-model integration: from measurements to simulated results

In order to model the cardiorespiratory system, MFS-measured inspired gas fractions along with inspired and expired flows become model inputs. Additional inputs are: (1) patient-specific age, sex, height and weight; (2) apparatus dead space, added by the MFS measurement head and by any other apparatus interposed between the gas source and the patients mouth; (3) an experimental file containing instructions on acceptable initial guesses for several physiological variables pertaining gas exchange and metabolism – the parameter set of interest[142].

Once initialised, the model continues to run driven by flows – gas and blood – and metabolism. A respiratory controller dictates gas flows from MFS-acquired measurements. A cardiac controller determines blood flows from cardiac output, a variable which, in this work, is fixed as part of the experimental file. A metabolic controller instructs gas exchange between blood and tissues based on oxygen consumption and carbon dioxide production. The problem solved by the model is the simulation of an individual's expired flow.

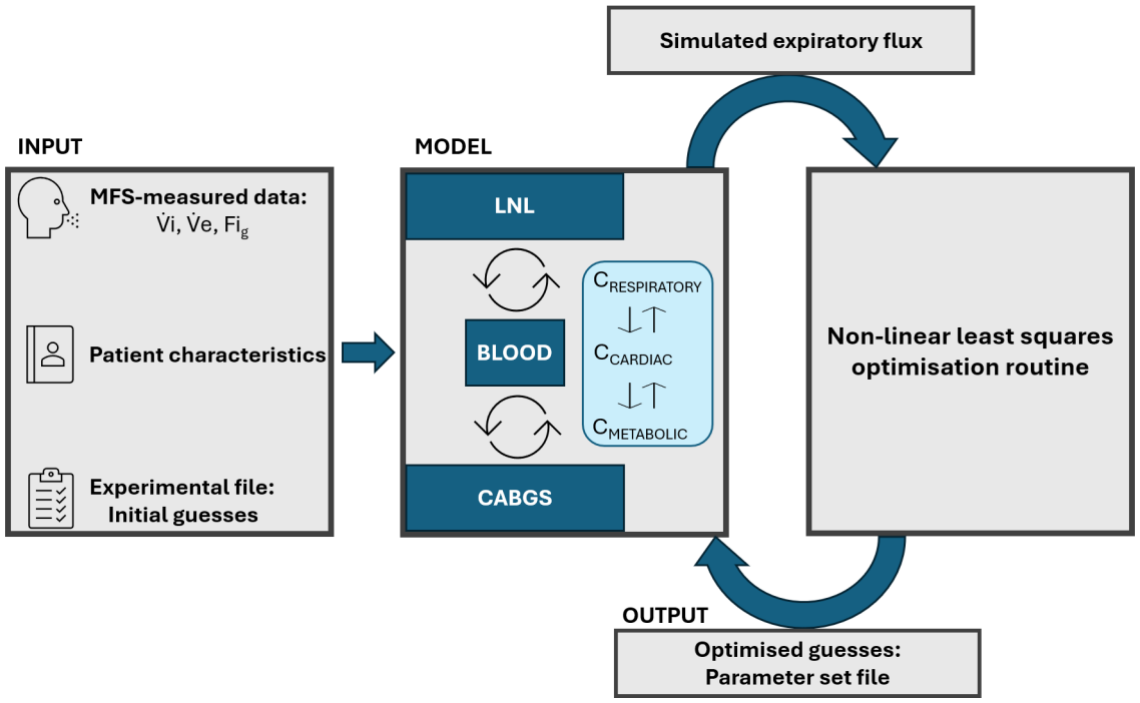

Figure 18. From MFS-measurements to gas exchange simulation: a step-by-step representation of CCP.

The cardiopulmonary model takes as inputs the MFS-measured data, including inspired gas fractions (Fi_g) and respired flows (inspired, $\dot{V}i$; expired, $\dot{V}e$) to generate simulated expiratory gas fractions, which allow for estimation of expiratory flux. Patient-specific characteristics help the model to personalise its output. An experimental file containing initial guesses for the most relevant physiological parameters is also provided to the model. The model circulates and exchanges respired gases under the influence of 3 controllers: respiratory ($C_{RESPIRATORY}$), dictated by gas flows; cardiac ($C_{CARDIAC}$), guided by experimental cardiac output; metabolic ($C_{METABOLIC}$), defined by oxygen consumption and carbon dioxide production rates. A non-linear least squares optimisation routine iteratively adjusts the experimental physiological parameters to minimise the difference between measured and simulated fluxes. After several iterations, the model outputs a final parameter set that best characterises the individual's cardiopulmonary physiology.

Upon completion of expired gas fractions simulation by the model, the NLLSOR algorithm initiates the process of model fitting – the procedure by which it determines the best match between measured and simulated gas fluxes. This is achieved by iteratively adjusting the

physiological variables of interest in the experimental file to minimise the squared difference between the measured and modelled fluxes. The fitting process is repeated four times using different initial parameter guesses to check that the same minimum is found each time and therefore that the minimum is likely to be a global minimum. Once this condition is satisfied, the model output is given as the optimised simulated parameter set which is the most likely to be representative of an individual's cardiopulmonary physiology (Figure 18). The parameter set file includes those lung inhomogeneity variables and absolute lung volumes described in Table 1. Of relevance to this work, it also includes modelled ideal partial pressure of CO_2 ($PiCO_2$), modelled oxygen consumption ($\dot{V}_{O2}^{mod}$), and modelled respiratory quotient (RQ^{mod}).

In addition to the NLLSOR, quality control measures are employed to ensure that the physiological parameters simulated by CCP are a good fit for the MFS-measured data. These will be discussed in sections 4.2.6 and 6.3.4.

3.2.5. Multi-breath nitrogen washout in cardiopulmonary modelling

In this thesis, the experimental protocol varied according to study objectives. In oxygen consumption studies, cardiopulmonary modelling was unnecessary, as all required data were obtained directly from MFS measurements. Detailed protocols for each metabolic studies are discussed in Chapter 4 and Chapter 5. By contrast, studies of absolute lung volumes – described in Chapter 6 and Chapter 7 – required cardiopulmonary modelling as an integral component of the protocol. In these cases, steady tidal breathing through the MFS was supplemented with a specific stimulus: the multi-breath nitrogen washout (MBNW).

A standard MBNW in healthy participants consists of breathing through the MFS for twelve minutes. The first seven minutes – the baseline phase – involve inhaling a gas mixture with a known FiO_2 (typically 0.21 for spontaneously ventilated subjects). In the final five minutes – the washout phase – FiO_2 is increased in a single step, washing oxygen into and nitrogen out of the lungs. The magnitude of the FiO_2 step determines whether the washout is partial or full: throughout this work, partial washouts are defined as an absolute FiO_2 increase of 0.2 from baseline, whereas full washouts involve raising the FiO_2 from baseline to 1.0.

Figure 19 displays a partial nitrogen washout dataset in a healthy participant, showing the cumulative volume uptake of O_2, CO_2, and N_2. Cumulative volumes are obtained by summing, over time, the product of each gas fraction and its flow rate. During baseline breathing, the slopes of the O_2 and CO_2 curves reflect the participant's metabolic rates – O_2 shows a positive slope (indicating uptake for respiration) and CO_2 shows a negative slope (reflecting its production and elimination). Nitrogen, which is not involved in metabolism, should ideally show no slope; this is known as the nitrogen balance and serves as an important quality control measure.

As discussed in section 2.4.1.4, the ratio of nitrogen washed out from the lungs to the change in the inspired fraction of N_2 is proportional to an individual’s lung volume. This information enables the model to estimate absolute lung volumes more reliably.

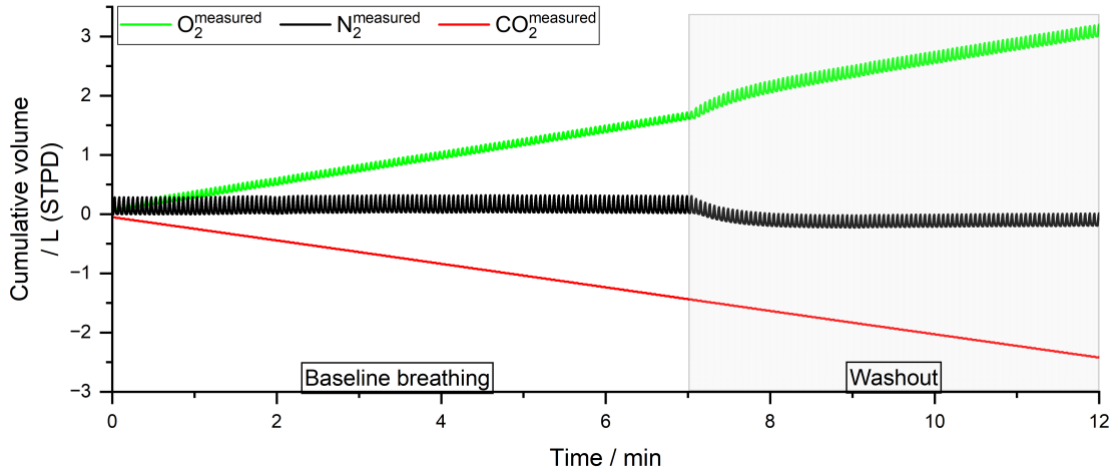

Figure 19. MFS recording of the breathing protocol used to model absolute lung volumes and lung inhomogeneity.

The graph displays cumulative volumes of oxygen, nitrogen, and carbon dioxide over a 12-minute tidal breathing protocol. During the first 7 minutes (baseline breathing phase), the participant breathes their baseline FiO_2 gas mixture. In the final 5 minutes (washout phase), the inspired oxygen fraction is increased – in this example by 0.2 – initiating a multi-breath nitrogen washout. As oxygen is introduced to the lungs, nitrogen is simultaneously washed out. This change provides the necessary model stimulus to estimate lung volume and assess inhomogeneity.

Finally, the shape of the washout phase gives additional insight into lung inhomogeneity. Simulated V_A and V_D are divided across the 125 LNL individual alveolar compartments – V_A equally and V_D unequally. Each group of 25 compartments is given a different dead space path length. The model compartments empty at different time constants, at a speed driven by their individual compliances. Therefore, the wider the compliance (σC_L) and dead space (σV_D) variances, the longer it will take for all gas to be washed out, and, therefore, to reach a plateau.

3.3. Clinical applications of CCP

CCP has been clinically applied to assess distinct lung physiology aspects in several pathologies, such as chronic obstructive pulmonary disease (COPD), asthma, COVID-19, and cystic fibrosis.

Use of the measurement component of CCP – the MFS – was first reported in a clinical setting in 2016 by *Ciaffoni et al*[54]. In this study, the MFS was employed longitudinally to measure oxygen consumption in a single mechanically ventilated patient throughout an elective abdominal aortic aneurism repair. Here, the feasibility of acquiring reliable real-time gas exchange measurements noninvasively within the mainstream airway in a clinical setting was confirmed. More than that, it was established that MFS measurements achieved a precision that was an order of magnitude higher and an accuracy two times better than other gas analysers[54].

Building on that foundation, cardiopulmonary modelling was developed and coupled with MFS measurements to construct the first complete CCP version. Its clinical debut took place in 2018, reported by *Mountain et al.*, who assessed lung inhomogeneity patterns across three distinct groups: healthy young adults, healthy older adults, and patients suffering from COPD[138]. These groups showed significant differences ($p < 0.001$) across all three modelled inhomogeneity parameters (σC_L, σV_D, σC_d), with the widest distributions of alveolar compliance, anatomic dead space, and lung perfusion occurring in the group with COPD[138].

In a subsequent study in 2022, *Smith et al.* corroborated these findings observing significantly higher alveolar compliance inhomogeneity, represented by σC_L, in patients with early-stage COPD when compared with age-matched healthy individuals[150]. It was

also shown that σC_L is more sensitive than the forced expired volume in one second (FEV1%) in identifying early-stage COPD (GOLD 1 & 2), identifying this parameter as a potential biomarker for early detection of small airways disease[150]. In fact, the latest study conducted by *Smith et al.* in 2024 has demonstrated that σC_L may become significantly altered even before symptoms or a COPD diagnosis are established, as early as 5 to 10 pack-years (where a pack-year is defined as smoking an average of twenty cigarettes per day for one year) into tobacco exposure[151]. In contrast, FEV1% remained similar across the groups studied: (1) healthy volunteers, (2) smokers with a 0 to 5 pack-year history and (3) those with between 5 and 10 pack-years[151].

An asthma study completed in 2020 by *Smith et al.* compared σC_L and FEV1% in an investigation including a group of patients with asthma and a group of healthy controls. Asthmatics showed increased σC_L alongside a lower FEV1% relative to controls[152]. These variables were, however, only weakly correlated, likely because they reflect different pathophysiological phenomena: FEV1% reflecting increased airways resistance and σC_L reflecting small airway ventilation inhomogeneity exacerbated by smooth muscle hyper-reactivity[152].

Continuing CCP applications in asthma, in 2025 *Alamoudi et al.* studied type-2 high asthma patients before and after initiating anti-IL5 or anti-IL5R biologic therapy[153]. Three to four months after commencing treatment, patients showed significant reductions in symptoms, blood eosinophil count, FEV1%, and σC_L – a marker of ventilation inhomogeneity. Based on a bimodal distribution, patients were stratified as σC_L responders or non-responders according to the magnitude of their σC_L change post-bronchodilator administration. Responders showed greater symptom improvement, larger FEV1% increases, and were more likely to achieve clinical remission at one year of treatment. These findings support

σC_L as a potential early predictor of disease activity in the lungs and of long-term response to biologics[153].

In 2023, *Sandhu et al.* studied a small cohort of cystic fibrosis patients comparing them with healthy controls[142]. Subjects with this genetic condition displayed rather large values for σC_L in addition to FRC volumes below those predicted from their physical characteristics. These variables were significantly different between disease and control cohorts[142].

CCP has also been employed to assess the long-term effects of COVID-19 on lung function. In 2024, *Magor-Elliott et al.* assessed patients treated in the community, on hospital wards, and within the ICU, after 6 months and at one year from the time of SARS-CoV-2 infection, comparing them against healthy controls who had never been infected by the virus[144]. When compared with controls, community and ward-treated subjects demonstrated significantly higher values of σC_L. Patients treated in the ICU, whether they received mechanical ventilation or not, exhibited an increase in anatomical dead space compared with controls. All hospitalised patients displayed a reduction in FRC values following recovery. Interestingly, regardless of disease severity, the lasting changes in inhomogeneity associated with COVID-19 were equivalent to ageing the patients' lungs by approximately 15 years[144].

To date, most of the published work involving CCP has focused on the study of lung inhomogeneity in awake self-ventilating participants. In this thesis, primarily mechanically ventilated individuals are studied, with an emphasis on investigating absolute lung volumes and oxygen consumption.

3.4. Summary

CCP is a recently developed, non-invasive technique designed to comprehensively assess cardiopulmonary function by integrating highly precise, time-resolved measurements of respiratory gas exchange with a detailed physiological model. The technique relies on the MFS, which employs laser absorption spectroscopy to continuously measure the composition and flow of respired gases every 10 milliseconds. These high-fidelity data are then input into a mechanistic cardiopulmonary model that simulates gas exchange dynamics through the integration of three submodels: a model of lung inhomogeneity, a model of the circulation and body gas stores, and a model of the physicochemical behaviour and transport of respired gases in the blood.

Clinically, CCP offers a powerful tool for evaluating subtle changes in lung physiology that may not be captured by conventional lung function tests. By quantifying parameters such as alveolar compliance, anatomical dead space, and vascular conductance distributions, CCP may aid in detection and/or monitoring of conditions such as COPD, asthma, cystic fibrosis, and COVID-19. Its ability to provide multidimensional insights into respiratory and cardiovascular function holds promise for enhancing disease diagnosis, treatment planning, and longitudinal patient monitoring.

Chapter 4. Preliminary study in awake healthy participants to compare MFS $\dot{V}_{O2}$ with the Douglas bag

Existing techniques for the measurement of $\dot{V}_{O2}$ are often impractical, invasive, imprecise, inaccurate, or a combination of these. The MFS measures $\dot{V}_{O2}$ directly, non-invasively, and within the mainstream airway. It offers high temporal resolution and overcomes many of the limitations associated with traditional methods. While initial laboratory evaluations have demonstrated superior precision and accuracy compared with commercially viable methods for measuring oxygen consumption, these assessments have largely relied on controlled experimental conditions involving passing gas mixtures of known composition and flow rates through the instrument. The performance of the MFS in the measurement of $\dot{V}_{O2}$ under clinically relevant conditions has not yet been systematically evaluated. Furthermore, no studies to date have compared MFS-derived $\dot{V}_{O2}$ measurements with a physiological gold standard.

4.1. Research aims and objectives

The primary aim of the study described in this chapter is to assess the accuracy of MFS-derived $\dot{V}_{O2}$ measurements against those obtained via the DB method, a well-established physiological reference. This comparison between methods was performed in spontaneously breathing healthy participants as a pilot study with the aim to evaluate the MFS performance against a physiological standard for respiratory gas exchange.

4.2. Methods

4.2.1. Ethical approval

The study was approved by the Scotland A Research Ethics Committee, reference 17/SC/0172. Of relevance to the experiments conducted in this thesis, ethics approval permitted the following: (i) recruitment of adult healthy volunteers identified via hospital clinics, research registries, or public advertisements; (ii) up to four visits per participant, each lasting no more than two hours; (iii) performance of repeated lung inhomogeneity tests (i.e., MFS and CCP), involving controlled variations of inspired gas composition while breathing through a mouthpiece with continuous monitoring; (iv) use of standard clinical pulmonary tests (spirometry, lung volumes, diffusing capacity, oscillometry) performed during the visit; (v) collection and analyses of expired gas samples. Study synopsis can be found in Appendix A.

All practices were conducted in conformity with the general principles of the Declaration of Helsinki, the guidelines for GCP, and the UK GDPR.

4.2.2. Participant recruitment

Volunteers for this observational study were recruited through general advertisements, including posts on social media platforms. Once potential participants expressed their interest to the research team, either via email or message, they were provided with additional details about the study, including the Participant Information Sheet. The eligibility criteria for participation in the study are described below.

(i) Inclusion criteria:

a. Male and female, aged 18 or above;

b. Willing and able to provide informed consent.

(ii) Exclusion criteria:

a. Inability to tolerate mouthpiece and/or nose clip;

b. Established diagnosis of major cardiac or respiratory disease;

c. Current smoker;

d. Pregnancy.

If eligibility was confirmed, the prospective participant was offered an in-person meeting with a member of the team to discuss their participation in the study.

4.2.3. Informed consent

Participants were given the opportunity to ask questions and ensure they fully understood the study before providing consent. They were provided with clear, accessible information regarding their right to withdraw at any time, as well as the implications of their participation. This process took place in an in-person meeting with a GCP-trained member of the research team, during which prospective participants had ample time to consider their decision. If the volunteer demonstrated both capacity and willingness to consent, verbal

and written consent were obtained. When consent was provided, the study visit typically took place shortly afterwards, on the same day.

4.2.4. Instrumental setup

Participants were connected to the MFS measurement head through a mouthpiece. An HME filter was interposed between the MFS and the mouthpiece to prevent cross-contamination and to ensure heat and moisture provision to the airways in view of a dry gas supply source. The participant had their nose occluded by a nose clip to ensure a good seal and prevent leaks, and was positioned sitting upright, with their back supported by a chair and their legs uncrossed (Figure 20). A circuit was connected to the back of the MFS providing the participant with a known flow and concentration of gas. Pulse oximetry was employed to monitor oxygen saturation and heart rate throughout the study.

Figure 20. Instrumental setup in spontaneously breathing participants.

Spontaneously ventilated participant breathing through the MFS head via mouthpiece, with an HME filter interposed. A gas supply source is fed to the back of the MFS head. Nose is occluded by nose clip to prevent leaks. Picture taken by Colin Beesley; Robbins' group holds copyright.

4.2.4.1. MFS warm-up and calibration

Prior to attaching a participant to the MFS, the device was turned on and allowed to warm-up for thirty minutes. This time was essential to heat the measurement cell temperature with the intent to: (1) prevent condensation within the measurement elements, such as mirrors, (2) match, to a better degree, device and body temperatures, enhancing gas exchange measurements. The measurement cell was heated to 35°C. Once the measurement cell had been fully warmed-up, calibration of the MFS was initiated.

Calibration was performed in two steps, lasting for a total of two to three minutes. First, low-flow pure N_2 (N4.8, 99.998% N_2; BOC Limited, UK) ran through the measurement cell to determine the baseline reading points for O_2, CO_2, and H_2O. Later, pure O_2 (N5.0, 99.999% O_2; BOC Limited, UK) was flowed to assess the path length of the O_2 optical cavity.

Upon completion of warm-up and calibration, which occurred once a day, the device would be ready for participant connection.

4.2.5. Experimental protocol

4.2.5.1. Data recording

This protocol was designed to simultaneously measure $\dot{V}_{O2}$ in spontaneously breathing participants using both the MFS and the DB method. To enable this, the MFS and the DB were connected in series within the same breathing circuit, as illustrated in Figure 21.

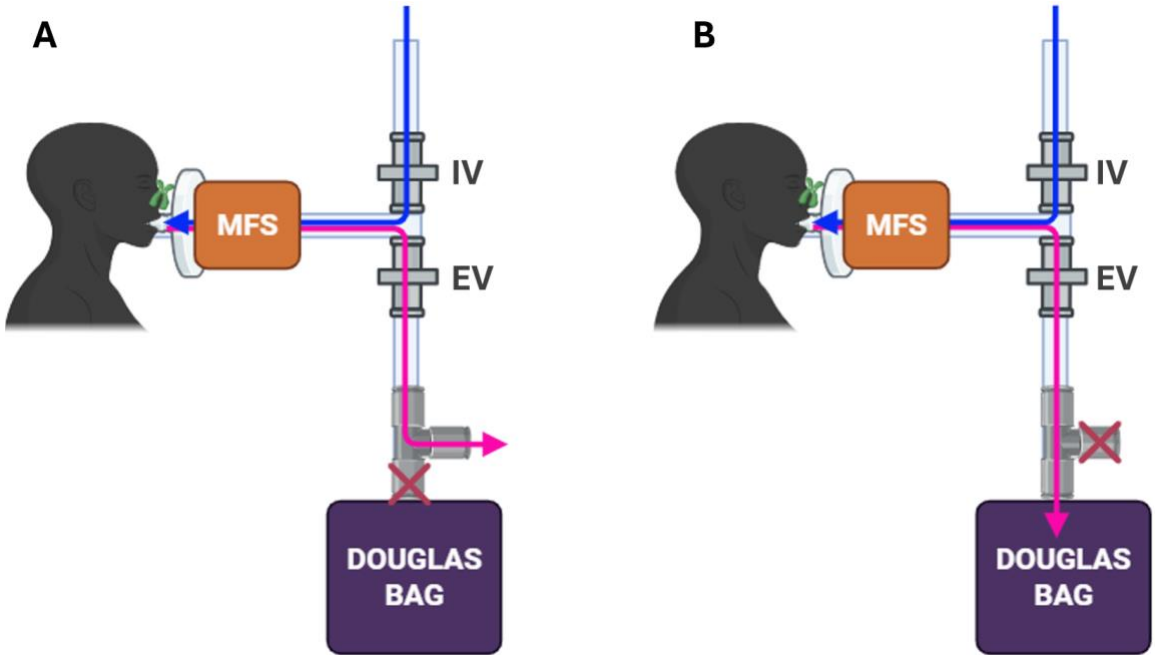

Figure 21. Schematic representation of the experimental setup for simultaneous measurements by the MFS and Douglas bag.

Inspiratory and expiratory flow directions are shown in blue and pink, respectively. Panel A: The three-way valve is closed to the DB during the acclimatisation period. Ambient air is inspired, through the MFS, by the participant. Expired gas is exhaled through the MFS back to the atmosphere. Panel B: Three-way valve is open to the DB and mixed expired gas is collected for analysis of composition and volume. IV = inspiratory valve; EV = expiratory valve. Created with Biorender.com.

Participants breathed ambient air through an open-ended circuit fitted with a unidirectional inspiratory valve, which allowed airflow only in the direction from the atmosphere toward the participant. Inspired air passed through the MFS measurement cell before reaching the participant. On exhalation, expired air returned through the MFS, passed a unidirectional expiratory valve, and entered the expiratory limb of the circuit.

A three-way valve was positioned between the expiratory limb and the DB. This allowed the operator to direct expired air either into the DB for collection or out into the atmosphere. In panel A, the valve is set to vent exhaled gas to the atmosphere; in panel B, it is switched to collect mixed expired gas in the DB.

Prior to data collection, each participant breathed through the system for five minutes. This initial period served two purposes: (1) to allow the participant to acclimatise to the equipment, including the mouthpiece, nose clip, and any additional resistance from the HME filter; and (2) to allow the $\dot{V}_{O2}$ trace to reach a steady state. During this time, the valve to the DB was briefly opened, flushing the bag and expiratory limb with mixed expired gas. The valve was then closed, and at the end of the period, the bag was disconnected, emptied, and reconnected to the system in preparation for formal measurements.

Data collection began immediately after this initial phase. The participant continued breathing through the system, with expired gas directed into the DB and $\dot{V}_{O2}$ simultaneously measured by the MFS. The collection phase ended once the participant had filled approximately two-thirds of a 150 L PVC DB (Harvard Apparatus Ltd, UK). The bag was then sealed and removed for analysis of gas volume and composition.

4.2.5.2. Preliminary checks

While the MFS provides $\dot{V}_{O2}$ in real time and breath-by-breath, the DB technique requires additional steps to determine the average rates of gas exchange. This involves measuring the total volume of mixed expired gas collected in the bag and analysing its composition.

To minimise the impact of known sources of error associated with the DB method, preliminary checks were conducted prior to data collection. These checks aimed to ensure the accuracy and reliability of both the gas meter used for volume measurement and the gas

analyser used for gas composition analysis. Additionally, the integrity of the breathing circuit and the DB was assessed to exclude leaks. The volume of expired gas collected in the DB was analysed utilising a Harvard dry gas meter (Hugo Sachs Elektronik, Germany). Prior to commencing the study, the gas meter was calibrated using a 3 L calibration syringe (Vitalograph, UK). The syringe was filled with fresh ambient air and emptied into the gas meter ten times, delivering a total volume of 30 L per trial. This process was repeated three times. In each trial, the gas meter recorded a volume of 29.9 L. These results were in keeping with the manufacturer's reported gas meter accuracy of ± 1.5%. The composition of mixed expired gas was analysed using the Scio Four Oxi gas analyser (Drager, Germany) with readings displayed on a connected Vista 120S monitoring device (Drager, Germany). The analyser was calibrated using: (1) a certified precision gas mixture containing 5% CO_2, 55% O_2, and 40% N_2O; (2) zero grade N_2 (N4.8, 99.998% N_2; BOC Limited, UK); and (3) high grade O_2 (N5.0, 99.999% O_2; BOC Limited, UK).

Upon introduction of the precision gas mixture, the analyser reported values of 4.9% CO_2, 55% O_2, and 38% N_2O. When flushed with zero grade N_2 and high grade O_2, the analyser reported values of 0% and 99% O_2, respectively. These measurements were consistent with the manufacturer's stated accuracy specifications (Table 2), which are expressed as a combination of absolute and relative error. For instance, for an oxygen concentration of 55%, the absolute error of ± 2.5 vol% corresponds to a range of 52.5% to 57.5%, while the inclusion of the relative error of ± 2.5% further expands the expected range to approximately 51.1% to 58.9%.

Gas species	Absolute error / vol%	Relative error / %
O_2	± 2.5%	± 2.5%
CO_2	± 0.43%	± 8%
N_2O	± 2%	± 8%

Table 2. Reported measurement accuracies for the Scio Four Oxi gas analyser.

Accuracy is expressed as a combination of absolute and relative error: ± (absolute vol% + % of measured value).

To ensure the integrity of the breathing circuit and the DB, a custom-built unidirectional fan with adjustable speed was used fully to evacuate the contents of the DB through the gas meter. In the presence of a leak, the gas meter would continue to register volume after the bag had emptied.

To test for potential leaks, the bag was filled with varying volumes of air and emptied into the gas meter across three trials. In each case, the gas meter reading ceased promptly once the bag was fully emptied, confirming that the system used in this study was free from detectable leaks.

4.2.5.3. Determination of $\dot{V}_{O2}$

As previously described, mixed expired gas was collected into a 150 L PVC DB until approximately two-thirds of its capacity was reached. At the end of the experiment, three 50 mL syringes were used to extract samples from the bag for gas composition analysis. The remaining volume in the bag was then emptied into the gas meter to determine the total mixed expired volume. $\dot{V}_{O2}$ was calculated using the following equation:

$$\dot{V}_{O2} = \frac{\left(Fi_{O_2} \times V^{insp}\right) - \left(Fme_{O_2} \times V^{mexp}\right)}{Time}$$

where FiO_2 is the dry fraction of inspired oxygen in ambient air; $FmeO_2$ is the dry fraction of mixed expired oxygen from the DB; V^{mexp} is the mixed expired volume (in L) converted to standard temperature and pressure, dry conditions (STPD); time is the duration of gas collection (in minutes); V^{insp} is the inspired volume, calculated using the Haldane transformation (in L / STPD). The values assigned to each variable and the steps used to derive them are summarised in Table 3.

4.2.5.4. Dealing with water vapour in the presence of an HME filter

The MFS requires the use of an HME filter, which reduces the water vapour pressure in the expired air collected in the DB. As $\dot{V}_{O2}$ is calculated under STPD conditions, and the experimental gas fractions and volumes are measured under ambient temperature and pressure, saturated (ATPS) conditions, it is necessary to convert all values from ATPS to STPD prior to calculating $\dot{V}_{O2}$. This conversion depends on an accurate estimate of the water vapour pressure (P_{H2O}) in the expired gas. However, direct measurement of P_{H2O} in the DB was not possible, as this would necessitate breaking the bag's seal. To address this, we utilised water vapour pressure measurements from the MFS to calculate a flow-weighted mean P_{H2O} across the sampling period.

Variable	Description	Measurement / Calculation / Assumption	Units
FiO_2	Inspired O_2 fraction of dry gas	= 0.2095	N/A
$FiCO_2$	Inspired CO_2 fraction of dry gas	= 0.0004	N/A
F_{meO2}	Mixed expired O_2 fraction of dry gas	$= Fme_{O_2\,(wet,\ measured)} \times \left(\frac{P_B}{P_B - P_{H2O}}\right)$	N/A
F_{meCO2}	Mixed expired CO_2 fraction of dry gas	$= Fme_{CO_2\,(wet,\ measured)} \times \left(\frac{P_B}{P_B - P_{H2O}}\right)$	N/A
V^{mexp}	Mixed expired volume (STPD)	$= V^{mexp}(ATP)_{(wet,\ measured)} \times \left(\frac{P_B - P_{H2O}}{760}\right) \times \left(\frac{273}{273 + T}\right)$	L
V^{insp}	Inspired volume (STPD)	$= V^{mexp} \times \left(\frac{F_{e_{N2}}}{F_{i_{N2}}}\right)$	L
Time	Test duration	Measured	sec
P_B	Barometric pressure	Measured (mercury barometer)	mmHg
P_{H2O}	Water vapour pressure in expired gas	Flow-weighted mean calculated from MFS data output	mmHg
T	Ambient temperature	Measured (temperature and humidity sensor)	°C
FiN_2	Inspired N_2 fraction of dry gas	= 0.79	N/A
FeN_2	Expired N_2 fraction of dry gas	$= 1 - F_{meO_2} - F_{me_{CO_2}}$	N/A

Table 3. Measurements, calculations, and assumptions employed to obtain $\dot{V}_{O2}$ through the Douglas bag method.

N/A = not applicable.

4.2.6. Quality control

A key quality control criterion applied in this and all the subsequent studies described in this thesis – whether based solely on MFS readings or incorporating cardiopulmonary modelling – was the evaluation of N_2 balances over time. As nitrogen is an inert gas (i.e., is neither consumed nor produced by the body), its balance over time should remain steady

and, in the ideal scenario, be equal zero. Trends of N_2 consumption or production may be interpreted as systematic errors or leaks, which, if sufficiently large, will interfere with the model estimation of absolute lung volumes and the MFS measurement of oxygen consumption. Datasets exhibiting an absolute N_2 balance greater than 60 $mL.min^{-1}$ were not analysed further.

4.2.7. Statistical analyses

All statistical analyses were conducted using SPSS version 30.0 (IBM Corp., USA), with statistical significance set at $p < 0.05$.

The relationship between $\dot{V}_{O2}$ values obtained via the MFS and those derived from DB measurements was assessed using Pearson's correlation coefficient. To evaluate differences in mean $\dot{V}_{O2}$ between the two methods, paired t-tests were performed.

Bland-Altman analysis was used to assess agreement between the two measurement techniques, with plots constructed to illustrate percentage bias and limits of agreement ($1.96 \times SD$; LoA).

Additionally, local deterministic (one-at-a-time) sensitivity analyses were performed to quantify the effect of measurement inaccuracies in water pressure, mixed expired volume, and gas fractions on the calculated $\dot{V}_{O2}$. These analyses examined the impact of varying P_{H2O}, V^{mexp}, F_{meCO2}, and F_{meO2} on $\dot{V}_{O2}$ outputs derived using the Haldane transformation.

4.3. Results

4.3.1. Baseline characteristics of participants

Sixteen healthy volunteers were included in the study. Relevant physical characteristics are displayed in Table 4.

PID	Age / yr	Sex	Height / m	Weight / kg	LBM / kg
1	20	F	1.73	64.0	48.1
2	20	M	1.85	87.5	71.0
3	19	M	1.71	76.5	61.5
4	20	F	1.70	49.3	39.6
5	20	M	1.76	76.7	62.8
6	20	F	1.67	49.0	39.1
7	26	M	1.78	75.5	61.7
8	23	M	1.80	76.5	63.2
9	23	M	1.84	73.5	62.5
10	24	M	1.82	77.3	63.9
11	27	M	1.80	68.0	57.7
12	20	F	1.74	63.0	47.8
13	22	M	1.84	73.5	62.5
14	34	M	1.75	75.5	59.5
15	25	F	1.69	67.5	48.1
16	26	M	1.79	63.5	54.9
Mean ± SD	23 ± 4	N/A	1.77 ± 0.06	69.8 ± 10.3	56.5 ± 9.3

Table 4. Baseline characteristics of spontaneously breathing participants.

PID = participant identification; LBM = lean body mass; F = female; M = male.

4.3.2. Summary of $\dot{V}_{O2}$ measurements

A typical recording of oxygen consumption measurement over time from the MFS is shown in Figure 22.

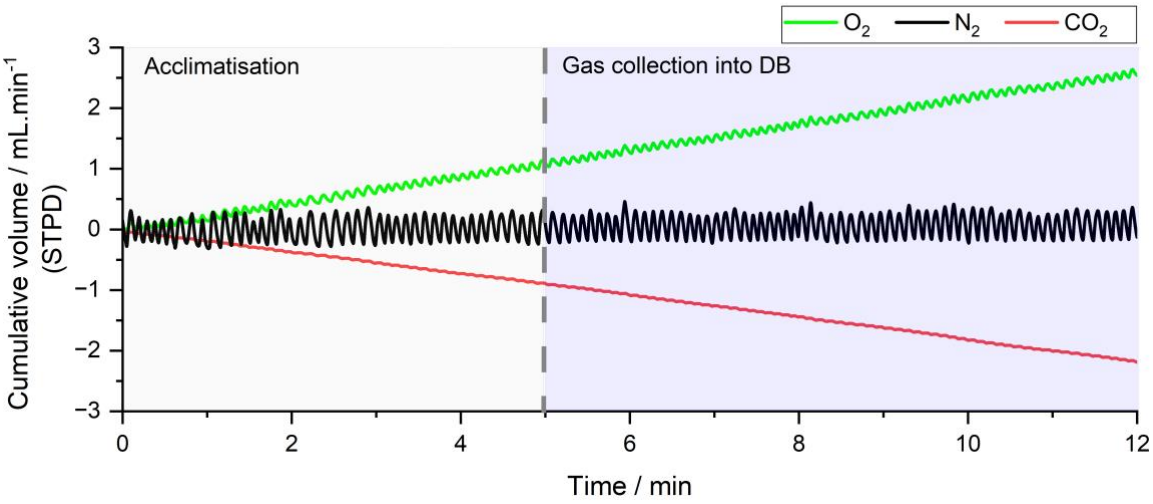

Figure 22. Typical MFS gas exchange recording during experiment.

During the initial 5 minutes, the participant had time to acclimatise to the study conditions: wearing a nose clip and breathing through a mouthpiece with mildly increased resistance due to the presence of an HME filter. At this stage, both the breathing circuit and the Douglas bag (DB) were rinsed with mixed expired gas. The DB was emptied and reconnected to the circuit just before gas collection started. In the following minutes, the participant inspired ambient air and breathed out into the DB. Collection continued until the bag was two thirds full, at which point the breathing test was concluded and the gas analysis commenced. O_2 (green) is consumed over time, CO_2 (red) is produced over time, and N_2 (black), as a balance gas, should be close to or equal zero. In this participant, the average gas exchange was calculated from minutes 5 to 12 ($\dot{V}_{O2}$ = 214 mL.min^{-1}; $\dot{V}_{CO2}$ = - 189 mL.min^{-1}; $\dot{V}_{N2}$ = 2.15 mL.min^{-1}).

Mean ± SD $\dot{V}_{O2}$ measured by the MFS was 291 ± 58 mL.min^{-1}, while the DB method yielded 299 ± 58 mL.min^{-1}. Within-participant differences in $\dot{V}_{O2}$ between methods are displayed in Figure 23.

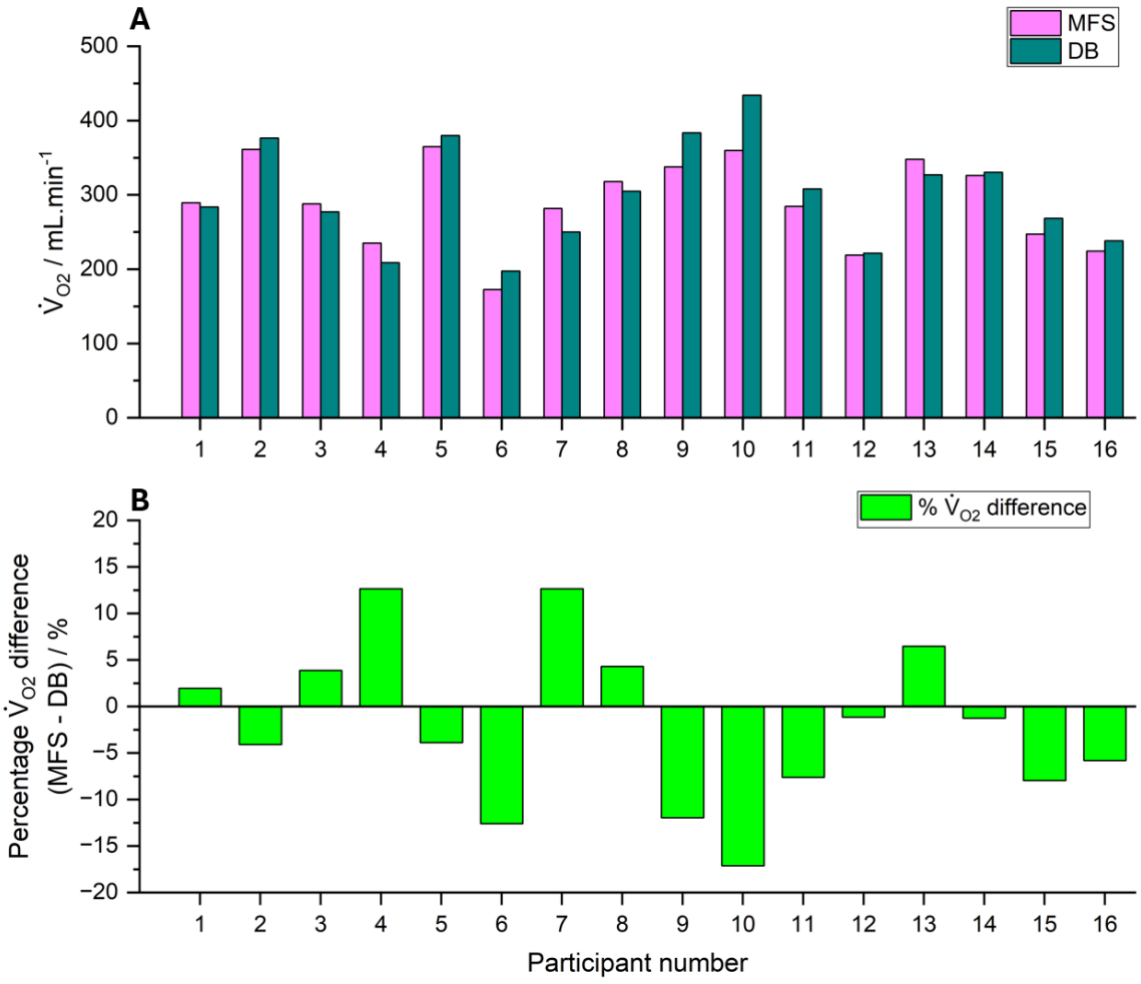

Figure 23. Individual absolute and percentage differences between $\dot{V}_{O2}$ measured by the MFS and estimated by the Douglas bag.

Sixteen participants are numbered in the x-axis of both panels. The difference in $\dot{V}_{O2}$ between methods is represented in mL.min^{-1} on panel A and as a percentage (MFS - Douglas bag) on Panel B. DB = Douglas bag.

4.3.3. Paired comparison of $\dot{V}_{O2}$ values

There was no statistically significant difference between $\dot{V}_{O2}$ values measured by the MFS and those estimated by the DB method ($t(15) = 1.204$, $p = 0.25$; Figure 24).

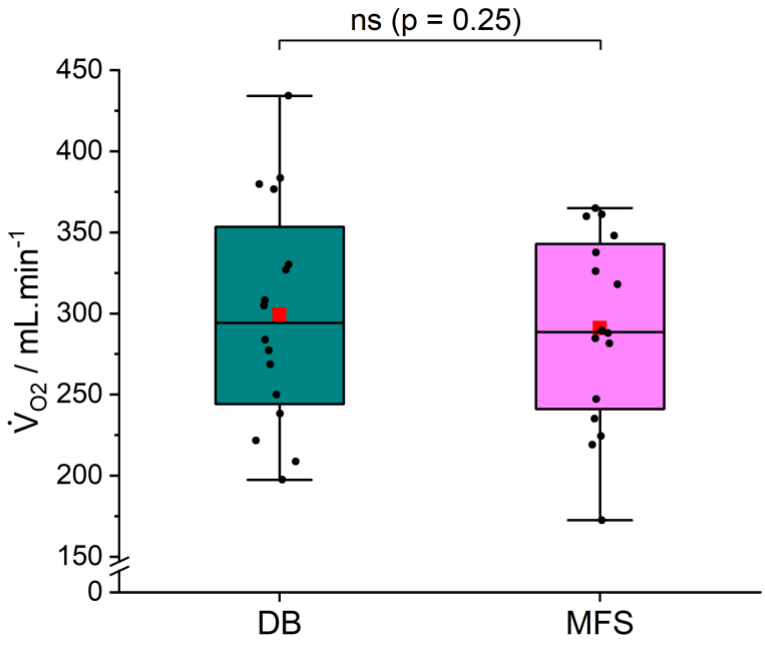

Figure 24. Box-plot showing the distribution of $\dot{V}_{O2}$ values measured by the MFS and estimated by the Douglas bag method.

The box extends from the first to the third quartile, with the central horizontal line in each box representing the median and the central red square representing the mean. Whiskers denote the range of values within 1.5 times the interquartile range from the lower and upper quartiles. Each $\dot{V}_{O2}$ value is shown as black dot onto the box-plot. No outliers were observed. The two methods showed similar central tendencies and spread, with no statistically significant difference between their means (t(15) = 1.204, p = 0.25). DB = Douglas bag.

4.3.4. Agreement between methods: Bland-Altman analysis

The agreement between $\dot{V}_{O2}$ measurements from the MFS and by the DB method is shown in Figure 25. Although he two measurements were strongly correlated (r = 0.92, $p < 0.0001$), Bland-Altman analysis revealed a mean percentage bias of - 2%, indicating that the MFS slightly underestimated $\dot{V}_{O2}$ relative to the DB. The 95% limits of agreement ranged from - 19% to + 15%.

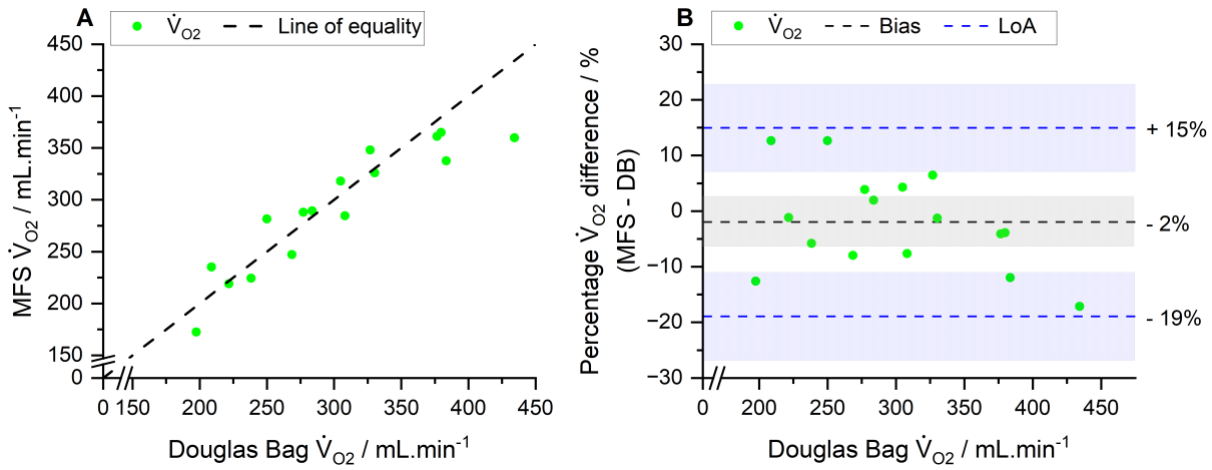

Figure 25. Relationship and agreement between $\dot{V}_{O2}$ values measured by the MFS and estimated by the Douglas bag method.

A: Correlation between methods. $\dot{V}_{O2}$ measurements acquired through both techniques were strongly correlated, as demonstrated by a tight fit of the data points to the line of identity and a high Pearson's coefficient ($r = 0.92$, $p < 0.0001$). B: Agreement between methods. Using the Douglas bag (DB) as the reference method (x-axis), the percentage difference between MFS and DB was calculated (y-axis). The MFS underestimated $\dot{V}_{O2}$ by 2% (or - 8 mL.min^{-1}) when compared with the DB. Limits of agreement ranged from - 19 to + 15% (or - 62 to + 45 mL.min^{-1}). The shaded grey and blue areas represent the 95% confidence interval for the bias and the limits of agreement, respectively.

4.3.5. Sensitivity of $\dot{V}_{O2}$ to measurement uncertainties

4.3.5.1. Water pressure uncertainty

The accuracy of P_{H2O} readings obtained using the MFS was validated against the Optidew dew-point sensor (Michell Instruments, UK), which detects the temperature at which condensation forms on a mirror – directly indicating water vapour pressure. This validation showed that the MFS measured P_{H2O} with an accuracy of ± 1 mmHg.

To assess the impact of this uncertainty in $\dot{V}_{O2}$, a local deterministic (one-at-a-time) sensitivity analysis was performed by varying each participant's P_{H2O} by ± 1 mmHg. The resulting changes were propagated through both the ATPS-to-STPD volume conversion and the correction of gas fractions using the Haldane transformation. This analysis demonstrated a mean ± 0.76% change in $\dot{V}_{O2}$ across participants. These findings indicate that P_{H2O} uncertainty, when estimated using MFS-derived flow-weighted averages, has a minimal effect on calculated $\dot{V}_{O2}$.

4.3.5.2. V_{mexp} uncertainty

The gas meter used to measure the mixed expired volume of the DB has a manufacturer-reported accuracy of ± 1.5%. To quantify the potential impact of this uncertainty, a one-at-a-time sensitivity analysis was performed by adjusting each participant's V^{mexp} by ± 1.5% accordingly. This resulted in a mean ± 1.5% change in $\dot{V}_{O2}$. The observed proportionality reflects the coupled scaling of inspired volume according to expired volume through the Haldane transformation.

4.3.5.3. F_{meCO2} uncertainty

The manufacturer reports an absolute error of ± 0.43 vol% and a relative error of ± 8% for CO_2 measurements. A sensitivity analysis was conducted by applying this combined uncertainty to F_{meCO2} values for each participant and recalculating $\dot{V}_{O2}$. The analysis showed a mean ± 1.9% change in $\dot{V}_{O2}$.

4.3.5.4. F_{meO2} uncertainty

According to the manufacturer, the gas analyser used to determine the F_{meO2} has an absolute error of ± 2.5 vol%, and an additional ± 2.5% relative error based on the measured value.

F_{meO2} for each participant was varied accordingly, and $\dot{V}_{O2}$ was recalculated using the Haldane transformation. This analysis resulted in a mean ± 21% change in $\dot{V}_{O2}$ (Figure 26, panels A and B). These results highlight that measurement error in F_{meO2} is the most significant source of $\dot{V}_{O2}$ uncertainty among all variables tested. When individual within-participant differences in $\dot{V}_{O2}$ between methods are replotted with error bars reflecting the uncertainty in F_{meO2} measurements, it becomes apparent that the observed differences fall within the expected range of measurement error (Figure 26C). This suggests that any discrepancies between methods can largely be attributed to uncertainty in F_{meO2} obtained for the DB $\dot{V}_{O2}$ estimates.

No specific tests were conducted to assess inaccuracies in the measurement of P_B and T. P_B was measured using a standard mercury barometer, instrument widely recognised for its accuracy and longstanding use as a reference standard against which modern devices are calibrated. T was measured with a reference-grade thermometer, accurate to within a few tenths of a degree Celsius.

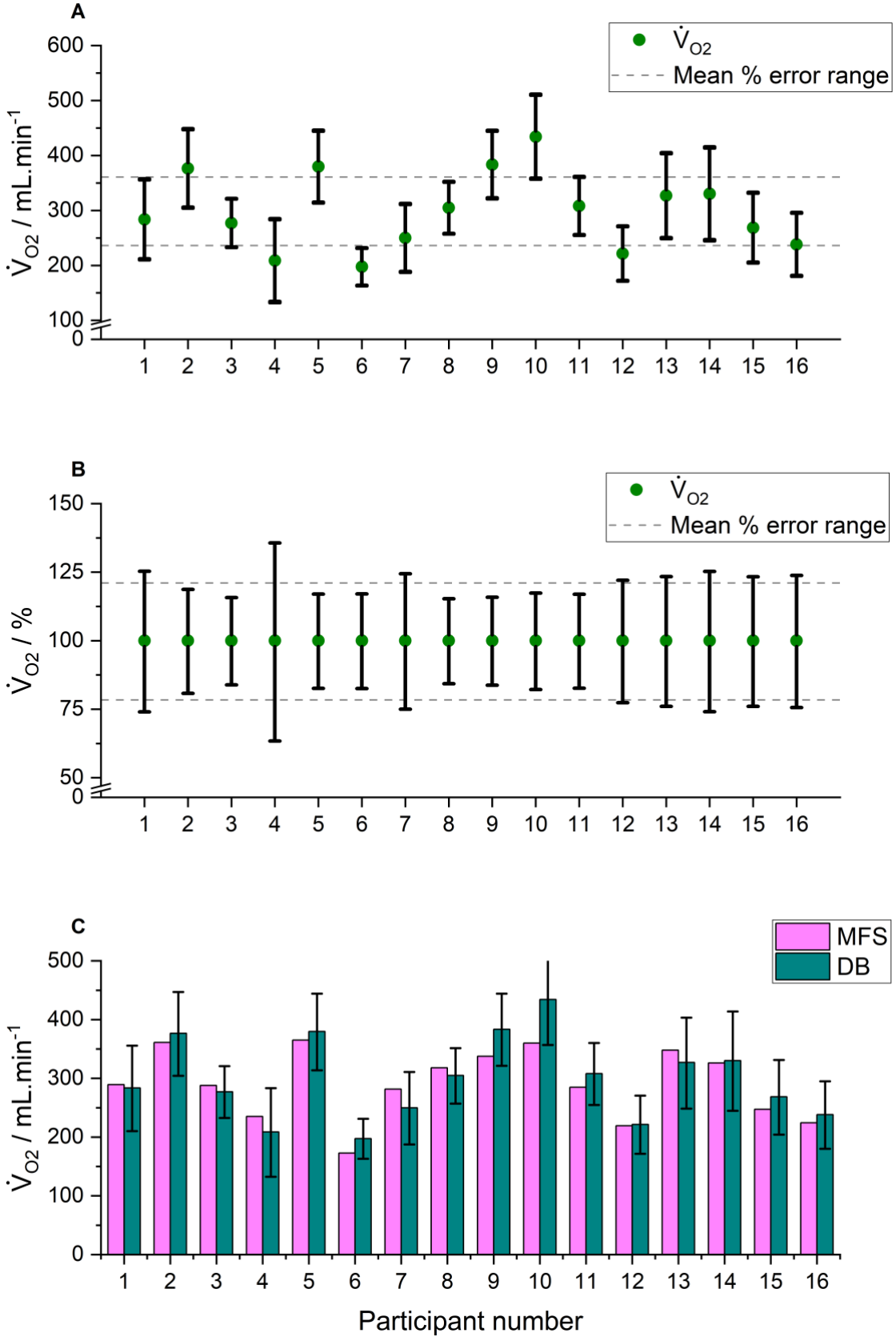

Figure 26. $\dot{V}_{O2}$ uncertainty in Douglas bag method introduced by measurement errors in F_{meO2}.

Each participant is represented individually on the x-axis. Panels A and B show $\dot{V}_{O2}$ (green dots) with corresponding error bars due to F_{meO2} uncertainty, expressed in absolute terms (mL.min^{-1}) and as a percentage of each participant's DB mean $\dot{V}_{O2}$, respectively. The grey dashed lines represent the mean uncertainty range around the mean $\dot{V}_{O2}$ across participants. Panel C shows a plot of $\dot{V}_{O2}$ values from the MFS and the DB, with error bars representing F_{meO2}-related uncertainty. The overlap of this uncertainty range with MFS-measured $\dot{V}_{O2}$ values could potentially account for all differences between the methods.

4.4. Discussion

4.4.1. Summary of findings

In spontaneously breathing participants, the MFS demonstrated a small mean bias in $\dot{V}_{O2}$ compared with the DB method, with a group-level mean difference of - 2%. The correlation between methods was excellent ($r = 0.92$, $p < 0.0001$), and the paired comparison showed no statistically significant difference in $\dot{V}_{O2}$ values ($t(15) = 1.204$, $p = 0.25$). Despite this, individual variability was notable. Eleven out of sixteen participants showed less than ± 8% difference relative to their mean DB $\dot{V}_{O2}$. The absolute bias was - 8 mL.min^{-1} (SD ± 27 mL.min^{-1}), and the 95% limits of agreement ranged from - 62 to + 45 mL.min^{-1}, corresponding to - 19% to + 15% in relative terms.

These findings provide a basis for evaluating how the MFS compares with existing commercial systems validated against the DB, particularly under resting conditions where relative variability can be more pronounced.

4.4.2. Comparison with prior studies at resting conditions

The DB method is regarded by the American Thoracic Society (ATS) as the gold standard for $\dot{V}_{O2}$ measurement[48] and it has been widely employed to validate emerging techniques,

both in spontaneously breathing and in mechanically ventilated individuals[42, 43, 154-156]. While the ATS outlines minimum performance criteria for gas analysers and volume measurement systems employed in the measurement of $\dot{V}_{O2}$ for cardiopulmonary exercise testing[48] (CPET), there are no such standards set out for the measurement of $\dot{V}_{O2}$ at rest. Additionally, there are no universal benchmarks to define what constitutes acceptable $\dot{V}_{O2}$ bias and LoA when comparing emerging techniques with the DB[157]. This has led to broad variation in reported performance metrics in the literature[157].

The low mean bias observed in this study (- 8 mL.min^{-1} or - 2%) is consistent with that reported for commercial devices validated against the DB method under resting conditions[154-156]. While the LoA in the present experiment were relatively wide, such variability is not unusual at low metabolic rates and has been observed across multiple validation studies in resting individuals.

Several studies illustrate this trend. *Nieman et al.* assessed 60 spontaneously breathing participants and reported a mean bias of + 2.83 mL.min^{-1} (+ 1.2%) when comparing the FitMate (Cosmed, Italy) system with the DB, with LoA ranging from - 20.0 to + 25.7 mL.min^{-1} (- 8.3% to + 10.6%)[154]. *Brehm et al.* compared the V_{max}ST breath-by-breath analyser (Sensormedics, Netherlands) with the DB in 10 individuals and found a $\dot{V}_{O2}$ bias of - 20 mL.min^{-1} (- 7.4%), with LoA from - 59 to + 19.2 mL.min^{-1} (- 21.9% to + 7.1%)[155]. *Crouter et al.* evaluated the COSMED K5 (Cosmed, Italy) in 15 participants and observed a bias of - 50 mL.min^{-1} (- 13.2%) using mixing chamber mode, with LoA from - 150 to 0 mL.min^{-1} (- 39.5% to 0%)[156]. In breath-by-breath mode, the bias improved to - 30 mL.min^{-1} (- 7.9%), but LoA still ranged widely from - 120 to + 20 mL.min^{-1} (- 34.2% to + 5.3%)[156].

These findings indicate that the agreement between the MFS and DB observed in the present study is within the expected range for $\dot{V}_{O2}$ measurements at rest, and that wide LoA is a common feature of method comparisons conducted under low metabolism conditions.

4.4.3. Accuracy of the Douglas bag method

While the DB remains the reference standard for measuring $\dot{V}_{O2}$, it is not without limitations[48]. Understanding these limitations is essential when considering agreement between the DB and the MFS. Measurement errors may originate not only from inaccuracies in gas analyser and volume meter readings, but also from practical and environmental factors such as incomplete bag emptying, gas diffusion, and inaccurate correction from ambient to standard conditions[51].

To mitigate these issues and ensure the highest possible measurement fidelity, several measures were taken in this study:

(i) Gas analyser accuracy: Errors in gas composition measurements can disproportionately affect calculated $\dot{V}_{O2}$. In this study, calibration of the gas analyser was performed using three precision gases: pure nitrogen, pure oxygen, and a calibration mixture containing 5% CO_2, 55% O_2, and 40% N_2O. For CO_2, the largest observed deviation was 0.1%. For O_2, the analyser consistently reported 99% when exposed to pure oxygen. Although this value falls within the manufacturer's specified accuracy limits, it likely reflects the display's limited resolution, as the device only reports oxygen concentrations to the nearest whole percent. As a result, even a true concentration of 99.999% would be displayed as either 99% or 100%, introducing an apparent absolute deviation of nearly 1% if rounded down rather than up.

(ii) Gas meter accuracy: As $\dot{V}_{O2}$ calculations using the DB depend on expired volume and the Haldane transformation to infer inspired volume, any bias in volume measurement proportionally affects $\dot{V}_{O2}$. The dry gas meter used in this study was calibrated using a 3 L syringe over three 30 L injections and demonstrated a consistent underreading of 0.33%. This is within the manufacturer's specified accuracy of ± 1.5%, consistent with ATS recommendations[48] (for CPET).

(iii) Residual volume minimisation: Incomplete emptying of the DB can introduce significant error[51]. To prevent this, a unidirectional fan system was developed in-house to facilitate full evacuation of the bag, eliminating the variability associated with manual emptying.

(iv) Leakage and diffusion control: To limit the diffusion of gases from the bag over time, a PVC bag – known for low permeability – was used. Bags were filled to no more than two-thirds capacity to minimise internal pressure gradients, and gas analysis was conducted immediately after collection. These precautions are consistent with previous evidence suggesting that if analysed within fifteen minutes, composition changes due to leakage are negligible[158].

(v) Environmental inputs (pressure and temperature): Barometric pressure and ambient temperature were measured at the time of each experiment to ensure accurate STPD corrections, rather than relying on assumed or average values.

(vi) Humidity correction: Neglecting the assessment of P_{H2O} significantly affects $\dot{V}_{O2}$ estimates, introducing errors as high as 25%[159]. The use of an HME filter meant expired gas collected in the DB could not be assumed to be fully saturated. To account for this, the P_{H2O} was estimated from simultaneous MFS data and incorporated into the dry gas calculations.

Despite these precautions, some degree of error – systematic or random – may persist. Measurement of $\dot{V}_{O2}$ using the DB system remains inherently sensitive to a range of small, compounding inaccuracies[43]. Therefore, when interpreting limits of agreement between DB and MFS, the potential limitations of the reference method itself must also be acknowledged[160].

4.4.4. Limitations

A key limitation of this study lies in the reported accuracy of the gas analyser used to determine the composition of mixed expired gas in the DB system. According to the manufacturer, the analyser has an accuracy of ± 2.5 vol% (absolute) plus an additional ± 2.5% relative error for oxygen measurements. This level of inaccuracy is substantially higher than the minimum performance criteria recommended by the ATS for gas exchange analysers used in CPET, where ± 1% error is expected[48]. While the ATS standards were developed for dynamic exercise measurements rather than resting conditions, the discrepancy remains too large to ignore, particularly given the sensitivity of $\dot{V}_{O2}$ calculations to small changes in oxygen concentration.

As proposed by *Critchley and Critchley*, the expected agreement between two measurement methods should reflect the combined uncertainty of each system, calculated using the root-sum-of-squares (RSS) of their respective accuracies[161]. Using this approach, we estimated that the DB, based on ATS tolerances (± 1% for O_2; ± 1% for CO_2; ± 3% for volume), would contribute an overall $\dot{V}_{O2}$ uncertainty of ± 5.22% in this cohort's dataset. For the MFS, estimating $\dot{V}_{O2}$ error is substantially more complex. A rigorous sensitivity analysis would require evaluating the compounding contribution of each inspired and expired gas species and flow, along with the effects of pressure, temperature, density, and viscosity on $\dot{V}_{O2}$ calculations. For simplicity, this analysis assumed that $\dot{V}_{O2}$ error ($err\dot{V}_{O2}$) was

proportional to the product of nitrogen balance ($\dot{V}_{N2}$) and the ratio of the fractions of inspired oxygen and nitrogen, as given by the following equation:

$$err\dot{V}_{O2} = \frac{FiO_2}{FiN_2} \times \dot{V}_{N2}$$

Based on this approach, the estimated MFS $\dot{V}_{O2}$ error was ± 1.59%. When combined via RSS, the predicted SD between DB and MFS should therefore fall within approximately ± 5.46%. Therefore, the expected LoA range would be ± 10.70% from the bias, with a total width of 21.40%.

However, the observed LoA spread was wider (34% width), corresponding to a ± 17% dispersion around the bias. The poor performance of the gas analyser in O_2 measurements relative to ATS benchmarks[48] is particularly concerning. Sensitivity analyses showed that the reported inaccuracy of the analyser for O_2 could translate into a standalone $\dot{V}_{O2}$ error of ± 21%, even when CO_2 and volume errors are excluded. Regrettably, this single factor could largely explain the width of the LoA observed in the present data.

Nevertheless, it should be noted that calibration results did not support such a poor level of performance. Deviations from known precision gas mixtures were relatively small, and it is possible that the manufacturer reported a worst-case specification to remain conservative. If the true analyser performance was better than stated, the actual error contribution would be smaller than the theoretical ± 21%. Still, this uncertainty complicates the interpretation of the findings. It does not invalidate the results, but it limits the extent to which the observed LoA can be attributed to the performance of the MFS or DB.

Assuming both the gas analyser and volume meter used in DB systems – as well as in any commercial metabolic device being validated against the DB – perform according to ATS standards[48], the maximum expected SD between methods would be approximately 7.38% (LoA range of 28.94%), based on combined uncertainty. Interestingly, however, only one of the validation studies we reviewed involving resting individuals reported LoA within this range when comparing these systems with the DB[154]. This suggests that even under ideal performance assumptions, additional sources of variability likely influence the agreement in real-world settings.

The observed discrepancy strongly suggests the influence of additional sources of random error beyond those accounted for by volume and concentration inaccuracies. For the MFS in comparison with the DB, the additional potential contributors to errors are summarised in Table 5.

Source of error	Type of error	Method affected	$\dot{V}_{O2}$ impact	Description
Timing mismatch (three-way valve opening and closing)	Operational	Both	Moderate	Slight delays or inconsistencies in switching between collection modes can desynchronize measurement periods, especially if breathing is variable.
Barometric pressure / temperature drifts	Environmental	DB	Low	Minor environmental changes during measurement can affect the accuracy of gas volume conversions to standard conditions.
Breath variability / postural change	Biological	Both	Moderate	Natural fluctuations in breathing pattern or body movement can transiently alter metabolic rate and ventilation, influencing $\dot{V}_{O2}$ readings.
Residual gas effects	Technical	DB	Low	Incomplete emptying of the DB may skew volume quantification.
Dead space effects	Technical	DB	Moderate	Rebreathing from system dead space may contaminate the gas sample and skew composition data
Methodological differences in $\dot{V}_{O2}$ calculation	Technical	Both	Low	Differences in how each method derives $\dot{V}_{O2}$ – e.g., end-expiratory volume regression fitting over time versus Haldane transformation with total volume-based averaging – can lead to discrepancies even with identical raw data.
P_{H2O} inconsistency	Technical	DB	Moderate	The assumption of P_{H2O} in DB to be equal of that measured by the MFS reduces this source of error, although it introduces mathematical coupling. However, the extent to which the gas analyser employed for DB readings dries the sample due to the presence of an integrated humidity filter is unknown. Inaccurate water vapour correction may lead to errors in converting gas volumes to dry conditions, particularly in DB calculations.

Table 5. Sources of random error in $\dot{V}_{O2}$ measurement.

Multiple sources of error can compromise the measurements of $\dot{V}_{O2}$ to varying extents.

Overall, the limitations discussed here highlight both the challenges in achieving accurate $\dot{V}_{O2}$ measurement and the vital importance of considering the accuracy of the reference system itself. The large observed LoA are likely the result of a combination of factors –

most notably, the high reported inaccuracy of the oxygen analyser used with the DB approach. However, additional sources of error, both technical and biological, likely contributed to the variability. These factors do not undermine the overall findings, but they do place necessary boundaries on how confidently method agreement can be interpreted. A more precise reference system and tighter environmental control may be required in future studies to determine the performance of the MFS with greater certainty.

4.5. Conclusion

This study represents the first direct comparison between the MFS and the DB method for measuring $\dot{V}_{O2}$ in spontaneously breathing healthy individuals at rest. Despite the known limitations of the reference method and the wide limits of agreement observed – which are consistent with those reported in similar physiological conditions – the MFS demonstrated low bias and overall good agreement with the DB.

These findings provide a basis for more challenging investigations. In particular, the use of MFS to achieve accurate data in mechanically ventilated patients, where measurement complexity is markedly increased. Subsequent studies in this thesis – described in Chapter 5 – will explore the utility of the device under those conditions, including its potential to detect clinically meaningful trends in $\dot{V}_{O2}$ over time in real-world critical care settings.

Chapter 5. An exploration of $\dot{V}_{O2}$ measurements generated by the MFS in critically ill patients

5.1. Introduction

Measurement of $\dot{V}_{O2}$ could provide clinicians with an index of the global adequacy of tissue oxygen utilisation. In the context of critical care, such assessments might facilitate evaluation of metabolic demand, guide therapeutic decision-making, and enable longitudinal monitoring of physiological trends. As previously discussed in Chapter 1, despite their potential clinical utility, $\dot{V}_{O2}$ measurements remain challenging to obtain in mechanically ventilated patients, a population for whom such data might be particularly valuable.

To date, the performance of the MFS for measuring $\dot{V}_{O2}$ in mechanically ventilated patients has not been comprehensively assessed. In addition, no studies to date have investigated the longitudinal reliability of its $\dot{V}_{O2}$ measurements in critically ill patients.

5.2. Research aims and objectives

The primary aim of this chapter was to evaluate the performance of the MFS for the measurement of $\dot{V}_{O2}$ in mechanically ventilated, critically ill patients.

To achieve this, several studies were conducted, setting out to: (i) assess the accuracy of MFS-derived $\dot{V}_{O2}$ measurements in mechanically ventilated patients in terms of systematic error (bias) and random error (imprecision); (ii) explore the feasibility and clinical application of longitudinal $\dot{V}_{O2}$ monitoring by the MFS in critical care.

5.3. Methods

5.3.1. Ethical approval

The study was approved by South Central – Oxford C Research Ethics Committee, reference 22/SC/0127. Of relevance to the experiments conducted in this thesis, ethics approval permitted the following: (i) recruitment of mechanically ventilated adult ICU patients with respiratory failure using consultee agreement under the Mental Capacity Act; (ii) insertion of the MFS into the ventilator circuit with data recording for up to twelve hours, involving brief disconnection from mechanical ventilator and adjustment of ventilation to compensate for instrumental dead space; (iii) brief and clinically safe changes in FiO_2 and end-tidal CO_2 to enable physiological measurements; (iv) transient interruption of active humidification and alternative utilisation of an HME filter for the duration of MFS connection; (v) access to routine clinical blood tests and monitoring data, with no additional sampling performed for research purposes; (vi) acquisition of data before and after quasistatic pressure-volume curves, before and after recruitment manoeuvres, and

throughout periods when no intervention is being conducted. Study synopsis can be found in Appendix A.

All practices were conducted in conformity with the general principles of the Declaration of Helsinki, the guidelines for Good Clinical Practice (GCP), and the UK General Data Protection Regulation (GDPR).

5.3.2. Patient recruitment

Recruitment took place at the Intensive Care Unit of the Royal Berkshire Hospital. Suitable patients were identified to the research team by the clinical team responsible for the patient. This observational cross-sectional study enrolled critically ill adults receiving mechanical ventilation via endotracheal tube according to the criteria below.

(i) Inclusion criteria:

   a. Male and female, aged 18 years or above;

   b. Receiving mechanical ventilation via an endotracheal tube on ICU.

(ii) Exclusion criteria:

   a. Consultee indicates patient would be likely to decline enrolment;

   b. Patient is receiving palliative care;

   c. Language barriers prevent sufficiently good communication with patient or consultee.

5.3.3. Informed consent

Potential patients were unable to give informed consent at the time of enrolment due to alterations in consciousness caused by illness, therapeutic sedation – which is necessary to facilitate mechanical ventilation – or both. Practice was therefore directed by the Mental

Capacity Act 2005. Assent was sought from an appropriate consultee, either in person or by telephone, to determine if the prospective patient would likely have agreed to participate. If no personal consultee was available, a professional consultee, independent of the treating and study teams, was approached. Patients were only enrolled if a consultee was available and believed that they would have agreed to take part in research; otherwise, they were not included.

Patients who survived and regained capacity during their hospital stay were approached on the ward – following discharge from ICU. The study was explained, and retrospective consent was sought to confirm their agreement for the use of data already collected. If a patient declined, their data were deleted, and they were withdrawn from the study. In cases where a patient died or did not regain capacity before hospital discharge, previously collected data were retained for analyses, as per consultee's original assent.

5.3.4. Instrumental setup

Patients were connected to the MFS measurement head via an endotracheal tube. An HME filter was interposed between the MFS and the endotracheal tube to prevent cross-contamination and to ensure heat and moisture provision to the airways in view of upper airway bypass and dry gas supply. All patients were receiving active humidification prior to enrolment in the study, and had it discontinued before in-line insertion of the HME filter. Additional critical care devices such as the flow sensor, capnography, and closed suctioning system were placed in between the MFS and the HME filter. A brief pause in mechanical ventilation was necessary to enable connection and disconnection of the MFS. During this time, lasting only a few seconds, the ventilator circuit was transiently opened. The MFS-HME system utilised introduced approximately an additional 100 mL of

apparatus dead space into the ventilator circuit. This was compensated for by adjusting ventilator settings slightly to increase minute volume.

The initial position of the patient was dorsal decubitus with head up at 30 degrees. A mechanical ventilator circuit was connected to the back of the MFS providing the patient with a known flow and concentration of gas (Figure 27). Monitoring was conducted in accordance with the patient's needs and dictated by the responsible medical team. At a minimum, patients were under continuous cardiovascular monitoring (electrocardiography and invasive blood pressure assessment), capnography, and pulse oximetry.

Each patient had the MFS connected into their ventilator circuit for a maximum of 12 hours. During this period, parameters of interest were measured utilising the MFS, the electronic clinical record (ECR), and the case report form (CRF).

Figure 27. Instrumental setup in mechanically ventilated patients.

Mechanically ventilated patient connected to the MFS head by an endotracheal tube with an HME filter interposed. Suction system, ventilator flow sensor, and capnography are placed in between the filter and the tube. The mechanical ventilator circuit is connected to the back of the MFS head.

5.3.4.1. MFS warm-up and calibration

These processes were described in detail in section 4.2.4.1. Two differences should be noted when conducting warm-up and calibration in mechanically ventilated patients: (i) as this cohort of subjects were receiving active humidification at 37°C (ventilator circuit y-piece temperature) prior to MFS attachment, an increase by 2°C from this baseline was deemed necessary to reduce the risk of residual condensation; (ii) the procedures were repeated after each individual patient as opposed to once a day.

5.3.5. Experimental protocol

5.3.5.1. Data recording: Electronic Clinical Record

Variables likely to affect $\dot{V}_{O2}$ in critically ill patients were prospectively identified by reviewing the literature. These included, but were not restricted to: FiO_2, body temperature, bolus fluids, vasopressor and inotropic drugs, feeding, sedation, neuromuscular blockade, renal replacement therapy, changes in haemoglobin concentration, physical activity (e.g., physiotherapy), surgical procedures, and mode of ventilation. These variables were monitored throughout the period of MFS connection and recorded in the patients' ECR as part of routine clinical care. Additional notes were entered in the CRF to ensure optimal time alignment between the occurrence of interventions which could potentially change $\dot{V}_{O2}$ and their documentation.

5.3.5.2. Data recording: Molecular Flow Sensor

Gas exchange trends for $\dot{V}_{O2}$, $\dot{V}_{CO2}$, $\dot{V}_{N2}$, and $\dot{V}_{H2O}$ were displayed on the MFS laptop controller in real time and were also recorded for retrospective analysis. Table 6 shows the parameters that were recorded by the MFS during the period of attachment.

MFS-recorded parameters		Units
$\dot{V}_{O2}$	Oxygen consumption	mL.min^{-1} (STP)
$\dot{V}_{CO2}$	Carbon dioxide production	mL.min^{-1} (STP)
$\dot{V}_{H2O}$	Water vapour production	mL.min^{-1} (STP)
$\dot{V}_{N2}$	Nitrogen balance*	mL.min^{-1} (STP)
F_{O2}	Fraction of oxygen, inspired and expired, dry	N/A
F_{CO2}	Fraction of carbon dioxide, inspired and expired, dry	N/A
F_{N2}	Fraction of nitrogen, inspired and expired, inspired and expired, dry	N/A
P_{H2O}	Partial pressure of water vapour, inspired and expired	kPa (STP)
C_{O2}	Molar concentration of oxygen, inspired and expired	mol.L^{-1}
C_{CO2}	Molar concentration of carbon dioxide, inspired and expired	mol.L^{-1}
C_{H2O}	Molar concentration of water, inspired and expired	mol.L^{-1}
C_{N2}	Molar concentration of nitrogen, inspired and expired	mol.L^{-1}
$C_{VOL}(O_2)$	Cumulative uptake of oxygen over time	L (STP)
$C_{VOL}(CO_2)$	Cumulative uptake of carbon dioxide over time	L (STP)
$C_{VOL}(H_2O)$	Cumulative uptake of water vapour over time	L (STP)
$C_{VOL}(N_2)$	Cumulative uptake of nitrogen over time	L (STP)
P	Airway pressure – throughout the respiratory cycle	kPa
T	Gas temperature	°C
$\dot{V}$	Total gas flow, inspired and expired	L.min^{-1}

Table 6. Parameters recorded by the MFS.

The MFS measures the molar concentration of respired gases and their flows, taking into consideration ambient pressure and temperature, in addition to gas density and viscosity. Gas concentrations are then converted into fractions of the total respired gas. Variables listed on the table above were continuously recorded by the MFS. STP = standard temperature (0°C) and pressure (101.325 kPa); N/A = not applicable; *a positive sign indicates apparent nitrogen uptake.

5.3.6. Accuracy studies

5.3.6.1. $\dot{V}_{O2}$ time series construction

Careful consideration was given to selectively including stable, sedated patients, whose $\dot{V}_{O2}$ and lung volumes were likely to remain relatively steady for the duration of the study.

As $\dot{V}_{O2}$ naturally fluctuates over time, even in resting healthy individuals, a secondary time series was retrospectively derived from the original MFS data to support reproducibility assessments. This was achieved by fitting regression lines to the end-expiratory cumulative volume of oxygen over a period of 3 minutes at approximately 30-minute intervals (Figure 28). These 3-minute averages of gas exchange rates – obtained for both for $\dot{V}_{O2}$ and $\dot{V}_{N2}$ – were utilised for statistical analyses and plot construction.

To minimise the influence of external disturbances on these measurements, care was taken to ensure that the 5 minutes preceding each intended averaging period were free from any clinical interventions. If any procedure occurred during this time – such as repositioning, medication administration, blood sampling, or flushing of lines or feeding tubes – the measurement window was postponed. A new 5-minute period of clinical inactivity was required before resuming the averaging period.

After the construction of the $\dot{V}_{O2}$ time series, ECR variables and CRF notes were retrospectively reviewed for associations between changes in variables known to affect $\dot{V}_{O2}$ and significant shifts in gas exchange trends. If a change in any of these variables appeared to cause a sustained alteration in $\dot{V}_{O2}$ across specific averaging periods – but not others – those data were flagged for further review and potential exclusion from analysis.

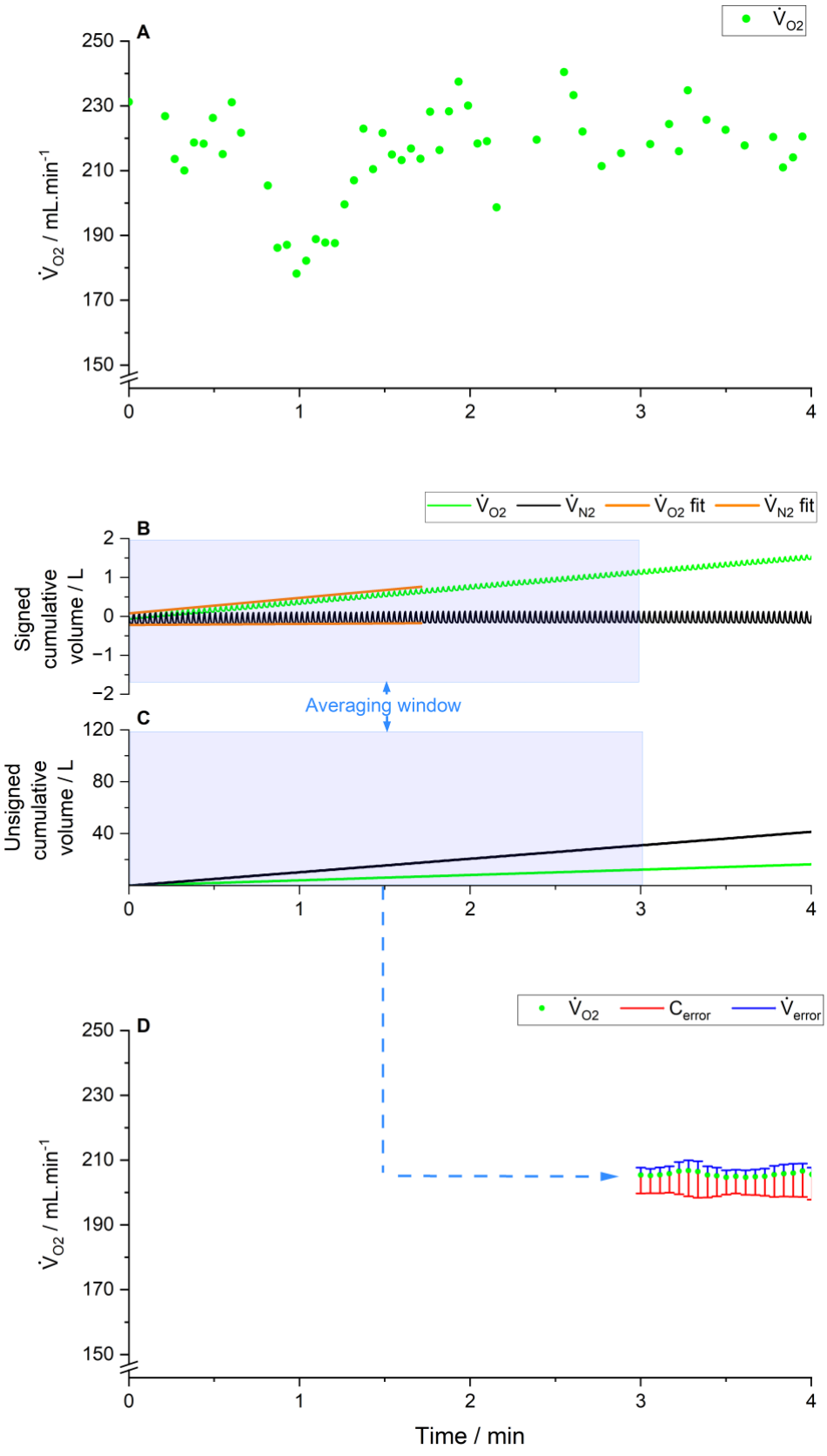

Figure 28. Calculation of $\dot{V}_{O2}$ by the MFS and $\dot{V}_{O2}$ timeline example.

$\dot{V}_{O2}$ was calculated as the slope of the regression line fitted to the end-expiratory cumulative volume of oxygen over time. This method smoothes $\dot{V}_{O2}$ fluctuations and allows a more representative value of $\dot{V}_{O2}$ to be obtained during the 3-minute averaging window. The same method was used to obtain the average $\dot{V}_{N2}$. Panel A: Untreated breath-by-breath $\dot{V}_{O2}$ measurements recorded over 4 minutes. Panel B: Regression line fitted over 3-minute window to obtain average $\dot{V}_{O2}$ and $\dot{V}_{N2}$. Oxygen was being consumed (upward trend of cumulative volume; positive sign), while nitrogen remained near zero (straight line of cumulative volume). Panel C: Total cumulative volumes of oxygen and nitrogen passing through the MFS over the specified period of time. The total amount of oxygen inhaled and exhaled was far greater than the volume of oxygen consumed by the body. Panel D: Example of $\dot{V}_{O2}$ timeline as displayed on the MFS laptop controller screen during the period of patient connection. Each green dot represents a 3-minute rolling average of $\dot{V}_{O2}$. The first $\dot{V}_{O2}$ measurement represents the average of the preceding 3 minutes, highlighted as the averaging window in panels B and C. Each $\dot{V}_{O2}$ average is accompanied by a confidence interval, estimated from nitrogen balance with subcomponents of concentration (in red) and flow (in blue) errors.

5.3.6.2. Estimating $\dot{V}_{O2}$ accuracy from $\dot{V}_{N2}$

There is no reference standard against which to determine the absolute accuracy of the $\dot{V}_{O2}$ measurements. In this work, nitrogen balance, as calculated by the MFS, was used as an internal reference to assess the accuracy of $\dot{V}_{O2}$ measurements. As discussed in section 3.2.4, nitrogen is considered a physiologically inert gas and should neither be consumed nor produced by the body under normal conditions. Therefore, in the absence of measurement errors and in the absence of ongoing adjustments in lung stores, $\dot{V}_{N2}$ should equal zero. Any deviation from zero indicates a measurement bias, which may arise from inaccuracies in flow measurement or in the determination of inspired and expired gas concentrations. Based on this principle, deviations in $\dot{V}_{N2}$ can serve as an internal consistency check, offering an estimate of $\dot{V}_{O2}$ measurement accuracy.

This section explores the relationship between errors in the measurement $\dot{V}_{O2}$ and the corresponding errors induced in the measurement of $\dot{V}_{N2}$ (i.e., the amount by which $\dot{V}_{N2}$ deviates from zero), with the intent of using these relationships to define the likely maximum absolute error in the measurement of $\dot{V}_{O2}$.

The MFS calculates $\dot{V}_{O2}$ by integrating the product of flow ($\dot{V}$) – which alternates in sign according to the direction of flow – and the molar concentration of oxygen (C_{O2}) over time (L):

$$\dot{V}_{O2} = \frac{1}{L}\int_0^L \dot{V}.C_{O2}dt$$

$\dot{V}_{N2}$ is calculated in the same way, but using molar concentration of nitrogen (C_{N2}):

$$\dot{V}_{N2} = \frac{1}{L}\int_0^L \dot{V}.C_{N2}dt$$

C_{N2} is not measured directly. Instead, it is calculated by subtracting the measured O_2, CO_2, and H_2O vapour concentrations from the total molar gas content at a given pressure (P) and temperature (T):

$$C_{N2} = \frac{P}{RT} - C_{O2} - C_{CO2} - C_{H2O}$$

where R is the ideal gas constant, C_{CO2} is the molar concentration of CO_2, and C_{H2O} is the molar concentration of H_2O vapour. The measurements for P, T, $\dot{V}$, C_{O2}, C_{CO2} and C_{H2O} are all made simultaneously by the MFS.

From the equations above, two important relationships emerge between errors in $\dot{V}_{O2}$ and $\dot{V}_{N2}$, depending on the source of error:

1) If the error in $\dot{V}_{O2}$, $err\dot{V}_{O2}$, arises from inaccuracies in C_{O2}, then the corresponding error in $\dot{V}_{N2}$ will be equal in magnitude but opposite in sign:

$$\dot{V}_{N2} = -\, err\dot{V}_{O2}$$

2) If the error in $\dot{V}_{O2}$ arises from inaccuracies in $\dot{V}$ measurement, then the error in $\dot{V}_{N2}$ will be proportional to the error in $\dot{V}_{O2}$:

$$\dot{V}_{N2} = \gamma . err\dot{V}_{O2}$$

where γ is the ratio between the total unsigned flow of N_2 and the total unsigned flow of O_2 through the sensor. γ cannot be known precisely, as this ratio will vary somewhat through the respiratory cycle, but it may be approximated by:

$$\gamma \approx \int_0^L |\dot{V}| C_{N2} dt \Big/ \int_0^L |\dot{V}| C_{O2} dt$$

Apart from measurement errors in C_{O2} and $\dot{V}$, there may also be measurement errors in P, T, C_{CO2} and C_{H2O}. These will induce further direct errors into the measurement of $\dot{V}_{N2}$, but not $\dot{V}_{O2}$. Indirectly, however, they may contribute to further error in the measurement of C_{O2} and $\dot{V}$. For C_{O2}, there will be a small effect of error in T on the spectral measurement of O_2. For $\dot{V}$, errors in P, T, C_{CO2} and C_{H2O} will to some degree affect the calculated values for viscosity and density that are used in the calculation of flow from pressure drop across the pneumotachograph. Thus, it is not possible to calculate the exact error in $\dot{V}_{O2}$ from the deviation of $\dot{V}_{N2}$ from zero because the relationship between the two depends on how the errors arise. Nevertheless, a small error in $\dot{V}_{N2}$ indicate that the error in $\dot{V}_{O2}$ will also be

small, and that the true value for $\dot{V}_{O2}$ can reasonably be expected to lie between the limits ($\dot{V}_{O2} - \dot{V}_{N2}$) and ($\dot{V}_{O2} + \dot{V}_{N2} / \gamma$). These are limits that can be determined at the same time as measurements of $\dot{V}_{O2}$ are made, providing a range of uncertainty for the $\dot{V}_{O2}$ result.

For simplicity, and as will be used throughout the remainder of this thesis, the error in $\dot{V}_{O2}$ caused by inaccuracies in C_{O2} is referred to as C_{error} ($C_{error} = - \dot{V}_{N2}$), while the error due to $\dot{V}$ measurement is referred to as $\dot{V}_{error}$ ($\dot{V}_{error} = \dot{V}_{N2} / \gamma$).

5.3.7. Statistical analyses

To evaluate the accuracy of $\dot{V}_{O2}$ measurements obtained using the MFS, we estimated systematic errors associated with flow and concentration measurements separately for each 3-minute $\dot{V}_{O2}$ average. Each average was sampled during a steady state period, approximately 30 minutes apart from each other, over several hours. The systematic errors were then used to build a confidence interval around each patient's mean $\dot{V}_{O2}$, with the upper and lower bounds defined by the average of all positive and negative errors, respectively. This approach allowed for an internal assessment of measurement accuracy in the absence of an external gold standard.

Statistical analyses were performed utilising SPSS version 30.0 (IBM Corp., USA), with significance established at $p < 0.05$.

To assess the variability of $\dot{V}_{O2}$ over time, descriptive statistics were calculated, including the mean and SD for each subject. The precision of $\dot{V}_{O2}$ measurements by the MFS over time was assessed using the coefficient of variation (CV), computed by dividing the SD by the mean $\dot{V}_{O2}$ for each individual and expressed as a percentage. This provided a normalised measure of intra-individual variability in $\dot{V}_{O2}$ across repeated assessments.

A one-way analysis of variance (ANOVA) was conducted to partition the total $\dot{V}_{O2}$ variance into between- and within-subject components. While multiple $\dot{V}_{O2}$ measurements were collected per patient, the analysis was not intended to model the effect of time or to assess within-subject correlations. Instead, patient identity was treated as a grouping factor to obtain the proportion of variability attributable to inter-individual differences versus intra-individual fluctuations across repeated measurements. From the resulting variance components, an intraclass correlation coefficient (ICC) was calculated to quantify the proportion of total variability in $\dot{V}_{O2}$ that was explained by differences between patients:

$$ICC = \frac{\sigma^2_{between}}{\sigma^2_{between} + \sigma^2_{within}}$$

where $\sigma^2_{between}$ is the variance in $\dot{V}_{O2}$ between subjects (captured by the mean squared error between subjects), and σ^2_{within} reflects the variance within subjects across repeated measurements.

5.4. Results

5.4.1. Baseline characteristics of patients in accuracy studies

Eighteen mechanically ventilated patients were studied. Three patients were excluded from the analysis due to missing data (n=2) or not meeting quality control criteria ($\dot{V}_{N2}$ > 60 mL.min^{-1}; n=1). A CONSORT-like diagram outlining the flow of patients across all studies in mechanically ventilated patients is available in Appendix B. Fifteen mechanically ventilated patients were retained for analysis and will be discussed in the following sections.

All patients were receiving therapeutic sedation, though the drug choice, the rate of infusion, and the depth of sedation varied significantly across the cohort. Two thirds of the patients were male, and the average age on recruitment was 56 years. Over 50% of the patients required at least one vasoactive drug to achieve a clinically targeted mean arterial blood pressure of 65 mmHg. The fraction of inspired oxygen with which the patients were ventilated varied from 0.21 to 0.40. Only 40% of the patients had been discharged home at 28 days following hospital admission. Relevant demographic and clinical characteristics are outlined in Table 7.

ID	Age / yr	Sex	Height / m	Weight / kg	LBM / kg	NMB	VD	RRT	Fever	FiO_2	Clinical condition	28-day outcome
17	45	M	1.85	82.0	60.6	N	Y	N	N	0.30	Pneumonia	DH
18	78	F	1.66	71.5	36.4	N	Y	N	Y	0.24 to 0.25	Liver abscess	Died
19	72	M	1.80	80.0	52.0	N	N	N	N	0.25	Post ROSC	ICU
20	43	F	1.62	72.0	42.9	N	N	Y	N	0.40	Hepatic encephalopathy	ICU
21	52	F	1.52	83.0	39.2	N	Y	N	N	0.21 to 0.30	Polypharmacy overdose	DH
22	64	M	1.70	127.7	56.2	N	Y	N	Y	0.21	Status epilepticus	Died
23	58	M	1.70	83.0	53.4	N	N	N	N	0.21	Delirium tremens	ICU
24	67	M	1.70	89.0	52.6	N	Y	N	N	0.21 to 0.30	Post ROSC	DH
25	66	M	1.78	67.0	47.1	N	N	N	N	0.25	Infective COPD exacerbation	DH
26	36	M	1.75	120.0	70.1	Y	N	N	CD	0.21 to 0.25	Post ROSC	Died
27	30	M	1.90	82.5	65.8	N	N	N	N	0.21	Delirium tremens	DH
28	52	F	1.58	51.8	33.6	N	Y	N	N	0.21	Intracranial haemorrhage	DW
29	52	F	1.70	114.0	48.4	N	Y	N	N	0.21	Symptomatic hyponatraemia	DW
30	52	M	1.63	112.0	56.0	N	Y	N	N	0.30	Urosepsis	Died
31	79	M	1.77	104.0	54.8	N	Y	N	N	0.21	Biliary sepsis	DH

Table 7. Patient characteristics on enrolment.

ID = patient identification number; M = male; F = female; N = no; Y = yes; NMB = neuromuscular blockade; VD = vasoactive drug; RRT = renal replacement therapy; CD = cooling device; FiO_2 = fraction of inspired oxygen; ROSC = return of spontaneous circulation following in- or out-of-hospital cardiac arrest; DH = discharged home; DW = discharged to hospital ward; ICU = remained as an ICU inpatient.

5.4.2. Accuracy

Each of the fifteen patients recruited completed between six and ten 3-minute $\dot{V}_{O2}$ averages during a minimum of three hours of continuous MFS monitoring. For every $\dot{V}_{O2}$ averaging window, potential sources of systematic measurement errors arising from inaccuracies in flow ($\dot{V}_{error}$) and gas concentration (C_{error}) measurements were estimated using the corresponding $\dot{V}_{N2}$ values.

Individual $\dot{V}_{O2}$ time series are displayed in Figure 29 to Figure 31. These figures present $\dot{V}_{O2}$ and associated errors as: (1) absolute values ($mL.min^{-1}$), (2) values normalised by lean body mass ($mL.min^{-1}.kg^{-1}$), and (3) percentages relative to each patient's mean $\dot{V}_{O2}$. Each time series is composed of 3-minute averages of $\dot{V}_{O2}$ (black dots), taken approximately every thirty minutes. Error bars indicate the estimated uncertainty in $\dot{V}_{O2}$ due to inaccuracies in concentration (in red) and flow measurement (in blue). The dashed grey lines represent ± 2 SD from the individual's mean $\dot{V}_{O2}$, calculated across all timepoints. Patients are numerically identified from 17 to 31.

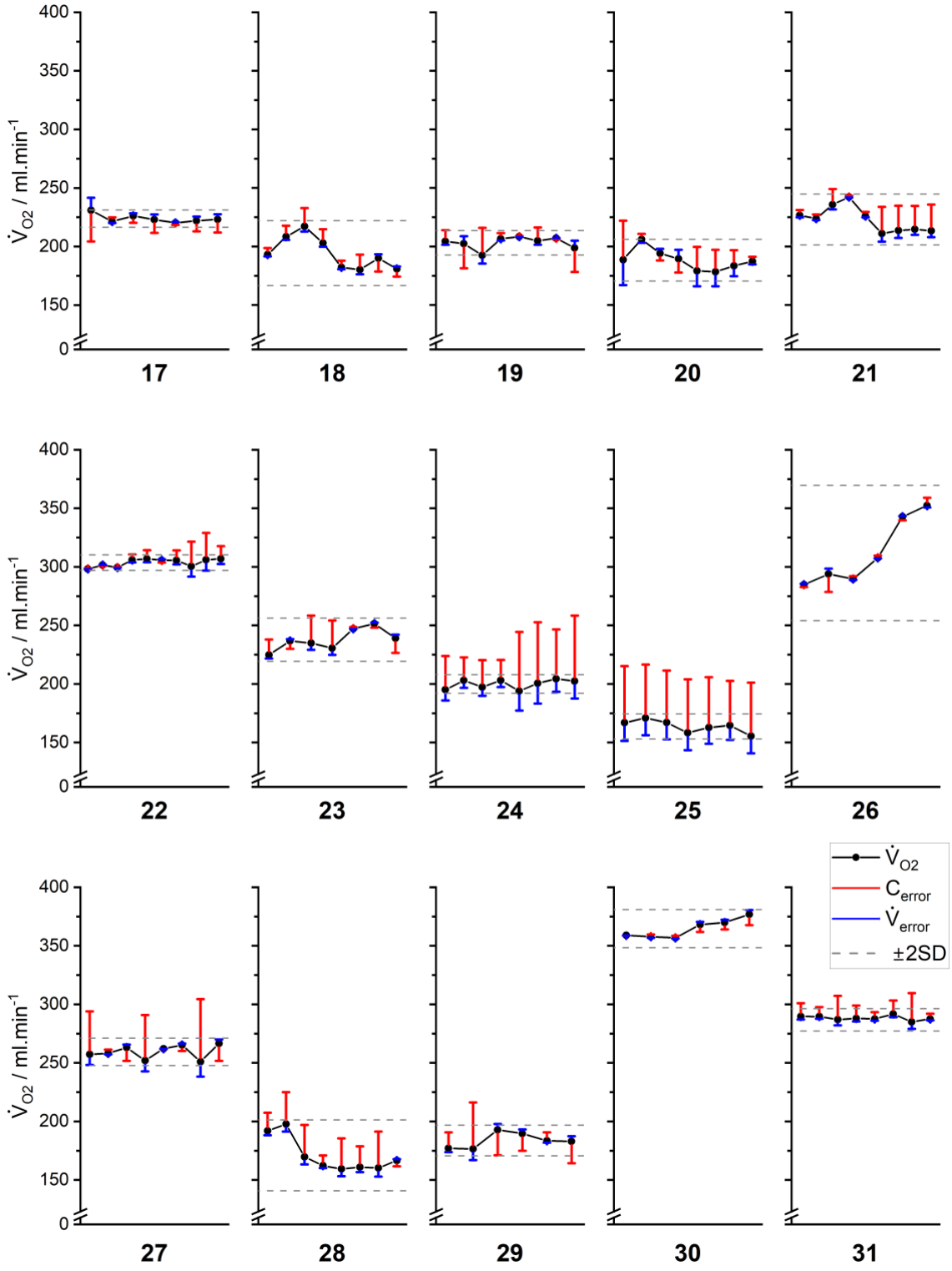

Figure 29. Individual time series of MFS-derived oxygen consumption measurements. $\dot{V}_{O2}$ and errors are absolute values.

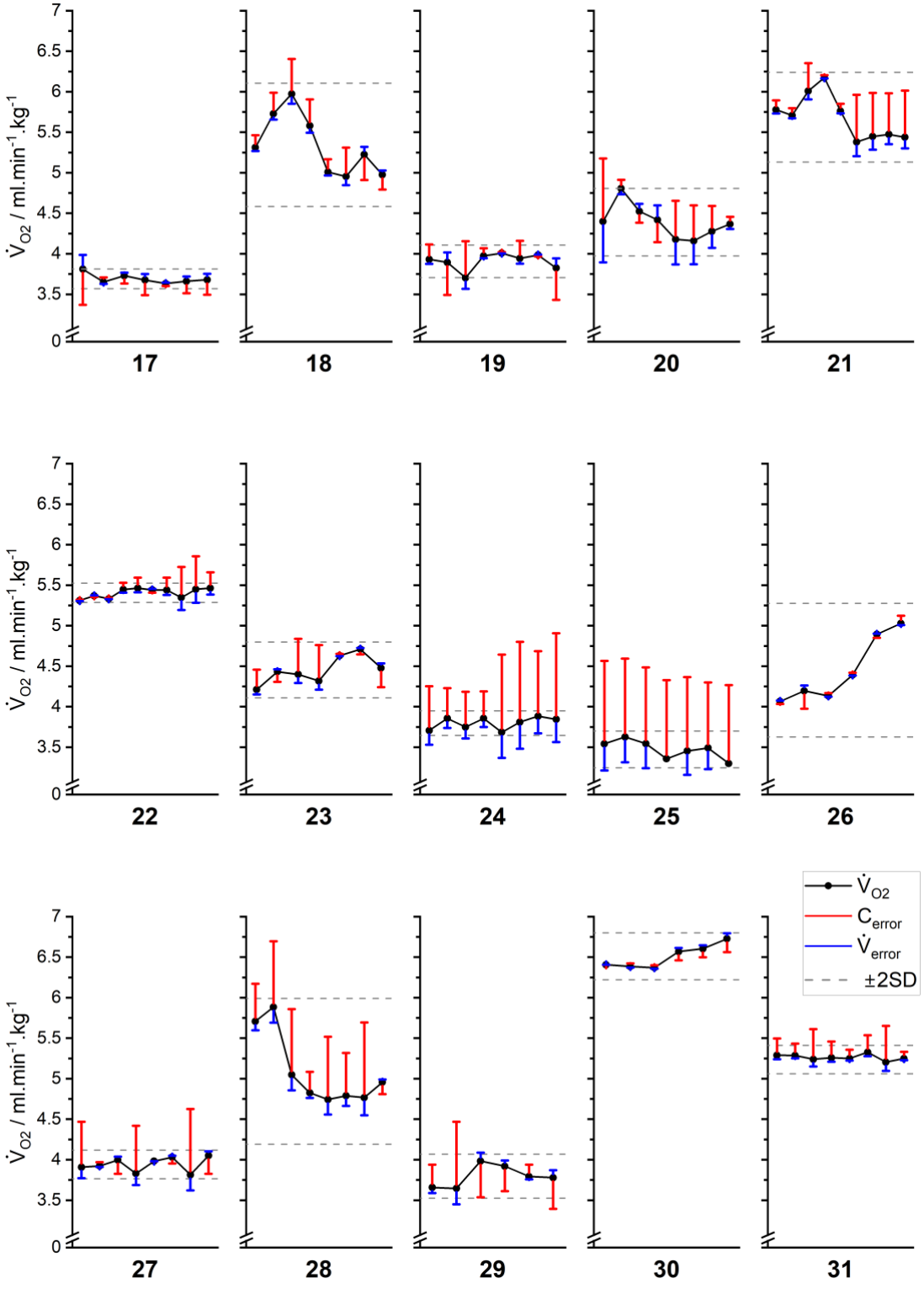

Figure 30. Individual time series of MFS-derived oxygen consumption measurements. $\dot{V}_{O2}$ and errors were normalised to lean body mass.

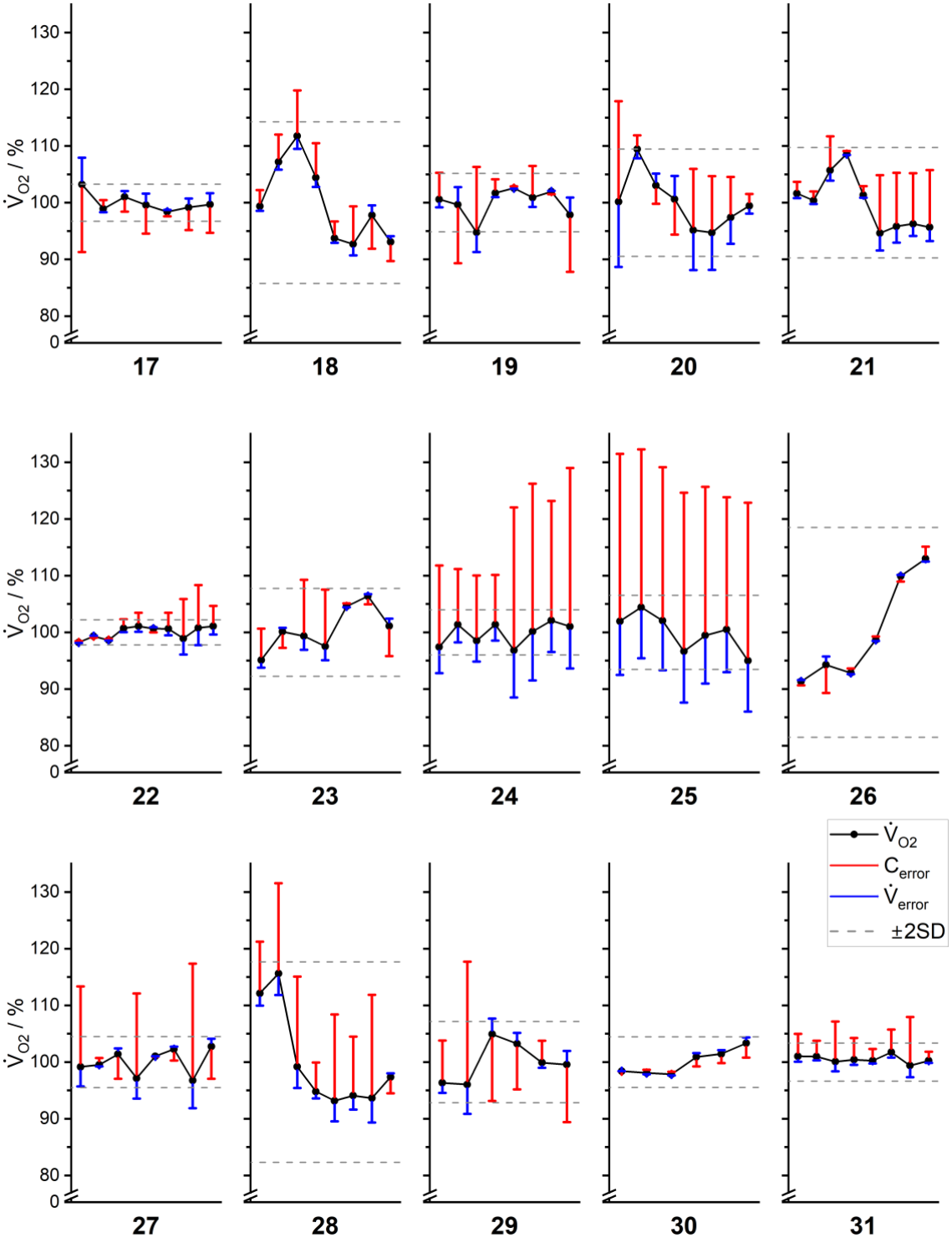

Figure 31. Individual time series of MFS-derived oxygen consumption measurements. $\dot{V}_{O2}$ and errors were normalised to mean $\dot{V}_{O2}$ and represented as a percentage of it.

Patients were initially recruited under the assumption of relative clinical stability, with no interventions affecting $\dot{V}_{O2}$ within five minutes preceding measurements and no interventions altering lung volumes for the duration MFS attachment. This approach was designed to facilitate the assessment of both bias and the instrument's precision in repeatedly measuring $\dot{V}_{O2}$ over a minimum of three hours.

However, retrospective evaluation of $\dot{V}_{O2}$ data, normalised by lean body mass, revealed clear systematic trends in five patients (IDs 18, 21, 26, 28, and 30; Figure 30). Upon reviewing CRF and electronic records, these $\dot{V}_{O2}$ variations were seen to correlate with distinct clinical events, indicating what could be genuine physiological changes rather than measurement errors.

Patient 18 exhibited elevated body temperature (38.5ºC) and fluctuating mean arterial pressure, accompanied by a varying noradrenaline requirement during the first half of measurements. Both temperature and noradrenaline infusion rate stabilised subsequently.

Patient 21 experienced a significant secretion burden, frequent coughing, and repeated endotracheal tube suctioning during the first five $\dot{V}_{O2}$ measurements, leading to increased muscle activity and, consequently, to initially elevated $\dot{V}_{O2}$ values.

Patient 26 demonstrated progressively rising $\dot{V}_{O2}$ values over the course of the study. This behaviour is likely associated with temperature fluctuations, as body temperature was actively controlled by an external cooling device.

Patient 28 was hypertensive at the start of the data acquisition but experienced a substantial drop in mean arterial pressure after the second measurement, requiring a noradrenaline infusion to be commenced. This abrupt change suggests the onset of shock, which corresponded to a sharp and sustained decline in $\dot{V}_{O2}$.

Patient 30 had received sedation and neuromuscular blockade as a bolus – midazolam and atracurium, respectively – for a percutaneous liver biopsy performed approximately one hour before the initial $\dot{V}_{O2}$ measurement. Given the patient's underlying liver failure, residual sedation effects likely contributed to initially reduced $\dot{V}_{O2}$ values, which later rose.

Although for this aspect of the work patients were sought in whom it was expected that oxygen consumption would remain reasonably stable, the dynamic and often unpredictable nature of critical illness – shaped by clinical interventions and evolving clinical course – resulted in the inclusion of individuals who experienced pathophysiological changes. This variability demonstrates the MFS's ability to capture meaningful trends in $\dot{V}_{O2}$ over time, reflecting a change in the patient's clinical condition.

5.4.2.1. Bias

The primary sources of uncertainty in $\dot{V}_{O2}$ measurement using the MFS arise from inaccuracies in flow and concentration measurements. These can be estimated from the nitrogen balance, by assuming that nitrogen behaves as an inert gas and is neither consumed nor produced by the body. Accordingly, any deviation from zero nitrogen exchange reflects systematic measurement error – i.e., bias – in either flow or concentration.

Flow and concentration errors are inherently signed in opposite directions and may vary in magnitude and direction from one measurement to another. This results in an asymmetric distribution of errors both within individual $\dot{V}_{O2}$ measurements and across the time series of each patient. To quantify this, an empirical confidence interval was calculated for each patient to indicate the uncertainty range within which their true $\dot{V}_{O2}$ values are likely to lie. For each patient:

(i) The upper bound of the $\dot{V}_{O2}$ confidence interval was defined as the average of all positive errors across the time series.

(ii) The lower bound was defined as the average of all negative errors.

This approach provides a patient-specific range that reflects the direction and magnitude of systematic error in $\dot{V}_{O2}$ measurement, while acknowledging its asymmetrical distribution. Table 8 displays the mean $\dot{V}_{O2}$ for each patient along with their correspondent confidence interval.

Patient ID	$\dot{V}_{O2}$ / mL.min^{-1}	$\dot{V}_{O2}$ / mL.min^{-1}.kg^{-1}	$\dot{V}_{O2}$ / %
17	224 [214, 228]	3.7 [3.5, 3.8]	100.0 [95.7, 101.9]
18	194 [190, 203]	5.3 [5.2, 5.6]	100.0 [97.7, 104.3]
19	203 [196, 211]	3.9 [3.8, 4.1]	100.0 [96.5, 103.9]
20	188 [178, 202]	4.4 [4.2, 4.7]	100.0 [94.7, 107.0]
21	223 [219, 235]	5.7 [5.6, 6.0]	100.0 [98.4, 105.6]
22	304 [300, 311]	5.4 [5.3, 5.5]	100.0 [98.9, 102.6]
23	238 [232, 247]	4.5 [4.4, 4.6]	100.0 [97.7, 104.0]
24	200 [189, 236]	3.8 [3.6, 4.5]	100.0 [94.5, 118.1]
25	164 [149, 208]	3.5 [3.2, 4.4]	100.0 [91.3, 127.1]
26	312 [308, 315]	4.5 [4.4, 4.5]	100.0 [98.7, 100.9]
27	259 [252, 277]	3.9 [3.8, 4.2]	100.0 [97.0, 106.7]
28	171 [166, 190]	5.1 [4.9, 5.7]	100.0 [97.0, 111.3]
29	184 [172, 196]	3.8 [3.6, 4.0]	100.0 [93.7, 106.7]
30	365 [361, 367]	6.5 [6.4, 6.5]	100.0 [99.0, 100.6]
31	288 [285, 300]	5.3 [5.2, 5.5]	100.0 [99.0, 104.2]
Mean $\dot{V}_{O2}$	233 [228, 248]	4.6 [4.5, 4.9]	100.0 [96.7, 107.0]

Table 8. Mean $\dot{V}_{O2}$ and confidence interval per patient.

Column 1 displays the patients, identified by numbers. Columns 2, 3, and 4, show the individual mean $\dot{V}_{O2}$ and their associated confidence intervals as, respectively: an absolute number (mL.min^{-1}), a function of lean body mass (mL.min^{-1}.kg^{-1}), and a percentage of the mean $\dot{V}_{O2}$ (%). Data are presented as mean [LB, UB], where UB is the upper bound of the confidence interval and LB is the lower bound of the confidence interval.

To explore the composition of this $\dot{V}_{O2}$ uncertainty, individual mean contributions from flow and concentration measurement errors were calculated as follows:

$$Mean\ flow\ error\ per\ patient = \left(\frac{1}{n}\right)\sum_{i=1}^{n}\left|\dot{V}error_i\right|$$

$$Mean\ concentration\ error\ per\ patient = \left(\frac{1}{n}\right)\sum_{i=1}^{n}\left|Cerror_i\right|$$

where n is the number of $\dot{V}_{O2}$ measurements obtained for a given patient. These values are summarised in Table 9 and Table 10, detailing the relative contributions of each error type to total $\dot{V}_{O2}$ uncertainty.

The total uncertainty width was defined as the difference between the upper and lower bounds of the confidence interval. This provides a single measure of the extent of $\dot{V}_{O2}$ uncertainty for each patient and is reported in Table 11.

Patient ID	$\dot{V}_{O2}$ FUW / mL.min^{-1}	$\dot{V}_{O2}$ FUW / mL.min^{-1}.kg^{-1}	$\dot{V}_{O2}$ FUW / %
17	4 ± 3	0.1 ± 0.1	1.8 ± 1.5
18	3 ± 1	0.1 ± 0.0	1.4 ± 0.6
19	3 ± 3	0.1 ± 0.1	1.7 ± 1.4
20	9 ± 6	0.2 ± 0.2	4.9 ± 3.4
21	4 ± 2	0.1 ± 0.1	1.6 ± 1.1
22	3 ± 3	0.1 ± 0.1	1.1 ± 1.1
23	3 ± 2	0.1 ± 0.0	1.2 ± 0.9
24	11 ± 5	0.2 ± 0.1	5.5 ± 2.3
25	14 ± 1	0.3 ± 0.0	8.7 ± 0.6
26	2 ± 2	0.0 ± 0.0	0.5 ± 0.5
27	5 ± 5	0.1 ± 0.1	1.9 ± 1.8
28	5 ± 2	0.1 ± 0.1	2.8 ± 1.3
29	5 ± 3	0.1 ± 0.1	2.5 ± 1.5
30	2 ± 1	0.0 ± 0.0	0.5 ± 0.4
31	3 ± 2	0.1 ± 0.0	1.0 ± 0.6
Mean ± SD	5 ± 5	0.1 ± 0.1	2.5 ± 2.6

Table 9. Average flow uncertainty width per patient.

All values are represented as the mean flow uncertainty width ± the SD of the mean. Column 1 displays the patients, identified by numbers. Columns 2, 3, and 4, show the flow uncertainty width as, respectively: an absolute number (mL.min^{-1}), a function of lean body mass (mL.min^{-1}.kg^{-1}), and a percentage of the mean $\dot{V}_{O2}$ (%). FUW = flow uncertainty width.

Patient ID	$\dot{V}_{O2}$ CUW / mL.min^{-1}	$\dot{V}_{O2}$ CUW / mL.min^{-1}.kg^{-1}	$\dot{V}_{O2}$ CUW / %
17	10 ± 8	0.2 ± 0.1	4.4 ± 3.7
18	10 ± 4	0.3 ± 0.1	5.1 ± 1.9
19	12 ± 9	0.2 ± 0.2	5.7 ± 4.5
20	14 ± 10	0.3 ± 0.2	7.5 ± 5.3
21	13 ± 9	0.3 ± 0.2	5.6 ± 4.2
22	8 ± 8	0.1 ± 0.1	2.6 ± 2.7
23	12 ± 9	0.2 ± 0.2	5.1 ± 3.8
24	36 ± 16	0.7 ± 0.3	18.1 ± 7.9
25	44 ± 3	0.9 ± 0.1	27.1 ± 1.9
26	5 ± 5	0.1 ± 0.1	1.7 ± 1.7
27	20 ± 20	0.3 ± 0.3	7.9 ± 7.7
28	19 ± 12	0. 6± 0.3	11.6 ± 5.6
29	19 ± 11	0.4 ± 0.2	10.5 ± 6.1
30	4 ± 3	0.1 ± 0.1	1.1 ± 0.9
31	12 ± 7	0.2 ± 0.1	4.2 ± 2.4
Mean ± SD	16 ± 14	0.3 ± 0.3	7.8 ± 7.8

Table 10. Average concentration uncertainty width per patient.

All values are represented as the mean concentration uncertainty width ± the SD of the mean. Column 1 displays the patients, identified by numbers. Columns 2, 3, and 4, show the concentration uncertainty width as, respectively: an absolute number (mL.min^{-1}), a function of lean body mass (mL.min^{-1}.kg^{-1}), and a percentage of the mean $\dot{V}_{O2}$ (%). CUW = concentration uncertainty width.

Patient ID	$\dot{V}_{O2}$ TUW / mL.min^{-1}	$\dot{V}_{O2}$ TUW / mL.min^{-1}.kg^{-1}	$\dot{V}_{O2}$ TUW / %
17	14 ± 12	0.2 ± 0.2	6.2 ± 5.2
18	13 ± 5	0.3 ± 0.1	6.5 ± 2.4
19	15 ± 12	0.3 ± 0.2	7.4 ± 5.9
20	23 ± 16	0.5 ± 0.4	12.3 ± 8.7
21	16 ± 12	0.4 ± 0.3	7.2 ± 5.2
22	11 ± 12	0.2 ± 0.2	3.7 ± 3.8
23	15 ± 11	0.3 ± 0.2	6.3 ± 4.7
24	47 ± 20	0.9 ± 0.4	23.6 ± 10.1
25	59 ± 4	1.2 ± 0.1	35.9 ± 2.6
26	7 ± 7	0.1 ± 0.1	2.2 ± 2.2
27	25 ± 25	0.4 ± 0.4	9.8 ± 9.5
28	25 ± 12	0.7 ± 0.3	14.3 ± 6.9
29	24 ± 14	0.5 ± 0.3	13.0 ± 7.5
30	6 ± 5	0.1 ± 0.1	1.6 ± 1.3
31	15 ± 9	0.3 ± 0.2	5.2 ± 3.0
Mean ± SD	21 ± 18	0.4 ± 0.4	10.3 ± 10.2

Table 11. Average total uncertainty width per patient.

All values are represented as the mean total uncertainty width ± the SD of the mean. Column 1 displays the patients, identified by numbers. Columns 2, 3, and 4, show the total uncertainty width as, respectively: an absolute number (mL.min^{-1}), a function of lean body mass (mL.min^{-1}.kg^{-1}), and a percentage of the mean $\dot{V}_{O2}$ (%). TUW = total uncertainty width.

Across all patients, the mean ± SD total uncertainty width was 10.3% ± 10.2% of the their mean $\dot{V}_{O2}$. Concentration error was the dominant source of uncertainty, contributing 7.8% ± 7.8%, approximately three times greater than the average flow error (2.5% ± 2.6%).

Two patients (24 and 25) exhibited higher-than-expected widths of uncertainty in $\dot{V}_{O2}$ measurements (see Figure 29 to Figure 31 and Table 9 to Table 11). During data collection, this issue was identified in real time by elevated nitrogen balance values displayed on the

MFS laptop controller interface. Post hoc investigation revealed that dust accumulation on the MFS's internal mirrors had impaired optical gas readings, which became noisier than usual. This was subsequently resolved by cleaning the device, and no similar issues were observed in following patients. Due to this transient technical issue, the inclusion of these patients discreetly changed the overall results. For completeness, Table 12 also presents total, flow, and concentration uncertainty widths with patients 24 and 25 excluded from the analysis.

Uncertainty	$\dot{V}_{O2}$ / mL.min^{-1}	$\dot{V}_{O2}$ / mL.min^{-1}.kg^{-1}	$\dot{V}_{O2}$ / %
Total	16 ± 13	0.3 ± 0.3	7.4 ± 6.5
Flow	4 ± 3	0.1 ± 0.1	1.8 ± 1.8
Concentration	12 ± 10	0.3 ± 0.2	5.6 ± 5.0

Table 12. Average uncertainty width per patient after exclusion of patients 24 and 25.

Patients 24 and 25 are excluded from this analysis. All values are represented as the mean uncertainty width ± the SD of the mean for total width of uncertainty and the uncertainty corresponding to flow and concentration inaccuracies. Columns 2, 3, and 4, show the total uncertainty width as, respectively: an absolute number (mL.min^{-1}), a function of lean body mass (mL.min^{-1}.kg-^{1}), and a percentage of the mean $\dot{V}_{O2}$ (%).

5.4.2.2. Precision

Given the identifiable clinical causes for the $\dot{V}_{O2}$ trends in patients 18, 21, 26, 28, and 30, these five patients were excluded from the precision analysis.

In the remaining 10 patients, the MFS demonstrated high precision in repeated $\dot{V}_{O2}$ measurements. The maximum coefficient of variation from the mean $\dot{V}_{O2}$ was 5%, with 60% of patients showing a SD ≤ 5 mL.min^{-1} from their mean $\dot{V}_{O2}$ (Table 13).

ANOVA was used to assess the variability in $\dot{V}_{O2}$ between and within patients. As anticipated, between-subject variability in $\dot{V}_{O2}$ was far greater than within-subject variability (Table 13). From these values, the ICC was calculated as 0.999, indicating that 99.9% of the total variability in $\dot{V}_{O2}$ was attributable to differences between patients. This high ICC demonstrates excellent reproducibility of $\dot{V}_{O2}$ measurements within individuals over time, with minimal within-subject variation.

Collectively, these findings suggest that the MFS is precise when used as a tool for monitoring $\dot{V}_{O2}$ over time in mechanically ventilated critically ill patients.

Patient ID	$\dot{V}_{O2}$ / mL.min^{-1}	$\dot{V}_{O2}$ / mL.min^{-1}.kg^{-1}	$\dot{V}_{O2}$ / %	CV / %
17	224 ± 4	3.7 ± 0.1	100 ± 2	2
19	203 ± 5	3.9 ± 0.1	100 ± 3	3
20	188 ± 9	4.4 ± 0.2	100 ± 5	5
22	304 ± 3	5.4 ± 0.1	100 ± 1	1
23	238 ± 9	4.5 ± 0.2	100 ± 4	4
24	200 ± 4	3.8 ± 0.1	100 ± 2	2
25	164 ± 5	3.5 ± 0.1	100 ± 3	3
27	259 ± 6	3.9 ± 0.1	100 ± 2	2
29	184 ± 7	3.8 ± 0.1	100 ± 4	4
31	288 ± 2	5.3 ± 0.0	100 ± 1	1
MSE (WP)	32.901	0.013		
MSE (BP)	17706.469	3.667		
F (p-value)	538.182 (< 0.001)	281.484 (< 0.001)		
ICC	0.999	0.999		

Table 13. MFS precision assessment table.

Data are presented as mean ± SD. Columns 2, 3 and 4 show the mean $\dot{V}_{O2}$ ± SD for each patient included expressed as absolute values (mL.min^{-1}), values normalised by lean body mass (mL.min^{-1}.kg^{-1}), and percentages relative to the patient's own mean $\dot{V}_{O2}$, respectively. Column 5 presents the coefficient of variation (CV) from the mean $\dot{V}_{O2}$. Summary metrics for the mean squared error (MSE) of between-patient variability (BP), within-patient variability (WP), their relationship (F = BP/WP), and intra-class correlation (ICC) are also provided.

5.5. Discussion

5.5.1. Summary of findings

The study as part of which these measurements were made was primarily intended to explore cardiopulmonary physiology in mechanically ventilated critically ill patients, and was not designed or regulated as a device trial. Nevertheless, the findings generated cannot

help but prompt consideration about potential clinical applications for the technique described, and these clearly merit brief discussion at this stage.

For such technique to be useful in clinical practice, it must demonstrate not only the ability to detect true physiological trends in $\dot{V}_{O2}$ (i.e., precision), but also the ability to report values that closely match the actual parameter of interest (i.e., accuracy). Put another way, it must be possible for any observed changes to be confidently attributed to the patient's pathophysiology, rather than to random or systematic measurement error.

In this study, the MFS showed strong performance on both fronts. Analyses demonstrated high precision and minimal bias, suggesting that the device provides accurate and reliable $\dot{V}_{O2}$ measurements, even under the challenging conditions posed by mechanical ventilation.

It can be argued that the cohort of mechanically ventilated patients enrolled in this study was one likely to benefit from continuous $\dot{V}_{O2}$ monitoring in critical care. All patients were severely ill at the time of enrolment, with over half requiring circulatory support. Several developed fever and one was undergoing active temperature management with a cooling device. Nearly two-thirds remained hospitalised 28 days after admission, underscoring the disease severity and clinical complexity of the cohort. These characteristics provided a rigorous test of $\dot{V}_{O2}$ measurement under typical ICU conditions.

It is important to emphasize that the results presented here do not represent technical specifications under controlled conditions, but rather the real-world performance of the instrument in a cohort of critically ill patients. Measuring $\dot{V}_{O2}$ in this setting is known to be significantly more complex than in awake spontaneously ventilated individuals. Prior studies have suggested that up to 90% of the total variability in metabolic readings stems from biological changes in the patient, while only 10% is attributable to technical error[157].

These biological fluctuations are particularly relevant in mechanically ventilated patients, where factors such as sedation, muscle activity, temperature, and haemodynamic status can all influence $\dot{V}_{O2}$ [162-167].

Further complicating the assessment, this study captured $\dot{V}_{O2}$ measurements over a considerably longer time frame than previous studies have achieved. Whereas many precision studies have opted to evaluate short-term repeatability to ensure the maintenance of a steady metabolic state[43, 47, 168], here measurements were spaced every thirty minutes across at least three hours. This design introduced greater opportunity for biological variability but better reflects how $\dot{V}_{O2}$ would be used for trend detection were the technique described herein using the MFS eventually to be exploited for clinical purposes.

As discussed in section 1.5.4, one of the enduring limitations of existing commercial devices designed for ICU use is the unreliability of $\dot{V}_{O2}$ readings. There is high inter-device variability and often poor precision and accuracy, in keeping with their reliance on the Haldane transformation[43, 47, 169]. Critically, they do not incorporate an internal mechanism to assess the quality or plausibility of each measurement. This leaves clinicians with no indication as to whether a given $\dot{V}_{O2}$ can be trusted.

The MFS addresses these limitations by: (i) providing high-precision, low-bias measurements; (ii) operating independently of the Haldane transformation and related assumptions; and (iii) offering built-in confidence intervals for each $\dot{V}_{O2}$ estimate, potentially delivering real-time quality control to the bedside.

The sections below explore some of these aspects in details, beginning with the provision of real-time quality control.

5.5.2. Real-time quality control in $\dot{V}_{O2}$ measurements

A major innovation of this study was the development of a real-time quality control strategy to assess the degree of uncertainty associated with each $\dot{V}_{O2}$ measurement on a breath-by-breath basis, without relying on external validation. This was accomplished by quantifying deviations from expected nitrogen balance ($\dot{V}_{N2} = 0$), which served as an internal check on the accuracy of both concentration and flow data. The dynamic estimation of confidence intervals around individual $\dot{V}_{O2}$ measurements represents a novel contribution to the field and marks a significant step forward in assessing the reliability of oxygen consumption monitoring in critical care.

The results of $\dot{V}_{O2}$ error estimation through $\dot{V}_{N2}$ in this critically ill cohort were reassuring. In the absence of technical issues, the mean confidence interval around $\dot{V}_{O2}$ was narrow – approximately 16 mL.min^{-1}, or 7.4%. In contrast, when technical issues were identified, as in patients 24 and 25, nitrogen balance deviated markedly from zero, and the system correctly flagged a broader uncertainty range, indicating that those measurements should be interpreted with caution. When these two patients are considered separately, the average confidence interval width rises to 53 mL.min^{-1}, or 29.8%.

To understand better what these confidence intervals represent, it is important to note that the maximum possible $\dot{V}_{O2}$ error is bounded by the magnitude of the nitrogen balance deviation. This imbalance arises from either flow or concentration inaccuracy, but as it represents a single value, the total error must be attributable either to one or divided between the two. If only one of these components is at fault, the full nitrogen imbalance can be attributed to it – meaning that the $\dot{V}_{O2}$ error equals either the full flow or concentration error. If both sources contribute simultaneously, their effects tend partially to cancel, as flow and concentration errors act in opposite directions, resulting in a smaller

apparent $\dot{V}_{O2}$ error. As both errors are derived from the same nitrogen deviation, it is not mathematically possible for both to occur at their full magnitude concurrently. In practice, consistent with findings from the DB versus MFS comparison, concentration inaccuracies were observed to be the dominant source of uncertainty, averaging three times greater than flow-related errors.

However, nitrogen imbalance can also be caused by factors unrelated to instrument performance. Small circuit leaks, even those below ventilator detection thresholds, can significantly distort nitrogen balance[170, 171]. For example, a 0.5% expiratory leak in a patient with minute ventilation of 6.3 $L.min^{-1}$ and FiO_2 of 0.21 would result in a false oxygen imbalance of approximately 25 $mL.min^{-1}$. As FiO_2 or minute ventilation increases, this effect is exacerbated. In reality, minor leaks are likely to occur, and not all deviations in nitrogen balance should be interpreted as true measurement errors.

In the present dataset, only one patient was excluded due to a nitrogen balance exceeding the predefined threshold (> 60 $mL.min^{-1}$). This individual had a suspected cuff leak, which was only communicated to the research team at the end of the study period. Notably, the ventilator failed to detect the leak, yet the MFS identified a nitrogen imbalance exceeding 80 $mL.min^{-1}$. In a real clinical application, this deviation would have produced an unacceptably wide confidence interval, potentially prompting clinicians to question the reliability of the corresponding $\dot{V}_{O2}$ values and alerting them to a possible patient safety issue. In this case, the implied $\dot{V}_{O2}$ error was up to four times greater than that average observed in the rest of the cohort, highlighting the utility of nitrogen balance as a built-in safeguard for identifying questionable measurements.

Transient changes in EELV can also affect $\dot{V}_{O2}$ measurement by altering the volume of gas retained in the lungs in between breaths[172, 173] – even in the absence of true metabolic changes. For example, following a sedation hold or a shift in patient position, an increase in EELV means more gas (including nitrogen) is stored in the lungs, while a decrease in EELV releases stored gas into the measured expiratory flow. These changes can disrupt nitrogen balance, potentially mimicking a change in $\dot{V}_{O2}$. However, because these fluctuations produce corresponding deviations in nitrogen balance, the MFS correctly registers greater uncertainty around $\dot{V}_{O2}$ estimates, reflected in wider confidence intervals. Were the technique to be exploited clinically in the future, this feature could potentially help prevent clinicians from misinterpreting such phenomena as real changes in $\dot{V}_{O2}$.

These findings underscore a critical limitation of traditional $\dot{V}_{O2}$ measurement methods: the assumption that nitrogen balance is always zero[174]. This simplification, central to the Haldane transformation and widely used in clinical devices, overlooks physiological and technical disturbances – including leaks, flow or concentration mismeasurements, and changes in lung volume – that can substantially distort $\dot{V}_{O2}$ values. The result is the calculation of apparent, rather than true, $\dot{V}_{O2}$.

The MFS addresses this gap by calculating $\dot{V}_{O2}$ directly from bidirectional flow and absolute molar concentrations of respired gases. This enables true measurement of oxygen consumption and calculation of nitrogen balance on a breath-by-breath basis – without relying on assumptions such as those required by the Haldane transformation.

Given the high accuracy of laser absorption spectroscopy used by the MFS for gas concentration analysis, most uncertainty in $\dot{V}_{O2}$ is likely to derive from flow measurement. Nevertheless, flow is measured directly in the main airway using a bidirectional sensor that

adjusts its measurements for gas density and viscosity, arguably making it more robust than conventional pneumotachographs or turbine-based systems.

In summary, by integrating nitrogen balance into each breath-by-breath measurement, the MFS not only estimates $\dot{V}_{O2}$ accurately, but also quantifies the uncertainty around each value. This capability represents a meaningful advance in metabolic monitoring – particularly in mechanically ventilated patients, where distinguishing true physiological shifts from artefact could be critical for result interpretation, clinical decision-making, and ultimately patient safety.

5.5.3. Precision of $\dot{V}_{O2}$ measurements by the MFS

The results of this study demonstrated that the MFS provides precise $\dot{V}_{O2}$ measurements in mechanically ventilated patients, as evidenced by a low coefficient of variation for the mean and high intraclass correlation coefficient. This indicates that the technique consistently produces similar $\dot{V}_{O2}$ values for a given individual under presumably stable clinical conditions.

There is currently no universal standard for what constitutes acceptable precision in metabolic measurements. However, in clinical practice, a variation of less than 10% in repeated $\dot{V}_{O2}$ measurements over five minutes is often considered acceptable for resting metabolic rate assessments[168]. In sedated, mechanically ventilated individuals, tighter variation – ideally within 5% – is typically recommended to define steady state[168].

Previous studies in similar populations have reported variable levels of precision. Historically, the now-retired Deltatrac II (GE healthcare, USA) was regarded as a benchmark for both high precision and low bias in $\dot{V}_{O2}$ measurement, with a study reporting

CV below 5%, similar to those found in the present analysis[42, 43]. By contrast, modern indirect calorimeters often exhibit higher variability[169], with CVs often exceeding 5%, and even 10%[43, 47].

The design of the present study deliberately challenged the MFS's precision by spacing out $\dot{V}_{O2}$ measurements at 30-minute intervals over several hours. This is in contrast to a number of prior studies, which typically assessed precision using tightly spaced averages over short periods of time – of the order of minutes rather than hours[43, 47]. The present approach was intended to replicate realistic clinical application conditions, where measurements are likely to be made at intervals to detect meaningful changes over time.

Even whilst sedated, mechanically ventilated patients may experience subtle fluctuations in sedation depth, temperature, ventilation, and haemodynamic status, all of which might influence $\dot{V}_{O2}$. Figure 29 to Figure 31 illustrate this variability, with modest fluctuations in $\dot{V}_{O2}$ observed within each patient. In the absence of identifiable interventions or relevant clinical changes, these fluctuations suggest that true physiological variation may have occurred in the background.

$\dot{V}_{O2}$ fluctuations of this kind are expected in both healthy and critically ill individuals, although their magnitude remains difficult to quantify. In a 24-hour monitoring study by *van Lanschot et al.*, diurnal variation in $\dot{V}_{O2}$ averaged around 3% in mechanically ventilated patients[175]. However, this analysis was based on 3-hour averaging windows, which likely smoothed out shorter-term fluctuations[175]. In contrast, *Jenkins et al.* reported between-day baseline $\dot{V}_{O2}$ variability greater than 15% based on 2-minute averages in mechanically ventilated patients who would then undergo physical rehabilitation[165].

In summary, these findings suggest that the MFS not only achieves a level of precision comparable to or better than existing technologies, but it also maintains this performance under real-world ICU conditions. This level of reliability is essential for interpreting trends over time – especially in settings where even modest changes in $\dot{V}_{O2}$ may carry important clinical implications.

5.5.4. Identifying $\dot{V}_{O2}$ trends in critical care

The findings discussed thus far in this chapter expand on the foundational work by *Ciaffoni et al.*[54], where a single anaesthetised patient underwent longitudinal $\dot{V}_{O2}$ monitoring intra-operatively. On that occasion, the MFS registered $\dot{V}_{O2}$ changes related to variations in blood pressure, vasoactive drug infusion, and ventilator settings[54].

The factors likely responsible for meaningful $\dot{V}_{O2}$ changes in patients 18, 21, 26, 28, and 30, are recognised in the literature to have an effect on $\dot{V}_{O2}$[163-165, 167, 176, 177]. However, an ability to register these effects accurately and non-invasively in this patient population has, until now, been lacking. One particularly illustrative case is patient 28, who transitioned from a hypertensive to a hypotensive state during the experiment, ultimately requiring escalating doses of noradrenaline to maintain a target mean arterial pressure. The MFS recorded a corresponding fall in oxygen consumption aligned with the onset and progression of shock. This observation is consistent with the final common pathway in all forms of shock: inadequate cellular oxygen utilisation[7, 12].

As discussed in Chapter 1, many of the interventions used to treat shock – such as fluid resuscitation, vasopressor infusion, blood transfusion, and increases in FiO_2 – are intended to augment oxygen delivery as a means to facilitate improved oxygen consumption[7, 12, 13, 26]. These interventions are not without risk, and can be harmful even

when cautiously delivered. Yet, their effects on tissue-level oxygen utilisation are either unknown or largely inferred, as current assessments rely on surrogate markers such as blood lactate concentration or $ScvO_2$. These markers are often insensitive to rapid changes and may be confounded by comorbidities or medications. Direct $\dot{V}_{O2}$ measurement might allow clinicians to guide interventions based on real-time physiological feedback. One possible application is to identify the point at which further therapy is unlikely to yield benefit, titrating treatments based on $\dot{V}_{O2}$ response. For example, if $\dot{V}_{O2}$ reaches a plateau despite a rising D_{O2}, this might indicate that oxygen delivery is appropriate and sufficient, and that further interventions directed at increasing D_{O2} could be withheld – thereby avoiding unnecessary harms from excessive treatment.

Another interesting example is patient 26, whose $\dot{V}_{O2}$ steadily increased during the period of MFS connection while on a cooling device for temperature control. Targeted temperature management is commonly used after return of spontaneous circulation following cardiac arrest to support neurological recovery[178]. Cooling devices are widely employed to prevent fever, which can worsen hypoxic-ischaemic brain injury by increasing the mismatch between oxygen supply and demand[178]. One of the goals of temperature control in this context is to reduce metabolic activity, especially of the brain[179]. A progressive rise in oxygen consumption in these cases may reflect a failure of the cooling strategy to achieve its intended effect. For example, if a patient is shivering in response to active cooling, this must be adequately managed to prevent a counterproductive increase in metabolic demand[179, 180]. Importantly, even in the absence of shivering – as absent in patient 26 – an increase in oxygen consumption may go unnoticed despite continuous conventional clinical monitoring, underscoring another potentially valuable application of real-time $\dot{V}_{O2}$ measurement.

Taken together, these observations help identify goals for future research. In particular, it would be desirable to study patients earlier in the course of their critical illness – prior to the onset of overt shock – to assess whether decline in $\dot{V}_{O2}$ may serve as an early warning sign of insipient shock. Additionally, tracking the $\dot{V}_{O2}$ response to specific interventions could support the development of $\dot{V}_{O2}$-guided therapy, where the goal becomes restoration of oxygen consumption itself rather than relying on surrogates. This approach may also have value in settings where metabolic control is desirable, such as in post-cardiac-arrest care. Used in this way, $\dot{V}_{O2}$ monitoring has the potential to act not only as a diagnostic and monitoring tool, but to provide a real-time therapeutic target – bringing the field one step closer to personalised, physiology-driven critical care.

5.5.5. Limitations

Several limitations of this study should be considered when interpreting the results. First, the study was conducted in a relatively small cohort. However, the primary aim was to evaluate the feasibility and performance of the MFS in critically ill mechanically ventilated patients. Similar small sample sizes have been employed in proof-of-concept studies for other gas exchange technologies and are appropriate for this early-phase evaluation.

Second, the 3-minute $\dot{V}_{O2}$ averaging period was selected arbitrarily. To balance this, measurements were spaced thirty minutes apart, which introduced the potential for greater biological variability between readings.

Third, although efforts were made to include clinically stable patients, unforeseen changes in patient condition may have influenced $\dot{V}_{O2}$ independently of device performance. To address this, the analyses were stratified into two groups: patients who remained stable over time (for precision assessment) and those with identifiable physiological changes (for

trends analyses). Whilst unplanned, this division ultimately strengthened the study by allowing the evaluation of the technique under both stable and dynamic conditions.

Fourth, although the MFS demonstrated promising accuracy in this cohort, its performance may have been affected by factors unrelated to measurement error, particularly leaks or changes in EELV, both of which can disrupt nitrogen balance[170-172].

Fifth, the FiO_2 levels in this study did not exceed 0.4. One of the main theoretical advantages of the MFS is its ability to measure $\dot{V}_{O2}$ accurately at high levels of FiO_2 without relying on the Haldane transformation. However, this strength could not be fully demonstrated in the present cohort due to moderate FiO_2 employed clinically – a potential consequence of seeking to enrol stable patients.

Finally, as there are many factors that can simultaneously influence $\dot{V}_{O2}$ in critical illness, it is difficult to attribute observed $\dot{V}_{O2}$ changes to specific interventions with absolute certainty. While major clinical events likely responsible for $\dot{V}_{O2}$ shifts were highlighted, the contribution of other subtler processes acting concurrently cannot be definitively ruled out.

5.6. Conclusion

This work represents the first evaluation of the performance of the MFS in critically ill, mechanically ventilated patients, specifically examining the reproducibility and accuracy of $\dot{V}_{O2}$ measurements obtained using the technique. Building on the previous findings of strong agreement with the established standard – the DB – the MFS demonstrated high precision for the measurement of $\dot{V}_{O2}$ in this population. Additionally, the development of confidence intervals around each $\dot{V}_{O2}$ measurement improves the reliability of the technique

in discerning signal from noise, a significant achievement in the metabolic measurements field.

These findings further the application of the MFS in the analyses of $\dot{V}_{O2}$ trends over time and open new avenues for future research focused on detecting $\dot{V}_{O2}$ trends at earlier stages of critical illness, including the progression from sepsis to septic shock – a major problem in clinical practice.

Chapter 6. An exploration of EELV estimates obtained by CCP in critically ill patients

6.1. Introduction

As discussed in Chapter 2, bedside assessments of absolute EELVs in mechanically ventilated patients might allow the intensivist to tailor ventilatory support and other interventions according to individual patient need, and to monitor their effectiveness in real time. Currently, however, the techniques available to the critical care clinician to assess such parameters non-invasively at the bedside are limited in both availability and practicality.

For example, body plethysmography (BPleth) – considered the gold standard for lung volume measurement – requires the patient to be placed in a sealed chamber, which is clearly unfeasible in mechanically ventilated individuals. Likewise, conventional MBNWs involving a step change in inspired oxygen from 0.21 to 1.0 are problematic. The use of

100% oxygen can induce hyperoxic atelectasis, and many ICU patients require elevated baseline FiO_2, making such step increase impossible.

The following experiments address the question of whether small, clinically insignificant, variations in FiO_2 can be used to measure absolute EELV in mechanically ventilated patients in the ICU with sufficient accuracy relative to the reference method that would be necessary to make them useful tools for patient management.

6.2. Research aims and objectives

The primary aim of this chapter was to evaluate the performance of CCP in estimating EELV in mechanically ventilated, critically ill patients.

To address this aim, three studies were conducted to: (i) compare EELV estimated by CCP under a full nitrogen washout stimulus with FRC measured by BPleth in awake healthy individuals; (ii) evaluate whether partial nitrogen washouts can substitute for full nitrogen washouts when estimating EELV using CCP both in awake healthy individuals and in mechanically ventilated patients; and (iii) assess the precision of EELV estimates obtained using CCP in mechanically ventilated patients.

6.3. Methods

Participant recruitment, informed consent, ethical considerations, and instrumental setup for healthy participants were discussed in Chapter 4, while Chapter 5 covered these aspects for mechanically ventilated patients. The following sections focus on study-specific experimental protocols and the corresponding statistical analyses.

6.3.1. Preliminary study in awake healthy participants

6.3.1.1. Comparison between CCP and BPleth FRC

Participants were studied during a single visit to the Churchill Hospital (Oxford, UK), during which they undertook serial assessments including spirometry, MBNW using the MFS, and BPleth.

Spirometry was performed in accordance with standard guidelines[181]. Each participant completed three manoeuvres, achieving repeatabilities within 5% of each other for forced expired volume in one second (FEV1), forced vital capacity (FVC)[182], and vital capacity (VC)[181]. Automated reports of lung function were printed for retrospective analysis, containing the highest values obtained for each of these three parameters.

Nitrogen washouts were performed using the MFS, as described in section 3.2.5. Each participant completed three 12-minute full MBNW trials. A minimum rest period of 15 minutes was observed between trials to allow for restoration of normal alveolar gas composition. The resulting gas exchange profiles were then processed to complete the CCP process, in which cardiopulmonary modelling and parameter estimation were used to derive FRC, as described in section 3.2.4.

BPleth was conducted with participants seated inside an airtight plethysmograph chamber. Trained respiratory technicians provided instruction on the breathing manoeuvres. These included tidal breathing, full inspiratory and expiratory efforts to determine TLC and RV, as well as forced expiratory manoeuvres for the assessment of airway resistance.

Plethysmography recordings were repeated until three technically acceptable measurements were obtained, resulting in a coefficient of variation from the mean of less

than 5% for FRC, in accordance with standard quality control criteria[67]. Upon completion, an output report was generated containing the arithmetic mean of the three FRC measurements.

6.3.1.2. CCP-derived FRC: full versus partial nitrogen washout comparison

Participants were assessed across two study visits at the Department of Physiology, Anatomy and Genetics (Sherrington Building, University of Oxford, UK). During each visit, two MBNW tests were performed: one using a full washout protocol and the other using a partial washout protocol, with a minimum rest period of 15 minutes between these to allow for gas equilibration. The full washout involved a step change in FiO_2 from 0.21 to 1.0, while the partial washout involved a step from 0.21 to 0.41. A mass flow controller (Robbins-Ritchie group, University of Oxford, UK) was employed to facilitate the delivery of predetermined fractions of inspired oxygen at a constant flow of 40 $L.min^{-1}$, while ensuring a smooth transition between baseline and washout phases.

In total, each participant completed four MBNWs – two partial and two full. Gas exchange data recorded by the MFS throughout the duration of all MBNWs were subsequently fed into the cardiopulmonary model for fitting upon completion of both study visits.

6.3.2. EELV estimates by CCP in mechanically ventilated patients

6.3.2.1. Data recording

Variables likely to influence EELV in mechanically ventilated patients were prospectively identified through a review of the literature. These included, but were not limited to: patient repositioning, mucus clearance, physiotherapy, adjustments to mechanical ventilation parameters, and prone positioning[182-186]. These variables were monitored throughout the

period of MFS connection and recorded in the patients' CRF to ensure accurate time alignment between any relevant interventions and their potential impact on EELV.

Respiratory mechanics were continuously recorded from the mechanical ventilator (Hamilton-C6, Hamilton Medical AG, Switzerland) using the manufacturer's Datalogger software (version 5.0, Hamilton Medical AG, Switzerland). Data were streamed in real time to the MFS laptop controller via an RS232 serial connection, and a complete ventilator data file was generated at the conclusion of each study session for retrospective analysis. Gas exchange data were recorded by the MFS, as described in Table 6.

The MBNW used in mechanically ventilated patients was based on that employed in awake participants but adapted to suit the ICU context. Here, the baseline phase was shortened from seven to five minutes to account for the more stable gas exchange conditions in sedated, ventilated patients. FiO_2 steps were also adjusted: while awake participants underwent full and partial washouts at fixed targets (0.21 to 1.0 and 0.21 to 0.41, respectively), ventilated patients underwent FiO_2 changes relative to their baseline requirement. Full washouts were defined as any step increase between 0.70 and 0.79, and partial washouts involved an absolute increase of 0.20 from the patient's baseline FiO_2. These protocol adjustments ensured the feasibility of performing MBNWs in critically ill patients for whom baseline FiO_2 was often higher than 0.21.

6.3.2.2. Data processing

To estimate EELV, gas exchange data recorded by the MFS were segmented into separate 10-minute data files, each containing a single MBNW. A parameter set file was obtained through CCP modelling for each individual washout file, as described in Chapter 3.

6.3.2.3. Data analysis

Repeated MBNW were conducted approximately every thirty minutes, with each patient undergoing at least six washouts. To ensure stable conditions for precision assessment, no clinical interventions – including medication adjustments, nutritional changes, etc. – were permitted during the 5-minute baseline phase. Likewise, in the fifteen minutes preceding the washout phase, no interventions known to change EELV were tolerated. If any such intervention occurred due to clinical need and was identified in real-time, the ongoing washout was discontinued. If a confounding intervention was identified retrospectively from review of the CRF and ECR, that particular washout was flagged for exclusion from the precision analysis.

To compare EELV estimates derived from full and partial nitrogen washouts, patients were required to have a baseline FiO_2 between 0.21 and 0.30. Patients meeting this criterion underwent two full nitrogen washouts in addition to a minimum of two partial washouts.

6.3.3. Model fitting

For all studies requiring cardiopulmonary modelling, a NLLSOR enabled fitting of the model to the measured data, as detailed in section 3.2.4. The fitting process typically required less than an hour and consisted of running the model along with its inputs through a high-performance computer system with remote access made available by the University of Oxford's Advanced Research Computing facility. Most of the cardiopulmonary model was written by contributors (see Appendix C) in MATLAB (R2022b, MathWorks Inc, USA), with a minor C++ contribution.

6.3.4. Quality control

In addition to monitoring nitrogen balance, as described in section 4.2.6, all modelling studies included visual inspection of the model's fit to the measured data as an additional quality control step. Although the model fit selected by the NLLSOR algorithm represents the best mathematical match to the measured data, it may not always reflect a physiologically accurate fit. Therefore, model performance was assessed by examining the cumulative residual difference between modelled and measured data, as well as by comparing modelled and measured cumulative volumes of gas exchanged throughout the experimental protocol (Figure 32). Datasets demonstrating poor agreement between modelled and measured data were excluded from further analysis.

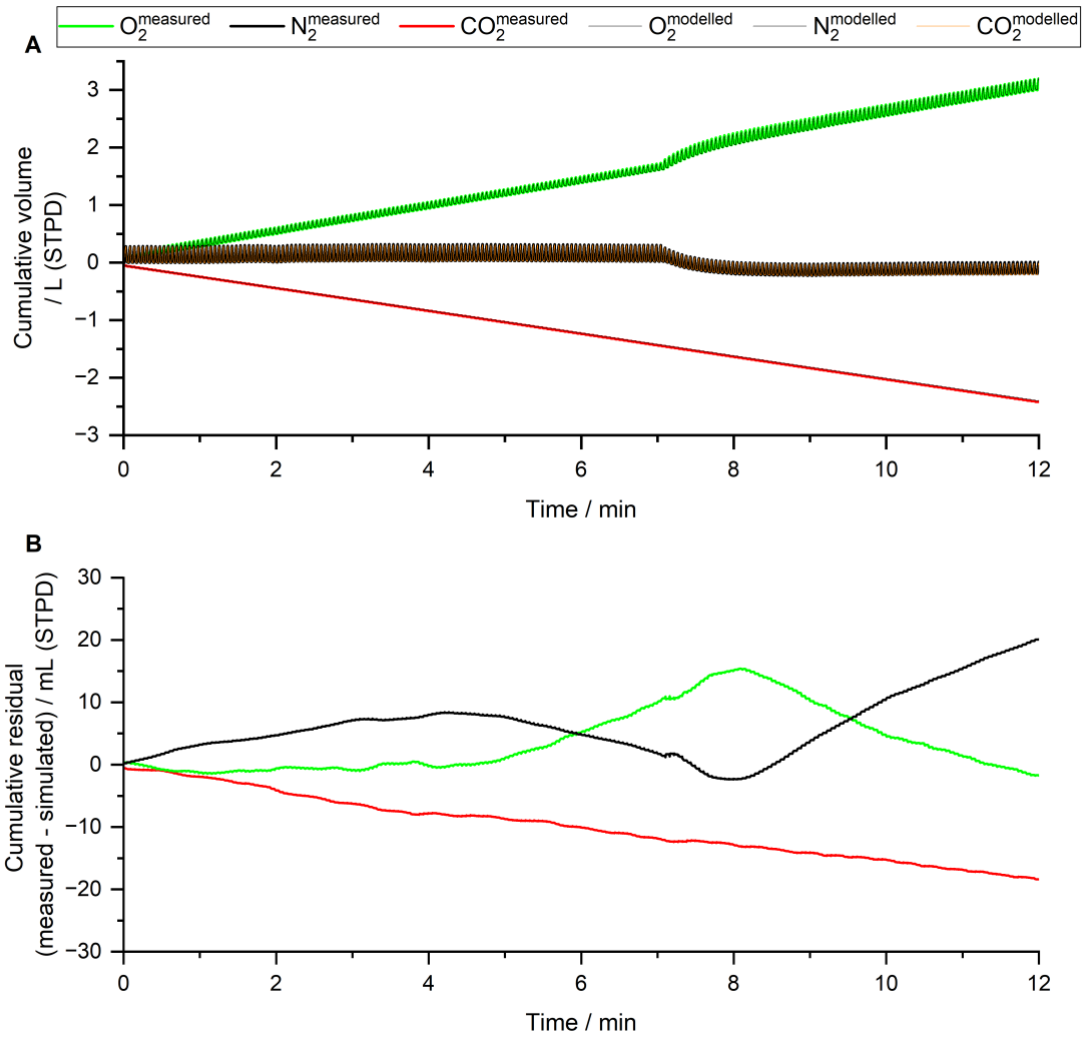

Figure 32. Quality control measures post model run.

Low residual differences between measured and modelled data and near-zero nitrogen balances indicate good quality of CCP generated datasets. A: Both measured and modelled cumulative volumes of oxygen, carbon dioxide, and nitrogen over time are represented. Nitrogen balance remains very close to zero (0.4 $mL.min^{-1}$ in this dataset) throughout baseline breathing phase. The fitting of the simulated data over the measured data is represented as a shade of grey behind the CO_2 and O_2 curves and a shade of orange behind the N_2 curve. The agreement is so significant that simulated data are almost completely overlapped by the measured data, visually indicating good quality of the dataset acquired. B: The residual cumulative difference between measured and modelled gas volumes over time is represented for oxygen (green), carbon dioxide (red) and nitrogen (black). During the baseline breathing phase the maximum residual difference was below 15 mL for each gas.

6.3.5. Statistical analyses

Statistical analyses were performed utilising SPSS version 30.0 (IBM Corp., USA), with significance established at $p < 0.05$.

The relationship between FRC values obtained by CCP and those derived from BPleth measurements was assessed using Pearson's correlation coefficient. Paired t-tests were used to evaluate differences in mean FRC between the two methods. Agreement between methods was assessed using Bland-Altman analysis, with plots constructed to illustrate percentage bias and LoA. The reproducibility of CCP FRC estimates over three repeated readings was assessed using CV and ICC.

The difference between FRCs and EELVs estimated using full and partial MBNWs – in awake and in mechanically ventilated patients, respectively – was assessed using univariate ANOVA, with EELV as the dependent variable, washout type (full or partial) as a fixed factor, and participant identity as a random factor. Pearson's correlation coefficient and Bland-Altman analysis were also performed to assess the relationship and agreement between full and partial washouts.

In mechanically ventilated patients, the precision of EELV measurements by CCP over time was assessed using CV and ICC. ANOVA was conducted to partition the total EELV variance into between- and within- subject components in order to facilitate ICC calculation.

For all paired t-tests, correlations, and Bland-Altman analyses reported in this chapter, repeated values obtained with the same method were averaged per participant prior to

analysis. This ensured one value per participant and preserved the assumption of independence required for these statistical approaches.

6.4. Results

6.4.1. Preliminary study: comparison of FRC measured by BPleth with that estimated by CCP

6.4.1.1. Baseline characteristics of participants

Fourteen healthy volunteers participated in the study. Relevant anthropometric and respiratory characteristics are displayed in Table 14. Participants exhibited normal lung function as assessed by spirometry, with all spirometry parameters (e.g., FEV1, FVC, and FEV1/FVC) within the normal range (> 80% predicted) as defined by the Global Lung Initiative (GLI) race-neutral predicted values[187].

Characteristic	Male (n = 9)	Female (n = 5)	All (n = 14)
Age / yr	30.6 ± 8.0	26.0 ± 7.0	28.9 ± 7.7
Height / m	1.78 ± 0.05	1.66 ± 0.06	1.74 ± 0.08
Weight / kg	78.9 ± 17.6	70.7 ± 11.8	75.9 ± 15.8
BMI / kg.m^{-2}	24.8 ± 5.2	26.0 ± 6.2	25.2 ± 5.4
FEV1 / L	4.2 ± 0.5	3.2 ± 0.4	3.8 ± 0.6
FEV1 / %pred	99.0 ± 14.3	100.1 ± 5.0	99.7 ± 11.6
FVC / L	5.0 ± 0.6	3.8 ± 0.7	4.6 ± 0.8
FVC / %pred	100.0 ± 12.1	103.8 ± 6.1	101.4 ± 10.1
FEV1 / FVC	0.8 ± 0.1	0.8 ± 0.0	0.8 ± 0.0
FEV1 / %pred	97.8 ± 7.1	97.2 ± 6.3	97.6 ± 6.5

Table 14. Baseline characteristics of healthy volunteers enrolled for the comparison between FRC estimated by CCP and measured by BPleth.

Values are mean ± SD. n = number of participants; %pred = percentage of predicted.

6.4.1.2. Summary of FRC measurements and estimates

A total of forty-two full MBNWs were conducted, comprising three trials per individual. CCP successfully estimated FRC in all but two measurements from one participant, where a modelling failure of unknown origin prevented estimation. As a result, this participant's single available CCP estimate was excluded from the reproducibility analysis but retained for the accuracy assessment.

For the BPleth method, each participant underwent a minimum of three FRC measurements. However, individual BPleth FRC values and the total number of measurements performed were not available to the research team. As only the average FRC measurements were available, the ability to conduct a direct comparison of within subject variability between the two methods was limited. Notably, BPleth measurements undergo strict quality control, with values exhibiting CV above 5% routinely excluded. In contrast, to calculate the average CCP FRC, all estimates were included irrespective of variation, which may inherently increase the observed variability.

CCP demonstrated high precision in repeated FRC estimations, evidenced by an average within-subject CV of 4 ± 2%, and individual values ranging from a minimum of 1% to a maximum of 8%. Eleven out of the thirteen participants included in the precision analysis exhibited CV values below 5%. CCP's performance thus closely matched the stringent quality control criteria of BPleth (CV < 5%). The calculated ICC was 0.98, indicating excellent reproducibility of CCP-derived FRC estimates within an individual, with the majority of the variance attributable to differences between individuals.

Mean FRC estimated by CCP was 3.3 ± 0.8 L compared with 3.4 ± 0.9 L measured by BPleth. Individual differences in FRC between methods are displayed in Figure 33, panel

A. Statistical analysis revealed no significant difference between FRC values estimated by CCP and those measured by BPleth ($t(13) = 1.726$, $p = 0.108$; Figure 33, panel B).

The correlation and agreement between CCP and BPleth FRC values is depicted in Figure 33, panels C and D. The two measurements were strongly correlated ($r = 0.96$, $p < 0.0001$). Bland-Altman analysis indicated a small mean percentage bias of - 3%, showing a tendency for CCP to underestimate FRC relative to BPleth. The 95% LoA ranged from - 20% to + 13%. This degree of agreement suggests that CCP provides an accurate estimate of FRC when compared to BPleth, the current reference standard.

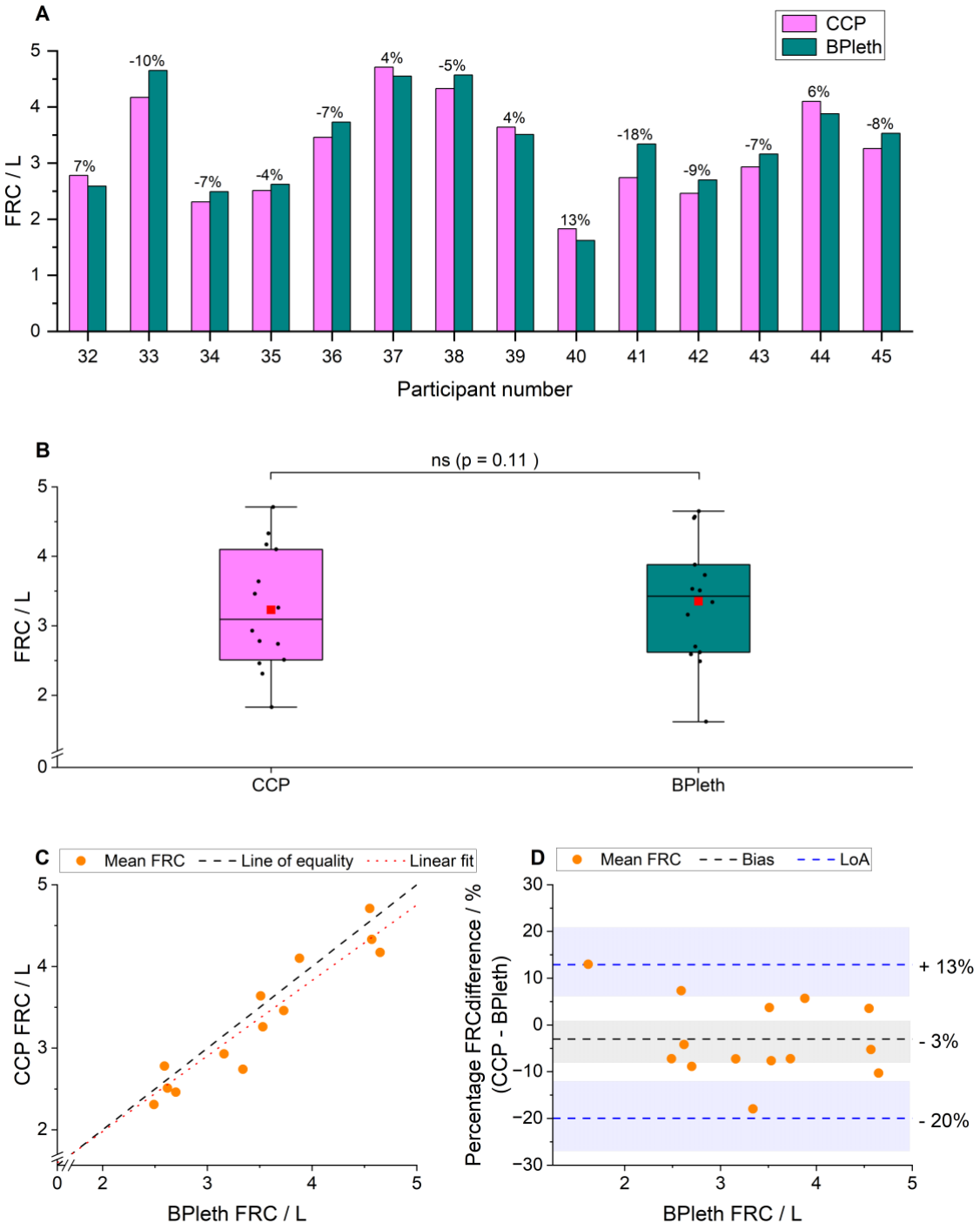

Figure 33. Individual and group comparison between FRC values estimated by CCP and measured by BPleth.

A: Individual absolute and percentage differences between methods. Fourteen participants are identified in the x-axis. The difference in FRC between methods is represented in litres in the y-axis and as a percentage (CCP - BPleth) at the top of each set of bars. B: Paired comparison between methods. The box extends from the first to the third quartile, with the central line in each box representing the median and the central red square representing the mean. Whiskers denote 1.5 times the interquartile range from the lower and upper quartiles. Each FRC value is shown as black dot. No outliers were observed. The two methods showed similar central tendencies and spread, with no statistically significant difference between their means ($t(13) = 1.726$, $p = 0.11$). C: Correlation between methods. FRC values obtained through both techniques were strongly correlated ($r = 0.96$, $p < 0.0001$). D: Agreement between methods. Using the BPleth as the reference method (x-axis), the percentage difference between CCP and BPleth was calculated (y-axis). CCP underestimated FRC by 3% (or 122 mL) when compared with BPleth, though this difference was not significant. Limits of agreement ranged from - 20 to + 13% (or - 641 to + 396 mL). The shaded grey and blue areas represent the 95% confidence interval for the bias and the limits of agreement, respectively.

6.4.2. Preliminary study: comparison of full and partial washout for the estimation of FRC

6.4.2.1. Baseline characteristics of participants

Twelve healthy participants were enrolled in the study, each completing both a full and a partial MBNW using the MFS during two separate study visits. One participant was excluded from all analyses due to CCP model outputs that did not meet quality control criteria. In another participant, CCP failed to generate an output for one of the two full washouts due to an unknown cause; all other data from this participant were retained for analysis. Baseline characteristics of the remaining eleven participants are presented in Table 15. A CONSORT-like diagram outlining the flow of patients across all studies in spontaneously breathing participants is available in Appendix B.

Characteristic	Male (n = 4)	Female (n = 7)	All (n = 11)
Age / yr	20.0 ± 0.0	22.0 ± 4.9	21.3 ± 3.9
Height / m	1.86 ± 0.07	1.71 ± 0.04	1.76 ± 0.09
Weight / kg	67.8 ± 9.1	63.0 ± 7.3	64.7 ± 7.9
BMI / kg.m^{-2}	19.6 ± 1.9	21.5 ± 2.3	20.8 ± 2.3

Table 15. Baseline characteristics of healthy volunteers enrolled for the comparison of full and partial MBNWs for the estimation of FRC.

Values are mean ± SD. n = number of participants.

6.4.2.2. Summary of FRC estimates

In total, forty-three washouts were analysed across the eleven participants included in the study: twenty-one full and twenty-two partial washouts.

Individual FRC estimates are displayed in Figure 34, panel A. While variability in the direction and magnitude of difference was observed across participants, over 70% of partial washouts yielded FRC values approximately equal to or lower than those obtained under a full washout stimulus. The within-participant percentage difference between washout types ranged from - 11% to + 7%.

On group comparison (Figure 34, panel B), there was no statistically significant difference observed in mean FRC between the two methods (full washout: 3.5 ± 0.9 L; partial washout: 3.3 ± 0.8 L; p = 0.07). A strong positive correlation was observed (r = 0.98; p = 0.0001; Figure 34, panel C), with most data points closely aligned with the line of equality.

Bland-Altman analysis (Figure 34, panel D) revealed a mean percentage bias of - 3%, indicating that partial washouts slightly underestimated FRC compared with full washouts. The 95% LoA ranged from - 13% to + 8%.

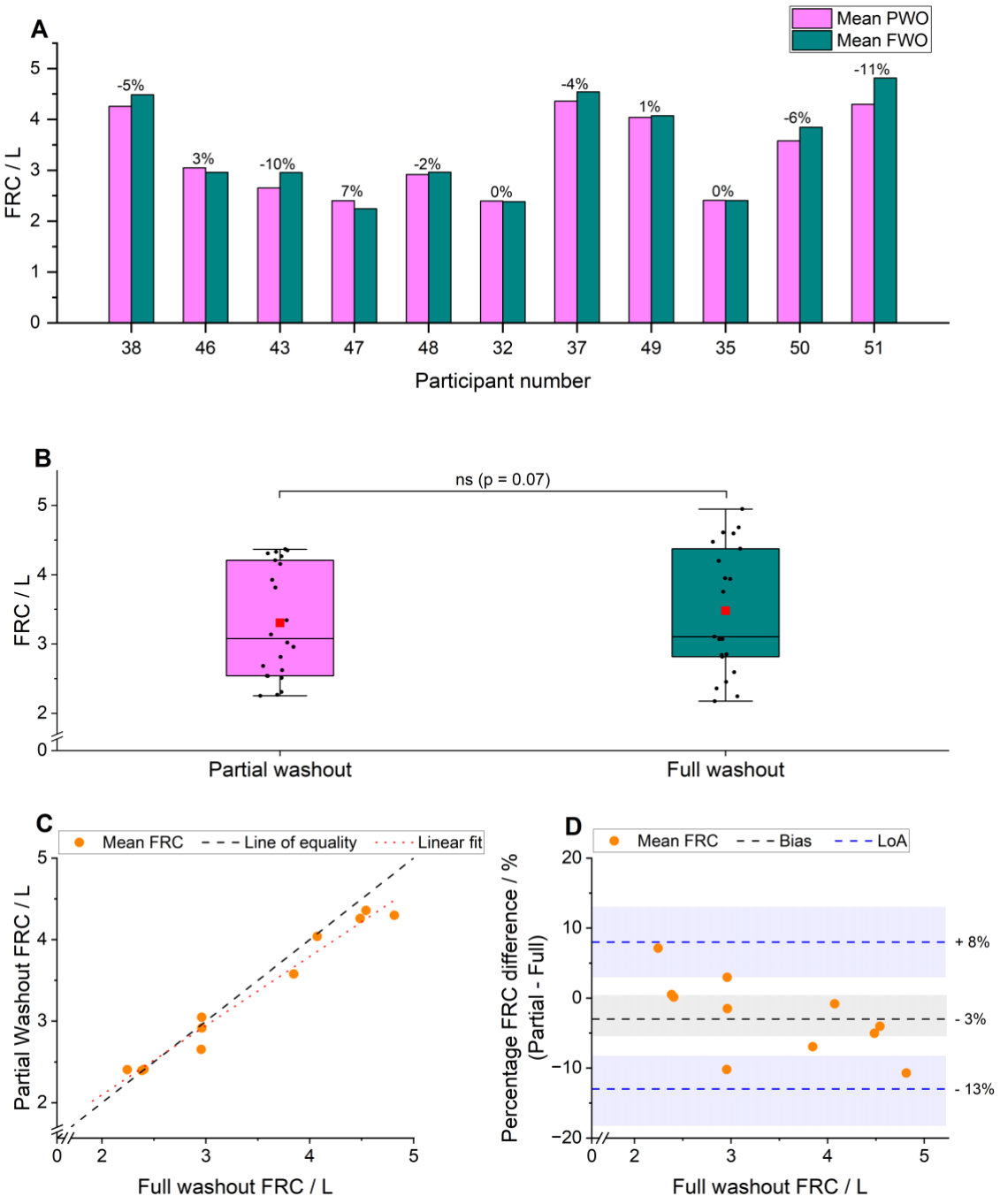

Figure 34. Comparison between full and partial nitrogen washouts in healthy volunteers.

A: Individual absolute and percentage differences between methods. Eleven participants are identified in the x-axis. The difference in FRC between methods is represented in litres in the y-axis and as a percentage (partial washout - full washout) at the top of each set of bars. B: Paired comparison between methods. The box extends from the first to the third quartile, with the central line in each box representing the median and the central red square representing the mean. Whiskers denote 1.5 times the interquartile range from the lower and upper quartiles. Each FRC value is shown as black dot. No outliers were observed. There was no statistically significant difference between the FRC means of the two methods ($F(1) = 4.08$, $p = 0.07$). C: Correlation between methods. FRC values obtained through both techniques were strongly correlated ($r = 0.98$, $p < 0.0001$). D: Agreement between methods. Using the full MBNW as the reference method (x-axis), the percentage difference between partial and a full washouts was calculated (y-axis). FRCs obtained under partial washout stimulus were, on average, 3% lower (or 106 mL) than those obtained with full washout. Limits of agreement ranged from - 13 to + 8% (or - 491 to + 279 mL). The shaded grey and blue areas represent the 95% confidence interval for the bias and the limits of agreement, respectively.

6.4.3. Estimating EELV in critical care

6.4.3.1. Baseline characteristics of patients

Data from seventeen critically ill mechanically ventilated patients were analysed in this study. Of these, nine patients underwent both full and partial nitrogen washouts for comparison, and fifteen were included in the precision analysis. Seven individuals contributed data to both analyses. A CONSORT-like diagram outlining the flow of patients across all studies in mechanically ventilated patients is available in Appendix B. Baseline characteristics of the full seventeen-patient cohort are presented in Table 16.

All patients were ventilated in a pressure-controlled mode throughout the duration of the study. The level of ventilatory support was modest, with average $P_{control}$ of 16 ± 5 cmH_2O,

PEEP of 6 ± 1 cmH_2O, and FiO_2 of 26 ± 5%. Arterial blood gases were near-normal ($PaCO_2$: 5.5 ± 0.7 kPa; PaO_2 10.0 ± 3.0 kPa).

Although only five patients had a primary lung condition and none met ARDS criteria[105], the mean P/F ratio of 37.7 ± 10.9 kPa (approximately 283 mmHg) indicates a mild oxygenation impairment in this cohort. Given that $PaCO_2$ values were within normal limits, hypoxaemia is unlikely to be due to global alveolar hypoventilation, and instead suggests a degree of ventilation-perfusion mismatch, possibly related to atelectasis, small airway closure, or subtle changes in pulmonary perfusion.

The average respiratory system dynamic compliance was 52 ± 19 $mL.cmH_2O^{-1}$, which is below the expected range for healthy lungs, but typical for a heterogeneous mechanically ventilated ICU population[188]. The 28-day mortality rate in this cohort was 23.5%, reflecting a high overall disease severity.

Characteristics	Values (n = 17)
Age / yr	56 ± 17
Male sex / n (%)	11 (64.7)
Height / m	1.72 ± 0.10
Weight / kg	87.9 ± 20.8
BMI / kg.m^{-2}	29.8 ± 7.8
28-day mortality / n (%)	4 (23.5)
$P_{control}$ / cmH_2O	16 ± 5
PEEP / cmH_2O	6 ± 1
RR / breaths.min^{-1}	19 ± 4
$PaCO_2$ / kPa	5.5 ± 0.7
PaO_2 / kPa	10.0 ± 3.0
FiO_2 / %	26 ± 5
P/F	37.7 ± 10.9
Tidal volume / mL.kg^{-1}	7.3 ± 2.6
Minute volume / L.min^{-1}	9.8 ± 2.2
C_{dyn} / $mL.cmH_2O$	52 ± 19

Table 16. Baseline characteristics of mechanically ventilated patients enrolled in the assessment of: (i) the precision of CCP in estimating EELV; (ii) the comparison of CCP-EELV estimates obtained using full versus partial washouts.

Data are expressed as mean ± SD. PEEP = positive end-expiratory pressure; $P_{control}$ = the pressure increment added to PEEP to deliver each breath in pressure-controlled mode of ventilation; RR = respiratory rate; $PaCO_2$ = arterial partial pressure of CO_2, obtained from an arterial blood gas; PaO_2 = arterial partial pressure of O_2, obtained from an arterial blood gas; P/F = ratio between PaO_2 and FiO_2; C_{dyn} = dynamic compliance of the respiratory system.

6.4.3.2. Comparison between full and partial washouts

Sixty-nine washouts were analysed across nine mechanically ventilated patients. Each individual underwent at least two full washouts (eighteen total) and two partial washouts (fifty-one total). The higher number of partial washouts reflects the inclusion of some of

these patients in the precision analysis, where partial washouts were more frequently repeated over time.

Individual EELV estimates are displayed in Figure 35, panel A. A near perfect correlation was observed between methods ($r = 0.99$; $p < 0.0001$; Figure 35, panel C), with data points tightly clustered around the line of equality. The linear fit closely overlapped the line of equality, indicating high consistency in CCP estimation of EELV between the different washout types.

The difference between values estimated using full and partial washouts was not statistically significant ($p = 0.71$; Figure 35, panel B). On average, the mean EELV was 1.9 ± 0.7 L for both washout types, differing only by a few tens of millilitres. Likewise, Bland-Altman analysis (Figure 35, panel D) revealed minimal bias (+ 1%) across techniques.

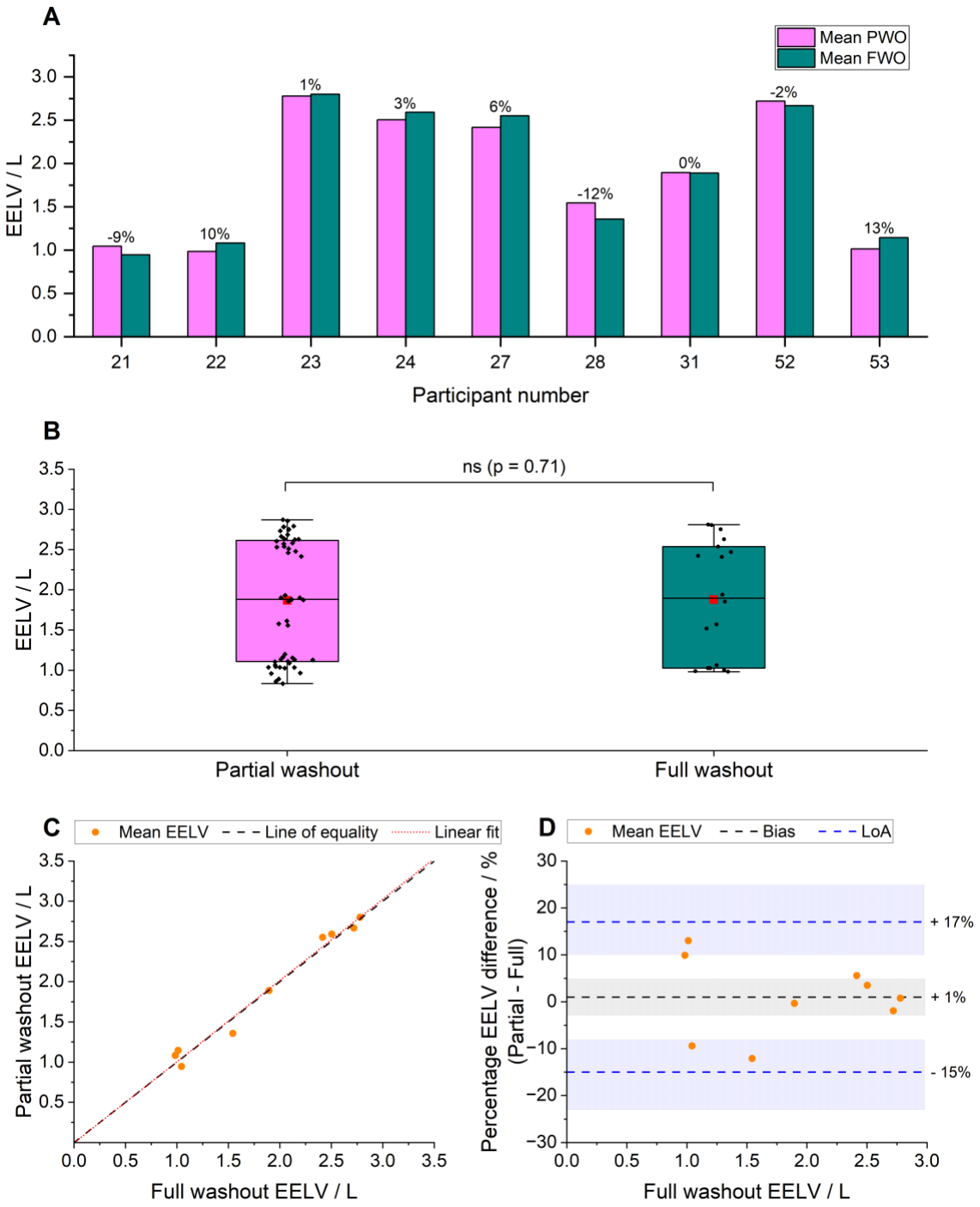

Figure 35. Comparison between full and partial nitrogen MBNWs for the estimation of EELV in mechanically ventilated patients.

A: Individual absolute and percentage differences between methods. Nine patients are identified in the x-axis. The difference in EELV between methods is represented in litres in the y-axis and as a percentage (partial washout - full washout) at the top of each set of bars. B: Paired comparison between methods. The box extends from the first to the third quartile, with the central line in each box representing the median and the central red square representing the mean. Whiskers denote 1.5 times the interquartile range from the lower and upper quartiles. Each EELV value is shown as black dot. No outliers were observed. There was no statistically significant difference between the EELV means using the two methods ($F(0.151) = 0.27$, $p = 0.71$). C: Correlation between methods. EELV values obtained through both techniques were strongly correlated ($r = 0.99$, $p < 0.0001$). D: Agreement between methods. Using the full MBNW as the reference method (x-axis), the percentage difference between partial and full washouts was calculated (y-axis). EELVs obtained under partial washout stimulus were, on average, 1% higher (or 14 mL) than those obtained with a full washout approach. Limits of agreement ranged from - 15 to + 17% (or - 203 to + 232 mL). The shaded grey and blue areas represent the 95% confidence interval for the bias and the limits of agreement, respectively.

6.4.3.3. Precision

Each of the fifteen mechanically ventilated patients in this study underwent a minimum of six partial washouts, resulting in a total of a hundred and three measurements. The average CV for EELV readings in this cohort was 5.8% (SD ± 4.4%), with values ranging from 1% to 18%. Sixty-seven percent of patients exhibited a CV ≤ 5%, and fourteen out of fifteen (93%) showed a CV ≤ 10%. The ICC was 0.996, indicating excellent reproducibility of EELV estimated from partial washouts.

The patients included in this precision analysis were the same as those included in the $\dot{V}_{O2}$ accuracy study using the MFS (section 5.4.2). Notably, the patients with the highest EELV variability (CV ≥ 9%) – patients 18, 21, 26, and 28 – were excluded from the $\dot{V}_{O2}$ precision analysis due to $\dot{V}_{O2}$ instability that appeared to arise due to pathophysiological changes during data acquisition.

Of these, only patient 18 had a clear explanation for EELV variability, with a high secretion burden, frequent suctioning, and coughing likely contributing to fluctuations in lung volume. For the remaining patients with higher CVs, no specific clinical interventions or events known to affect lung volume were documented during the measurement period or identified on post-hoc CRF and ECR review. Therefore, they were retained in the analysis.

Patient ID	Mean / L	SD / L	CV / %
17	1.34	0.02	2
18	1.83	0.16	9
19	2.07	0.09	5
20	1.90	0.12	6
21	0.95	0.09	10
22	1.08	0.05	5
23	2.80	0.05	2
24	2.59	0.12	5
25	2.82	0.15	5
26	0.82	0.09	10
27	2.55	0.07	3
28	1.36	0.25	18
29	1.70	0.06	4
30	1.68	0.04	2
31	1.89	0.02	1

MSE (WP)	0.012
MSE (BP)	2.828
F (p-value)	235.568 (< 0.001)
ICC	0.996

Table 17. EELV precision assessment.

Columns 2, 3 and 4 show, respectively, the mean, SD, and CV of EELV estimates by CCP for each patient included. Summary metrics for the mean squared error (MSE) of between-patient variability (BP), within-patient variability (WP), their relationship (F = BP/WP), and intra-class correlation (ICC) are also provided. ID = dentification number.

6.5. Discussion

6.5.1. Comparison of CCP with BPleth

CCP estimates of FRC were closely aligned with those obtained via BPleth, the current gold standard. This agreement held for both bias and precision, supporting the use of CCP in measuring absolute lung volumes in awake individuals.

According to the most recent ERS/ATS consensus, repeated MBNW-derived FRC should demonstrate a CV below 10%[67]. In commercial practice, measurements outside this threshold are typically discarded, which may lead to an apparent, but not actual, measure of test precision in published data[189-191]. In contrast, all CCP trials were retained in this study, yet every participant's data met the most stringent "Grade A" quality criteria[67]. The average CV of FRC using CCP was 4 ± 2%, closely matching the < 5% benchmark recommended for BPleth[67] – with the advantage of not requiring a sealed chamber or participant cooperation.

While *in vitro* precision data for commercial MBNW devices are available[192], *in vivo* validation studies remain scarce, as many publications exclude measurements that fall outside ATS/ERS repeatability criteria. Moreover, substantial variation between devices has been reported. For example, two widely used systems – the Exhalyzer D (Eco Medics AG, Switzerland) and the EasyOne Pro (ndd Medizintechnik AG, Switzerland) – have shown poor agreement with each other[190, 193]. The Exhalyzer D, which has been used clinically for over a decade, was only recently corrected for an oxygen-carbon dioxide sensor crosstalk that had introduced systematic errors in FRC of approximately 10%[194]. Similarly, a signal correction for the EasyOne Pro was implemented in 2024, revealing that prior uncorrected values may have been overestimated by more than 10%[195].

As expected, CCP tended to report slightly lower FRC values than BPleth, although this difference was neither statistically nor clinically significant. This is consistent with physiological principles: MBNW methods measure only ventilated lung compartments, while BPleth includes non-communicating volumes such as trapped gas. In healthy individuals, where gas trapping is minimal, both methods are expected to converge. This expectation was borne out in the present cohort. Similar findings have been reported in the literature[88, 196, 197], although some studies describe a significant bias between the two methods even in healthy subjects[189, 193, 198, 199], with the direction and magnitude of the discrepancy varying.

One likely contributor to the strong agreement observed in this study is the longer washout period used during CCP (5 minutes), compared with the typical 2 to 3 minutes in commercial MBNW protocols (e.g., stopping at $1/40^{th}$ of the baseline nitrogen concentration)[200]. This extended washout may have allowed for better ventilation of slow compartments and improved completeness of nitrogen clearance.

Although direct comparisons with BPleth are not possible in mechanically ventilated patients, the present findings suggest that CCP can deliver reproducible and physiologically accurate FRC estimates. The combination of a highly time-resolved measurement system (MFS) and extended washout duration likely contributed to the observed precision, supporting CCP as a tool for bedside lung volume assessment in the study of mechanically ventilated individuals.

6.5.2. Comparison of full and partial MBNWs to estimate EELV

Across both study cohorts – healthy volunteers and mechanically ventilated critically ill patients – partial and full FiO_2 washouts yielded comparable estimates of FRC or EELV

when using CCP. While the direction of bias between cohorts differed, these differences were neither clinically nor statistically significant, supporting the clinical equivalence of the two approaches.

The motivation to minimise the FiO_2 step change stems from two key concerns: (i) the risk of oxygen-induced absorption atelectasis; and (ii) the fact that many ICU patients are ventilated on elevated baseline FiO_2, making a full washout (0.79 FiO_2 rise) impossible. The relationship between high inspired oxygen levels and atelectasis is well established: alveolar collapse occurs more rapidly and at higher V/Q ratios when FiO_2 approaches 1.0[201]. Prolonged intra-operative exposures to high oxygen tensions can cause EELV reductions that persist for more than 24 hours[202].

To the best of this author's knowledge, to date, no studies have systematically explored how various small FiO_2 steps affect FRC measurements during MBNW in healthy spontaneously breathing individuals. Given that commercial devices are often unable to maintain adequate signal alignment at full washouts, it seems unlikely that they would perform well employing small FiO_2 changes, which may compromise volume accuracy. For example, *Maisch et al.* found that when comparing a pair of FRCs derived from a 0.29 FiO_2 step to another pair obtained from a 0.79 step, the bias was small (- 2.6%) but the limits of agreement were very wide (- 24.5 to + 17.1%)[203]. At the 0.29 delta FiO_2, FRCs generated by MBNW were on average 11.7% lower than those obtained with BPleth (- 42.8% to + 19.3% LoA)[203]. *Heinze et al.* reported similarly wide variability when comparing FRCs obtained through a 0.6 FiO_2 step with BPleth[88].

In mechanically ventilated patients, *Olegard et al.* compared EELV estimates in mechanically ventilated patients using 0.1 and 0.3 FiO_2 steps and reported a small mean

bias (- 9 mL), but quite wide LoA (± 356 mL), despite all measurements being completed in less than an hour[85]. In the current study, despite a larger FiO_2 step (≥ 0.7) and a significantly longer measurement window, CCP achieved LoA approximately 40% narrower than those reported by *Olegard et al.*[85], likely reflecting the higher precision of the latter approach.

The findings reported here are consistent with findings by *Wrigge et al.*, who used mass spectrometry to compare MBNW-based EELVs from FiO_2 steps of 0.2, 0.3, 0.4, and 0.7 in postoperative patients[204]. The device employed in their study is likely to have been more technically robust than its commercial counterparts, as it directly measured nitrogen with high precision while employing corrections for delays and viscosity changes[204]. These investigators found a small bias (1.2%) and relatively narrow LoA (± 7.8%) when comparing 0.2 vs 0.7 FiO_2 steps[204]. However, their study involved only patients with healthy lungs and short measurement intervals (15 minutes), in contrast with the prolonged protocol employed in the present thesis study, which allowed patients with lung disease to be included – factors that will necessarily have introduced greater variability.

In summary, CCP-derived EELV estimates obtained via partial FiO_2 washouts can be seen to be comparable to those from full washouts, both in healthy spontaneously breathing individuals and in critically ill mechanically ventilated patients. These findings are reassuring and support the use of partial washouts as a more practical and safer alternative in the intensive care setting.

6.5.3. Precision of EELV estimates in mechanically ventilated patients

The present study demonstrates that CCP provides acceptable precision for estimating EELV in mechanically ventilated patients. Unlike previous studies involving MBNW-based techniques[85, 87, 204-207], this study was conducted over an extended period – spanning several hours – with at least six measurements per patient. It included patients with and without lung disease and allowed transient oscillations between assisted and controlled modes in patients with lighter sedation, reflecting real-world ICU variability. Despite these more challenging conditions, CCP achieved a low average coefficient of variation of 5.8% (SD ± 4.4%), with 93% of patients exhibiting a CV ≤ 10%, and an ICC of 0.996 – indicating excellent reproducibility. Even under this broader variability, CCP's performance matched or exceeded that of previous studies using duplicate EELV measurements, which report mean CVs below 7%[85, 87, 204-207].

Some of the observed variability is likely attributable to true physiological changes in lung volume, rather than device imprecision. This is supported by the study's extended timeframe, during which patients may have experienced subclinical variations in factors that can modify lung volumes. The ability to capture these variations is key to ensure CCP's suitability not only for accurate measurement, but also for meaningful longitudinal monitoring.

Compared with traditional MBNW devices, CCP eliminates a critical limitation: the need for breath-by-breath synchronisation and post hoc correction for gas timing and concentration changes. Conventional systems require complex alignment between flow and gas sensors, which are physically separated in the breathing circuit. These alignment procedures are vulnerable to error, particularly in mechanically ventilated patients with

irregular or dyssynchronous breathing. In fact, even systems that claim to bypass synchronisation requirements[87] (e.g., by using end-tidal rather than the entire breath for volume estimation) require correction for the early "gas front" after an FiO_2 step, where gas concentrations vary rapidly between breaths[84]. Failure to apply such corrections appropriately has been shown to result in errors of 10-20% in both bench and clinical settings[204, 206]. Recent "recall" corrections to commercial devices, as discussed, illustrate how pervasive these issues can be[194, 195].

In contrast, CCP's unique advantage lies in its fully integrated, time-resolved data stream: flow and gas signals are recorded at the same point in the circuit, eliminating the need for any time alignment. Viscosity is also measured on the spot, and, consequently, gas flows do not require further adjustment. This not only reduces technical error but also enables prolonged measurement protocols with high precision and minimal drift – a key requirement for identifying real changes in lung volume rather than artifacts introduced by measurement technique.

Together, these findings support CCP as a robust, reproducible, and adaptable tool for assessing EELV in mechanically ventilated patients, including under conditions that would challenge the reliability of conventional methods.

6.5.4. Limitations

6.5.4.1. Technical

While the promise of CCP is considerable, it must be recognised that the MFS has been developed as a scientific instrument for research purposes rather than as a medical device. As such there are a number of challenges that would need to be overcome before it could be suitable for widespread use in the clinical setting.

First, the measurement head together with the bacterial filter that is required between the ventilator circuit and the patient both add to dead space, which is undesirable, especially in patients for whom lung protective ventilation is indicated. The measurement head is also relatively bulky and requires its own mechanical arm to support it.

Second, the MFS is yet to be tested to ensure its accuracy remains satisfactory under the conditions posed by active humidification. While the MFS has performed well in such conditions for short periods of time in healthy volunteers and for twelve hours using a bespoke lung simulator, it is yet to be tested for prolonged periods of time in mechanically ventilated individuals. Currently, the interposition of an HME filter is essential.

Third, the patient cannot receive nebulised medications with the measurement head in situ. The cavity mirrors become coated with the nebulised drug, which impairs gas composition analysis.

Finally, estimation of the model parameters from the raw data sometimes requires an hour or more of computing time, and so the code would require substantial optimisation in order to make measurements available in a timely manner for patient management.

6.5.4.2. Experimental

Several experimental limitations should be acknowledged. First, the sample size was small, although appropriate for a proof-of-concept investigation.

Second, while CCP-derived FRC values were compared with the gold standard of BPleth in healthy individuals, no reference method was available for mechanically ventilated patients. As such, the accuracy of CCP in the ICU setting could not be directly assessed.

Third, some of the variability observed in repeated CCP measurements likely reflects genuine changes in lung volume rather than technical noise. In mechanically ventilated patients, this may have occurred due to the extended duration of the measurement period. In healthy individuals, such changes may have arisen from minor variations in position between repeated lung volume readings.

Finally, mechanically ventilated patients exhibited significant heterogeneity. While this reflects true ICU complexity, it may also undermine the instrument's performance compared to studies conducted in more controlled conditions.

6.6. Conclusion

This chapter explored the application of CCP for estimating EELV in mechanically ventilated patients, a context where accurate, repeatable lung volume assessment may be clinically important yet remains technically challenging. Across a small but diverse cohort, CCP demonstrated high measurement consistency under true ICU conditions, with routine care maintained and observations conducted for a prolonged period of time. These findings suggest that CCP may offer a practical and technically robust alternative to traditional MBNW techniques, particularly given its ability to overcome the challenges of synchronisation.

The study also examined whether smaller step changes in inspired oxygen – more suitable for critically ill patients – could be used effectively for CCP-based EELV estimation. The results indicate that partial washouts provide equivalent estimates to full washouts. In healthy participants, CCP-derived FRC values showed close agreement with those measured by BPleth, offering additional confidence in the validity of the present approach.

Taken together, these investigations offer preliminary evidence supporting the feasibility of CCP for bedside lung volume assessment in mechanically ventilated patients. The accuracy and precision demonstrated here set the stage for future investigations into a possible clinical role for CCP in critical care, including its potential for assessing lung recruitability and the effects of commonly performed manoeuvres (e.g., RMs and prone positioning).

Chapter 7. Measurement of EELV in critically ill patients undergoing a Recruitment Manoeuvre

7.1. Introduction

Recruitment manoeuvres are generally considered in the context of a mechanically ventilated patient who is suspected to have regions of the lung that are unventilated. These manoeuvres may help to re-inflate collapsed regions such that they then contribute effectively to gas exchange. However, the clinical benefit of RMs is highly variable, and indiscriminate application may increase the risk of VILI without benefit.

To guide the use of RMs, a rational assessment of lung recruitability is key, enabling identification of those patients who are more likely to benefit. Yet, existing indices of recruitability often disagree, and their results are sensitive to the protocols and methods used to generate them.

Likewise, methods to assess the effectiveness of RMs – both in regards to lung volumes and ventilation distribution – remain limited. While several studies have conducted CT imaging both before and after a RM to evaluate recruitment[117, 124, 130, 208, 209], this approach is impractical for routine clinical care and, furthermore, it does not allow for sequential measurement to determine whether any benefit of the manoeuvre is sustained.

7.2. Research aims and objectives

The primary aim of the experiments presented in this chapter was to explore the potential clinical utility of CCP to assess lung recruitment in mechanically ventilated patients undergoing a RM.

The objectives of this study were to: (i) quantify the absolute changes in EELV following a quasistatic PV curve and a sustained inflation RM using CCP-derived volume estimates; (ii) examine the relationship between CCP volume-based indices and conventional lung recruitability variables; (iii) examine the relationship between CCP volume-based indices and the volume recruited during sustained inflation (V_{rec}); (iv) evaluate ventilation inhomogeneity through σC_L before and after a RM.

7.3. Methods

Patient recruitment, informed consent, ethical considerations, and instrumental setup for mechanically ventilated patients were discussed in Chapter 5. Data recording, data processing, model fitting, and quality control checks were conducted as described on sections 6.3.2.1, 6.3.2.2, 6.3.3, and 6.3.4 respectively. Study-specific aspects of the

experimental protocol and appropriate statistical analyses will be discussed in the following sections.

7.3.1. Quasistatic PV curve and RM

Throughout MFS monitoring, patients continued to receive routine clinical care. In some cases, this included clinician-led assessment of lung recruitability using PV curves, sometimes followed by the performance of a RM if felt to be clinically indicated. These procedures were not conducted as part of the research protocol, but rather according to clinician preference.

Pressure-volume curves were generated and RMs were delivered by the ventilator using the built-in P/V Tool (Hamilton Medical AG, Switzerland). Clinicians were reminded of the protocol[211] recommended by the manufacturer [210], however, the approach taken – including pressure settings, inflation rate, and duration – was ultimately left entirely to the discretion of the treating clinician. In all cases, PV curves were generated using low-flow inflation-deflation cycles, and RMs were delivered as sustained inflations. The suggested parameters are summarised in Table 18 and described in greater detail in the manufacturer's clinical white paper and accompanying publication by *Chiumello et al*[130, 210].

Manoeuvre	Variable	Ref	Definition
PV curve	P_{start} / cmH_2O	5	Airway pressure at the beginning of the manoeuvre
	P_{top} / cmH_2O	40	Top airway pressure at the end of inflation
	Ramp speed / $cmH_2O.sec^{-1}$	2	Speed with which airway pressure changes
	End PEEP / cmH_2O	5	Airway pressure at the end of the manoeuvre
RM	P_{start} / cmH_2O	CP	Airway pressure at the beginning of the manoeuvre
	P_{top} / cmH_2O	40	Top airway pressure at the end of inflation
	Ramp speed / $cmH_2O.sec^{-1}$	5	Speed with which airway pressure changes
	T_{pause} / sec	10	Time period of sustained inflation
	End PEEP / cmH_2O	15	Airway pressure at the end of the manoeuvre

Table 18. Reference values for quasistatic pressure-volume curves and recruitment manoeuvres.

Reference values (Ref) suggested for the use of P/V Tool (Hamilton Medical AG, Switzerland)[210]. CP = current PEEP; the PEEP to which the patient was exposed before a RM was performed.

Given that RMs were implemented solely at the discretion of the clinical team, the study did not restrict enrolment to patients meeting the Berlin definition of ARDS. Inclusion criteria for mechanically ventilated patients were outlined in section 5.3.1.

7.3.2. Lung recruitability

Several established indices derived from the quasistatic pressure-volume curve were used to assess lung recruitability and were compared with absolute volumes and their corresponding metrics estimated by CCP. These indices are illustrated in Figure 36, panels A and B.

The normalised maximum distance percentage (NMD%) was calculated as the ratio between the maximal vertical distance separating inflation and deflation limbs of the PV

curve (D_{max}) and the maximal lung volume achieved at the top airway pressure (V_{top}), expressed as a percentage:

$$NMD\% = (D_{max}/V_{top}) \times 100$$

Patients with an NMD% of 41% or higher were considered to have a high potential for lung recruitment, while those below this threshold were considered to have limited recruitability[130]. In addition to the normalised index, D_{max} alone was used directly as an indicator of lung recruitability.

Hysteresis of the PV curve was explored using three different metrics. Raw hysteresis (in $cmH_2O.mL$), was calculated as the polygonal area contained between the inspiratory and expiratory limbs of the curve. Two hysteresis ratios were additionally computed through raw hysteresis normalisation by: (i) the product of the pressure span of the curve (P_{top} minus P_{start}) and V_{top}, in %; (ii) the product of the pressure span of the curve and the predicted body weight of the patient, in $mL.kg^{-1}$.

7.3.3. Volume recruited during sustained inflation

The volume recruited during the sustained inflation phase of the RM (V_{rec}) was utilised to evaluate the efficacy of lung recruitment. This was calculated as the difference in lung volume determined from the RM curve at the end versus the beginning of the sustained inflation period. The method is illustrated in Figure 36, panel C.

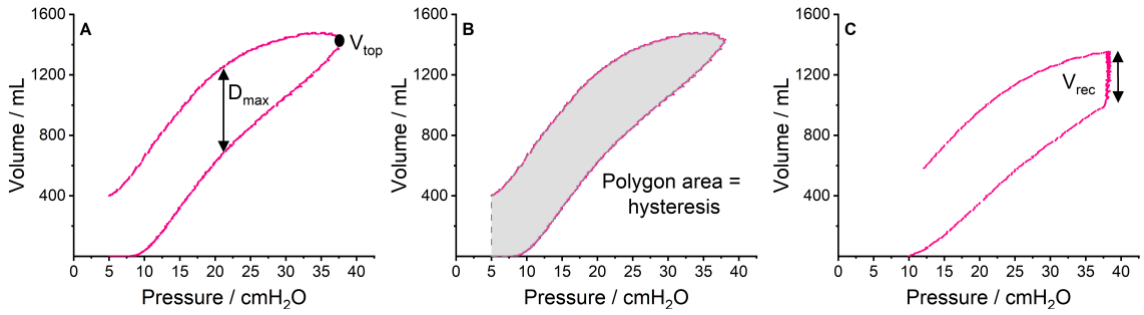

Figure 36. Assessment of lung recruitability with the P/V Tool and volume recruited by a recruitment manoeuvre through existing indices.

Panel A: calculation of the normalised maximum distance percentage (NMD%), defined as the maximum vertical distance (D_{max}) between inflation and deflation limbs of the PV curve, normalised by the maximal lung volume at top airway pressure (V_{top}). Panel B: calculation of hysteresis, measured as the polygonal area enclosed between the inspiratory and expiratory limbs of the PV loop. Panel C: Volume recruited during the sustained inflation phase of the RM (V_{rec}), calculated as the difference between the start and end of the sustained inflation phase at supranormal pressure.

7.3.4. Individual ranges of normal lung volumes

For each mechanically ventilated patient undergoing a RM, an individualised normal EELV range was calculated based on the upper and lower predicted bounds for FRC defined by the GLI[211]. Predicted FRC values were obtained by inputting patient-specific characteristics (age, height, and sex) into the GLI reference equation calculator[211]. A reduction factor to 75% was applied to account for the known effect of supine positioning on the lung volume[59, 60]. The calculation of the modified EELV bounds was conducted as follows:

$$pFRC_{UB} = (calculated\ upper\ bound\ value\ \times 0.75)$$

$$pFRC_{LB} = (calculated\ lower\ bound\ value \times 0.75)$$

where $pFRC_{UB}$ and $pFRC_{LB}$ are, respectively, the upper and lower bound GLI-predicted FRC values modified to account for supine position.

7.3.5. Predicted body weight

Predicted body weight (PBW) was calculated based on patient sex and height[96]. For male patients: $PBW\ (kg) = 50 + 0.91 \times (height\ in\ cm - 152.4)$. For female patients: $PBW\ (kg) = 45.5 + 0.91 \times (height\ in\ cm - 152.4)$.

7.3.6. CCP-derived absolute volume and inhomogeneity metrics

The absolute volume metrics estimated using CCP are summarised on Table 19.

Variable	Definition
$EELV_{BRM}$	EELV before RM
$EELV_{ARM}$	EELV after RM
V_{PEEP}	Volume added to EELV by the presence of PEEP
$V_{\Delta PEEP}$	Volume added to, or deducted from, EELV by a change in PEEP
$EELV_{ZEEP}$	EELV at zero PEEP
$Z\sigma C_L$	Z-score for ventilation inhomogeneity, represented by σC_L
ΔEELV	Total change in EELV following RM
ΔEELV / PBW	Total change in EELV normalised by PBW
ΔV_A	Total change in V_A following RM
ΔV_A / PBW	Total change in V_A normalised by PBW
ΔRM	Change in EELV following RM discounted from $V_{\Delta PEEP}$
ΔRM / PBW	Change in EELV discounted from $V_{\Delta PEEP}$ normalised by PBW

Table 19. Definition of CCP-derived absolute volume and inhomogeneity metrics.

7.3.6.1. EELV calculation

EELV was calculated as the sum of V_A and V_D, both retrieved from the parameter set file at the conclusion of CCP.

7.3.6.2. Volume added by changes in positive end-expiratory pressure

The CCP model does not automatically distinguish the proportion of alveolar volume attributable to applied positive end-expiratory pressure (V_{PEEP}). During EELV reproducibility assessments, the determination of V_{PEEP} was unnecessary since all MBNW were conducted under constant PEEP conditions.

However, when PEEP changed – as often occurred following a recruitment manoeuvre – it became necessary to separate the additional volume introduced by the new PEEP level ($V_{\Delta PEEP}$) from total alveolar recruitment. This differentiation was essential to understand the lung volume changes resulting specifically from a recruitment manoeuvre.

To calculate $V_{\Delta PEEP}$, linearity of the respiratory system compliance was assumed. First, the difference in applied PEEP before ($PEEP_{BRM}$) and after ($PEEP_{ARM}$) a RM was determined. Dynamic compliance was then calculated as the slope of a single-breath pressure-volume loop recorded during the baseline phase of the post-RM MBNW (C_{ARM}; Figure 38). $V_{\Delta PEEP}$ was then computed[124] as:

$$V_{\Delta PEEP} = (PEEP_{ARM} - PEEP_{BRM}) \times C_{ARM}$$

The single-breath curve from which C_{ARM} was derived was representative of the patient's lung mechanics, as shown in Figure 37. In this example, thirty consecutive breaths closely overlapped, indicating minimal breath-to-breath variability.

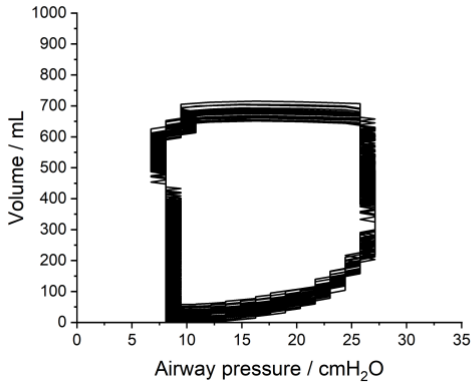

Figure 37. Defining a representative tidal breath to measure dynamic compliance

Thirty consecutive tidal breaths are plotted to illustrate the consistency of lung mechanics during the measurement period. The tight overlap between individual pressure-volume loops reflects minimal breath-to-breath variability, supporting the use of a single representative breath to calculate dynamic compliance.

7.3.6.3. End-expiratory lung volume at zero PEEP

The end-expiratory volume at zero PEEP ($EELV_{ZEEP}$) was estimated by subtracting V_{PEEP} from CCP-derived EELV obtained before a RM ($EELV_{BRM}$). V_{PEEP} was calculated as the product of the applied PEEP and the dynamic compliance before a RM (C_{BRM}), using the pressure difference between the PEEP during MBNW and zero:

$$EELV_{ZEEP} = EELV_{BRM} - (PEEP_{BRM} \times C_{BRM})$$

This method assumed linear pressure-volume behaviour over the range between PEEP and zero pressure.

7.3.6.4. Absolute volume recruitment induced by a RM

To quantify recruited lung volume, a partial MBNW was performed immediately before and approximately thirty minutes after a RM was performed. This allowed the calculation of EELVs for the corresponding periods. Two main measures of volume recruitment were derived: ΔEELV and ΔRM.

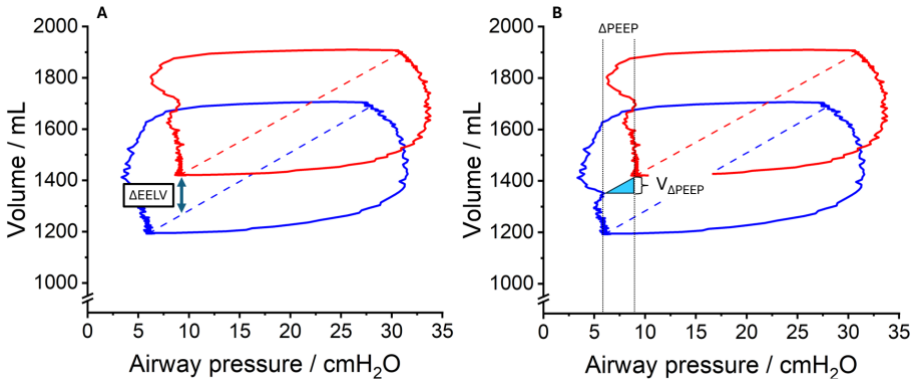

Figure 38. Calculating ΔEELV, $V_{\Delta PEEP}$, and ΔRM

Each figure contains two single-breath PV loops from a patient of the study: one before (in blue) and one after a RM (in red). The curves are offset on the y-axis by the absolute EELV derived from CCP. Dashed lines represent the dynamic compliance before (C_{BRM}; in blue) and after (C_{ARM}; in red) a RM. (A) The total change in end-expiratory lung volume (ΔEELV) corresponds to the vertical difference in volume between two single-breath PV loops. (B) The volume attributable to the change in PEEP ($V_{\Delta PEEP}$) is obtained from multiplying the change in PEEP between the two PV loops (ΔPEEP), by the dynamic compliance after a RM. By subtracting $V_{\Delta PEEP}$ from ΔEELV, the absolute volume recruited (ΔRM) can be determined.

The total change in end-expiratory lung volume was calculated as the simple difference between post-recruitment EELV ($EELV_{ARM}$) from pre-recruitment EELV ($EELV_{BRM}$) values. This calculation did not differentiate between the volume recruited and a change in volume resulting from altered PEEP levels.

$$\Delta EELV = EELV_{ARM} - EELV_{BRM}$$

To obtain ΔRM, the total change in absolute lung volume was corrected for any volume shift attributable to alterations in PEEP. Specifically, the volume change caused by varying PEEP ($V_{\Delta PEEP}$) was subtracted from ΔEELV.

$$\Delta RM = \Delta EELV - V_{\Delta PEEP}$$

7.3.6.5. Absolute volume change induced by PV curve

The calculations described above were repeated to assess whether performing a PV curve alone could induce measurable changes in EELV. In this analysis, PEEP remained constant; therefore, correction for changes in PEEP was not necessary.

7.3.6.6. Z-scores for ventilation inhomogeneity

Z-scores for σC_L ($Z\sigma C_L$) were calculated to assess the degree of ventilation inhomogeneity relative to age-predicted norms. The reference equation was derived from *Alamoudi et al.*[212], where predicted σC_L ($\sigma C_{L,predicted}$) was estimated using the following regression model:

$$\sigma C_{L,predicted} = 2.062 - 0.966 \times \ln(age) + 0.146 \times \ln(age)^2$$

The Z-score was then calculated for each patient using:

$$Z\sigma C_L = (\sigma C_{L,observed} - \sigma C_{L,predicted})/0.0738$$

Where 0.0738 represents the SD of residuals (root mean square error) reported for the model, and the observed σC_L ($\sigma C_{L,observed}$) is that retrieved from the CCP output file.

A $Z\sigma C_L$ between ± 1.65 was considered normal. Values greater than + 1.65 were considered above the upper limit of normal, corresponding to the 95th percentile, while those below - 1.65 were below the lower limit of normal, corresponding to the 5th percentile. Patients were classified as having normal or high ventilation inhomogeneity based on these thresholds.

7.3.7. Statistical analyses

Statistical analyses were performed utilising SPSS version 30.0 (IBM Corp., USA), with significance established at $p < 0.05$. Data were analysed using descriptive statistics to evaluate responses to RM and assess deviations from normal values. Results are given as mean ± SD unless stated otherwise. To assess the impact of RM, paired t-tests were used to compare pre- and post-RM values for key parameters, including $Z\sigma C_L$ and volume-based indices. Pearson's correlation coefficient and linear regression were computed to explore associations between CCP-derived absolute volume changes and existing indices of lung recruitability and volume recruitment.

7.4. Results

7.4.1. Baseline characteristics of patients

Seventeen critically ill mechanically ventilated patients were considered for inclusion in this analysis. Five, however, did not proceed to the analysis phase. In one patient, nebulised salbutamol administration compromised the quality of the MFS readings. In three cases, data recording was stopped after acquiring the quasistatic pressure-volume curve because the clinical team decided not to proceed with a recruitment manoeuvre. In the final case, CCP modelling was unable to retrieve results for unknown reasons. The remaining twelve

patients formed the final analysis cohort: the RM group. Their baseline characteristics are summarised in Table 20. A CONSORT-like diagram outlining the flow of patients across all studies in mechanically ventilated patients is available in Appendix B.

Similar to the group of patients described in section 6.4.3.3, all individuals in the RM analysis were ventilated in pressure-controlled mode. However, the RM group showed evidence of more severe respiratory impairment, with higher pressures required to prevent lung collapse, along with worse oxygenation indices and lung mechanics.

The mean inspiratory pressure in the RM group was only modestly higher than in the EELV precision patient cohort (section 6.4.3.3; 18 ± 3 cmH_2O; + 12%), while PEEP was more markedly elevated, averaging 10 ± 3 cmH_2O – an upward difference of almost 70%. These higher ventilatory pressures were accompanied by greater oxygen requirement and worse oxygenation indices, indicating more severely impaired gas exchange. The average baseline FiO_2 and P/F ratios were, respectively, 40 ± 13% and 26.4 ± 6.6 kPa. Dynamic compliance of the respiratory system was also significantly reduced, averaging 29 ± 6 $mL.cmH_2O^{-1}$ – nearly half of the mean value observed in section 6.4.3.3.

Notably, despite a more complex respiratory management, the 28-day mortality was lower in the RM group: only one in twelve patients died by day 28. Another eight patients remained hospitalised, either in intensive care units or on the wards, suggesting prolonged illness and delayed recovery.

All patients were receiving treatment for lower respiratory tract infection at the time of enrolment, including cases of community-acquired pneumonia, hospital-acquired pneumonia, and ventilator-associated pneumonia. None met formal diagnostic criteria for ARDS.

The mean tidal volume, normalised to predicted body weight, was 7.6 ± 0.7 $mL.kg^{-1}$. It should be remembered that tidal volumes were adjusted to maintain adequate minute-volume ventilation in the context of increased apparatus dead space introduced by the MFS and HME filter.

Characteristics	Values (n = 12)
Age / yr	53 ± 10
Male sex / n (%)	8 (66.7)
Height / m	1.69 ± 6.32
Weight / kg	81.3 ± 17.6
BMI / $kg.m^{-2}$	28.7 ± 7.1
28-day mortality / n (%)	1 (8.3)
$P_{control}$ / cmH_2O	18 ± 3
PEEP / cmH_2O	10 ± 3
RR / $breaths.min^{-1}$	22 ± 3
$PaCO_2$ / kPa	6.2 ± 1.2
PaO_2 / kPa	10.6 ± 2.1
FiO_2 / %	40 ± 13
P/F	26.4 ± 6.6
Tidal volume / $mL.kg^{-1}$	7.6 ± 0.7
Minute volume / $L.min^{-1}$	10.7 ± 2.0
C_{dyn} / $mL.cmH_2O$	29 ± 6

Table 20. Baseline characteristics of the RM group.

Data are expressed as mean ± SD. PEEP = positive end-expiratory pressure; $P_{control}$ = the pressure increment added to PEEP to deliver each breath in a pressure-controlled mode of ventilation; RR = respiratory rate; $PaCO_2$ = arterial partial pressure of CO_2, obtained from an arterial blood gas; PaO_2 = arterial partial pressure of O_2, obtained from an arterial blood gas; P/F = ratio between PaO_2 and FiO_2; C_{dyn} = dynamic compliance of the respiratory system.

7.4.2. Determination of EELV before a RM

$EELV_{BRM}$ was estimated using CCP. From this value, $EELV_{ZEEP}$ was calculated by subtracting the volume attributable to applied PEEP, as described in section 7.3. Both $EELV_{BRM}$ and $EELV_{ZEEP}$ were compared against a normal-volumes reference range, defined as the values contained within 75% of the minimum and the maximum GLI-predicted FRCs.

Figure 39 presents the $EELV_{BRM}$ and $EELV_{ZEEP}$ values for each of the twelve patients, alongside the corresponding reference range. The average $EELV_{BRM}$ and $EELV_{ZEEP}$ in this cohort was 1.9 ± 0.8L and 1.6 ± 0.8L, respectively. At zero PEEP, seven patients had EELV values below the lower limit of the normal range. When including the volume attributable to PEEP, $EELV_{BRM}$ fell within the normal range in eight out of the twelve patients. Remarkably, a substantial proportion of patients already exhibited EELV values within the normal range prior to the RM.

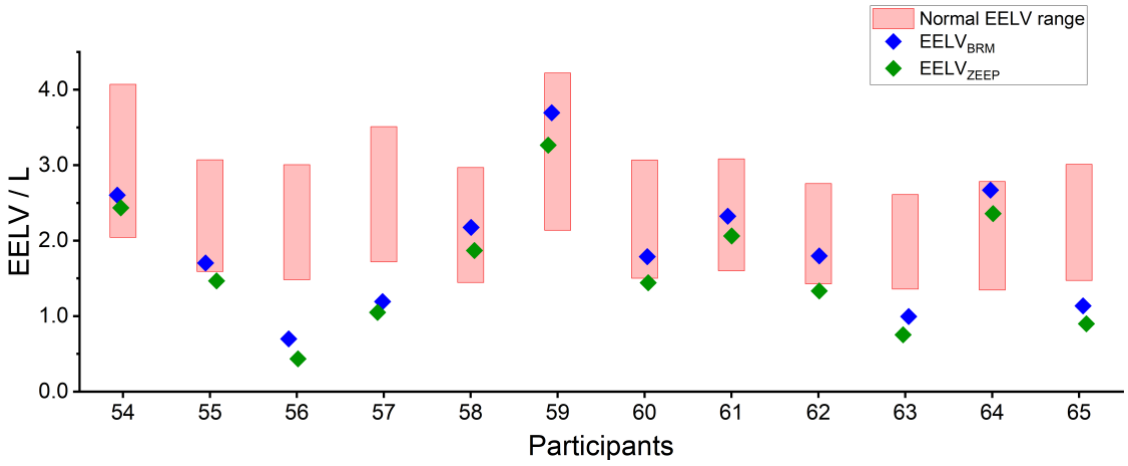

Figure 39. End-expiratory lung volumes before recruitment manoeuvre.

Blue diamonds represent EELV measured prior to a RM (EELV$_{BRM}$), and green diamonds represent estimated EELV at zero PEEP (EELV$_{ZEEP}$). Shaded pink bars indicate the predicted normal-volumes range, defined as the values contained within 75% of the upper and lower bounds of GLI-predicted functional residual capacity. Data are shown for each individual patient – twelve in total in the RM group.

7.4.3. EELV estimates before and after a quasistatic PV curve and RM

End-expiratory lung volume was estimated using CCP before and after two interventions: a low-flow quasistatic PV curve, and a sustained inflation RM. Figure 40 and Figure 41 present the single-breath PV loops for each patient. Unlike standard ventilator-generated PV loops, which are typically referenced to a volume baseline of zero, the loops presented here were offset using CCP-derived EELV estimates. This enabled anchoring of each loop to an absolute lung volume, allowing direct visualisation of the volume shifts induced by each procedure. Vertical displacement of the loops on the y-axis reflects changes in EELV. The slope between the end-inspiratory and end-expiratory points of the pressure-volume loop provides an estimate of dynamic compliance.

Following recording of the quasistatic PV curve, most patients showed minimal change in EELV, including patients 54, 59, 60, 61, 62, and 63. Others demonstrated clear upward shift, consistent with volume recruitment (patients 55, 56, and 58). Conversely, patients 57, 64, and 65 showed downward PV loop displacement, suggesting a net fall in EELV despite unchanged PEEP.

Changes in EELV were more pronounced after the RM. Patients were stratified into high and low recruiters based on median ΔEELV normalised to PBW. High recruiters (patients 55, 56, 57, 58, 59, and 63) had a mean ΔEELV of 305 mL (4.7 $mL.kg^{-1}$ PBW), with a mean ΔRM of 258 mL (4.0 $mL.kg^{-1}$ PBW). Among these, patient 58 exhibited a consistent increase in lung volume following both interventions. Low recruiters (patients 54, 60, 61, 62, 64, and 65) showed minimal or negative volume changes, with patients 64 and 65 again displaying EELV reductions after the RM.

Dynamic compliance (dashed lines) remained relatively stable across both procedures for most patients. Exact values of EELV, measured PEEP, dynamic compliance, and calculated recruitment volumes for each patient are summarised in Table 21.

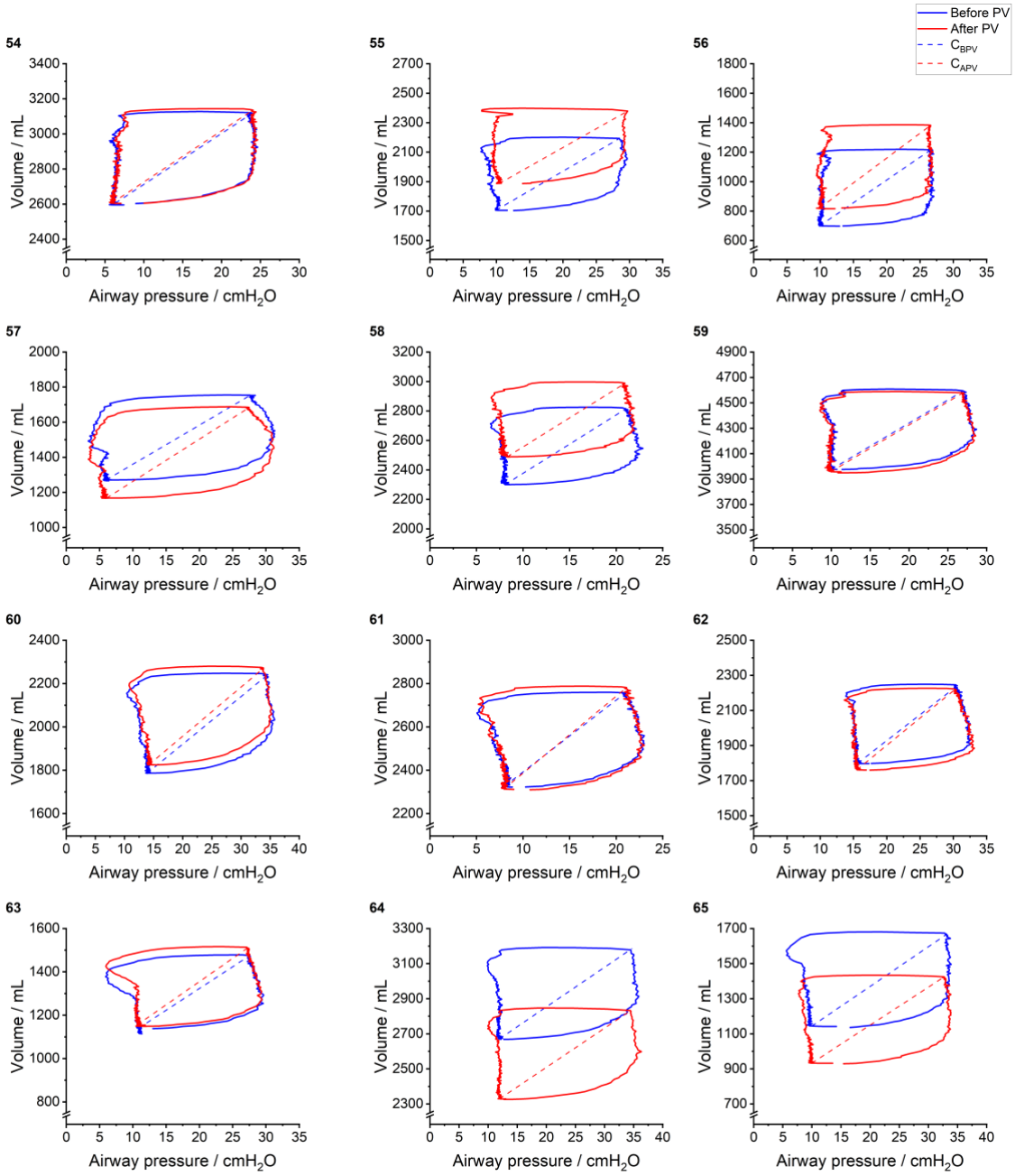

Figure 40. Pressure-volume loops before and after quasistatic inflation-deflation recording.

Pressure-volume loops obtained before (blue) and after (red) a quasistatic inflation-deflation PV recording in twelve mechanically ventilated patients. Dashed lines indicate dynamic compliance before (blue; C_{BPV}) and after (red; C_{APV}) the intervention. Each curve has been offset on the volume axis according to the absolute EELV estimated by CCP, enabling visualisation of volume shifts resulting from the recording.

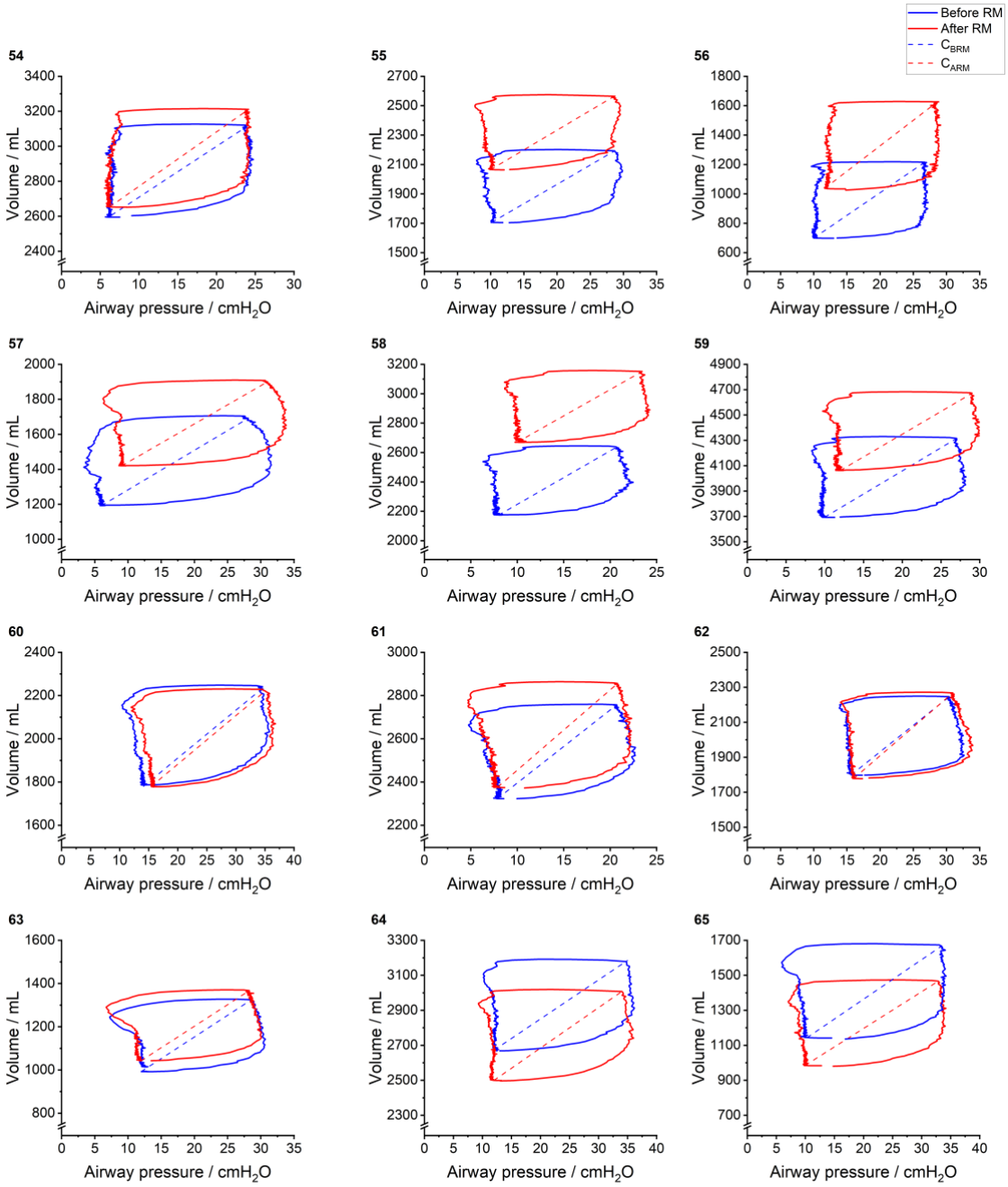

Figure 41. Pressure-volume loops before and after a recruitment manoeuvre.

Pressure-volume loops obtained before (blue) and after (red) a sustained inflation recruitment manoeuvre in twelve mechanically ventilated patients. Dashed lines indicate dynamic compliance before (blue) and after (red) the procedure. The curves are referenced to absolute EELV, estimated using CCP, allowing the effects of the RM on functional lung volume to be visualised as vertical shifts in the loops for each patient.

	Patient ID											
	54	**55**	**56**	**57**	**58**	**59**	**60**	**61**	**62**	**63**	**64**	**65**
$EELV_{BRM}$ / mL	2603	1704	700	1192	2175	3694	1786	2323	1798	994	2669	1136
$EELV_{ARM}$ / mL	2651	2066	1026	1420	2670	4065	1780	2372	1781	1043	2496	980
C_{BRM} / mL.cmH_2O	28	25	29	23	37	41	24	35	31	20	26	24
C_{ARM} / mL.cmH_2O	30	25	34	22	39	39	25	41	33	20	26	22
$PEEP_{BRM}$ / cmH_2O	6.1	9.3	9.1	6.2	8.2	10.4	14.2	7.5	15.0	12.0	12.1	10.1
$PEEP_{ARM}$ / cmH_2O	6.1	9.3	11.3	9.1	10.2	12.2	15.6	7.6	14.7	11.9	12.2	9.8
ΔEELV / mL	48	362	326	228	496	371	-7	49	-17	49	-172	-156
$V_{\Delta PEEP}$ / mL	0	0	75	64	78	70	35	4	-10	-1	3	-6
ΔRM / mL	48	362	251	164	418	301	-42	45	-7	50	-175	-150

Table 21. Recruitment metrics before and after a recruitment manoeuvre.

For each of the twelve patients, the table presents absolute EELV values before ($EELV_{BRM}$) and after ($EELV_{ARM}$) a sustained inflation RM, measured in millilitres (mL). Dynamic compliance before (C_{BRM}) and after (C_{ARM}) the RM is shown in mL.cmH_2O^{-1}, alongside corresponding PEEP (measured). The net change in EELV (ΔEELV) and volume recruited specifically due to the RM after accounting for PEEP-related effects (ΔRM) are also listed. $V_{\Delta PEEP}$ refers to the estimated change in lung volume attributable to changes in PEEP between conditions.

7.4.4. Assessment of lung recruitability

Several established surrogate indices of lung recruitability were compared with the change in EELV following RM discounted from $V_{\Delta PEEP}$ (ΔRM), as estimated using CCP. All volumetric indices were normalised to PBW where appropriate to facilitate comparison across patients.

Figure 42 displays the relationships between ΔRM / PBW and a selection of physiological parameters previously proposed to reflect lung recruitability. These included the maximum vertical distance between quasistatic PV curve limbs (D_{max}), the normalised maximal

distance (NMD), the respiratory system compliance before a RM (C_{BRM}), PV curve hysteresis (in $cmH_2O.mL^{-1}$), and two hysteresis-derived ratios (one normalised to PV curve geometry, and one to PBW). No statistically significant correlations were found between ΔRM / PBW and any of these indices. The strongest trend was observed with C_{BRM} ($r = 0.472$; $p = 0.121$), which showed a moderate, though non-significant, positive correlation.

Further exploratory analyses examined the relationship between C_{BRM} and additional CCP-derived recruitment metrics, including ΔEELV, ΔRM, and ΔV_A, along with their PBW-normalised counterparts. These results are summarised in Table 22. All variables demonstrated moderate positive correlations with C_{BRM}, indicating that individuals with higher compliance before a RM tended to exhibit greater volume recruitment. The strongest trend was observed with ΔV_A ($r = 0.545$; $p = 0.067$), followed by ΔEELV ($r = 0.529$; $p = 0.077$) and ΔRM ($r = 0.511$; $p = 0.089$).

Collectively, these findings suggest that traditional surrogate markers of lung recruitability may not reliably reflect the absolute volume of lung recruited following a RM. Among all tested variables, C_{BRM} showed the most consistent, albeit non-significant, association with absolute recruitment metrics.

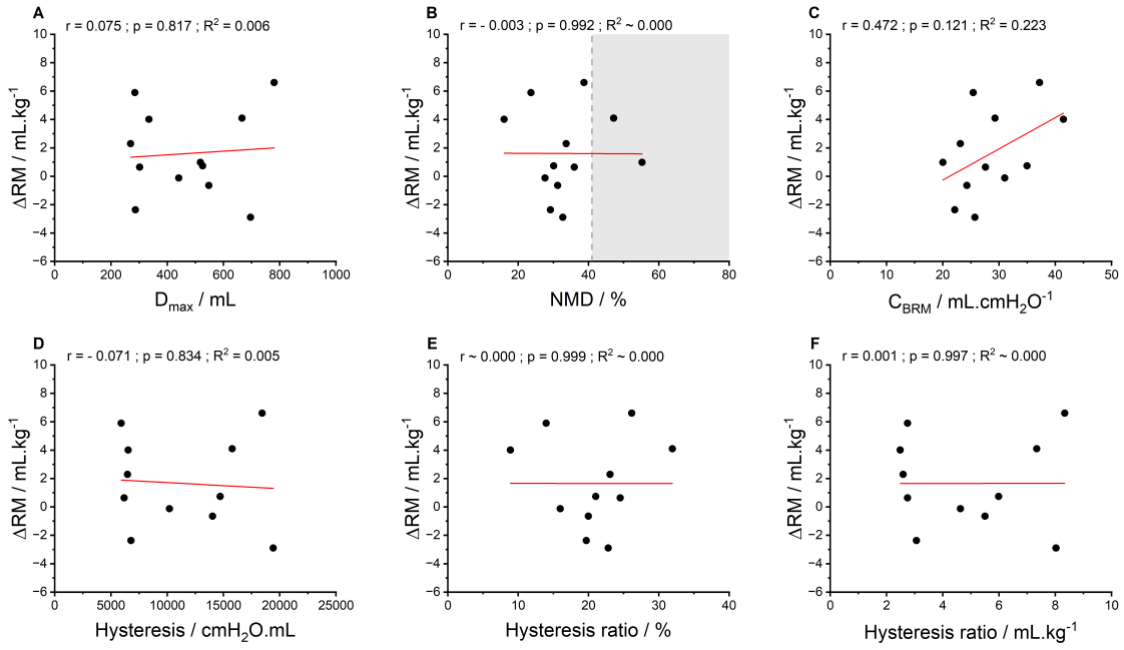

Figure 42. Correlation between ΔRM normalised to PBW and common surrogate markers of lung recruitability.

Scatter plots showing the relationship between the change in absolute volume following RM discounted from $V_{\Delta PEEP}$, normalised to PBW (ΔRM / mL.kg^{-1}), and various indices: (A) maximum vertical distance between PV curve limbs (D_{max}); (B) normalised maximal distance (NMD); (C) dynamic compliance before RM (C_{BRM}); (D) PV curve hysteresis (cmH$_2$O.mL^{-1}); (E) hysteresis ratio normalised to pressure span and the maximal volume of the curve; and (F) hysteresis ratio normalised to pressure span and PBW. Red lines show the best-fit linear regression. None of the correlations reached statistical significance.

Variable	Pearson's coefficient to C_{BRM}	p-value
ΔEELV	0.529	0.077
ΔEELV / PBW	0.492	0.104
ΔRM	0.511	0.089
ΔRM / PBW	0.472	0.121
ΔV_A	0.545	0.067
ΔV_A / PBW	0.506	0.094

Table 22. Correlation between C_{BRM} and CCP-derived estimates of absolute lung recruitment.

Pearson correlation coefficients and associated p-values are reported for the relationship between C_{BRM} and six recruitment metrics: ΔEELV, ΔRM, ΔV_A, and their PBW-normalised counterparts. All correlations were positive and moderate in strength, though none were statistically significant.

7.4.5. Assessment of lung volume response to a RM

Associations were explored between the lung volume recruited during the sustained inflation phase of the RM (V_{rec}) and the change in absolute recruited volume as estimated by CCP analysis (ΔRM). Unlike traditional indices of recruitability, V_{rec} is not a predictive measure but rather reflects the volume gained transiently during the RM, at supranormal airway pressures.

As shown in Figure 43, no statistically significant correlations were observed between V_{rec} (panel A) or V_{rec} / PBW (panel B) and ΔRM / PBW. This finding may be due to methodological differences between the two assessments. V_{rec} is captured during the RM itself – under high inflation pressures – and reflects an immediate mechanical response. In contrast, ΔRM values were derived from measurements taken approximately 30 minutes after a RM, at a new baseline airway pressure, and thus represent a more stable post-recruitment lung volume.

These findings suggest that the volume gained during a RM may not reliably predict the volume retained after a period of mechanical ventilation at typical pressures, further underscoring the distinction between transient inflation and sustained recruitment.

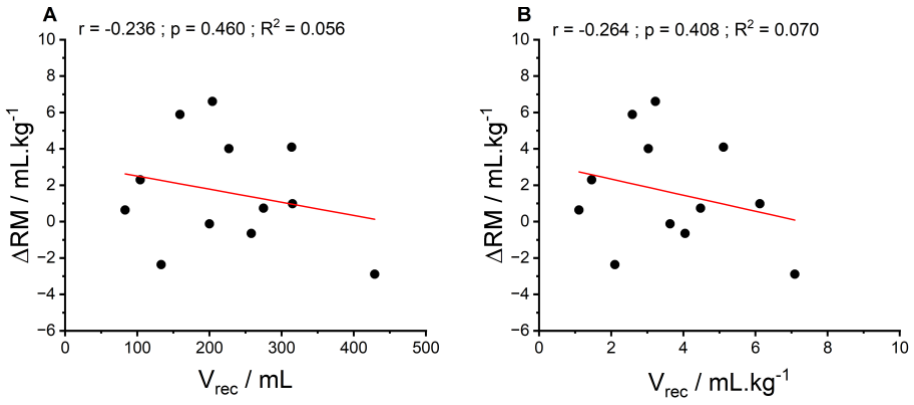

Figure 43. Correlation between V_{rec} and CCP-derived lung recruitment.

Scatter plots showing the relationship between the volume recruited during sustained inflation (V_{rec}) and ΔRM / PBW. Panel A shows the V_{rec} in mL; Panel B shows V_{rec} normalised to predicted body weight. No statistically significant correlations were observed.

7.4.6. Effect of a RM on EELV after one hour

To evaluate the persistence of RM-induced changes in lung volume, an additional EELV measurement was acquired with CCP one hour following the RM in five of the six patients previously classified as high recruiters (patients 56, 57, 58, 59, and 63). Patient 55 was excluded due to the absence of a follow-up measurement. Figure 44 and Figure 45 display representative PV loops before RM (blue), thirty minutes after RM (red), and one hour post RM (green) for each patient.

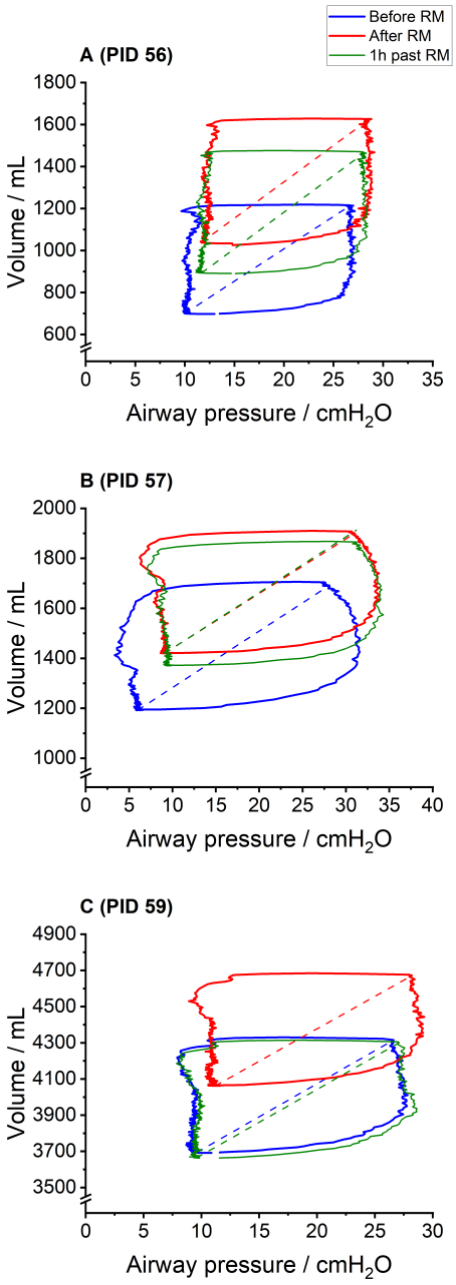

Figure 44. Pressure-volume loops before, thirty minutes after, and one hour after a RM in patients 56, 57, and 59.

PV loops are shown for three patients classified as high recruiters. Each panel displays PV data obtained before (blue), thirty minutes post RM (red), and one hour post RM (green). Dashed lines represent dynamic compliance during inflation at each time point. Curves are aligned to absolute EELV estimates from CCP. In all three patients, lung volume decreased at the one-hour follow-up compared with the thirty-minute post-RM measurement, consistent with partial derecruitment. In patient 59, PEEP was returned to pre-RM levels at one hour post intervention.

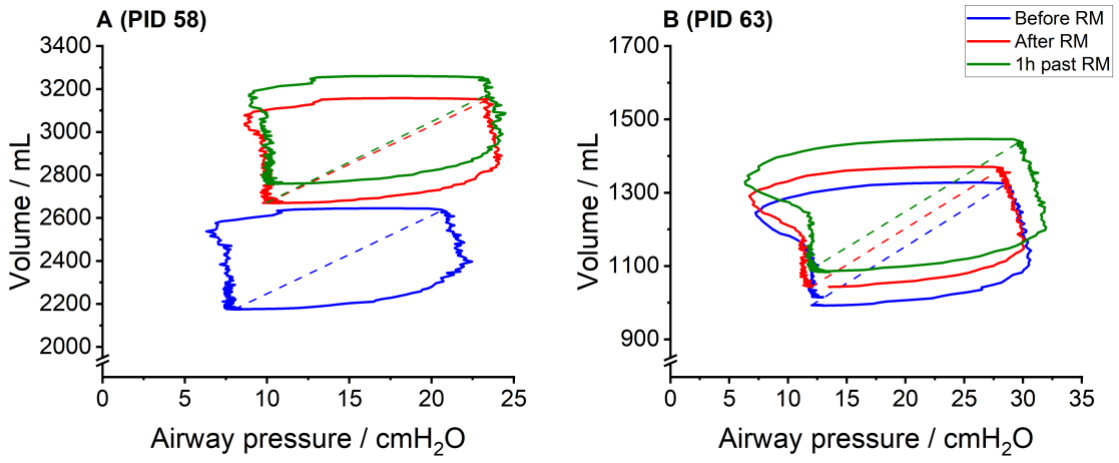

Figure 45. Pressure-volume loops before, thirty minutes after, and one hour after a RM in patients 58 and 63.

PV loops are shown for two patients classified as high recruiters. Blue, red, and green lines correspond to measurements taken before, thirty minutes after, and one hour after the RM, respectively. Dashed lines indicate dynamic compliance during inflation. Loops are offset using CCP-derived absolute EELV values. Both patients demonstrated a further increase in lung volume one hour after RM, suggestive of delayed and/or sustained recruitment.

The effects observed one hour after RM varied between individuals. In patients 56, 57, and 59 (Figure 44), EELV decreased relative to values measured thirty minutes post RM, indicating partial derecruitment. In contrast, patients 58 and 63 (Figure 45) exhibited further increases in EELV beyond the levels observed at thirty minutes post RM, suggestive of delayed or ongoing recruitment. In patients 57, 58, and 63, however, the change in EELV at one hour relative to values from thirty minutes following the RM was less than ± 5% (maximum 89 mL), which may fall within the expected range of physiological or measurement variability rather than reflecting a true change in lung volume.

Notably, patient 59 was the only individual in whom PEEP was returned to pre-RM levels by the clinical team between thirty minutes and one hour following the procedure. In this

patient, the total volume loss observed one hour after the RM was 401 mL, of which 338 mL could not be attributed to changes in PEEP ($V_{\Delta PEEP}$ = - 64 mL), suggesting substantial derecruitment to baseline pre-RM EELV.

No consistent pattern could be identified to explain the heterogeneity in volume trajectories observed one hour after RM.

7.4.7. Assessment of lung inhomogeneity before and after a RM

Ventilation inhomogeneity, represented by σC_L, was elevated in most patients before the RM. Specifically, nine out of twelve patients had Z-scores for σC_L ($Z\sigma C_{L\text{-}BRM}$) above the upper limit of normality (Z > 1.65), based on age-predicted reference values. Only patients 57, 61, and 62 had Z-scores within the normal range.

The mean $Z\sigma C_{L\text{-}BRM}$ was 3.2 ± 2.2. The most extreme value occurred in patient 54, who had a $Z\sigma C_{L\text{-}BRM}$ of 8.8 – more than five times the upper limit of normal and over five SDs above the group mean. This severe ventilation inhomogeneity is likely to have been related to the patient's known history of asthma, bronchiectasis, and previous smoking.

After a RM, there was a non-significant increase in σC_L Z-scores ($Z\sigma C_{L\text{-}ARM}$), with a post-RM group mean of 3.6 ± 2.3 ($t(11) = -1.757$; $p = 0.107$; Figure 46). Two patients (61 and 62) who initially had normal σC_L values, shifted into the abnormal range post RM, suggesting that the RM may have negatively impacted ventilation distribution in their cases. Full individual results, including raw σC_L values, Z-scores, and classification before and after a RM, are presented in Table 23.

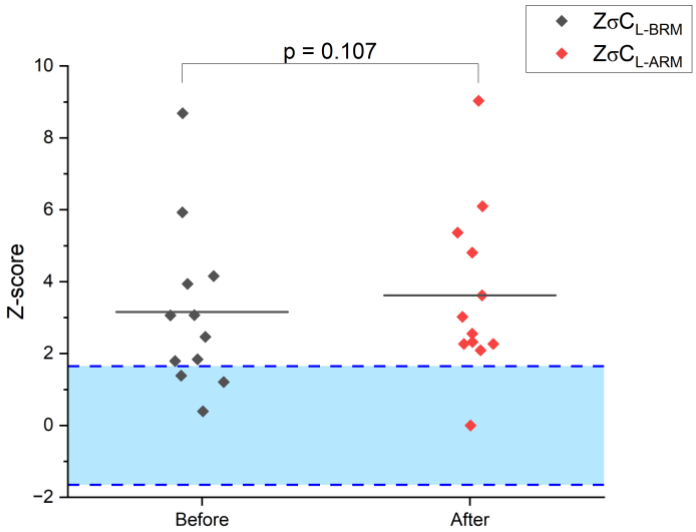

Figure 46. Z-scores for σCL before and after a RM.

Individual Z-scores are shown before ($Z\sigma C_{L\text{-}BRM}$) and after ($Z\sigma C_{L\text{-}ARM}$) the RM. The dashed dark blue lines represent the upper and lower limit of normal (Z = ± 1.65). The normal Z-score range is represented in light blue. The grey lines represent the mean $Z\sigma C_L$ for each group. The majority of the patients exhibited abnormal σC_L values prior to the RM, with a trend toward further increases afterwards. Two patients (61 and 62) crossed from the normal to the abnormal range following the RM. No statistically significant difference was observed overall (p = 0.107).

	Patient ID											
	54	**55**	**56**	**57**	**58**	**59**	**60**	**61**	**62**	**63**	**64**	**65**
$\sigma C_{L\text{-}BRM}$	1.22	0.74	0.82	0.60	0.63	0.79	0.65	0.63	0.55	0.85	0.91	0.73
$Z\sigma C_{L\text{-}BRM}$	8.7	3.1	3.9	1.2	1.8	2.5	1.8	1.4	0.4	4.2	5.9	3.1
Classification BRM	H	H	H	N	H	H	H	N	N	H	H	H
$\sigma C_{L\text{-}ARM}$	1.25	0.78	0.93	0.51	0.67	0.80	0.67	0.75	0.69	0.90	0.92	0.67
$Z\sigma C_{L\text{-}ARM}$	9.0	3.6	5.4	0.0	2.3	2.6	2.1	3.0	2.3	4.8	6.1	2.3
Classification ARM	H	H	H	N	H	H	H	H	H	H	H	H

Table 23. Individual σC_L values before and after a RM.

Individual σC_L values, Z-scores, and classifications before and after the recruitment manoeuvre. Raw σC_L values and corresponding Z-scores are shown for each patient before (BRM) and after (ARM) the RM. Z-scores were computed using age-adjusted prediction equations, with a threshold of $Z > 1.65$ defining elevated ventilation inhomogeneity[212]. Patient 54 demonstrated an exceptionally high $Z\sigma C_{L\text{-}BRM}$ of 8.7. Classifications are denoted as high (H) and normal (N) based on Z-score thresholds.

7.5. Discussion

7.5.1. Summary of findings

There is an ongoing debate as to whether RMs are safe and the manner in which they impact patient outcomes[108, 109, 137, 213-216]. Although RMs have shown potential benefit in re-aerating previously collapsed areas of the lung susceptible to atelectrauma, they may also over-distend the lung leading to volutrauma, furthering VILI[217]. To a large degree, uncertainties surrounding the pathophysiological effects of RMs arise as a consequence of the lack of accurate bedside techniques to monitor their short and long-term consequences.

The experiments discussed in Chapter 6 have confirmed that it is possible to impose small, clinically insignificant, variations in FiO_2 in mechanically ventilated patients, and from these extract highly precise measurements of lung volumes using CCP. Here, twelve

mechanically ventilated ICU patients (the RM group) undergoing treatment for acute infectious lung conditions received RMs at the discretion of the clinical team. Most patients were ventilated with moderate inspiratory and end-expiratory pressures and exhibited impaired oxygenation and low respiratory compliance.

In this cohort, most patients had baseline EELV within the expected range even before a RM was performed. Volume recruitment following a RM varied considerably between patients, and, in many cases, the observed apparent gains in EELV diminished within one hour. Across the cohort, commonly used surrogate indices of lung recruitability showed no significant correlation with CCP-derived absolute lung volume recruitment metrics. Among the measured parameters, C_{BRM} showed a moderate, though statistically non-significant, association with the total change in absolute volume. The correlation persisted when assessing C_{BRM} against ΔRM, showing that this limited correlation was not explained by any change in PEEP post RM. Baseline ventilation inhomogeneity was well above normal in the majority of the patients studied and did not change significantly following the RM, though a modest trend towards an increase in inhomogeneity was observed after the procedure.

The interpretation of these findings is discussed in more detail in the following sections.

7.5.2. Baseline EELV and the rational to performing a RM

All patients in the RM cohort were undergoing treatment for pneumonia – either community-acquired, hospital-acquired, or ventilator-associated – which likely contributed to their reduced lung volumes. In such cases, regional alveolar consolidation, atelectasis, increased intrapulmonary shunt, and reduced compliance may all have reduced the volume available for gas exchange[218-220]. These effects can be especially pronounced in

mechanically ventilated individuals, where volumes are already compromised by sedation, a reduction in diaphragmatic tone, and the adverse effects of supine body positioning[62]. Therefore, low EELV at ZEEP in this cohort is expected.

Notably, in three of these seven patients, the application of moderate PEEP alone was sufficient to restore EELV to within the normal predicted range. This observation reinforces the well-established role of PEEP in counteracting lung volume loss[63]. *Bikker et al.* reported that EELV was on average 42% of the expected (in the sitting position) in a cohort of mechanically ventilated individuals with primary lung disease ventilated at a PEEP of 5 cmH_2O[63]. In the present RM group, EELV at ZEEP was 52% of that predicted for healthy individuals in the supine position. The volume rose by almost 10% when accounting for V_{PEEP}.

One of the most striking findings in this cohort was that, at levels of PEEP set by the clinical team, most patients had EELV within the predicted normal range even before the RM was performed. It is important to reinforce here that this reference was based on GLI-derived FRC values for spontaneously breathing individuals – for whom the lung volumes are naturally higher – and adjusted by 25% to reflect supine positioning. RMs, by definition, are aimed at re-aerating collapsed areas of the lung so that the restored volume can effectively contribute towards gas exchange, though, as already discussed, they are not risk free. This finding raises an important question: if clinicians had known that lung volumes were already within normal range at baseline, would the recruitment manoeuvre still have been indicated?

While this study was not designed to address this question directly, the ability to assess EELV non-invasively at the bedside may provide new opportunities to guide recruitment

strategies more selectively. In particular, distinguishing between patients whose lung volumes remain low despite PEEP versus those who have already achieved near-normal lung volumes could help avoid unnecessary or potentially harmful interventions.

7.5.3. Effects of PV curve recording and RM on EELV

Computed cardiopulmonography has proven capable of assessing both the immediate and delayed effects of a RM on EELV. While some patients showed substantial and sustained gains in lung volume, others experienced only transient recruitment or even early derecruitment despite no significant change in ventilator settings. This heterogeneity likely reflects individual underlying differences in lung pathology, regional compliance, and susceptibility to atelectasis and overdistension.

Interestingly, brief exposures to supranormal airway pressures – such as those delivered during recording of a quasistatic PV curve, without a sustained inflation phase – elicited measurable lung recruitment in some patients. This suggests that even transient increases in inspiratory pressure may be sufficient to reopen certain lung units[103, 104]. However, the larger and more consistent responses seen after a formal RM indicate that the duration of the exposure also contributes meaningfully to the extent of recruitment [103, 104].

The fact that several “high recruiters” experienced partial derecruitment within one hour raises important questions about these volume gains. If the benefits of RM wear off within sixty minutes, is the manoeuvre truly justified? Should RMs be repeated periodically to maintain lung volume, or should they be reserved only for specific indications, such as after disconnection from the ventilator? Without tools to track lung volume over time, such decisions can only be made empirically.

One must be careful not to overinterpret the findings of this observational study. The longitudinal assessment of EELV displayed here is cross-sectional by nature. As a snapshot of the dynamic lung function, one reading may selectively capture a momentaneous drift or increase in volume and misrepresent the longer-term EELV trend. For instance, while the observed changes in EELV suggest recruitment or derecruitment after a quasistatic PV curve or RM, causality cannot be definitively established. Moreover, post-RM PEEP settings were not standardised. While some patients underwent formal decremental PEEP titration, others had arbitrarily chosen or unchanged PEEP levels. These variations may have influenced the extent to which recruitment was sustained or lost.

Despite these limitations, the study demonstrates that CCP, by enabling repeated EELV assessments, provides a practical means to objectively evaluate the effects of relevant clinical interventions – such as a RM – on lung volume. This technique may eventually support clinicians in the development of more individualised treatment strategies at the bedside.

7.5.4. Limitations of lung recruitability and lung recruitment indices

A key finding in this cohort was the lack of correlation between CCP-derived absolute recruitment and several indices commonly used to estimate lung recruitability and lung recruitment. Parameters obtained before or during recording of the quasistatic PV curve – such as hysteresis (and their normalised variants), D_{max}, NMD%, and C_{BRM} – and during the RM curve (i.e., V_{rec}) showed no significant association with ΔEELV, ΔRM, or ΔV_A.

Among all indices tested, only C_{BRM} demonstrated a moderate, albeit statistically non-significant, correlation with CCP-derived lung recruitment. This is plausible and such an

effect has been described in the literature[127-129], as patients with higher baseline compliance may be better able to accommodate additional volume when exposed to higher pressures. However, the relationship is unlikely to be linear or universal; focal inhomogeneities in poorly compliant lungs may still permit recruitment in specific regions.

Overall, these findings underscore a fundamental limitation of indirect markers: they are dependent on measurement timing, technique, and the mathematical definitions employed. Take hysteresis as an example. Although it has been proposed as a marker of recruitable volume, its calculation varies widely across published studies – reported either as an absolute pressure-volume area or normalised by pressure span, maximum inflation volume, or predicted body weight[127, 130, 221]. *Chiumello et al.* found that a hysteresis ratio (but not the raw area) correlated with CT-estimated alveolar recruitment[130]. In contrast, *Henzler et al.* reported correlations for both hysteresis area and another hysteresis ratio[221]. However, the methods used not only different lung recruitability indices deriving from hysteresis, but also different definitions of recruitment (i.e., non-aerated to aerated versus poorly aerated and non-aerated to aerated), and different methods to assess it (i.e., voxel-by-voxel versus anatomical delineation)[130, 221]. This lack of standardisation across studies compromises comparability and weakens the evidence base for these indices.

Some studies have compared PV-curve-derived estimates of recruitment with absolute PEEP-induced changes in lung volume measured by MBNW or helium dilution[124, 222]. When PV curves are offset by absolute volume baselines (e.g., EELV), correlations tend to emerge – but the values remain significantly different[124, 222]. It remains unclear whether these correlations are physiologically meaningful or merely reflect mathematical coupling arising from the use of a shared EELV reference. In the present study, quasistatic PV curves were not recorded in duplicate and were not offset by CCP-estimated EELV, preventing

the performance of such analysis. However, given the findings in the present cohort, it is likely that unreferenced curves would not correlate with absolute volume recruitment.

The lack of correlation between CCP-derived recruitment and these conventional indices may also reflect differences in when and how each measurement was taken. They may simply be measuring different physiological phenomena. PV-derived indices are obtained before the RM, during passive, low-flow inflation, and are designed to predict recruitability rather than confirm it. Notably, studies that report correlations with CT often ensured the scan was performed at the same pressure level as the start of the PV curve[124, 223]. Aligning measurement conditions in this way may have improved the observed correlations.

V_{rec} presents a distinct case, as it is the only measure acquired during the RM itself, capturing the volume gained during sustained inflation at supranormal pressures, and the only index supposed to indicate the effectiveness of lung recruitment rather than recruitability. However, it does not account for whether that volume remains recruited under normal ventilator conditions. The lack of correlation between V_{rec} and CCP-derived ΔRM reflects this limitation – a transient volume gain does not necessarily indicate durable improvement in lung volume or gas exchange. Thus, V_{rec} may capture mechanical inflation, but not meaningful, sustained alveolar recruitment.

In contrast, in the present cohort, CCP was used to quantify lung volume at a new post-RM steady state, about thirty minutes after the intervention. It did not estimate potential recruitment, nor capture transient volume shifts, but measured the actual volume retained under clinically relevant ventilator settings. The temporal dissociation between a RM and its clinical effect highlights the importance of longitudinal assessment. The ability of CCP to measure lung volume in a steady state after a RM offers an opportunity to evaluate

whether recruitment was successful and durable. From a clinical perspective, this may be a more meaningful indicator of RM effectiveness, while it does not resolve the problem of lung recruitability prediction to support the rational use of RMs.

From a practical perspective, it would not be feasible to perform multiple nitrogen washouts during or immediately after a RM, due to rapid changes in EELV and the time required for gas stores re-equilibration. For example, *Maggiore et al.* reported a 6% underestimation of EELV when measurements were taken immediately after a recording of a PV curve compared with those obtained fifteen minutes later[128]. A thirty-minute follow-up window aligns well with clinical workflows and could be sufficient to detect whether the RM effect has persisted. If no lasting recruitment is evident at that point, one must ask whether the intervention provided any tangible benefit at all.

7.5.5. CCP for the assessment of ventilation inhomogeneity

Ventilation inhomogeneity – as quantified by σC_L – was elevated in the majority of sedated, mechanically ventilated patients in this cohort prior to the RM. This is not unexpected as the reference Z-scores for σC_L are derived from healthy, upright spontaneously breathing individuals, in whom natural diaphragmatic movement and posture favour more uniform ventilation distribution[212]. In contrast, mechanical ventilation imposes positive pressure in a supine, often immobile patient, which tends to redistribute ventilation towards non-dependent lung regions, leaving dependent zones underinflated. Even in the absence of lung pathology, these factors could increase σC_L[224]. In critically ill patients with underlying lung disease, as it is the case of the present cohort, this heterogeneity is likely to be further amplified.

The highest pre-RM σC_L value was observed in a patient with a known history of asthma, bronchiectasis, and previous smoking – conditions that are well-recognised to cause ventilation heterogeneity[225-227]. These features would be expected to contribute to marked regional disparities in compliance, leading to an elevated σC_L even before the effects of mechanical ventilation are considered[150-153, 228].

The performance of a RM did not significantly change σC_L at the group level, though a very modest, non-significant increase in mean inhomogeneity was observed. Interestingly, two patients transitioned from within-normal to above-normal σC_L Z-scores post RM. While RMs and appropriate PEEP settings can potentially reduce stress and strain on aerated regions by opening collapsed alveoli[229], excessive pressures may instead cause counterproductive regional overdistension. This may explain the apparent deterioration in σC_L in these two patients, suggesting that RMs may have worsened ventilation heterogeneity.

In a recent perspective on the future of mechanical ventilation, *Gattinoni et al.* argued that quantifying ventilation inhomogeneity is an essential step for adequately tailoring care and preventing lung injury[230]. CCP modelling provides a potential solution: by estimating σC_L, clinicians could gain insight into whether the aerated fraction of the lung is expanding relatively evenly during ventilation, or whether some parts are being relatively over- or under-distended. Consequently, reliable information pertaining to volutrauma and atelectrauma, both of which are key drivers of ventilator-induced lung injury[217, 231, 232], could be made available to the treating clinician. With further clinical investigations, σC_L could serve as an index of ventilation quality and response to interventions in mechanically ventilated patients.

7.5.6. Limitations

In addition to the technical considerations already discussed in section 6.5.4.1, the present study has several experimental limitations.

First, the sample size was relatively small and did not include any patient with a confirmed diagnosis of ARDS, which is a major population for whom lung recruitability and recruitment manoeuvres are relevant. As a result, patients had low average stress and strain and several established indices of lung recruitability – for instance, hysteresis ratio and NMD% – were considered normal when compared with previous studies in individuals with ARDS. Both the small sample size and the lack of ARDS cases mean that the findings may not capture the full spectrum of lung recruitability and RM effects typically seen in that setting.

Second, the lack of a consistent, validated reference standard for lung recruitability complicates efforts to benchmark CCP-derived recruitment estimates and underscores the challenge of drawing conclusions about any potential predictive power. Although several indices were evaluated, none demonstrated a statistically significant correlation with CCP measures.

Third, CCP evaluates recruitment at different timepoints and ventilator settings than lung recruitability indices, V_{rec}, and CT scans. As briefly discussed in section 7.5.4, this may limit the ability of the present study to establish meaningful correlations given the truly different physiological aspects of such measurements.

Finally, the observational nature of the study preserved clinician autonomy but introduced important variability in how recruitment manoeuvres were performed and quasistatic PV

curves recorded. Inflation pressures and pressure spans were not standardised across patients, which could have introduced confounding effects on the measured outcomes, especially if no normalisation had been conducted. While this reflects real-world practice and may enhance external validity, it also limits the ability to control for procedural factors when interpreting the data.

7.6. Conclusion

This study demonstrated that CCP provides a viable non-invasive bedside approach for quantifying absolute lung volumes and lung inhomogeneity in the assessment of the effects of RMs in mechanically ventilated patients. CCP successfully demonstrated changes in EELV before and after RMs, capturing not only immediate but also short-term effects. The findings revealed substantial inter-individual variability in the response to RMs, with some patients exhibiting significant recruitment and others showing transient or even negative changes in lung volume.

Importantly, the study showed that several indices commonly used to estimate lung recruitability and lung recruitment did not correlate with CCP-derived recruitment metrics, which reveals the limitations of such tools in detecting true absolute lung volume changes. In this cohort, a CCP-derived ventilation inhomogeneity index was elevated in most patients and remained largely unchanged following RMs, providing additional information on the mechanical stress posed by mechanical ventilation.

These results support the potential of CCP as a bedside tool to inform and personalise mechanical ventilation strategies. By enabling precise assessment of lung volume and lung

inhomogeneity, CCP may eventually help clinicians tailor interventions more effectively and avoid unnecessary or potentially harmful manoeuvres.

Chapter 8. Overall conclusions

An aphorism historically attributed to Galileo Galilei states: “measure what can be measured, and make measurable what cannot be.” Yet in critical care practice, a measurement is only meaningful if it is accurate and yields information that can be acted upon at the bedside. This thesis has sought to explore whether two such challenging variables – absolute EELV and $\dot{V}_{O2}$ – can be reliably quantified in mechanically ventilated patients. Both are dynamic and physiologically central to understanding health and disease, but have long resisted simple, trustworthy measurement in critical care settings. This limitation has constrained the clinicians’ ability to appreciate their importance in managing the critically ill patient. By employing new approaches – the MFS alone and CCP – and by examining their strengths and limitations, this work asked not only whether these variables could be made measurable, but also whether doing so might provide meaningful insight into patient pathophysiology and care.

In the case of $\dot{V}_{O2}$, the MFS demonstrated good agreement with DB measurements in healthy volunteers and was able to provide precise and reproducible values in mechanically ventilated patients. To address the longstanding limitation of unreliable single

measurements, this thesis introduced an internal quality control approach, constructing confidence intervals based on nitrogen balance. This increased confidence in the values obtained and provided a framework for determining whether these were narrow enough to be clinically actionable. Additionally, the MFS was able to detect changes in $\dot{V}_{O2}$ associated with fluctuations in body temperature, muscle activity, and haemodynamic status, demonstrating that meaningful physiological trends can indeed be captured in real time. Perhaps the most exciting potential clinical application of $\dot{V}_{O2}$ monitoring might be in the early recognition and management of shock, where $\dot{V}_{O2}$ offers a direct marker of supply-demand balance. Future studies should focus on patients at risk of developing shock, followed longitudinally, to determine whether $\dot{V}_{O2}$ monitoring can anticipate its onset, guide therapy, and improve outcomes.

For lung volumes, CCP provided precise estimates of EELV under actual ICU conditions, offering a practical alternative to traditional washout techniques. Partial washouts, more suitable for critically ill patients, achieved results equivalent to full washouts, and CCP-derived values in healthy volunteers agreed closely with BPleth. When applied before and after a RM, CCP revealed highly variable recruitment volumes and demonstrated that many existing indices of lung recruitability did not correlate with the actual change in absolute lung volume. The balance between recruitment and overdistension was further assessed by measuring ventilation inhomogeneity, which remained largely unchanged following the manoeuvre. These findings reveal both the feasibility of bedside EELV measurements and the limitations of current lung recruitability indices, placing the role and effects of recruitment manoeuvres into perspective. Overall, they underscore the need for more individualised and rational ventilatory strategies, particularly when applying interventions that may carry harmful consequences.

Some technical barriers remain before studies employing the MFS and CCP can be more widely applied in mechanically ventilated patients. These include reducing the dead space introduced by the MFS, ensuring compatibility with active humidification, and shortening the computational time required for CCP modelling. Addressing these issues will make the techniques safer, more practical, and better suited for continuous monitoring of critically ill patients.

Taken together, this thesis demonstrates that two physiological variables long considered impractical to measure in critical care – $\dot{V}_{O2}$ and EELV – can in fact be quantified at the bedside with accuracy and reliability sufficient to provide clinically meaningful insight. While further refinements are needed, the ability to track these variables opens the door to more individualised, physiology-based management of the critically ill. The contribution of this work is not the development of instruments, but the demonstration that elusive aspects of cardiopulmonary physiology can be rendered visible; and in doing so, might guide more precise and safer care. To return to Galileo's aphorism, measurement is only worthwhile if it advances understanding; this thesis offers a step toward making that possible in the most demanding of clinical settings.

Appendix A: Ethics detailing

Below are the synopses of the two ethical approvals under which all studies presented in this thesis were conducted.

Studies in mechanically ventilated patients (22/SC/0127)

Study Title	An observational study of the relationship between pressure-volume curves and recruitability of the lung in mechanically ventilated critically ill patients with respiratory failure		
Internal ref. no. / short title	Recruitment manoeuvres in critically ill patients		
Study registration	NCT05508724 (ClinicalTrials.gov)		
Sponsor	University of Oxford | Research Governance, Ethics & Assurance Team Boundary Brook House, Churchill Drive, Headington, Oxford OX3 7GB		
Funder	University of Oxford | Internal Funds Sherrington Building, Sherrington Road, Oxford OX1 3PT		
Study Design	Observational study		
Study Participants	Critically ill adult patients with respiratory failure receiving invasive mechanical ventilation on an Intensive Care Unit		
Sample Size	60		
Planned Study Period	3 years and 3 months		
Planned Recruitment period	01/05/2022 to 01/08/2025		
	Objectives	Outcome Measures	Timepoint(s)
Primary	To determine whether parameters derived from the airway pressure-volume curve predict changes in static measures of lung volume in response to recruitment manoeuvres	Functional residual capacity	Before and after recruitment manoeuvre
Secondary	To determine if and how anatomic dead space and ventilatory inhomogeneity changes in response to recruitment manoeuvres	Anatomic dead space Standard deviation for ventilation inhomogeneity across the lungs	Before and after recruitment manoeuvre.
Intervention(s)	No interventions additional to routine clinical care		
Comparator	Within patient changes in lung parameters before and after a recruitment manoeuvre in a given patient		

Table A 1. Synopsis of ethics 22/SC/0127.

Studies in healthy volunteers (17/SC/0172)

Study Title	An assessment of novel non-invasive indices of lung function in patients with respiratory disease.
Study Design	Observational study in patients and healthy volunteers.
Study Participants	Patients with established or suspected respiratory diagnoses (e.g. asthma, COPD, interstitial lung disease, pleural disease, cystic fibrosis and bronchiectasis) and healthy volunteers.
Planned sample size	Up to 700.
Planned study period	Six years and six months (February 2017 – Jan 2027)
Primary Objective	To determine the range and reproducibility of novel non-invasive indices of lung function across a range of respiratory diseases, and to compare these indices with those measured in normal volunteers.
Secondary Objective	To assess the impact of routine clinical interventions and of mild-moderate exercise on our novel indices of lung function.
Interventions	Measurements of lung function will be made via a *Lung Heterogeneity Test*, which involves breathing on a mouthpiece with the nose occluded for up to 30 min. During this period the inspired gas may be enriched with oxygen (up to 100%), carbon dioxide (up to 8%), nitrogen (to facilitate exposure to hypoxia) and/or trace amounts of acetylene, methane or carbon monoxide (<1%). On each day of study, a venous blood sample would also be taken, and conventional pulmonary function testing performed. Volunteers will undertake a maximum of 16 *Lung Heterogeneity Tests* during their involvement with the study, with no more than four tests on one day. Tests may be performed before and after clinical interventions/procedures, but these would be undertaken only as part of routine clinical care, rather than being undertaken for the study *per se*. For some participants, one or more *Lung Heterogeneity Tests* may be performed during mild-moderate exercise on a cycle ergometer. Some participants may be asked to undertake a computed tomography scan of the lungs as an optional procedure.

Table A 2. Synopsis of ethics 17/SC/0172

Appendix B: CONSORT-like diagram

The following CONSORT-like flow diagrams summarise the progression of patients through the study, from enrolment to inclusion in the final analysis. Within this thesis, patient identifiers are assigned only to those included in the analytical datasets. Numbering is sequential and corresponds to the order in which patients are presented in the results chapters: Patient 1 appears in Chapter 4 and Patient 65 in Chapter 7. Some identifiers occur in multiple studies, reflecting patients who contributed data to more than one cohort.

Studies in mechanically ventilated patients (22/SC/0127)

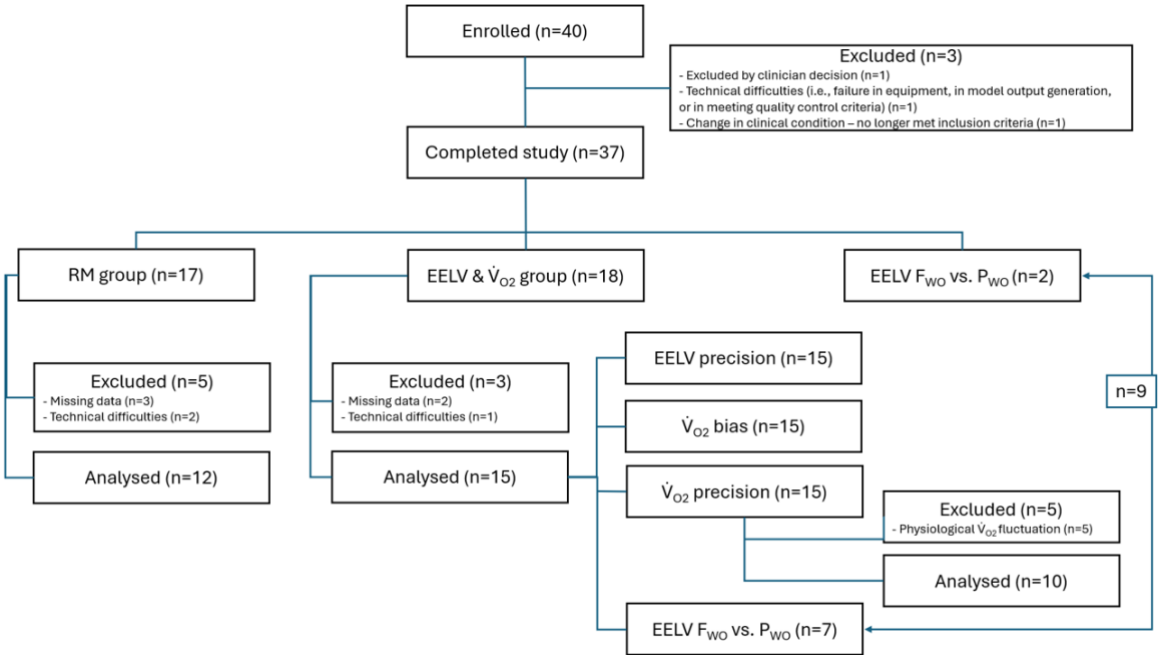

Figure C 1. CONSORT-like diagram reporting patient flow through all studies conducted in mechanically ventilated patients.

F_{WO} = full nitrogen washout; P_{WO} = partial nitrogen washout; n = number of patients.

Screening logs were not systematically recorded for this study; therefore, the precise number of patients screened cannot be reported. Clinical estimates suggest that at least 200 patients were assessed for eligibility, although most were excluded at the screening stage due to failure to meet inclusion criteria or the presence of exclusion criteria. A small proportion of otherwise eligible patients were not enrolled due to lack of consultee consent. No patients withdrew consent after regaining capacity.

Studies in healthy volunteers (17/SC/0172)

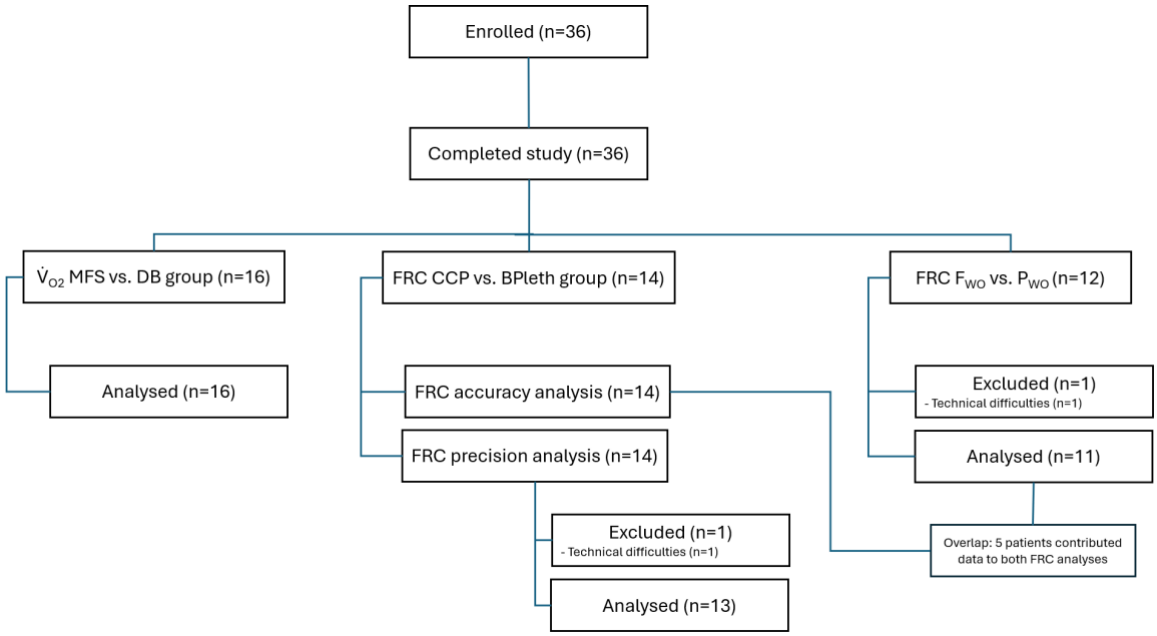

Figure C 2. CONSORT-like diagram reporting patient flow through all studies conducted in spontaneously breathing participants.

F_{WO} = full nitrogen washout; P_{WO} = partial nitrogen washout; n = number of patients. Technical difficulties encompass failure in model output generation and failure in meeting quality control criteria.

Appendix C: Contributions

The studies in healthy volunteers and mechanically ventilated patients reported in this thesis involved the clinical application of an instrument developed by the Robbins-Ritchie group (University of Oxford, UK). This marked the first systematic use of the instrument in mechanically ventilated individuals. Both the MFS and CCP modelling required ongoing maintenance and updates to ensure safe data acquisition and accurate processing. A team of physicists, chemists, and engineers supported optimisation of the instrument, development of analytical tools, and troubleshooting.

Two Final Honours School (FHS) undergraduate students, supervised by this author, contributed to participant recruitment and data collection in healthy volunteers. Interim results from these studies were submitted as essays for their University of Oxford examinations.

All data analysis and interpretation in this thesis were carried out by this author under the supervision of Prof. Peter A. Robbins and Prof. Matthew C. Frise. A list of contributors and their specific roles is provided below.

Studies in mechanically ventilated patients

Prof Matthew C Frise – Principal Investigator at the Royal Berkshire Hospital; conception and design of study; assistance in securing ethical approval.

Prof Peter A Robbins – conception and design of study; assistance in securing ethical approval.

Dr Christoph Schranz (Hamilton Medical AG) – contribution to study design; loan of memory box to record mechanical ventilation parameters.

Dr Dominik Novotni (Hamilton Medical AG) – contribution to study design; loan of memory box to record mechanical ventilation parameters.

Prof Liza Keating (Royal Berkshire Hospital) – assistance in site implementation and promoting the study amongst Critical Care consultants.

Research nurses (Royal Berkshire Hospital) – assistance in recruiting and consenting patients; master file maintenance on site.

Dr Dominic Sandhu – CCP programming and optimisation tailored to mechanically ventilated individuals; CCP modelling troubleshooting.

Dr Graham Richmond – MFS maintenance; software development and optimisation for oxygen consumption analysis both in real time and post data acquisition.

John Couper – MFS maintenance.

Study comparing BPleth and CCP

Prof Peter A Robbins and Prof Nick Talbot – conception and design of study.

Ella McLoughlin (FHS) – recruitment of volunteers; assistance running MFS data acquisition.

Respiratory technicians (Churchill Hospital) – body plethysmography data acquisition and output file generation.

Dr Dominic Sandhu – CCP modelling troubleshooting.

Dr Graham Richmond – MFS maintenance.

Study comparing full and partial MBNW in healthy volunteers

Prof Peter A Robbins and Prof Nick Talbot – conception and design of study.

Ella McLoughlin (FHS) – recruitment of volunteers; assistance running MFS data acquisition.

Dr Dominic Sandhu – CCP modelling troubleshooting.

Dr Graham Richmond – MFS maintenance.

Study comparing DB and MFS

Prof Peter A Robbins and Prof Nick Talbot – conception and design of study.

Benjamin Fuller (FHS) – recruitment of volunteers; assistance running MFS data acquisition.

Dr Graham Richmond – MFS maintenance.

John Couper – development of an automated fan to enable slow emptying of Douglas bag into a volume gas analyser.

References

(1) West JB, Luks A. West's respiratory physiology: the essentials. Wolters Kluwer; 2021.

(2) Lumb AB, Thomas CR. Nunn's applied respiratory physiology. Elsevier; 2020.

(3) Leach RM, Treacher DF. The pulmonary physician in critical care * 2: oxygen delivery and consumption in the critically ill. *Thorax* 2002;57:170–177.

(4) Kane AD, Kothmann E, Giussani DA. Detection and response to acute systemic hypoxia. *BJA Educ* 2020;20:58–64.

(5) Barcroft J. Physiological effects of insufficient oxygen supply. *Nature* 1920;106:125–129.

(6) Treacher DF, Leach RM. Oxygen transport - 1. Basic principles. *BMJ* 1998;317:1302–1306.

(7) Cecconi M, De Backer D, Antonelli M *et al*. Consensus on circulatory shock and hemodynamic monitoring. Task force of the European Society of Intensive Care Medicine. *Intensive Care Med* 2014;40:1795–1815.

(8) Vincent J, De Backer D. Circulatory shock. *N Engl J Med* 2013;369:1726–1734.

(9) De Backer D, Zhang H, Vincent JL. Models to study the relation between oxygen consumption and oxygen delivery during an acute reduction in blood flow: comparison of balloon filling in the inferior vena cava, tamponade, and hemorrhage. *Shock* 1995;4:107–112.

(10) Ronco JJ, Fenwick JC, Tweeddale MG *et al*. Identification of the critical oxygen delivery for anaerobic metabolism in critically ill septic and nonseptic humans. *JAMA* 1993;270:1724–1730.

(11) Cain SM. Appearance of excess lactate in anesthetized dogs during anemic and hypoxic hypoxia. *Am J Physiol* 1965;209:604–610.

(12) Vincent J, De Backer D. My paper 20 years later: effects of dobutamine on the VO_2/DO_2 relationship. *Intensive Care Med* 2014;40:1643–1648.

(13) Bersten AD, Handy J. Oh's intensive care manual. Elsevier; 2018.

(14) Gilbert EM, Haupt MT, Mandanas RY *et al*. The effect of fluid loading, blood transfusion, and catecholamine infusion on oxygen delivery and consumption in patients with sepsis. *Am Rev Respir Dis* 1986;134:873–878.

(15) Haupt MT, Gilbert EM, Carlson RW. Fluid loading increases oxygen consumption in septic patients with lactic acidosis. *Am Rev Respir Dis* 1985;131:912–916.

(16) Vincent JL, Roman A, De Backer D *et al*. Oxygen uptake/supply dependency. Effects of short-term dobutamine infusion. *Am Rev Respir Dis* 1990;142:2–7.

(17) Shoemaker WC, Appel PL, Waxman K *et al*. Clinical trial of survivors' cardiorespiratory patterns as therapeutic goals in critically ill postoperative patients. *Crit Care Med* 1982;10:398–403.

(18) Shoemaker WC, Montgomery ES, Kaplan E *et al*. Physiologic patterns in surviving and nonsurviving shock patients. Use of sequential cardiorespiratory variables in defining criteria for therapeutic goals and early warning of death. *Arch Surg* 1973;106:630–636.

(19) Shoemaker WC, Appel PL, Kram HB *et al*. Prospective trial of supranormal values of survivors as therapeutic goals in high-risk surgical patients. *Chest* 1988;94:1176–1186.

(20) Gattinoni L, Brazzi L, Pelosi P *et al*. A trial of goal-oriented hemodynamic therapy in critically ill patients. SvO2 Collaborative Group. *N Engl J Med* 1995;333:1025–1032.

(21) Böhrer H, Schmidt H, Bach A. Elevation of systemic oxygen delivery in the treatment of critically ill patients. *N Engl J Med* 1994;331:1161.

(22) Mohr PA, Monson DO, Owczarski C *et al*. Sequential cardiorespiratory events during and after dextran-40 infusion in normal and shock patients. *Circulation* 1969;39:379–393.

(23) Connors AFJ, Speroff T, Dawson NV *et al*. The effectiveness of right heart catheterization in the initial care of critically ill patients. SUPPORT Investigators. *JAMA* 1996;276:889–897.

(24) Polanczyk CA, Rohde LE, Goldman L *et al*. Right heart catheterization and cardiac complications in patients undergoing noncardiac surgery: an observational study. *JAMA* 2001;286:309–314.

(25) Sandham JD, Hull RD, Brant RF *et al*. A randomized, controlled trial of the use of pulmonary-artery catheters in high-risk surgical patients. *N Engl J Med* 2003;348:5–14.

(26) Rivers E, Nguyen B, Havstad S *et al*. Early goal-directed therapy in the treatment of severe sepsis and septic shock. *N Engl J Med* 2001;345:1368–1377.

(27) ProCESS Investigators, Yealy DM, Kellum JA *et al*. A randomized trial of protocol-based care for early septic shock. *N Engl J Med* 2014;370:1683–1693.

(28) ARISE Investigators, ANZICS Clinical Trials Group, Peake SL *et al*. Goal-directed resuscitation for patients with early septic shock. *N Engl J Med* 2014;371:1496–1506.

(29) Mouncey PR, Osborn TM, Power GS *et al*. Trial of early, goal-directed resuscitation for septic shock. *N Engl J Med* 2015;372:1301–1311.

(30) Nguyen HB, Jaehne AK, Jayaprakash N *et al*. Early goal-directed therapy in severe sepsis and septic shock: insights and comparisons to ProCESS, ProMISe, and ARISE. *Crit Care* 2016;20:160.

(31) Chawla LS, Zia H, Gutierrez G *et al*. Lack of equivalence between central and mixed venous oxygen saturation. *Chest* 2004;126:1891–1896.

(32) Wacharasint P, Nakada T, Boyd JH *et al*. Normal-range blood lactate concentration in septic shock is prognostic and predictive. *Shock* 2012;38:4–10.

(33) Jansen TC, van Bommel J, Mulder PG *et al*. The prognostic value of blood lactate levels relative to that of vital signs in the pre-hospital setting: a pilot study. *Crit Care* 2008;12:R160.

(34) Nguyen HB, Rivers EP, Knoblich BP *et al*. Early lactate clearance is associated with improved outcome in severe sepsis and septic shock. *Crit Care Med* 2004;32:1637–1642.

(35) Wilson RF, Christensen C, LeBlanc LP. Oxygen consumption in critically-ill surgical patients. *Ann Surg* 1972;176:801–804.

(36) Duff JH, Groves AC, McLean AP *et al*. Defective oxygen consumption in septic shock. *Surg Gynecol Obstet* 1969;128:1051–1060.

(37) Oshima T, Berger MM, De Waele E *et al*. Indirect calorimetry in nutritional therapy. A position paper by the ICALIC study group. *Clin Nutr* 2017;36:651–662.

(38) West JB. The collaboration of Antoine and Marie-Anne Lavoisier and the first measurements of human oxygen consumption. *Am J Physiol Lung Cell Mol Physiol* 2013;305:L775–L785.

(39) Frankenfield DC. On heat, respiration, and calorimetry. *Nutrition* 2010;26:939–950.

(40) Haldane JS. Methods of air analysis. Griffin; 1912.

(41) Douglas CG. A method for determining the total respiratory exchange in man. *J Physiol* 1911;42:17–18.

(42) Tissot S, Delafosse B, Bertrand O *et al*. Clinical validation of the Deltatrac monitoring system in mechanically ventilated patients. *Intensive Care Med* 1995;21:149–153.

(43) Black C, Grocott MPW, Singer M. Metabolic monitoring in the intensive care unit: a comparison of the Medgraphics Ultima, Deltatrac II, and Douglas bag collection methods. *Br J Anaesth* 2015;114:261–268.

(44) Bredbacka S, Kawachi S, Norlander O *et al*. Gas exchange during ventilator treatment: a validation of a computerized technique and its comparison with the Douglas bag method. *Acta Anaesthesiol Scand* 1984;28:462–468.

(45) Cournand A, Riley RL, Breed ES *et al*. Measurement of cardiac output in man using the technique of catheterization of the right auricle or ventricle. *J Clin Invest* 1945;24:106–116.

(46) Gidwani UK, Mohanty B, Chatterjee K. The pulmonary artery catheter: a critical reappraisal. *Cardiol Clin* 2013;31:545–565.

(47) Rehal MS, Fiskaare E, Tjäder I *et al*. Measuring energy expenditure in the intensive care unit: a comparison of indirect calorimetry by E-sCOVX and Quark RMR with Deltatrac II in mechanically ventilated critically ill patients. *Crit Care* 2016;20:54.

(48) American Thoracic Society, American College of Chest Physicians. ATS/ACCP Statement on cardiopulmonary exercise testing. *Am J Respir Crit Care Med* 2003;167:211–277.

(49) Sundström M, Tjäder I, Rooyackers O *et al*. Indirect calorimetry in mechanically ventilated patients. A systematic comparison of three instruments. *Clin Nutr* 2013;32:118–121.

(50) Cooper JA, Watras AC, O'Brien MJ *et al*. Assessing validity and reliability of resting metabolic rate in six gas analysis systems. *J Am Diet Assoc* 2009;109:128–132.

(51) Shephard RJ. Open-circuit respirometry: a brief historical review of the use of Douglas bags and chemical analyzers. *Eur J Appl Physiol* 2017;117:381–387.

(52) Levinson MR, Groeger JS, Miodownik S *et al*. Indirect calorimetry in the mechanically ventilated patient. *Crit Care Med* 1987;15:144–147.

(53) Phang PT, Cunningham KF, Ronco JJ *et al*. Mathematical coupling explains dependence of oxygen consumption on oxygen delivery in ARDS. *Am J Respir Crit Care Med* 1994;150:318–323.

(54) Ciaffoni L, O'Neill DP, Couper JH *et al*. In-airway molecular flow sensing: A new technology for continuous, noninvasive monitoring of oxygen consumption in critical care. *Sci Adv* 2016;2:e1600560.

(55) Intensive Care National Audit and Research Centre (ICNARC). Case mix programme public report 2022-23. 2024:15.

(56) Chiumello D, Carlesso E, Cadringher P *et al*. Lung stress and strain during mechanical ventilation for acute respiratory distress syndrome. *Am J Respir Crit Care Med* 2008;178:346–355.

(57) Janssens JP, Pache JC, Nicod LP. Physiological changes in respiratory function associated with ageing. *Eur Respir J* 1999;13:197–205.

(58) Peters U, Suratt BT, Bates JHT *et al*. Beyond BMI: obesity and lung disease. *Chest* 2018;153:702–709.

(59) Lumb AB, Nunn JF. Respiratory function and ribcage contribution to ventilation in body positions commonly used during anesthesia. *Anesth Analg* 1991;73:422–426.

(60) Ibañez J, Raurich JM. Normal values of functional residual capacity in the sitting and supine positions. *Intensive Care Med* 1982;8:173–177.

(61) Koo MC, Au R, Hague CJ *et al*. Expiration CT gas trapping measures with texture-based radiomics improves association with lung function and lung function decline in COPD. *Acad Radiol* 2025;32:3711–3721.

(62) Hedenstierna G, Edmark L. The effects of anesthesia and muscle paralysis on the respiratory system. *Intensive Care Med* 2005;31:1327–1335.

(63) Bikker IG, van Bommel J, Reis Miranda D *et al*. End-expiratory lung volume during mechanical ventilation: a comparison with reference values and the effect of positive end-expiratory pressure in intensive care unit patients with different lung conditions. *Crit Care* 2008;12:R145.

(64) Meneely GR, Kaltreider NL. The volume of the lung determined by Helium dilution. Description of the method and comparison with other procedures. *J Clin Invest* 1949;28:129–139.

(65) Chiumello D, Cressoni M, Chierichetti M *et al*. Nitrogen washout/washin, helium dilution and computed tomography in the assessment of end expiratory lung volume. *Crit Care* 2008;12:R150.

(66) Patroniti N, Bellani G, Manfio A *et al*. Lung volume in mechanically ventilated patients: measurement by simplified helium dilution compared to quantitative CT scan. *Intensive Care Med* 2004;30:282–289.

(67) Bhakta NR, McGowan A, Ramsey KA *et al*. European Respiratory Society/American Thoracic Society technical statement: standardisation of the measurement of lung volumes, 2023 update. *Eur Respir J* 2023;62:2201519.

(68) Patroniti N, Bellani G, Cortinovis B *et al*. Role of absolute lung volume to assess alveolar recruitment in acute respiratory distress syndrome patients. *Crit Care Med* 2010;38:1300–1307.

(69) Weaver LJ, Pierson DJ, Kellie R *et al*. A practical procedure for measuring functional residual capacity during mechanical ventilation with or without PEEP. *Crit Care Med* 1981;9:873–877.

(70) Heldt GP, Peters RM. A simplified method to determine functional residual capacity during mechanical ventilation. *Chest* 1978;74:492–496.

(71) Di Marco F, Rota Sperti L, Milan B *et al*. Measurement of functional residual capacity by helium dilution during partial support ventilation: in vitro accuracy and in vivo precision of the method. *Intensive Care Med* 2007;33:2109–2115.

(72) Barber DC, Brown BH. Applied potential tomography. *J Br Interplanet Soc* 1989;42:391–393.

(73) Hinz J, Hahn G, Neumann P *et al*. End-expiratory lung impedance change enables bedside monitoring of end-expiratory lung volume change. *Intensive Care Med* 2003;29:37–43.

(74) Frerichs I, Amato MBP, van Kaam AH *et al*. Chest electrical impedance tomography examination, data analysis, terminology, clinical use and recommendations: consensus statement of the TRanslational EIT developmeNt stuDy group. *Thorax* 2017;72:83–93.

(75) Wrigge H, Zinserling J, Muders T *et al*. Electrical impedance tomography compared with thoracic computed tomography during a slow inflation maneuver in experimental models of lung injury. *Crit Care Med* 2008;36:903–909.

(76) Gattinoni L, Chiumello D, Cressoni M *et al*. Pulmonary computed tomography and adult respiratory distress syndrome. *Swiss Med Wkly* 2005;135:169–174.

(77) Gattinoni L, Caironi P, Pelosi P *et al*. What has computed tomography taught us about the acute respiratory distress syndrome? *Am J Respir Crit Care Med* 2001;164:1701–1711.

(78) Austin JH, Müller NL, Friedman PJ *et al*. Glossary of terms for CT of the lungs: recommendations of the Nomenclature Committee of the Fleischner Society. *Radiology* 1996;200:327–331.

(79) Gattinoni L, Pesenti A, Bombino M *et al*. Relationships between lung computed tomographic density, gas exchange, and PEEP in acute respiratory failure. *Anesthesiology* 1988;69:824–832.

(80) Desai SR, Hansell DM. Lung imaging in the adult respiratory distress syndrome: current practice and new insights. *Intensive Care Med* 1997;23:7–15.

(81) Darling RC, Cournand A, Mansfield JS *et al*. Studies on the intrapulmonary mixture of gases. I. Nitrogen elimination from blood and body tissues during high oxygen breathing. *J Clin Invest* 1940;19:591–597.

(82) Newth CJ, Enright P, Johnson RL. Multiple-breath nitrogen washout techniques: including measurements with patients on ventilators. *Eur Respir J* 1997;10:2174–2185.

(83) Weismann D, Reissmann H, Maisch S *et al*. Monitoring of functional residual capacity by an oxygen washin/washout; technical description and evaluation. *J Clin Monit Comput* 2006;20:251–260.

(84) Fretschner R, Deusch H, Weitnauer A *et al*. A simple method to estimate functional residual capacity in mechanically ventilated patients. *Intensive Care Med* 1993;19:372–376.

(85) Olegård C, Söndergaard S, Houltz E *et al*. Estimation of functional residual capacity at the bedside using standard monitoring equipment: a modified nitrogen washout/washin

technique requiring a small change of the inspired oxygen fraction. *Anesth Analg* 2005;101:206–212.

(86) Edmark L, Auner U, Enlund M *et al*. Oxygen concentration and characteristics of progressive atelectasis formation during anaesthesia. *Acta Anaesthesiol Scand* 2011;55:75–81.

(87) Olegård C, Søndergaard S, Pålsson J *et al*. Validation and clinical feasibility of nitrogen washin/washout functional residual capacity measurements in children. *Acta Anaesthesiol Scand* 2010;54:370–376.

(88) Heinze H, Schaaf B, Grefer J *et al*. The accuracy of the oxygen washout technique for functional residual capacity assessment during spontaneous breathing. *Anesth Analg* 2007;104:598–604.

(89) Petousi N, Talbot NP, Pavord I *et al*. Measuring lung function in airways diseases: current and emerging techniques. *Thorax* 2019;74:797–805.

(90) Hedenstierna G. The recording of FRC: is it of importance and can it be made simple? *Intensive Care Med* 1993;19:365–366.

(91) Pelosi P, Croci M, Calappi E *et al*. Prone positioning improves pulmonary function in obese patients during general anesthesia. *Anesth Analg* 1996;83:578–583.

(92) Maggiore SM, Lellouche F, Pigeot J *et al*. Prevention of endotracheal suctioning-induced alveolar derecruitment in acute lung injury. *Am J Respir Crit Care Med* 2003;167:1215–1224.

(93) Heinze H, Sedemund-Adib B, Heringlake M *et al*. Changes in functional residual capacity during weaning from mechanical ventilation: a pilot study. *Anesth Analg* 2009;108:911–915.

(94) Gattinoni L, Protti A, Caironi P *et al*. Ventilator-induced lung injury: the anatomical and physiological framework. *Crit Care Med* 2010;38:S539–S548.

(95) Heinze H, Eichler W. Measurements of functional residual capacity during intensive care treatment: the technical aspects and its possible clinical applications. *Acta Anaesthesiol Scand* 2009;53:1121–1130.

(96) Acute Respiratory Distress Syndrome Network, Brower RG, Matthay MA *et al*. Ventilation with lower tidal volumes as compared with traditional tidal volumes for acute lung injury and the acute respiratory distress syndrome. *N Engl J Med* 2000;342:1301–1308.

(97) Amato MB, Barbas CS, Medeiros DM *et al*. Effect of a protective-ventilation strategy on mortality in the acute respiratory distress syndrome. *N Engl J Med* 1998;338:347–354.

(98) Maisch S, Reissmann H, Fuellekrug B *et al*. Compliance and dead space fraction indicate an optimal level of positive end-expiratory pressure after recruitment in anesthetized patients. *Anesth Analg* 2008;106:175–181.

(99) Suter PM, Fairley B, Isenberg MD. Optimum end-expiratory airway pressure in patients with acute pulmonary failure. *N Engl J Med* 1975;292:284–289.

(100) Huh JW, Jung H, Choi HS *et al*. Efficacy of positive end-expiratory pressure titration after the alveolar recruitment manoeuvre in patients with acute respiratory distress syndrome. *Crit Care* 2009;13:R22.

(101) Caironi P, Cressoni M, Chiumello D *et al*. Lung opening and closing during ventilation of acute respiratory distress syndrome. *Am J Respir Crit Care Med* 2010;181:578–586.

(102) Hodgson C, Goligher EC, Young ME *et al*. Recruitment manoeuvres for adults with acute respiratory distress syndrome receiving mechanical ventilation. *Cochrane Database Syst Rev* 2016;11:CD006667.

(103) Arnal J, Paquet J, Wysocki M *et al*. Optimal duration of a sustained inflation recruitment maneuver in ARDS patients. *Intensive Care Med* 2011;37:1588–1594.

(104) Marini JJ. Recruitment maneuvers to achieve an "open lung": whether and how? *Crit Care Med* 2001;29:1647–1648.

(105) Matthay MA, Arabi Y, Arroliga AC *et al*. A New Global Definition of Acute Respiratory Distress Syndrome. *Am J Respir Crit Care Med* 2024;209:37–47.

(106) Gattinoni L, Pesenti A. The concept of "baby lung". *Intensive Care Med* 2005;31:776–784.

(107) Meade MO, Cook DJ, Guyatt GH *et al*. Ventilation strategy using low tidal volumes, recruitment maneuvers, and high positive end-expiratory pressure for acute lung injury and acute respiratory distress syndrome: a randomized controlled trial. *JAMA* 2008;299:637–645.

(108) Writing Group for the Alveolar Recruitment for Acute Respiratory Distress Syndrome Trial (ART) Investigators, Cavalcanti AB, Suzumura ÉA *et al*. Effect of lung recruitment and titrated positive end-expiratory pressure (PEEP) vs low PEEP on mortality in patients with acute respiratory distress syndrome: a randomized clinical trial. *JAMA* 2017;318:1335–1345.

(109) Hodgson CL, Cooper DJ, Arabi Y *et al*. Maximal recruitment open lung ventilation in acute respiratory distress syndrome (PHARLAP). A phase II, multicenter randomized controlled clinical trial. *Am J Respir Crit Care Med* 2019;200:1363–1372.

(110) Pensier J, de Jong A, Hajjej Z *et al*. Effect of lung recruitment maneuver on oxygenation, physiological parameters and mortality in acute respiratory distress syndrome patients: a systematic review and meta-analysis. *Intensive Care Med* 2019;45:1691–1702.

(111) Futier E, Constantin J, Pelosi P *et al*. Noninvasive ventilation and alveolar recruitment maneuver improve respiratory function during and after intubation of morbidly obese patients: a randomized controlled study. *Anesthesiology* 2011;114:1354–1363.

(112) Reinius H, Jonsson L, Gustafsson S *et al*. Prevention of atelectasis in morbidly obese patients during general anesthesia and paralysis: a computerized tomography study. *Anesthesiology* 2009;111:979–987.

(113) Writing Committee for the PROBESE Collaborative Group of the PROtective VEntilation Network (PROVEnet) for the Clinical Trial Network of the European Society of Anaesthesiology, Bluth T, Serpa Neto A *et al*. Effect of intraoperative high positive end-expiratory pressure (PEEP) with recruitment maneuvers vs low PEEP on postoperative pulmonary complications in obese patients: a randomized clinical trial. *JAMA* 2019;321:2292–2305.

(114) Dyhr T, Bonde J, Larsson A. Lung recruitment manoeuvres are effective in regaining lung volume and oxygenation after open endotracheal suctioning in acute respiratory distress syndrome. *Crit Care* 2003;7:55–62.

(115) Lapinsky SE, Mehta S. Bench-to-bedside review: Recruitment and recruiting maneuvers. *Crit Care* 2005;9:60–65.

(116) de Matos GFJ, Stanzani F, Passos RH *et al*. How large is the lung recruitability in early acute respiratory distress syndrome: a prospective case series of patients monitored by computed tomography. *Crit Care* 2012;16:R4.

(117) Gattinoni L, Caironi P, Cressoni M *et al*. Lung recruitment in patients with the acute respiratory distress syndrome. *N Engl J Med* 2006;354:1775–1786.

(118) Grasso S, Mascia L, Del Turco M *et al*. Effects of recruiting maneuvers in patients with acute respiratory distress syndrome ventilated with protective ventilatory strategy. *Anesthesiology* 2002;96:795–802.

(119) Crotti S, Mascheroni D, Caironi P *et al*. Recruitment and derecruitment during acute respiratory failure: a clinical study. *Am J Respir Crit Care Med* 2001;164:131–140.

(120) Pelosi P, Cadringher P, Bottino N *et al*. Sigh in acute respiratory distress syndrome. *Am J Respir Crit Care Med* 1999;159:872–880.

(121) Gattinoni L, Pelosi P, Suter PM *et al*. Acute respiratory distress syndrome caused by pulmonary and extrapulmonary disease. Different syndromes? *Am J Respir Crit Care Med* 1998;158:3–11.

(122) Malbouisson LM, Muller JC, Constantin JM *et al*. Computed tomography assessment of positive end-expiratory pressure-induced alveolar recruitment in patients with acute respiratory distress syndrome. *Am J Respir Crit Care Med* 2001;163:1444–1450.

(123) Chiumello D, Brioni M. Severe hypoxemia: which strategy to choose. *Crit Care* 2016;20:132.

(124) Chiumello D, Marino A, Brioni M *et al*. Lung recruitment assessed by respiratory mechanics and Computed Tomography in patients with acute respiratory distress syndrome. What is the relationship? *Am J Respir Crit Care Med* 2016;193:1254–1263.

(125) Jonson B, Richard JC, Straus C *et al*. Pressure-volume curves and compliance in acute lung injury: evidence of recruitment above the lower inflection point. *Am J Respir Crit Care Med* 1999;159:1172–1178.

(126) Ranieri VM, Eissa NT, Corbeil C *et al*. Effects of positive end-expiratory pressure on alveolar recruitment and gas exchange in patients with the adult respiratory distress syndrome. *Am Rev Respir Dis* 1991;144:544–551.

(127) Demory D, Arnal J, Wysocki M *et al*. Recruitability of the lung estimated by the pressure volume curve hysteresis in ARDS patients. *Intensive Care Med* 2008;34:2019–2025.

(128) Maggiore SM, Jonson B, Richard JC *et al*. Alveolar derecruitment at decremental positive end-expiratory pressure levels in acute lung injury: comparison with the lower inflection point, oxygenation, and compliance. *Am J Respir Crit Care Med* 2001;164:795–801.

(129) Vieillard-Baron A, Prin S, Chergui K *et al*. Early patterns of static pressure-volume loops in ARDS and their relations with PEEP-induced recruitment. *Intensive Care Med* 2003;29:1929–1935.

(130) Chiumello D, Arnal J, Umbrello M *et al*. Hysteresis and lung recruitment in acute respiratory distress syndrome patients: a CT scan study. *Crit Care Med* 2020;48:1494–1502.

(131) Giovanazzi S, Nocera D, Catozzi G *et al*. Assessment of recruitment from CT to the bedside: challenges and future directions. *Crit Care* 2025;29:64.

(132) Chen L, Del Sorbo L, Grieco DL *et al*. Potential for lung recruitment estimated by the recruitment-to-inflation ratio in acute respiratory distress syndrome. A clinical trial. *Am J Respir Crit Care Med* 2020;201:178–187.

(133) Costa ELV, Borges JB, Melo A *et al*. Bedside estimation of recruitable alveolar collapse and hyperdistension by electrical impedance tomography. *Intensive Care Med* 2009;35:1132–1137.

(134) Richard J, Maggiore SM, Mercat A. Clinical review: bedside assessment of alveolar recruitment. *Crit Care* 2004;8:163–169.

(135) Karbing DS, Panigada M, Bottino N *et al*. Changes in shunt, ventilation/perfusion mismatch, and lung aeration with PEEP in patients with ARDS: a prospective single-arm interventional study. *Crit Care* 2020;24:111.

(136) Griffiths MJD, McAuley DF, Perkins GD *et al*. Guidelines on the management of acute respiratory distress syndrome. *BMJ Open Respir Res* 2019;6:e000420.

(137) Fan E, Del Sorbo L, Goligher EC *et al*. An official American Thoracic Society/European Society of Intensive Care Medicine/Society of Critical Care Medicine clinical practice guideline: mechanical ventilation in adult patients with acute respiratory distress syndrome. *Am J Respir Crit Care Med* 2017;195:1253–1263.

(138) Mountain JE, Santer P, O'Neill DP *et al*. Potential for noninvasive assessment of lung inhomogeneity using highly precise, highly time-resolved measurements of gas exchange. *J Appl Physiol (1985)* 2018;124:615–631.

(139) Mazurenka M, Orr-Ewing A, Peverall R *et al*. 4. Cavity ring-down and cavity enhanced spectroscopy using diode lasers. *Annu Rep Prog Chem , Sect C: Phys Chem* 2005;101:100–142.

(140) Cummings B, Hamilton ML, Ciaffoni L *et al*. Laser-based absorption spectroscopy as a technique for rapid in-line analysis of respired gas concentrations of O2 and CO2. *J Appl Physiol (1985)* 2011;111:303–307.

(141) Weldon V, O'Gorman J, Pérez-Camacho JJ *et al*. Spectroscopic Based Oxygen Sensing Using VCSEL and DFB Single Frequency Laser Diodes. *Conference on Lasers and Electro-Optics Europe* 1996:CWB6.

(142) Sandhu D, Redmond JL, Smith NMJ *et al*. Computed cardiopulmonography and the idealized lung clearance index, iLCI(2.5), in early-stage cystic fibrosis. *J Appl Physiol (1985)* 2023;135:205–216.

(143) O'Neill DP, Robbins PA. A mechanistic physicochemical model of carbon dioxide transport in blood. *J Appl Physiol (1985)* 2017;122:283–295.

(144) Magor-Elliott SRM, Fullerton CJ, Richmond G *et al*. A dynamic model of the body gas stores for carbon dioxide, oxygen, and inert gases that incorporates circulatory transport delays to and from the lung. *J Appl Physiol (1985)* 2021;130:1383–1397.

(145) Wilson TA, Beck KC. Contributions of ventilation and perfusion inhomogeneities to the VA/Q distribution. *J Appl Physiol (1985)* 1992;72:2298–2304.

(146) Beck KC, Johnson BD, Olson TP *et al*. Ventilation-perfusion distribution in normal subjects. *J Appl Physiol (1985)* 2012;113:872–877.

(147) International Commission on Radiological Protection. Report of the task group on reference man. *Ann ICRP* 1979;3:iii–iv.

(148) Spencer RP, Chaudhuri TK. Quantitative estimates of changes in splenic size during life. *Yale J Biol Med* 1969;41:333–339.

(149) Mazzoleni A, Curtin ME, Wolff R *et al*. On the relationship between heart weights, fibrosis, and QRS duration. *J Electrocardiol* 1975;8:233–236.

(150) Smith NMJ, Magor-Elliott SRM, Fullerton CJ *et al*. The Lognormal Lung: A new approach to quantifying lung inhomogeneity in COPD. *Front Physiol* 2022;13:1032126.

(151) Redmond JL, Kendall F, Smith NMJ *et al*. Computed cardiopulmonography for the detection of early smoking-related changes in the lungs of young individuals who smoke. *Chest* 2024;165:1107–1110.

(152) Smith NMJ, Couper J, Fullerton CJ *et al*. Novel measure of lung function for assessing disease activity in asthma. *BMJ Open Respir Res* 2020;7:e000531.

(153) Alamoudi A, Petralia L, Smith NMJ *et al*. Effects of biologic therapy on novel indices of lung inhomogeneity in patients with severe type-2 high asthma. *BMJ Open Respir Res* 2025;12:e002721.

(154) Nieman DC, Austin MD, Benezra L *et al*. Validation of Cosmed's FitMate in measuring oxygen consumption and estimating resting metabolic rate. *Res Sports Med* 2006;14:89–96.

(155) Brehm M, Harlaar J, Groepenhof H. Validation of the portable VmaxST system for oxygen-uptake measurement. *Gait Posture* 2004;20:67–73.

(156) Crouter SE, Antczak A, Hudak JR *et al*. Accuracy and reliability of the ParvoMedics TrueOne 2400 and MedGraphics VO2000 metabolic systems. *Eur J Appl Physiol* 2006;98:139–151.

(157) Hodges LD, Brodie DA, Bromley PD. Validity and reliability of selected commercially available metabolic analyzer systems. *Scand J Med Sci Sports* 2005;15:271–279.

(158) Shephard RJ. A critical examination of the Douglas bag technique. *Med Sci Sports Exerc* 2012;44:1407.

(159) Beaver WL. Water vapor corrections in oxygen consumption calculations. *J Appl Physiol* 1973;35:928–931.

(160) Cecconi M, Rhodes A, Poloniecki J *et al*. Bench-to-bedside review: the importance of the precision of the reference technique in method comparison studies--with specific reference to the measurement of cardiac output. *Crit Care* 2009;13:201.

(161) Critchley LA, Critchley JA. A meta-analysis of studies using bias and precision statistics to compare cardiac output measurement techniques. *J Clin Monit Comput* 1999;15:85–91.

(162) Kress JP, O'Connor MF, Pohlman AS *et al*. Sedation of critically ill patients during mechanical ventilation. A comparison of propofol and midazolam. *Am J Respir Crit Care Med* 1996;153:1012–1018.

(163) Cohen D, Horiuchi K, Kemper M *et al*. Modulating effects of propofol on metabolic and cardiopulmonary responses to stressful intensive care unit procedures. *Crit Care Med* 1996;24:612–617.

(164) Manthous CA, Hall JB, Olson D *et al*. Effect of cooling on oxygen consumption in febrile critically ill patients. *Am J Respir Crit Care Med* 1995;151:10–14.

(165) Jenkins TO, Karbing DS, Rees SE *et al*. Metabolic cost of physical rehabilitation in mechanically ventilated patients in critical care: an observational study. *BMJ Open Respir Res* 2025;12:e002878.

(166) Collings N, Cusack R. A repeated measures, randomised cross-over trial, comparing the acute exercise response between passive and active sitting in critically ill patients. *BMC Anesthesiol* 2015;15:1.

(167) Terao Y, Miura K, Saito M *et al*. Quantitative analysis of the relationship between sedation and resting energy expenditure in postoperative patients. *Crit Care Med* 2003;31:830–833.

(168) Compher C, Frankenfield D, Keim N *et al*. Best practice methods to apply to measurement of resting metabolic rate in adults: a systematic review. *J Am Diet Assoc* 2006;106:881–903.

(169) De Waele E, Honore PM, Spapen HD. New generation indirect calorimeters for measuring energy expenditure in the critically ill: a rampant or reticent revolution? *Crit Care* 2016;20:138.

(170) Dietrich KA, Romero MD, Conrad SA. Effects of gas leak around endotracheal tubes on indirect calorimetry measurement. *JPEN J Parenter Enteral Nutr* 1990;14:408–413.

(171) Bracco D, Chioléro R, Pasche O *et al*. Failure in measuring gas exchange in the ICU. *Chest* 1995;107:1406–1410.

(172) Wessel HU, Stout RL, Bastanier CK *et al*. Breath-by-breath variation of FRC: effect on VO2 and VCO2 measured at the mouth. *J Appl Physiol Respir Environ Exerc Physiol* 1979;46:1122–1126.

(173) Girardi M, Gattoni C, Stringer WW *et al*. Current definitions of the breathing cycle in alveolar breath-by-breath gas exchange analysis. *Am J Physiol Regul Integr Comp Physiol* 2023;325:R433–R445.

(174) Wilmore JH, Costill DL. Adequacy of the Haldane transformation in the computation of exercise VO2 in man. *J Appl Physiol* 1973;35:85–89.

(175) van Lanschot JJ, Feenstra BW, Vermeij CG *et al*. Accuracy of intermittent metabolic gas exchange recordings extrapolated for diurnal variation. *Crit Care Med* 1988;16:737–742.

(176) Harding J, Kemper M, Weissman C. Midazolam attenuates the metabolic and cardiopulmonary responses to an acute increase in oxygen demand. *Chest* 1994;106:194–200.

(177) Kreymann G, Grosser S, Buggisch P *et al*. Oxygen consumption and resting metabolic rate in sepsis, sepsis syndrome, and septic shock. *Crit Care Med* 1993;21:1012–1019.

(178) Nolan JP, Sandroni C, Böttiger BW *et al*. European Resuscitation Council and European Society of Intensive Care Medicine guidelines 2021: post-resuscitation care. *Intensive Care Med* 2021;47:369–421.

(179) Choi HA, Badjatia N, Mayer SA. Hypothermia for acute brain injury: mechanisms and practical aspects. *Nat Rev Neurol* 2012;8:214–222.

(180) Badjatia N. Hyperthermia and fever control in brain injury. *Crit Care Med* 2009;37:S250–S257.

(181) Graham BL, Steenbruggen I, Miller MR *et al*. Standardization of spirometry 2019 update. An official American Thoracic Society and European Respiratory Society technical statement. *Am J Respir Crit Care Med* 2019;200:e70–e88.

(182) Reshia FAA, Salameh B, Alsadaan N *et al*. Enhancing pulmonary function and arterial blood gas readings through immediate chest physiotherapy among extubated patients in ICU. *J Int Med Res* 2023;51:3000605231208600.

(183) Lee AL, Burge AT, Holland AE. Airway clearance techniques for bronchiectasis. *Cochrane Database Syst Rev* 2015;2015:CD008351.

(184) Froese AB. Gravity, the belly, and the diaphragm: you can't ignore physics. *Anesthesiology* 2006;104:193–196.

(185) Perchiazzi G, Rylander C, Vena A *et al*. Lung regional stress and strain as a function of posture and ventilatory mode. *J Appl Physiol (1985)* 2011;110:1374–1383.

(186) Sudy R, Dereu D, Lin N *et al*. Respiratory effects of pressure support ventilation in spontaneously breathing patients under anaesthesia: Randomised controlled trial. *Acta Anaesthesiol Scand* 2024;68:311–320.

(187) Bowerman C, Bhakta NR, Brazzale D *et al*. A race-neutral approach to the interpretation of lung function measurements. *Am J Respir Crit Care Med* 2023;207:768–774.

(188) Arnal J, Garnero A, Saoli M *et al*. Parameters for simulation of adult subjects during mechanical ventilation. *Respir Care* 2018;63:158–168.

(189) Tonga KO, Robinson PD, Farah CS *et al*. In vitro and in vivo functional residual capacity comparisons between multiple-breath nitrogen washout devices. *ERJ Open Res* 2017;3:11.

(190) Singer F, Houltz B, Latzin P *et al*. A realistic validation study of a new nitrogen multiple-breath washout system. *PLoS One* 2012;7:e36083.

(191) Poncin W, Singer F, Aubriot A *et al*. Agreement between multiple-breath nitrogen washout systems in children and adults. *J Cyst Fibros* 2017;16:258–266.

(192) Raaijmakers L, Jensen R, Stanojevic S *et al*. Validation of multiple breath washout devices. *J Cyst Fibros* 2017;16:e22–e23.

(193) Zwitserloot AM, van den Born EJ, Raaijmakers LHA *et al*. Differences in lung clearance index and functional residual capacity between two commercial multiple-breath nitrogen washout devices in healthy children and adults. *ERJ Open Res* 2020;6:247.

(194) Wyler F, Oestreich M, Frauchiger BS *et al*. Correction of sensor crosstalk error in Exhalyzer D multiple-breath washout device significantly impacts outcomes in children with cystic fibrosis. *J Appl Physiol (1985)* 2021;131:1148–1156.

(195) Oestreich M, Wyler F, Buess C *et al*. Signal-correction errors in the EasyOne Pro LAB multiple-breath washout device significantly impact outcomes in children and adults. *J Appl Physiol (1985)* 2024;136:460–471.

(196) Cliff IJ, Evans AH, Pantin CF *et al*. Comparison of two new methods for the measurement of lung volumes with two standard methods. *Thorax* 1999;54:329–333.

(197) Bayfield K, Alton E, Irving S *et al*. Comparison of functional residual capacity (FRC) from two multiple breath washout (MBW) systems and body plethysmography. *European Respiratory Society* ;48:PA1231.

(198) Zwitserloot A, Raaiijmakers L, Fuchs S *et al*. Comparison of FRC And TLC measured in whole body plethysmography and multiple breath washout in healthy adult volunteers. *Am J Respir Crit Care Med* 2014;189:A2988.

(199) Isaac SM, Jensen R, Anagnostopoulou P *et al*. Evaluation of a multiple breath nitrogen washout system in children. *Pediatr Pulmonol* 2020;55:2108–2114.

(200) Robinson PD, Latzin P, Verbanck S *et al*. Consensus statement for inert gas washout measurement using multiple- and single- breath tests. *Eur Respir J* 2013;41:507–522.

(201) Hedenstierna G, Edmark L. Mechanisms of atelectasis in the perioperative period. *Best Pract Res Clin Anaesthesiol* 2010;24:157–169.

(202) Grandville Bdl, Petak F, Albu G *et al*. High inspired oxygen fraction impairs lung volume and ventilation heterogeneity in healthy children: a double-blind randomised controlled trial. *Br J Anaesth* 2019;122:682–691.

(203) Maisch S, Boehm SH, Weismann D *et al*. Determination of functional residual capacity by oxygen washin-washout: a validation study. *Intensive Care Med* 2007;33:912–916.

(204) Wrigge H, Sydow M, Zinserling J *et al*. Determination of functional residual capacity (FRC) by multibreath nitrogen washout in a lung model and in mechanically

ventilated patients. Accuracy depends on continuous dynamic compensation for changes of gas sampling delay time. *Intensive Care Med* 1998;24:487–493.

(205) Heinze H, Sedemund-Adib B, Heringlake M *et al*. The impact of different step changes of inspiratory fraction of oxygen on functional residual capacity measurements using the oxygen washout technique in ventilated patients. *Anesth Analg* 2008;106:1491–1494.

(206) Zinserling J, Wrigge H, Varelmann D *et al*. Measurement of functional residual capacity by nitrogen washout during partial ventilatory support. *Intensive Care Med* 2003;29:720–726.

(207) Bikker IG, Scohy TV, Ad J J C Bogers *et al*. Measurement of end-expiratory lung volume in intubated children without interruption of mechanical ventilation. *Intensive Care Med* 2009;35:1749–1753.

(208) Coppola S, Froio S, Marino A *et al*. Respiratory mechanics, lung recruitability, and gas exchange in pulmonary and extrapulmonary acute respiratory distress syndrome. *Crit Care Med* 2019;47:792–799.

(209) Protti A, Santini A, Pennati F *et al*. Lung response to a higher positive end-expiratory pressure in mechanically ventilated patients with COVID-19. *Chest* 2022;161:979–988.

(210) Hamilton Medical. P/V Tool® Pro user guide: assessing lung recruitability and performing recruitment maneuvers in adult patients. 2021.

(211) Hall GL, Filipow N, Ruppel G *et al*. Official ERS technical standard: Global Lung Function Initiative reference values for static lung volumes in individuals of European ancestry. *Eur Respir J* 2021;57:2000289.

(212) Alamoudi A, Sandhu D, Bithell TDE *et al*. Computed cardiopulmonography: Effects of physical characteristics on lung parameter estimates. *Exp Physiol* 2025.

(213) Grasselli G, Calfee CS, Camporota L *et al*. ESICM guidelines on acute respiratory distress syndrome: definition, phenotyping and respiratory support strategies. *Intensive Care Med* 2023;49:727–759.

(214) Dianti J, Tisminetzky M, Ferreyro BL *et al*. Association of positive end-expiratory pressure and lung recruitment selection strategies with mortality in acute respiratory distress syndrome: a systematic review and network meta-analysis. *Am J Respir Crit Care Med* 2022;205:1300–1310.

(215) Goligher EC, Hodgson CL, Adhikari NKJ *et al*. Lung recruitment maneuvers for adult patients with acute respiratory distress syndrome. A systematic review and meta-analysis. *Ann Am Thorac Soc* 2017;14:S304–S311.

(216) Ball L, Serpa Neto A, Trifiletti V *et al*. Effects of higher PEEP and recruitment manoeuvres on mortality in patients with ARDS: a systematic review, meta-analysis,

meta-regression and trial sequential analysis of randomized controlled trials. *Intensive Care Med Exp* 2020;8:39.

(217) Cipulli F, Vasques F, Duscio E *et al*. Atelectrauma or volutrauma: the dilemma. *J Thorac Dis* 2018;10:1258–1264.

(218) Mink SN, Light RB, Wood LD. Effect of pneumococcal lobar pneumonia on canine lung mechanics. *J Appl Physiol Respir Environ Exerc Physiol* 1981;50:283–291.

(219) Hanly P, Light RB. Lung mechanics, gas exchange, pulmonary perfusion, and hemodynamics in a canine model of acute Pseudomonas pneumonia. *Lung* 1987;165:305–322.

(220) Light RB. Pulmonary pathophysiology of pneumococcal pneumonia. *Semin Respir Infect* 1999;14:218–226.

(221) Henzler D, Hochhausen N, Dembinski R *et al*. Parameters derived from the pulmonary pressure volume curve, but not the pressure time curve, indicate recruitment in experimental lung injury. *Anesth Analg* 2007;105:1072–1078.

(222) Dellamonica J, Lerolle N, Sargentini C *et al*. PEEP-induced changes in lung volume in acute respiratory distress syndrome. Two methods to estimate alveolar recruitment. *Intensive Care Med* 2011;37:1595–1604.

(223) Lu Q, Constantin J, Nieszkowska A *et al*. Measurement of alveolar derecruitment in patients with acute lung injury: computerized tomography versus pressure-volume curve. *Crit Care* 2006;10:R95.

(224) Victorino JA, Borges JB, Okamoto VN *et al*. Imbalances in regional lung ventilation: a validation study on electrical impedance tomography. *Am J Respir Crit Care Med* 2004;169:791–800.

(225) Poncin W, Reychler G, Leeuwerck N *et al*. Short-term effect of autogenic drainage on ventilation inhomogeneity in adult subjects with stable non-cystic fibrosis bronchiectasis. *Respir Care* 2017;62:524–531.

(226) Verbanck SAB, Polfliet M, Schuermans D *et al*. Ventilation heterogeneity in smokers: role of unequal lung expansion and peripheral lung structure. *J Appl Physiol (1985)* 2020;129:583–590.

(227) Svenningsen S, Eddy RL, Lim HF *et al*. Sputum eosinophilia and magnetic resonance imaging ventilation heterogeneity in severe asthma. *Am J Respir Crit Care Med* 2018;197:876–884.

(228) Magor-Elliott SRM, Alamoudi A, Chamley RR *et al*. Altered lung physiology in two cohorts after COVID-19 infection as assessed by computed cardiopulmonography. *J Appl Physiol (1985)* 2022;133:1175–1191.

(229) Barbas CSV, de Matos GFJ, Pincelli MP *et al*. Mechanical ventilation in acute respiratory failure: recruitment and high positive end-expiratory pressure are necessary. *Curr Opin Crit Care* 2005;11:18–28.

(230) Gattinoni L, Marini JJ, Collino F *et al*. The future of mechanical ventilation: lessons from the present and the past. *Crit Care* 2017;21:183.

(231) Pelosi P, Rocco PRM, Gama de Abreu M. Close down the lungs and keep them resting to minimize ventilator-induced lung injury. *Crit Care* 2018;22:72.

(232) Fan E, Checkley W, Stewart TE *et al*. Complications from recruitment maneuvers in patients with acute lung injury: secondary analysis from the lung open ventilation study. *Respir Care* 2012;57:1842–1849.